CHROMATIN ACCESSIBILITY CHANGES DURING ADIPOSE BEIGING AND MELANOCYTE STEM CELL ACTIVATION

A Dissertation

Presented to the Faculty of the Graduate School

of Cornell University

in Partial Fulfillment of the Requirements for the Degree of

Doctor of Philosophy

by

Seoyeon Lee

August 2022

ABSTRACT

CHROMATIN ACCESSIBILITY CHANGES DURING
ADIPOSE BEIGING AND MELANOCYTE STEM CELL ACTIVATION

Seoyeon Lee, Ph. D.
Cornell University 2022

The study of chromatin accessibility has been fundamentally important to understand gene regulatory networks underlying cellular behavior. I performed a single-nucleus assay for transposase-accessible chromatin (snATAC-seq) to characterize the changes in cellular heterogeneity and chromatin accessibility during adipose beiging and melanocyte stem cell activation.

In the first part of my thesis research, by applying snATAC-seq on adipose tissue, I identified distinct cell types in adipose tissue. I found substantial changes in adipocytes with an increase in abundance of beige adipocytes in response to thermogenic stimuli. I characterized a gene regulatory network during adipose beiging and identified commonality and heterogeneity of gene programs activated by two major thermogenic stimuli.

In the second part of my dissertation, I aimed to characterize melanocyte stem cells and their progeny and delineate the mechanisms and key regulators in melanocyte stem cell activation. By applying snATAC on sorted melanocytes, I identified three major cell states and characterized their chromatin states. The cell states vary by hair follicle cycles and environmental cues. I revealed potential regulators for activation of stem cell fate. Our data provide insights into cellular heterogeneity and gene regulatory networks underlying changes of cellular behaviors by analyzing chromatin states at a single-cell level.

BIOGRAPHICAL SKETCH

Seoyeon Lee was born and raised in Seoul, Korea. She attended Ewha Womans University in Seoul, earning a B.S. and M.S. in Nutritional Sciences. After graduating, she continued her research at California Institute of Technology, where she got intrigued by single-cell methods. She began doctoral studies and joined the lab of Dr. Paul Soloway at Cornell University. There she devoted several years to study chromatin accessibility changes in complex tissues at a single-cell level and to develop computational skills to analyze sequencing data. For her thesis, she studied dynamic chromatin accessibility changes during adipose beiging and melanocyte stem cell activation at a single-cell level.

ACKNOWLEDGEMENTS

I owe a debt of gratitude to my advisor, Paul Soloway; for his unwavering support and mentorship over the years of my PhD. He has set an example of excellence as a scientist, mentor, and role model. He has been extremely helpful in guiding me on my academic path. With his help, I could go beyond my comfort zone and enjoy my research.

I would like to show my deep appreciation for my committee members, Praveen Sethupathy, Daniel Berry, and Kimberley O'Brien, for their invaluable discussion, guidance, and support. I am so appreciative to have these incredible scientists on my committee.

I would like to give big thanks to the members of the Soloway lab, Roman Spektor for his valuable advice at the beginning of my PhD and Blane Harlan for inspiring discussions.

I would like to give special thanks to my collaborators and the Genomics facility staff; Nothing I've done would be possible without them.

Finally, I am very grateful to my family and friends for their love, support, and constant encouragement throughout my PhD. They all made me feel warm throughout my time in Ithaca even in cold winter.

TABLE OF CONTENTS

LIST OF FIGURES

LIST OF TABLES

LIST OF ABBREVIATIONS

Adrb3	β3-adrenergic receptor
aMcSC	Activated melanocyte stem cell
APC	Adipocyte progenitor cell
ATAC-seq	Assay for transpose accessible chromatin sequencing
BAT	Brown adipose tissue
ChIP-seq	Chromatin immunoprecipitation sequencing
CL	CL-316,243
CRISPR-Cas9	Clustered, regularly interspaced, short palindromic repeats (CRISPR) and CRISPR-associated protein 9
CUT&RUN	Cleavage under targets and release using nuclease
dCas9	Catalytically inactive CRISPR-associated protein 9
dMC	Differentiated melanocyte
DNase-seq	Deoxyribonuclease I hypersensitive sites sequencing
DNL	*De novo* lipogenesis
ECM	Extracellular matrix
FA	Fatty acid
FAIRE-seq	Formaldehyde-assisted isolation of regulatory elements sequencing
FAME	Fatty acid methyl esters
FANS	Fluorescence-assisted nuclei sorting
FDR	False discovery rate
FISH	Fluorescence *in situ* hybridization
GC-MS	Gas-chromatography mass spectrometry
GO	Gene ontology
GREAT	Genomic regions enrichment of annotations tool
GRN	Gene regulatory network
gRNA	Guide RNA
H&E	Hematoxylin and eosin
HAT	Histone acetyltransferases
HDAC	Histone deacetylase
HDM	Histone demethylase
HMT	Histone methyltransferases
iWAT	Inguinal white adipose tissue
KEGG	Kyoto encyclopedia of genes and genomes
KNN	K-nearest neighbor
LSA	Latent semantic analysis
McSC	Melanocyte stem cell
ME	Mosaic end

MERFISH	Multiplexed error-robust fluorescence *in situ* hybridization
Methyl-seq	Methylation sequencing
miRNA	MicroRNA
MNase-seq	Micrococcal nuclease digestion with sequencing
MUFA	Monounsaturated fatty acid
PCR	Polymerase chain reaction
PTM	Post-translational modification
PUFA	Polyunsaturated fatty acid
qMcSC	Quiescent melanocyte stem cell
RT	Room temperature
scATAC-seq	Single-cell assay for transpose accessible chromatin sequencing
scRNA-seq	Single-cell RNA-sequencing
seqFISH	Sequential fluorescence *in situ* hybridization
SFA	Saturated fatty acid
snATAC-seq	Single-nucleus assay for transpose accessible chromatin sequencing
SNN	Shared neighbor network
snRNA-seq	Single-nucleus RNA-seq
SVF	Stromal vascular fraction
TF	Transcription factor
TF-IDF	Term frequency-inverse document frequency
TSS	Transcription start site
UFA	Unsaturated fatty acid
UMAP	Uniform manifold approximation and projection
UVB	Ultraviolet-B
VEC	Vascular endothelial cell
VSMC	Vascular smooth muscle cell
WAT	White adipose tissue

Chapter 1: Introduction

1. Regulation of chromatin

Chromatin is a highly organized complex of DNA and protein that form chromosomes. The massive amount of DNA is condensed in a highly compact form in the nucleus of eukaryotic cells. DNA tightly wound around histone proteins are considered closed chromatin, and DNA with loose structure is permissible for transcription, called open chromatin. In eukaryotes, these compact or loose packaging of the genes in chromatin is tightly linked to transcriptional regulation. Transcriptional regulation is how cells control which genes to be turned up or down. Through the gene regulation, different cells can activate a different set of genes as needed. Gene regulation processes are often mediated by changes in chromatin structure and transition between a more open chromatin state and a more closed and compact chromatin state. When chromatin state in some regions becomes more open, the open regions are exposed for transcription of the genes. During cell differentiation and development, the chromatin is constantly undergoing modifications, thereby exposing different regions of DNA to chromatin binding factors. The chromatin compaction and assembly can be regulated by (1) remodeling of nucleosomes, (2) histone modifications, (3) DNA modifications or methylation, and (4) non-histone DNA binding proteins, which also can be modulated by chromatin.

1.1. Chromatin (nucleosome) remodeling

The fundamental subunit of chromatin is nucleosome. The nucleosome consists of about 146bp of DNA wrapped around histone proteins (Kornberg,

1974; Luger et al., 1997). The nucleosome organization by chromatin compaction and assembly regulates DNA to be more or less accessible to DNA binding factors, transcriptional machinery and vice versa. The nucleosome occupancy is highly dynamic across the genome, creating different chromatin accessibility states: open (accessible genomic regions with sparse nucleosome occupancy), permissive, or closed (inaccessible genomic regions with dense nucleosome occupancy). The process of opening and closure is called chromatin remodeling. Chromatin remodelers or nucleosome regulators can reconstruct nucleosomes and histone-DNA interactions by sliding, disrupting, or assembling nucleosomes (Bruno et al., 2003; Hamiche et al., 1999; Lorch et al., 1999).

Landscape of chromatin accessibility broadly reflects chromatin dynamics across the genome and interactions of promoters, enhancers, and chromatin-binding factors which collaboratively regulate gene programs. The landscape of chromatin accessibility varies by cell types and cellular states and changes dynamically in response to environmental and developmental cues. Aberrations in chromatin remodeling is associated with human diseases (Sims and Reinberg, 2004; Staub et al., 2006). Therefore, the study of chromatin accessibility and remodeling is important to the understanding of gene regulation and disease.

The major nucleosome structure alterations utilize the energy from ATP hydrolysis to move, eject or restructure nucleosomes. The key enzymes involved in this process are called ATP-dependent chromatin remodeling factors. Most ATP-dependent remodeling factors are typically composed of multiple subunits with an ATPase subunit. Four distinct families of ATP-dependent chromatin remodeling factors are SWI/SNF (switch/sucrose-non-

fermenting), ISWI (imitation switch), CHD (chromodomain-helicase-DNA binding) and INO80 (inositol requiring 80). The function of ATP-dependent chromatin remodeling on a nucleosome varies, however, the common outcome is the change of nucleosomal positions along the DNA by disrupting histone-DNA interactions (Hamiche *et al.*, 1999; Längst et al., 1999).

Beyond previously known ATP-dependent chromatin remodeling factors which use the energy of ATP hydrolysis, pioneer factors are transcription factors that open closed chromatin to activate transcription by introducing active-chromatin histone modifications at closed chromatin, specifically enhancers (Iwafuchi-Doi and Zaret, 2016; Larson et al., 2021; Mayran and Drouin, 2018). Pioneer factors conduct the initial steps of opening of enhancer chromatin which allow the subsequent binding of additional factors for transcription activation. Uniquely, pioneer factors are able to recognize the DNA in closed chromatin that are inaccessible to other DNA binding proteins. Thus, pioneer factors hold potential for therapy to correct cell fate specification by regulating enhancer activity.

1.2. Histone modifications

A key component of chromatin regulation is histone modifications. Approximately 146bp of DNA are tightly wrapped around a histone octamer that consists of two copies of each of the histones H2A, H2B, H3, and H4 (Luger *et al.*, 1997). The assembly of histones starts with the association of a tetramer of histone H3-H4, followed by the incorporation of H2A-H2B dimers. The positive charges of histones allow histones to tightly bind to the negative charges of the DNA. Thereby, histones can block other non-histone DNA binding proteins from binding to certain regions of DNA. Post-

translational modifications (PTMs) in histone alter chromatin compaction and transcription but not limited to transcription. PTMs include lysine acetylation, arginine and lysine methylation, phosphorylation, ubiquitination, deamination, sumoylation, proline isomerization, and others (Arnaudo and Garcia, 2013; Kouzarides, 2007). There are three known protein machinery; histone writers, erasers, and readers that modify these PTMs. Writers are histone modifying enzymes that add PTMs to histones. Writers include histone acetyltransferases (HAT) and histone methyltransferases (HMT) (Gillette and Hill, 2015). Erasers are histone demodifying enzymes that remove specific PTMs from histone substrate. Histone deacetylases (HDACs) and histone demethylases (HDMs) are proteins removing acetyl groups and methyl groups from histones respectively (Gillette and Hill, 2015). Lastly, readers such as SWI/SNF recognize PTM marks (Gillette and Hill, 2015). The readers that recognize these PTMs recruit various components of the signaling network to chromatin, mediating process such as chromatin remodeling, DNA damage response, apoptosis, and cell-cycle regulation (Kouzarides, 2007; Musselman et al., 2012).

Specifically, histone acetylation and phosphorylation reduce the positive charge of histones and disrupt histone-DNA interactions. This leads to opening packed chromatin structure and enables non-histone DNA binding proteins and transcription machineries to bind, facilitating active transcription. In contrast, histone methylation does not alter the charge of histones. The effects of methylation on gene activity vary depending on the degree and specific residues of methylation. The most common sites for methylation marks are lysine and arginine residues in histones. Histone arginine methylation exists in mono-methylated (me1), or di-methylated (me2). The

degree of methylation of histone lysine can be mono (me1), di (me2), or tri (me3) methylation. Typically, mono-methylation of H3K4 is considered as an activating mark, specifically for enhancers (Heintzman et al., 2007), whereas H3K9 and H3K27 methylations are repressive marks (Barski et al., 2007; Bernstein et al., 2005). Aberrant histone modifications can lead to defects in development and numerous diseases.

1.3. DNA methylation

Another mechanism to control transcription is through methylation of the DNA strand. These modifications affect the transcription by controlling recruitment of transcription factors, HDACs, chromatin remodelers and/or RNA polymerase (Zhang et al., 1998). Methylation of the DNA strand involves transfer of a methyl group to cytosine bases converting to 5-methylcytosine. Methylation often results in repression of transcription by attracting proteins involved in deacetylation of histones, leading to compact chromatin. Likewise, demethylated DNA often recruits histone acetyltransferases, allowing histones to remain acetylated which then promotes transcription by weakening interactions between DNA and histones.

1.4. Transcription factors

Transcription factor proteins are one of the main regulators of gene transcription, besides RNA polymerase that initiate and regulate transcription. Transcription factors regulate gene activity by binding to certain DNA sequences (motifs) in the genome. Transcription factors help control transcription in the right cells at the right time. Thus, dysregulation of

transcription factors is associated with human diseases and developmental disorders (Boyadjiev and Jabs, 2000; Bradner et al., 2017; Lee and Young, 2013).

Transcription factors function in the cell nucleus and contain DNA-binding and transcription activation or repression domains. Chromatin accessibility affects transcription factor binding activity by modulating when and where transcription factors bind their targets to regulate gene transcription. Most of transcription factors cannot bind to closed chromatin (Zaret and Mango, 2016).

Genetic elements can regulate gene expression in *cis* (on the same allele) or in *trans* (on both alleles). While *trans*-regulatory elements or *trans*-acting factors affect the gene transcription on both alleles, *cis*-regulatory elements or *cis*-acting factors act on the same chromosomal allele. *Trans*-regulatory elements including transcription factors interact with *cis*-regulatory elements. *Cis*-regulatory elements are generally noncoding DNA regions that regulate gene transcription such as promoters and enhancers. Promoters are close to the gene that is being transcribed. Enhancers which can be intragenic or extragenic function to enhance transcription, typically 100bp to 1kb short. Thus, gene transcription is regulated by the interplay of regulatory elements at gene promoters and enhancers. Nucleosomes are often depleted at *cis*-regulatory regions that interact with sequence-specific DNA-binding transcription factors (Lee et al., 2004; Yue et al., 2014). Overall, open and closed chromatins can represent transcriptionally active or repressed states of genes, often containing binding sites for transcription factors.

2. High-throughput sequencing assays to measure chromatin states

Section 1 detailed the function and importance of chromatin organization and chromatin regulators to our understanding of gene regulation. High-throughput sequencing assays have been developed to profile DNA methylation, chromatin accessibility, histone modification, and protein-DNA interaction. The development of techniques coupled with next generation sequencing enables us to analyze genome-wide landscapes. ChIP-seq (Chromatin immunoprecipitation sequencing) (Johnson et al., 2007), ChIP-exo (Rhee and Pugh, 2011), CUT&RUN (Cleavage under targets and release using nuclease) sequencing (Skene and Henikoff, 2017), and CUT&TAG (Cleavage under targets and tagmentation) sequencing (Kaya-Okur et al., 2019) have been used to study histone modification and DNA-protein interaction. Whole-genome bisulfite sequencing or Methyl-seq (Methylation sequencing) (Lister et al., 2009) are used to measure genome-wide DNA methylation levels. DNase-seq (Deoxyribonuclease I hypersensitive sites sequencing) (Boyle et al., 2008), MNase-seq (Micrococcal nuclease digestion with sequencing) (Schones et al., 2008), FAIRE-seq (Formaldehyde-assisted isolation of regulatory elements sequencing) (Giresi et al., 2007), and ATAC-seq (Assay for transpose accessible chromatin sequencing) (Buenrostro et al., 2013) are used to profile chromatin accessibility. These methods identify the regions of DNA that are not protected by bound proteins. By measuring chromatin accessibility, nucleosome depleted regions, transcription factor footprints, and active regulatory elements can be examined. These methods do not require specific target proteins, histone marks or antibodies to be determined. Thus, the analysis is not restricted to specific transcription factors or histone modifications. Moreover, chromatin accessibility is associated with changes

in DNA methylation and 3D genome architecture (Zhong et al., 2021). Therefore, the assays described in this section focus on the current genome-wide high-throughput arrays measuring chromatin accessibility.

Several assays exist to probe nucleosome-depleted areas of the genome. DNase-seq utilizes DNase I to digest nucleosome-depleted DNA. Low concentration of DNase I preferentially cuts nucleosome-free genomic regions (DNase I hypersensitive sites), while DNA regions tightly wrapped in nucleosome are relatively less susceptible to digestion with DNase. During gene activation, DNase I hypersensitive sites often contain altered chromatin conformation for open chromatin (Wu et al., 1979). Loss or temporal destabilization of nucleosomes with the collaborative action of ATP-dependent nucleosome- and histone-remodelers, chromatin structure is disrupted (Henikoff, 2008). Therefore, DNase-seq can identify active regions of the genome by sequencing DNase-digested fragments.

Another array based on the doublet enzymatic cleavage of DNA fragments is MNase-seq. Digestion of nuclei or chromatin using MNase derived from *Staphylococcus aureus* has been widely used for mapping nucleosome position (Schlesinger et al., 2013). Since nucleosome-associated DNA is relatively insensitive to MNase digestion, MNase preferentially digests DNA in between nucleosomes, while nucleosome-protected DNA remains intact. Thus, MNase-seq indirectly measures chromatin accessibility by identifying the regions of the genome occupied by nucleosomes and other DNA binding factors.

Unlike other enzymatic methods, FAIRE-seq is based on a biochemical method. Briefly, DNA-protein complexes are crosslinked using formaldehyde (Giresi *et al.*, 2007). Chromatin is then subsequently sheared

by sonication, and phenol-chloroform extracted. Then nucleosome-depleted regions of the genome are separated and sequenced. FAIRE-seq can avoid any sequence bias introduced by endonucleases, but has small signal-to-noise ratio compared to other methods.

Lastly, ATAC-seq is a popular method for measuring chromatin accessibility across the genome. ATAC-seq method was first published in 2013 (Buenrostro *et al.*, 2013). ATAC-seq relies on hyperactive Tn5 transposase which can only access open chromatin regions (Adey et al., 2010; Goryshin and Reznikoff, 1998). Much like DNase I, Tn5 transposase has low efficiency on DNA wrapped around nucleosomes. The method can be separated into three major steps: nuclei isolation, tagmentation, and amplification. Unlike FAIRE-seq, it doesn't require crosslinking before or after nuclei isolation. During tagmentation, Tn5 transposase binds and cuts accessible DNA and adds short oligonucleotides of known sequence (adaptors) simultaneously (Buenrostro *et al.*, 2013). DNA fragments are then amplified by PCR. ATAC-seq reads contain variable length of DNA, including nucleosome-free regions to mono-, di- to poly-nucleosomal regions. These different length of DNA reads provide information about the positions of nucleosomes.

Although extant methods such as DNase-seq and MNase-seq can also profile chromatin accessibility, they often require millions of cells as input material. In contrast, ATAC-seq is relatively rapid, information rich and compatible with low input as little as 500-5000 cells with low-background. Even though early protocols suffered from a high proportion of mitochondrial reads, it was significantly reduced by an optimized protocol, Omni-ATAC (Corces et al., 2017). ATAC-seq assay is now one of the most popular

approaches to investigate epigenetic profiles for its sensitivity across many different cell/tissue types, and compatibility with other methods. Importantly, ATAC-seq is compatible with other methods for cell separation and isolation, such as cell sorting, making it possible for single-cell analysis which will be discussed further in the section 3.

3. Single-cell/single-nucleus analysis

3.1. Single-cell arrays

Section 2 detailed the techniques enabled us to measure chromatin accessibility in a population of cells or complex tissues. While it is highly informative in a homogeneous population, heterogeneity from multiple cell populations and complex tissues is averaged out. Therefore, changes in a small population or rare cells can be missed by bulk analysis. Single-cell methods enable us to identify different cell types and heterogenous cell states in an unbiased way, quantify cell type abundances, and evaluate the effects of genotype, treatment, and development on individual cell types. Advances in single-cell technologies have allowed us to generate data for single cells in a relatively simple and cost-effective manner and have been adapted to ATAC-seq. In 2015, two single-cell ATAC-seq (scATAC-seq) methods were introduced with two different strategies. Greenleaf group used microfluidics chip (Fluidigm C_1) to capture individual cells then performed tagmentation, followed by library amplification (Buenrostro et al., 2015). Shendure group integrated ATAC-seq and a combinatorial indexing for multiplex barcoding of single cells, called sci-ATAC-seq (single-cell ATAC sequencing using combinatorial indexing), which does not require any specialized equipment (Cusanovich et al., 2015). In the method, nuclei in 96-

wells are exposed to barcoded transposase loaded with sequencing adapters. The nuclei are then pooled and sorted into a second plate using fluorescence-assisted nuclei sorting (FANS). During polymerase chain reaction (PCR) for DNA amplification, second barcodes with indexed primers are added. The use of two-stage combinatorial indexing during tagmentation and PCR achieve high cell throughput. Single cells can be identified based on the two rounds of combinatorial indexing after sequencing. In addition to these approaches, several strategies and improvements of the technology have been introduced, including plate-based single-cell ATAC-seq protocol (Chen et al., 2018) and dscATAC-seq (droplet single-cell assay for transposase-accessible chromatin using sequencing) (Lareau et al., 2019). Droplet-based workflow which was originally used for single-cell RNA-seq (scRNA-seq) increased throughput of scATAC-seq. In this approach, individual droplets capture a bead that contains indexed primers and pre-tagmented nuclei in bulk with Tn5 transposase. After breaking the emulsion, barcoded DNA is pooled and amplified. Droplet-based workflow using the Chromium platform from 10x Genomics has been widely used in various techniques. While the droplet-based 10X Genomics Chromium platform is a cost effective and time saving method discussed here, combinatorial indexing approach is highly scalable with the use of multiple rounds of combinatorial indexing. In this strategy, barcoding and pooling steps can be repeated as many times as needed, and increasing the overall complexity of barcoding capacity in a cost effective way. And as each round of cell indexing can be used to identify different samples, it enables separation of large numbers of samples to be multiplexed within a single experiment. Moreover, ligation-based indexing step has been utilized for additional

indexing to increase throughput to even larger scale and eliminate the necessity for FANS sorting. Seelig group introduced a ligation-based single-cell method called SPLiT-seq, which uses multiple rounds of pooling, splitting, and ligation (Rosenberg et al., 2018). It was first employed to measure single-cell transcriptomes. sci-ATAC-seq3 is an improved sci-ATAC-seq assay utilizing the three levels of combinatorial indexing by introducing ligation based indexing (Domcke et al., 2020). The barcode space can be expanded to even larger barcoding space with additional rounds of ligation. This further reduces costs and achieves larger scales.

3.2. Single-cell data analysis

Single-cell data analysis tools enable us to analyze large amount of sequencing data and identify (1) cell types and distinct cell states based on shared features, (2) changes in cell abundance, (3) differentially expressed or accessible features (genes, windows/bins, or peaks) between conditions or among cell types, and (4) cell-cell interaction based on ligand-receptor expression or accessibility. These analyses provide insights into how specific cell types in a complex tissue respond to genetic, environmental, developmental or pathologic changes, or at what genomic locations are the focus of those responses. Analyzing the single-cell data is much more complicated and requires computational tools. scRNA-seq data analysis tools such as Monocle (Trapnell et al., 2014) and Seurat (Stuart et al., 2019) were established earlier. Although scRNA-seq and scATAC-seq data analysis workflow share common steps such as alignment, cell clustering and identifying differentially active features, the bioinformatics tools for scRNA-seq data analysis lack comprehensiveness in their ability to process

scATAC-seq data. Some approaches differ to account for the difference in readout (gene expression *vs* chromatin accessibility) and features (genes *vs* binned genome or peaks). Specifically, the sparsity of genomic datasets in scATAC-seq data present computational challenges as the maximum total signal at a genomic locus is limited by the copy number of DNA, which results in generating 0, 1, or 2 reads from each element within a diploid genome. Several algorithms have been suggested to analyze scATAC-seq data. First of all, since the majority of accessible regions in cell-by-bin/window or cell-by-peak matrix is “0”, most of strategies for scATAC-seq data binarize the raw count feature matrix so that “0” represents either closed chromatin or missing value. Non-zero elements with more than 1 counts are converted to "1". Next, to get around the sparsity issue, latent semantic analysis (LSA) has been used to cluster cells based on the similarity of chromatin accessibility (Cusanovich *et al.*, 2015). LSA was originally designed for natural language data due to its sparsity and noise (Granja et al., 2021). An alternative approach is representing data by k-mer words associated with features such as transcription factor motifs. occupancy of the sequencing reads from each (Ma et al., 2020).

The output of ATAC-seq is reads enriched in genomic locations (called peaks). ATAC-seq data contain the genomics features such as promoter, gene body, exon, intronic, and intergenic regions. One of the easiest ways to annotate peaks is mapping peaks to a nearby gene based on the genomic location. Understanding how changes in chromatin accessibility associated with their target genes is important to understand the molecular basis of cellular responses to genetic, environmental, developmental or pathological changes, and specifically, to identify the regulatory sequences that respond,

and their target genes. However, identifying the functions of differentially accessible genes are still challenging. Therefore, several approaches have been developed. One approach to infer transcription factor motif associated accessibility is chromVAR (Schep et al., 2017). ChromVAR estimates the variability of transcription factor motif occurrence within open chromatin regions in individual cells. While regulatory elements are enriched in physically proximity such as promoters, distal elements such as enhancers can be also correlated with the distant target promoters. To address these challenges, an algorithm, cicero (Pliner et al., 2018), infers *cis*-regulatory interactions in the genome by examining co-accessibility between enhancers and promoters. Recently, more frameworks for the analysis of single-cell chromatin data have been dedicated to scATAC-seq analysis such as snapATAC (Fang et al., 2021), Signac (Stuart et al., 2021), and ArchR (Granja *et al.*, 2021). These provide almost end-to-end analysis of single-cell ATAC-seq data and incorporate many existing tools, such as chromVAR and cicero. The analysis includes defining cell types and states, identifying key master regulators such as transcription factors, identifying differentially accessible elements and gene regulatory networks, and constructing trajectories.

4. Multi-omics

ATAC-seq and RNA-seq report distinct but related genomic features. Linking between chromatin accessibility and gene expression can reveal the role of chromatin structure in regulating gene expression. Likewise, data from multiple modalities enable us to gain complementary layers of information. Recent advances in technologies allow us to generate

multimodal datasets and integrate them to provide the comprehensive understanding of cells' biological networks. Omics technologies are high-throughput biochemical assays measure molecules from a biological sample comprehensively and simultaneously. Multi-omics is an integrative approach in which data sets are measurements of multiple "omes", such as genome, transcriptome, epigenome, proteome, and lipidome. Each of the genomic tools provides a different perspective. Yet, studying only a single layer of information provides a piece of the whole picture. For example, lipidomics analysis provides what genomics cannot, detailed insights into the state of a cell's metabolism. Transcriptomic studies provide information at the transcriptional level, but there are many underlying entities contribute to the transcription. Likewise, transcriptional level can contribute to another biological state of a cell. Thus, multiomics hold great potential for revealing associations of the layers of molecular properties of each cell or tissue. New technologies have been developed to capture multiple properties from the same sample or even same cell and to provide a more complete and informative view. The most rapid progress has been made in genomics and transcriptomics.

4.1. Joint profiling

Joint single-cell measurements of gene expression and DNA regulatory element activity holds great promise as a tool to understand transcriptional regulation. Particularly, capturing RNA and ATAC is the most widely used multilevel single-cell methods to explore associations between a regulatory network and a transcriptional state. The advancements of chromatin accessibility along with transcription profiling include sci-CAR (Cao et al.,

2018), PAIRED-seq (Zhu et al., 2019), SHARE-seq (Ma *et al.*, 2020), SNARE-seq (Chen et al., 2019b), and Smart3-ATAC (Cheng et al., 2021). Simultaneous profiling of transcriptome and epigenome on the same cells enables direct matching of epigenomic and transcriptional regulation, which provide more comprehensive understanding of the role of chromatin structure in regulating gene expression.

4.2. Integrative analysis

An alternative approach for the integrative analysis is combining publicly available dataset of single-omics data. In my thesis, my major focus is profiling chromatin accessibility using snATAC-seq. ATAC-seq has several advantages compared to other genomic tools. While RNA-seq is a powerful method to measure gene expression, it does not provide information about the underlying regulatory networks. ATAC-seq provides important component of these regulatory regions governing the expression programs. The features measured by ATAC-seq including accessible chromatin regions across the whole genome are typically 10-20x larger than the size of the features usually limited to expressed genes identified by RNA-seq (Chen et al., 2019a). The larger feature size could be valuable in distinguishing cell dynamics underlying variable cell states in complex tissues. Even though ATAC-seq can predict which genes are likely to be more transcribed based on reads in promoters and genes, it does not provide information about transcription level. Moreover, while ATAC-seq enables prediction of candidate promoters and enhancers. it does not directly map promoters and enhancers like PRO-seq (Kwak et al., 2013) or ChRO-seq (Chu et al., 2018). Still, ATAC-seq holds great potential to identify

candidate genes and regulatory elements. For better understanding of the flow of information and comprehensive analysis, here, I used publicly available scRNA-seq and ChIP-seq data and performed lipidomics analysis. Combination of multiomics data from publicly available expression and ChIP-seq data are used to further answer the questions which are limited to answer by ATAC-seq alone to reveal the relationship between epigenetic regulation and gene regulation.

Chapter 2: Remodeling of gene regulatory networks underlying thermogenic stimuli-induced adipose beiging

Seoyeon Lee[1], Abigail M. Benvie[1], Hui Gyu Park[2], Roman Spektor[3], Blaine Harlan[3], J Thomas Brenna[1,2], Daniel C. Berry[1], Paul D. Soloway[1,4]

[1]Division of Nutritional Sciences, College of Agriculture and Life Sciences, Cornell University, Ithaca, New York 14853, USA.
[2]Dell Pediatric Research Institute, Departments of Chemistry, Pediatrics, and Nutrition, Dell Medical School and the College of Natural Sciences, University of Texas at Austin, Austin, Texas 78712, USA.
[3]Field of Genetics, Genomics, and Development, Department of Molecular Biology and Genetics, Cornell University, Ithaca, New York 14853, USA.
[4]Department of Biomedical Sciences, College of Veterinary Medicine, Cornell University, Ithaca, New York 14853, USA.

Author contributions:

S.L., P.D.S., and D.C.B. conceived this study. S.L., P.D.S., D.C.B., and J.T.B. designed the experiments. S.L. carried out the snATAC-seq library preparation and data analyses. A.B. carried out the mouse experiment. H.G.P. performed the lipidomics experiment. R.S. and B.H. contributed to snATAC-seq sample preparation and provided suggestions on the data analysis. S.L. wrote the draft and S.L., P.D.S., and D.C.B. edited the manuscript. P.D.S. supervised this study.

Abstract

Beige adipocytes are induced by cold temperatures or β3-adrenergic receptor (Adrb3) agonists. They create heat through glucose and fatty acid (FA) oxidation, conferring metabolic benefits. The distinct and shared mechanisms by which these treatments induce beiging are unknown. Here, we perform single-nucleus assay for transposase-accessible chromatin sequencing (snATAC-seq) on adipose tissue from mice exposed to cold or an Adrb3 agonist to identify cellular and chromatin accessibility dynamics during beiging. Both stimuli induce chromatin remodeling that influence vascularization and inflammation in adipose. Beige adipocytes from cold-exposed mice have increased accessibility at genes regulating glycolytic processes, whereas Adrb3 activation increases cAMP responses. While both thermogenic stimuli increase accessibility at genes regulating thermogenesis, lipogenesis, and beige adipocyte development, the kinetics and magnitudes of the changes are distinct for the two stimuli. Accessibility changes at lipogenic genes are linked to functional changes in lipid composition of adipose. Both stimuli tend to decrease the proportion of palmitic acids, a saturated FA in adipose. However, Adrb3 activation increases the proportion of monounsaturated FAs, whereas cold increases the proportion of polyunsaturated FAs. These findings reveal common and distinct mechanisms of cold and Adrb3 induced beige adipocyte biogenesis, and identify the unique functional consequences of manipulating these pathways *in vivo*.

Introduction

Adipose tissues have a central role in maintaining systemic energy homeostasis (Cypess and Kahn, 2010a; b). Specifically, white adipose tissue (WAT) is considered a key regulator of energy storage and distribution and

regulates a myriad of local and distal metabolic responses (Wu et al., 2012). In contrast, reducing the environmental temperature can recruit and activate brown adipose tissue (BAT) to dissipate stored energy as heat via non-shivering thermogenesis(Cypess and Kahn, 2010a; b). To accomplish thermogenesis, brown adipocytes contain specialized mitochondria that express a high level of uncoupling protein 1 (UCP1), which can disconnect the electron transport chain by collapsing the proton gradient, generating heat rather than chemical energy (Cypess and Kahn, 2010a; b). In addition to brown adipocytes, cold temperature exposure can produce brown-like fat cells within WAT depots (Rosenwald et al., 2013). These so-called beige or brite adipocytes resemble brown fat cells in that they consume glucose and fatty acids (FAs) to perform thermogenesis (Cypess and Kahn, 2010b). In addition to cold temperatures, several other stimuli such as β3-adrenergic receptor (Adrb3) agonists, and peroxisome proliferator activated receptor gamma (PPARγ) agonists have been shown to promote beige adipocyte biogenesis (Jiang et al., 2017a; Jiang et al., 2017b; Ohno et al., 2012). Regardless of the beige adipocyte inducer, it appears that the activation of thermogenesis plays a critical role in shifting energy expenditure and mobilization of glucose and lipids from the blood. Additionally, identification and activation of human BAT have been linked to averting diet-induced weight gain and insulin resistance (Cypess and Kahn, 2010a). Thus, defining the cellular and transcriptional regulators of beige adipocyte formation under various beige fat-inducers could aid in developing targeted therapies to counteract metabolic disease.

Cold exposure stimulates the sympathetic nervous system to release norepinephrine, which activates adipose beiging through Ardb3 (Cypess and Kahn, 2010b). Due to the importance of Adrb3 signaling, Adrb3 agonists are

often interchangeably used with cold exposure to mimic cold stimulation of BAT (Burl et al., 2018; Rajbhandari et al., 2019). Although the two stimuli share major pathway features, distinct effects of cold exposure and Adrb3 agonists on beiging have been reported (Jiang *et al.*, 2017a). Lineage tracing studies, genetic necessity tests, and pharmacological strategies have suggested that cold temperatures stimulate WAT resident perivascular adipocyte progenitor cells (APCs) to undergo *de novo* adipocyte formation (Berry et al., 2016; Jiang *et al.*, 2017a). However, compared to cold, it has been reported that Adrb3 activation stimulates pre-existing white adipocytes to convert into beige adipocytes (Jiang *et al.*, 2017a). The mechanisms underlying the emergence of beige adipocytes remain incompletely characterized. It is also unknown whether these mechanisms differ when cold or Adrb3 activation induces beiging. Moreover, of clinical relevance, the use of Adrb3 agonists is contraindicated due to off-target side-effects such as tachycardia and hypertension (Arch, 2011). Yet recent efforts have identified a more selective Adrb3 agonist, mirabegron, which is clinically used to treat overactive bladder conditions, demonstrating clinical promise to improve metabolism in obese humans by stimulating beige fat formation but without the cardiometabolic effect (Michel et al., 2020). However, beyond the understanding of different cellular sources to generate beige fat much remains about the cellular, molecular, and metabolic differences between cold temperature- and Adrb3-induced beige fat. Critically, understanding these differences would be essential for enhancing clinical care to foster metabolic fitness and promote white fat loss.

The resolving power of single-cell technologies have enabled the characterization of cellular heterogeneity, and their transcriptional and epigenomic states in complex tissues (Cao et al., 2019; Cusanovich et al., 2018;

Preissl et al., 2018). Recently, single-cell RNA-sequencing (scRNA-seq) and single-nucleus RNA-sequencing (snRNA-seq) were applied to characterize cell populations in mature adipocytes and/or the stromal vascular fraction (SVF) of adipose tissue (Biagi et al., 2021; Burl *et al.*, 2018; Rabhi et al., 2020; Rajbhandari *et al.*, 2019; Sun et al., 2020; Vijay et al., 2020). While these studies have yielded tremendous insights into the transcriptomes of white and beige adipose tissues, only a few studies have attempted to discern differences between cold exposure and Adrb3 activation (Li et al., 2021; Rabhi *et al.*, 2020). Revealing gene regulatory networks (GRNs) is of significant interest as the interplay of *trans*-acting regulatory factors and *cis*-acting regulatory elements likely control the emergence of beige adipocytes and their metabolic programs. Yet, despite the importance of chromatin states, adipose tissues are a poorly represented node in chromatin state datasets.

Here, we performed single-nucleus assay for transposase-accessible chromatin with high-throughput sequencing (snATAC-seq) on WAT collected across the beige adipogenic time course induced by cold exposure or CL-316,243 (CL), a Adrb3 agonist. We characterized GRNs for the beige adipogenic process and developmental trajectory of cellular changes accompanying adipose tissue beiging. A comparative analysis for commonality and heterogeneity of two thermogenic agents showed that cold temperatures increase gene accessibility regulating glycolytic processes, whereas Adrb3 activation increases cAMP responses. Moreover, while we observed changes in thermogenic, lipogenic, and beige fat development genes in response to cold and Adrb3 activation, these responses had unique kinetics and magnitudes. Interestingly, we observed changes in lipogenic genes that could be attributed to functional changes in WAT lipid composition. Both cold and CL increased FA

elongation, but Adrb3 activation more induced the formation of monounsaturated FAs (MUFAs). Taken together, our analysis provides insights into mechanisms underlying beiging, and the shared and distinct effects of cold and Adrb3 activation on WAT.

Results

snATAC-seq reveals distinct cell types in inguinal adipose tissue

In order to understand the dynamic chromatin remodeling during adipose tissue beiging, we performed snATAC-seq of inguinal WAT (iWAT) from mice exposed to cold temperature (6°C) or treated with CL at room temperature (RT; 22°C) for 0, 1, 3, or 7 days (Fig. 1a). Histological assessment showed both cold exposure and CL induced beige adipocyte formation in iWAT depots (Supplementary Fig. 1a). Nuclei from whole adipose tissues were used to obtain cell types in entire iWAT to overcome technical bias related to isolation of cells or SVF. A total of 32,552 cells passed quality control from seven groups (day0RT, day1C, day3C, day7C, day1CL, day3CL, and day7CL) and three individual mice for each group (Supplementary Fig. 2a-s).

To identify the cell types, we performed dimensionality reduction and unsupervised clustering based on top 50% variable peaks using Signac (Hao et al., 2021; Stuart *et al.*, 2021). This revealed 12 highly consistent cell clusters, visualized using uniform manifold approximation and projection (UMAP) (Fig. 1b). We annotated clusters using differentially accessible genes, gene ontology (GO) analysis, cell type specific marker genes, transcription factor (TF) motif enrichment, and GREAT analysis (Fig. 1c and Supplementary Fig. 3a-e). We further confirmed that the annotation is consistent with the cell type identities predicted by publicly available adipose tissue scRNA-seq and snRNA-seq data

with high correlation rates (Supplementary Fig. 3f,g). Adipocytes constitute about 90% of adipose tissue volume but comprise only 20% of total cells (Rosen and Spiegelman, 2014). In agreement with our expectation, we found an average of 22% of adipocytes in our snATAC-seq dataset (Supplementary Fig. 4a,b). The average proportion of other non-adipocyte cell types in our dataset was about 72% for immune cells, 3% for APCs, and 2% for stromal cells (Supplementary Fig. 4a).

Dynamic changes in adipocytes and identification of thermogenic beige adipocytes

We analyzed the changes in cell abundance in response to cold and CL treatment in each cell type (Fig. 1d). However, the differential abundance testing of discrete clusters relies on predefined clusters and limits the ability to detect shifts in cell states within clusters. Thus, to further analyze the abundance changes caused by cold and CL treatment without relying on discrete clusters, we used Milo (Dann et al., 2022) to assign cells to neighborhoods having similar cellular states. The neighborhoods around adipocytes showed the highest variation in the log2 fold changes of their UMAP coordinates after cold and CL treatment. This indicated, that adipocytes underwent especially dynamic changes in their responses to cold and CL relative to other cell types (Fig. 1e,f and Supplementary Fig. 4c-h).

Mature adipocyte populations have high accessibility at the *Pparg* gene and differentially accessible peaks in these cells are enriched for PPARG motifs (Fig. 2a,b). Two distinct adipocyte populations were distinctively separated from other populations on the UMAP and identified as white or adipocytes and beige (Fig. 1b,2c). The proportion of beige adipocytes gradually increased from 1% to

5% with increased exposure time to both cold or CL treatments (Fig. 1d,2d). Among neighborhoods identified by Milo (Dann *et al.*, 2022), those around beige adipocytes were increased after cold and CL treatment compared to day 0 at RT, confirming accumulation of beige adipocytes (Fig. 1e,f and Supplementary Fig. 4c-h).

General adipocyte marker genes were highly accessible in both adipocyte populations, while beige/brown adipocyte marker genes were highly accessible in beige adipocyte population (Fig. 2e). The top five genes enriched in white adipocytes were *Car3, Lrp3, Tenm4, Trabd2d*, and *Cmklr1* (Fig. 2f); whereas the top five genes enriched in beige adipocytes were *Slc4a4, Ucp1, Pank1, Ppargc1b*, and *Gyk* (Fig. 2f). GO analysis revealed that the genes enriched in beige adipocytes are related to FA oxidation and thermogenesis (Fig. 2g). KEGG pathway analysis showed that the genes enriched in beige adipocytes are also associated with PPAR signaling pathway and FA metabolism (Fig. 2h). Taken together, the cluster we identified as beige adipocytes showed clear thermogenic signatures compared to white adipocytes.

Beige-specific cis- and trans-acting gene regulatory networks

Chromatin accessibility analysis reveals key GRNs including TFs and *cis*-regulatory elements underlying dynamic genetic and epigenetic program. To comprehensively characterize GRNs activated in beige adipocytes, we identified genomic regions with higher accessibility in beige adipocytes, which we refer to as beige-specific peaks. We firstly performed GREAT analysis (McLean et al., 2010) to predict biological functions of the beige-specific peaks using annotations of the nearby genes. Predicted functions of the beige-specific regions were related to brown fat cell differentiation and FA oxidation (Fig. 3a),

providing additional confidence in our original identification of beige adipocytes. We further extended these analyses by focusing on distal beige-specific peaks not residing in annotated genes. Using cicero (Pliner *et al.*, 2018), we analyzed co-accessible peaks and identify putative *cis*-regulatory interactions and the genomes that are more likely to be enhancers of the linked genes. For instance, a set of beige-specific peaks in the upstream of *Ucp1* showed high co-accessibility with each other and *Ucp1* promoter (Fig. 3b). Similarly, other sets of co-accessible beige-specific peaks were linked to genes including *Ppara, Pdk4, Ppargc1b, Acot11, Arhgef37, Slc4a4, Col27a1, Dio2, Elovl6*, *Kcnk3*, and *Ppargc1a*. These genes themselves exhibited high accessibility in beige adipocytes (Supplementary Fig. 5a). If intergenic beige-specific peaks include functional enhancers that are active in beige adipocytes, we expected to find H3K27ac marks associated with the beige-specific peaks. To make this determination, we referred published H3K27ac ChIP-seq data collected from white and beige adipocytes (Roh et al., 2018). Over 6,000 beige-specific peaks overlapped with regions carrying H3K27ac (Supplementary Fig. 5b). These overlapping regions included peaks upstream of *Ucp1* that were co-accessible with the *Ucp1* promoter in beige adipocytes that were largely absent from white adipocytes (Fig. 3b). This indicates that the beige-specific peaks are likely to include a large number of functional enhancers active in beige cells.

To gain further understanding of the GRNs in beige adipocytes, we contrasted TF binding motifs enriched in beige-specific, vs white-specific peaks. Motifs enriched in beige adipocytes included members of the ESRR, MEF2, ROR, NR2, and NR4 families (Fig. 3c and Supplementary Fig. 5c,d). It was previously reported that peroxisome proliferator-activated receptor coactivator-1α (PGC-1α), a key regulator for brown adipose, promoter has two MEF2-

binding sites and its transcriptional activation is mediated by MEF2 (Czubryt et al., 2003). Especially, ESRRα and ESRRβ were the most highly variable motifs in adipocytes (Fig. 3d). Whereas the footprint pattern of the general adipose regulator PPARγ was similar between white and beige adipocytes (Fig. 3e), beige adipocytes showed a distinct TF footprint for ESRRα (Fig. 3f). Loss of ESRR isoforms was shown to reduce thermogenic capacity of BAT upon adrenergic stimulation (Brown et al., 2018). These results collectively highlight specific regulation of ESRR and its importance in beige adipocytes. In addition to ESRR and MEF2, NR2 and NR4 family members can be functionally important to induce beiging. Especially, NR4A family members were shown to bind to a regulatory region of *Ucp1* and enhance *Ucp1* expression in mouse and human adipocytes (Kumar et al., 2008). On the other hand, the most enriched TF motifs in white adipocytes is NR3C family that serves as glucocorticoid receptors (GR) (Fig. 3c). GR can function as a TF and bind to glucocorticoid response elements. It was reported that excess glucocorticoids reduce the thermogenic activity of BAT and inhibit the expression of *Ucp1*, suggesting that glucocorticoids are negative regulators of BAT thermogenesis (Soumano, 2000; Strack et al., 1995; Thuzar et al., 2018; Viengchareun et al., 2001). In accordance with this, GR ChIP-seq data showed that NR3C1 and NR3C2 were enriched during re-warming of beige adipocytes at thermoneutrality (30°C), suggesting that NR3Cs are involved in whitening of beige adipocytes (Roh *et al.*, 2018). Collectively, these results demonstrate that our snATAC-seq data revealed positive and negative transcriptional regulators of beige adipocyte development.

PGC-1α is a key transcriptional coactivator of white-to-brown transition and regulates pathways including mitochondrial FA oxidation (Finck and Kelly, 2006)

and mitochondrial biogenesis (Czubryt *et al.*, 2003; Huss et al., 2004; Schreiber et al., 2004; Vega et al., 2000). To get better insights into how PGC-1α functionally relates to beige-specific peaks we identified, we intersected the beige-specific peaks with PGC-1α binding sites which were obtained from publicly available PGC-1α ChIP-seq data from BAT (Chang et al., 2018). We found that 50%, or 465 beige-specific peaks overlapped with PGC-1α binding sites, while only 1 white-specific peaks overlapped with PGC-1α binding sites (Fig. 3g and Supplementary Fig. 5e). Notably, *Ucp1* upstream has three beige-specific peaks which are PGC-1α binding sites, and overlapped with H3K27ac marks (Fig. 3b). In addition, *Pdk4, Slc4a4*, and *Ppara* also have three beige-specific peaks that have binding motifs for PGC-1α (Fig. 3h). These genes themselves exhibited high accessibility and expression level in beige adipocytes that arose upon cold and CL treatment (Supplementary Fig. 5f-h). These results strongly suggest that PGC-1α, in concert with the TF motifs enriched in beige-specific peaks identified in the present study play important roles in beige adipocyte function.

To identify potential target genes of beige-specific TFs and their coactivator PGC-1α, we identified the genes satisfying four criteria: (1) Tight linkage to beige-specific peaks, (2) having binding motifs for TFs enriched in beige adipocytes obtained from JASPAR2020 (Fornes et al., 2020) or cisbp database (Weirauch et al., 2014), (3) have validated binding sites for ESRRα (Chaveroux et al., 2013), MEF2α (Wales et al., 2014), and PGC-1α (Chang *et al.*, 2018) based on published ChIP-seq data, (4) overlap with H3K27ac27 marks in beige adipocytes. Among genes satisfying all criteria, *Pdk4* was identified as a target gene for beige-specific TFs and their coactivator (Fig. 3h-j and Supplementary Fig. 5i). The binding sites for PGC-1α, ESRRs, MEF2s, NR2s, and NR4s were

all enriched at beige-specific peaks at the locus; accordingly, *Pdk4* is a nexus for their coordinated regulation (Fig. 3h-k and Supplementary Fig. 5i). PDK4 enzyme inactivates the pyruvate dehydrogenase complex (PDH), resulting in a decrease in the formation of acetyl-CoA from glucose and a metabolic shift from glucose oxidation to FA oxidation (Cadoudal et al., 2008). The recent loss-of-function study revealed that FA oxidation was blunted in *Pdk4* knockdown human adipose-derived stem cells (Barquissau et al., 2016). Taken together, these data reveal the GRNs including TFs and *cis*-regulatory elements and their potential target genes underlying beiging process.

Transcription factor modules associated with beige adipocyte developmental trajectories

Our finding that the TFs function coordinately at beige-specific peaks motivated us to identify TF modules for beige adipocyte development. Three TF modules were revealed by unsupervised hierarchical clustering based on the similarity of TF activity computed by chromVAR (Schep *et al.*, 2017) across all individual adipocytes (Fig. 4a). Module 1 contained NR3C, TEAD, and STAT family motifs. It was previously shown that knockdown of TEAD4 increased expression of PPARγ and C/EBPα, master regulators for adipogenesis (Zhang et al., 2018). Also, adipocyte specific STAT1 knockout promoted PGC-1α expression and enhanced mitochondrial function in WAT depots (Cox et al., 2020). Therefore, the module 1 may represent negative regulators in beige adipogenic process. Module 3 consisted of ROR, NR2, NR4, ESRR, and MEF family motifs, which were enriched in beige adipocytes. The module 3 transcriptional regulators play critical roles in mitochondrial biogenesis and thermogenesis by interacting with PGC-1α in beige adipocytes (Czubryt *et al.*,

2003; Huss *et al.*, 2004; Schreiber *et al.*, 2004; Vega *et al.*, 2000). Lastly, module 2 contains C/EBP, RXR, PPAR, and NFI family motifs. RXRs play an important role in *Ucp1* induction in brown adipocytes (Nie et al., 2017). RXRs can form heterodimers with PPARs (Chandra et al., 2008). PPARα regulates adipogenesis and FA oxidation (Goto et al., 2011). C/EBPs function with PPARγ to promote adipocyte development (Rosen et al., 2002). Also, it was reported that NFIA binds to brown fat-specific enhancers prior to brown-fat cell differentiation along with C/EBPβ in WAT and BAT (Hiraike et al., 2017). The motifs in the module 2 have relatively higher correlations with both module 1 and module 3, suggesting intermediate states or shared features between white and beige adipocytes for adipocyte development.

Given these results, and the facts that (1) individual cells can move between cell states in the same cell type, and (2) cells may exist in transition between states (Altschuler and Wu, 2010), we sought to find a path covering the heterogeneous cellular states in the context of continuous beige adipocyte developmental trajectory. We constructed pseudotime trajectory of adipocytes. The inferred trajectory passes from one point where most of day 0 cells are located and to another where most of day 7 cells are located on UMAP (Fig. 4b). In line with our TF module analysis, the activity of TF motifs in module 3 was enriched in the later stage of trajectory, whereas the activity of TF motifs in module 1 was depleted (Fig. 4c). The activity of C/EBPβ and NFIA in module 2 were not significantly changed or gradually increased respectively (Fig. 4c). We ordered the genes based on changes in gene accessibility over pseudotime trajectory (Fig. 4d and Supplementary Fig. 6a,b). It showed that adipocytes lose gene accessibility of *Med16, Nnat, Car3*, and *Fads3* at early stage (Fig. 4d,e), and there is a gradual gain of accessibility for *Acly, Me1*, and *Acaca* at the

intermediate stage (Fig. 4d). As we expected, *Ucp1* was highly accessible at the later stage (Fig. 4d,e). Additionally, *Otop1, Cidea, Ppargc1b, Elovl6, Slc4a4, Ppara*, and *Pank1* were highly accessible in later pseudotime (Fig. 4d).

Finally, we identified positively correlated genes and TFs across pseudotime during beige adipocyte development. The cells at the later developmental stage gained accessibility at *Ppara, Esrra*, and *Mef2d* genes and their corresponding TF motifs (Fig. 4f,g). Specifically, the cells with high *Esrra* gene accessibility also had high ESRRA motif accessibility (Fig. 4h,i). Collectively, these emerging patterns of TF-encoding gene and TF motif accessibility across the adipocyte trajectory define mechanisms underlying environmentally-induced and transcriptionally-controlled adipocyte beiging (Fig. 4j).

Adipose progenitors and vascular network expansion in inguinal adipose tissue

Beige adipocytes can arise via transdifferentiation of unilocular mature adipocytes (Barbatelli et al., 2010; Rosenwald *et al.*, 2013) but also by *de novo* differentiation from various progenitors (Berry *et al.*, 2016; Chen et al., 2019c; Jiang *et al.*, 2017a). In our snATAC-seq data, two subtypes of APCs were identified (Fig. 5a). *Pdgfra*, a marker for APCs, was accessible in both APC clusters (Fig. 5b). APC1 was uniquely marked by accessibility at *Ebf2, Cd34*, and *Ly6a* (*Sca1*), whereas APC2 had higher accessibility at *Pdgfrb* and mural cell marker genes including *Acta2* and *Myh11* (Fig. 5b).

APCs reside in a vascular niche, and thus, the development of APCs is closely related to the vasculature (Berry *et al.*, 2016; Han et al., 2011; Jiang *et al.*, 2017a). In our snATAC-seq data, two stromal cell types were identified, vascular endothelial cells (VECs) and vascular smooth muscle cells (VSMCs).

VECs were uniquely marked by accessibility at endothelial cell marker genes such as *Pecam1* and *Chd5*, while VSMCs had higher accessibility at smooth muscle cell marker genes including *Mylk4, Myh4, Myog, Myf5*, and *Myod1* (Fig. 5b). We found that the abundance of VEC and VSMC tended to increase following cold and CL treatment (Fig. 1d). Since they are two essential cell types in blood vessels, the expansion of VEC and VSMC populations is closely associated with vessel growth. In line with this, the genes enriched in VECs were related to vasculature development (Fig. 5c).

To gain insights into how the expansion of vasculature is regulated in iWAT, we used ligand-receptor pairs to infer cellular communication (Jin et al., 2021). This analysis revealed that adipocytes are likely to interact with VEC through vascular endothelial growth factor (VEGF) signaling, mainly through *Vegfra* and *Vegfr1* (Fig. 5d,e). VEGF is a major growth factor that promotes the proliferation of endothelial cells and the growth of new blood vessel in adipose tissue (Ferrara et al., 2003). WAT vascular expansion is important for formation and maintenance of APC niche (Jiang *et al.*, 2017b). These results suggest that vascular cells and adipocytes in iWAT form a reciprocal feedback loop to promote angiogenesis in a paracrine manner and expansion of vascular cells provides a niche for APCs.

Decreased abundance of inflammatory immune cells after cold and CL treatment

Immune cells are another critical constituent of the adipose microenvironment that influence adipose tissue function and metabolic homeostasis (Choe et al., 2016). In our snATAC-seq data, we found lymphocytes, including B cells, CD4+ and CD8+ T cells, and myeloid cells,

including macrophages and dendritic cells (Fig. 6a,b). We observed a significant decrease in cell abundance of myeloid origin, especially dendritic cells after cold and CL treatment (Fig. 1d). Compared to other immune cells, the motifs for NF-kB family, including RELA, REL, NF-kB1, and NF-kB2, were highly enriched in dendritic cells (Fig. 6c,d). NF-kB is a key mediator of cytokine signaling and NF-kB signaling activates transcription of various proinflammatory genes (Lawrence, 2009). Consistently, GO analysis showed that the genes enriched in dendritic cells at day 0 are associated with NF-kB signaling pathway (Fig. 6e). These results suggest that dendritic cells in adipose tissue contribute to proinflammatory microenvironment, mainly through NF-kB signaling, and thus, a decrease in dendritic cell population may prevent activation of inflammatory responses after cold exposure and CL treatment.

Shared and distinct mechanisms of cold exposure and CL responses in adipocytes

It has been suggested that beige adipocytes produced by different thermogenic stimuli may have unique genetic signatures and different metabolic properties (Jiang *et al.*, 2017a). Therefore, we examined similarities and differences of activated gene programs resulting from cold and CL treatments. We first identified genes that were more accessible after 1, 3, and 7 days of cold or CL treatment compared to day 0 (Fig. 7a and Supplementary Fig. 7a-i). We next identified those genes that had elevated accessibility in both treatment groups, or in just one treatment group at the 3 or 7 day time points (Fig. 7b and Supplementary Fig. 7j-l). This strategy enabled us to identify shared and distinct mechanisms by which these exposures lead to beiging. GO analysis showed that the genes enriched after both cold and CL treatment were associated with

ribose phosphate metabolic process, fatty acid and acyl-CoA metabolic process, and adaptive thermogenesis (Fig. 7c). The genes more enriched after cold exposure were involved in glycolytic process (Fig. 7d); whereas the genes enriched in CL were related to GTPase activity and cAMP signaling (Fig. 7e). These findings are consistent with the facts that Adrb3 activation, like other G protein-coupled receptor signaling cascades, triggers cAMP signaling pathways; and in the case of Adrb3 activation, this leads to induction of thermogenesis (Harms and Seale, 2013).

The genes that are commonly more accessible by cold and CL treatment for 1, 3, and 7 days were involved in FA metabolism, specifically *de novo* lipogenesis (*DNL*) (Fig. 7a). Interestingly, we found some kinetic differences in accessibility of lipogenic genes between cold and CL across time course (Fig. 7f). In cold, the accessibility of lipogenic genes gradually increased from day 1 to day 7, whereas peak accessibility of lipogenic genes was shown at day 3 in CL. In contrast, the accessibility of glycolytic genes gradually increased after cold exposure, while no significant changes were observed after CL treatment (Fig. 7g). Therefore, cold and CL share common pathways during beiging, yet differ in specific signaling cascades and in timing of changes in gene accessibility.

Cold and CL alter the composition of lipid classes in inguinal adipose tissue

The genes encoding enzymes involved in *DNL* and FA elongation such as *Acaca, Acly, Fasn*, and *Elovl6* underwent profound changes in adipocytes after cold exposure and CL treatment (Fig. 7a and Supplementary Fig. 8a,b). Fatty acid synthetase (FAS), encoded by *Fasn*, converts malonyl-CoA into palmitic

acid, a major product of *DNL* (Lodhi et al., 2011). Then, saturated FA (SFA) and unsaturated FA (UFA) can be further elongated by FA elongases (ELOVLs) (Lodhi *et al.*, 2011). If any of these changes were functionally important, we expect that FAs extracted from adipose tissue would exhibit different profiles from RT after cold or CL treatment, or that profiles found in cold and CL may differ as well. Therefore, we measured a total of 21 lipid species from the same iWAT used for snATAC-seq by gas-chromatography mass spectrometry (GC-MS)-based lipid profiling. The most abundant free FAs were oleic acid (18:1n-9), linoleic acid (18:2n-6), and palmitic acid (16:0), making up around 82% of the FA content of the depot (Fig. 7h and Supplementary Fig. 8c). Palmitoleic acid (16:1n-7), stearic acid (18:0), and vaccenic acid (18:1n-7) were the next most abundant free FAs, which account for 10% (Fig. 7h and Supplementary Fig. 8c).

Based on the composition of major FAs and its elongation products, we calculated the metabolic activity of elongation and found that both cold and CL significantly increased the ratio of elongation (Fig. 7i). Consistently, our snATAC-seq analysis showed changes in FA elongation and accessibility of Elovl6, a gene encoding a key enzyme that catalyzes the elongation of FAs (Fig. 2h,7a), providing evidence for the correlation between chromatin accessibility and their functional modulation of lipid profiles. Next, we characterized changes in lipid composition after cold and CL treatment. Despite the increased elongation by both cold and CL, different types of FAs were increased by cold and CL. Strikingly, CL treatment significantly increased the proportion of oleic acid, a major component of monounsaturated FA (MUFA), not cold treatment (Fig. 7h,j). In addition, the proportion of some lipid species have opposite dynamics between cold and CL. For example, cold exposure tended to

decrease palmitic acid gradually over time course, while CL treatment dramatically decreased palmitic acid at day 1 then restored to the day 0 level by day 7 of CL treatment (Fig. 7h). Accordingly, the ratio of UFA to SFA had opposite trends between cold and CL over the time course of our study (Fig. 7k). Overall, these results reveal that both cold and CL treatment increase abundance of longer chain FAs in adipose, but they have distinct outcomes on FA saturation in adipose with the different dynamics (Fig. 7l).

Discussion

Here we provide first comprehensive atlas of iWAT at chromatin status at single-nucleus resolution in response to two major thermogenic stimuli. Our analyses identified changes in cell abundances, patterns of differential gene accessibility across the time course of the treatments, beige-specific enhancers and TF motif modules regulating beige adipocyte development, and a pseudotime trajectory for beige adipocyte development. These changes created functional consequences in FA metabolism detectable by lipidomics analysis. Collectively, our data report the genes and GRNs underlying the developmental emergence of beige adipocytes, as well as the metabolic consequences in adipose during responses to cold exposure and CL treatment.

Mature adipocytes underwent the most profound changes, with a beige adipocyte population accumulating in iWAT with increased exposure time of both stimuli (Fig. 1d-f,2d). The abundance of beige adipocytes increased to a similar level between cold and CL (Fig. 1d), however, the abundance of total adipocytes was in the range of 18% to 23% after cold exposure and about 20% to 37% after CL treatment (Supplementary Fig. 4b). This may indicate that CL generates more white adipocytes which can be further trans-differentiated into

beige adipocytes. This may support the notion that Adrb3 activation by CL initiates beige adipocyte formation by converting pre-existing white adipocytes into beige adipocytes, while cold induces the formation of beige adipocytes directly from progenitor cells (Jiang *et al.*, 2017a).

In addition to detecting beige adipocyte emergence during cold and CL responses, we detected two major APCs in iWAT. Both APCs had higher accessibility at *Pdgfra* (Fig. 5b). APC1 had higher accessibility of genes for stem cell surface markers such as *Ly6a* (*Sca1*) and *Cd34*; whereas, APC2 had higher accessibility at mural cell marker genes including *Pdgfrb* and *Acta2* (Fig. 5b). Our results are consistent with a recent lineage tracing study identifying two major adipocyte progenitors, *Pdgfra*+ and *Pdgfra*+/*Pdgfrb*+, using dual recombinase-mediated genetic labeling (Han et al., 2021). The genes upregulated in *Pdgfra*+/*Pdgfrb*+ cells were associated with wounding responses and likely correspond to APC2 in our snATAC-seq data (Fig. 5c) (Han *et al.*, 2021). We originally hypothesized that the origins of adipocytes would be revealed by characterizing intermediate cells between clusters, which may represent transition states of cells differentiating from their precursors. However, linkages representing transition cells, were lacking in the UMAP embedding from our snATAC-seq data. We reasoned that this could be due to the small number of APCs in our data. Therefore, our inference of adipocyte trajectory was limited to mature adipocyte populations. Further investigation into transition states of cells from progenitors and genetic memory could help elucidate how new adipocytes are generated in response to thermogenic stimuli.

Several lines of evidence suggest that beige adipocyte progenitors reside among mural cells within the vasculature (Berry *et al.*, 2016; Jiang et al., 2014). We found that stromal cell abundance tended to increase with cold and CL

treatment (Fig. 1d). Our results show that the vasculature expansion is influenced by VEGF signaling between adipocytes and VECs through the *Vegfra* and *Vegfr1* ligand-receptor pair (Fig. 5e). An important feature of this mechanism may involve PGC-1α and ESRRα binding motifs, which we found were enriched in beige adipocytes, and others have reported were important in skeletal muscle angiogenesis by *Vegfa* (Arany et al., 2008).

Besides detecting adipocytes, their precursors and vascular cells, we detected dendritic cells and macrophages in iWAT, and their reductions during the exposure intervals (Fig. 1d). Evidence indicates these immune cell reductions are important to the adipocyte changes we report. First, NF-kB pathway activation in dendritic cells stimulates proinflammatory gene expression and inflammatory responses leading to metabolic disorders in insulin sensitive tissues (Baker et al., 2011; Lawrence, 2009); accordingly, reduced inflammatory cell abundances after CL and cold exposure may limit the appearances of these disorders. Second, knockout of IκB kinase ε (IKKε) which is upregulated by NF-kB was shown to promote thermogenesis and prevent HFD induced obesity in mice (Chiang et al., 2009); accordingly, fewer cells utilizing NF-kB signaling after CL and cold exposure may also promote thermogenesis. Collectively, these results suggest that both cold and CL promote thermogenesis and prevent activation of NF-kB pathway in adipose tissue by suppressing dendritic cell recruitment in adipose tissue.

An important question in thermogenic stimuli induced beiging is difference between two most widely used thermogenic agents, cold and CL treatment. Pseudotime trajectories were quite similar for developing beige adipocytes emerging upon both CL and cold exposure (Supplementary Fig. 6a,b). Additionally, the fold-changes in gene accessibility after cold and CL treatment

compared to RT were positively correlated for the two treatments (Supplementary Fig. 9a,b). Despite these similarities, there were notable differences in responses to the two thermogenic stimuli. Genes involved in glycolysis were relatively more activated by cold stress (Fig. 7d,g). Specifically, *Eno1* was highly accessible in cold-induced beige adipocytes (Supplementary Fig. 9c). This is consistent with the findings from Chen et al. who reported that many glycolytic genes were up-regulated in a subset of beige adipocytes formed during cold adaptation in the absence of β-AR signaling (Chen *et al.*, 2019c). In contrast, CL treatment activated gene programs associated with cAMP responses and regulation of G-proteins relatively more compared to cold (Fig. 7e and Supplementary Fig. 9d-i). These findings suggest that cold and CL exert their effects through distinct mechanisms, with cold triggering extra beige fat formation via β-AR independent changes in regulation of genes involved in glucose metabolism.

A key finding from our analyses was that the genes involved in *DNL* exhibited markedly increased accessibility after both cold and CL treatment for 1, 3, and 7 days (Fig. 7a and Supplementary Fig. 8a). In agreement with our results, 4 days of cold exposure and CL treatment also increased gene expression levels of lipogenic genes in snRNA-seq data (Supplementary Fig. 8b) (Rajbhandari *et al.*, 2019). These results suggest that induction of beiging is accompanied by an activation of lipogenesis. Lipogenesis may contribute to thermogenesis through futile cycling of FA synthesis and oxidation by maintaining the availability of endogenous FAs as fuel for heat production (Guilherme et al., 2020; Mottillo et al., 2014). Indeed, the finding that *Pdk4* was enriched in beige adipocytes may be relevant to shifting energy source from glucose to FA in beige adipocytes, resulting in an increased demand for lipids (Barquissau *et al.*,

2016). It is noteworthy that both FA synthesis (anabolic) and FA oxidation (catabolic) processes were activated after thermogenic stimuli, indicating these are not mutually exclusive responses.

Changes in chromatin accessibility at genes involved in FA metabolism led to functional alterations in lipid composition in adipose tissue. Not all FAs are oxidized at the same rates, which may explain the changes in the cellular accumulation of FAs. SFAs with longer chain length are oxidized at slower rates, while oleic acid among MUFAs, and α-linolenic acid (18:3n-3) and linoleic acid among PUFAs, are oxidized at faster rates (Leyton et al., 1987). We reported that CL significantly increased the relative abundance of oleic acid, whereas cold increased the relative abundance of linoleic acid. These results suggest that cold and CL have distinct influences on FA oxidation, and thereby lead to differences in the lipid composition of adipose tissue.

Our lipid analysis revealed that cold treatment tended to increase the relative abundance of PUFAs, and increased the UFA:SFA ratio from day 1 to day 7 (Fig. 7j,k). This may represent an important adaptive change in animals living in cold conditions. UFAs, and especially PUFAs, have lower melting temperatures relative to SFAs. The increased MUFA and PUFA levels seen in adipose in cold-exposed mice may preserve fluidity of storage lipids, enabling them to be readily accessed by lipases and used as energy sources (Kostal et al., 1998). Additionally, membrane phospholipids have higher fluidity when they are composed of UFAs, which may be important in cold temperatures (Tiku et al., 1996). The increased abundance of PUFAs caused by cold exposure may also be beneficial for preserving membrane fluidity. These effects of cold exposure on lipid composition of adipose may be most important to poikilothermic animals, whose body temperatures varies with the environmental temperature (Tiku *et*

al., 1996), but they may be important for cutaneous and subcutaneous tissues in homeotherms, which maintain thermal homeostasis at internal tissues.

In addition to the differences we found between CL and cold that affect signaling and glycolytic pathways, there were notable chromatin state and lipid differences, some of which may underlie cardiac pathologies associated with CL treatments, contraindicating the use of this drug in people. First, consistent with reports that activation of Adrb3 affects cardiac contractility in human (Michel *et al.*, 2020), we found that CL treatment opened chromatin at genes associated with cardiac muscle contraction (Fig. 7e). Interestingly, a recent study suggested that overstimulation by isoproterenol, a β1- and β2-AR agonist, promoted the release of palmitic acid, palmitoleic acid, and oleic acid from adipose tissue, which caused myocardial fibrosis and apoptosis (Thiele et al., 2021). Importantly, they showed the cardioprotective effects of the inhibition of adipose triglyceride lipase activity in adipose tissue (Thiele *et al.*, 2021). We also reported an increase in the proportion of oleic acid after CL treatment, but not cold treatment (Fig. 7h). Collectively, our data might support the notion for an adipose tissue-heart communication in the development of cardiac diseases by regulating gene accessibility and lipid content in adipose tissue. Second, there were different kinetics in timing of gene accessibility changes and lipid species between cold and CL (Fig. 7f,g). Lastly, it was shown that treatment with oleic acid increased intracellular levels of cAMP in skeletal muscle cells (Lim et al., 2013). Thus, it might be conceivable that oleic acid increased after CL treatment promoted the changes in accessibility of genes involved in cAMP signaling pathway. However, as CL activates Adrb3 receptor, a major pathway activating thermogenesis in beige cells, it is possible that these differences were observed due to different effects/dosages of endogenous norepinephrine

induced by CL. Additionally, there may be differences in kinetics of the responses to CL and cold exposures that are read out as chromatin state differences. Future studies will be needed to demonstrate the effects of lipids and metabolic properties of adipocytes changed by cold and CL treatment.

Our analyses were mainly based on chromatin accessibility which may or may not be directly linked to the transcription state. Nonetheless, publicly available snRNA-seq data were used to pinpoint the specific changes in our analyses. Transcriptional changes may or may not lead to changes in translated protein, or protein activities. By assaying lipid profiles in the same tissues used for chromatin analysis, we were able to characterize functional physiologic and metabolic changes that accompanied gene accessibility changes. In summary, this study highlights underlying gene regulatory mechanisms for beige adipocyte development and the common and distinct properties of cold and Adrb3-induced beige adipocytes. These findings could provide pivotal insights into clinical utility of environmental and pharmacological beige stimuli.

Materials and Methods

Animals

All animal experiment was in accordance with approved protocols by the Institutional Animal Care and Use Committee (IACUC) at Cornell University (Protocol number 2017-0063). Six-weeks-old C57BL/6J mice were purchased from Jackson Laboratories. Mice were acclimated to the facility and maintained at room temperature (RT, 22°C) for two-weeks before intervention. Mice were randomly assigned to cold (6°C) or CL-316,243 (CL, 1 mg/kg), a β3-adrenergic receptor (Adrb3) selective agonist treatment group. Mice were exposed to cold and Adrb3 agonist for 0, 1, 3, or 7 days.

Histological staining

Adipose tissues were fixed in 10% formalin, paraffin embedded, and sectioned at 5µm thickness with a microtome. Slides were deparaffinized, rehydrated, and stained with hematoxylin and eosin (H&E).

Tn5 transposase purification & loading

Tn5 was produced as described with no modifications (Picelli et al., 2014). Tn5 transposase was generated by assembling pre-annealed ME-A and ME-B (IDT, standard desalting; Supplementary Table 1). Oligonucleotides (IDT, standard desalting) were annealed at 95°C for 2 min followed by cooling to 25°C at a 0.1°C/s cooling rate. Annealed ME-A and ME-B oligos were each mixed in a 1:1 ratio Tn5 transposase and incubated with for 30 min at room temperature. Eight A-transposomes and twelve B-transposomes were formed to generate 96 unique transposome combinations.

Nuclei isolation from adipose tissue

Inguinal adipose tissues were collected from mice before any intervention and after 1, 3 or 7 days of cold exposure or CL treatment and frozen at -80°C. All steps were performed on ice or at 4°C. To avoid perturbations caused by isolating cells, whole adipose tissues were used to extract nuclei without isolating mature adipocytes or SVF. Whole adipose tissues were minced on dry ice. 80-100 mg of chopped adipose tissue were transferred to a chilled 40 mL Dounce Homogenize containing 25 mL homogenize buffer (320 mM sucrose, 0.1 mM EDTA, 0.1 % NP40 (28324, ThermoFisher), 5 mM $CaCl_2$, 3 mM $Mg(Ac)_2$, 10 mM Tris pH 7.8, protease inhibitors (88666, Pierce), 0.016 mM PMSF, 0.33 mM β-mercaptoethanol) (Corces *et al.*, 2017). Tissue was homogenized

immediately via 10 gentle strokes of the loose pestle and then 10 gentle strokes of the tight pestle on ice using a Dounce tissue grinder (357546, Wheaton). The homogenate was filtered through a 40 µm nylon mesh (10199-658, VWR) and centrifuged for 10 min at 500 g. The top fat layer was discarded, and the supernatant was transferred into a new tube without disrupting the pellet. The samples were then resuspended in 5 vol. of ice-cold ATAC-resuspension wash buffer (10 mM Tris-HCl pH 7.4, 10 mM NaCl, 3 mM $MgCl_2$ and 0.1% Tween 20 in water) and centrifuged for 5 min at 500 g in a swinging bucket rotor centrifuge (5920R, Eppendorf). Nuclei pellets were resuspended in 1X tagmentation buffer (10 mM Tris pH 7.4, 5 mM $MgCl_2$, 10 % DMF, 33 % 1X PBS (without Ca++ and Mg++), 0.1 % Tween-20, 0.01 % Digitonin (BN2006, ThermoFisher)). The number of nuclei was counted using a hemocytometer.

snATAC-seq with combinatorial indexing

snATAC-seq was performed as described previously (Preissl *et al.*, 2018), with minor modifications. Nuclei concentration was adjusted to 160,000 nuclei/mL in 1X tagmentation buffer. 8 µL of nuclei were distributed into each well of a 96-well plate (1,280 nuclei/well) containing 1 µL of each ME-A or ME-B carrying barcoded transposome per well at ~1.5 µM. Tagmentation was performed at 50°C for 30 min. Following tagmentation, 10 µL of 40 µM EDTA was added each well and the plate was incubated at 37°C for 15 min to terminate the Tn5 reaction. Next, 20 µL of sort buffer (2 % BSA and 2 mM EDTA in PBS) was added to each well. All wells were pooled and centrifuged for 5 min at 500 g. Nuclei were resuspended in sort buffer with 10% DMSO and frozen at -80°C until ready for fluorescence activated nuclei sorting (FANS).

After thawing at 37°C for 1 min, nuclei were centrifuged for 5 min at 500 g and resuspended in 1 mL of sort buffer. Nuclei were filtered through a 35 µm mesh (352235, Corning) and stained with 3 µM Draq7 (ab109202, Abcam) before FANS. 25 Draq7+ nuclei were sorted into each well of second 96-well plates containing 16.5 µL of elution buffer (2 % BSA and 10 mM Tris pH 8.0) using a BD FASC Melody. Gating was selected to isolate single Draq7+ nuclei. After sorting, plates were frozen at -80°C.

For PCR amplification, 2 µL of 0.2% SDS were added to each well and the plate was incubated for 7 min at 55°C to denature transposase. 2.5 µL of 10% Triton X-100 were added to each well to quench SDS. 1.5 µL of 25 µM Primer i5 and 1.5 µL of 25 µM Primer i7 (Supplementary Table 1) were added to each well and the plate was gently vortexed and spun down briefly. 25 µL of PCR mix (Q5 DNA polymerase (M0491, NEB), 2 mM dNTP, Q5 buffer and 1X GC Enhancer) were added to each well. PCR was performed using the following protocol: 72°C 5 min, 98°C 30 sec, 13 cycles of: [98°C 10 sec, 63°C 30 sec, 72°C 30 sec], 72°C 5 min, held at 4°C. All wells were pooled. Amplified DNA libraries were purified using MinElute columns (28004, Qiagen) using a vacuum apparatus (19413, Qiagen), washed twice with 750 µL Buffer PE (19065, Qiagen) and spun down at maximum speed for 1 min. Samples were eluted twice with warm elution buffer (10 mM Tris pH 8). The size selection was performed using Ampure XP Bead (A63880, Beckman Coulter). The concentration of each pooled PCR plate library was measured using a Qubit dsDNA HS Assay Kit (Q32851, Invitrogen) and library fragment distribution was quantified on Agilent Bioanalyzer. Libraries were subjected to digital PCR on a Bio-Rad QX200 droplet digital PCR. Libraries were loaded at 8 pM on a mid-lane output PE 150bp. Libraries were sequenced on a Nextseq500 sequencer

(Illumina) using custom read primers (Supplementary Table 1); custom recipe for the following, read 1: [36 imaged cycles], Index 1: [8 imaged cycles, 27 dark cycles, 8 imaged cycles], Index 2: [8 imaged cycles, 21 dark cycles, 8 imaged cycles], Read 2: [36 imaged cycles].

snATAC-seq data pre-processing

Fastq files from two sequencing runs were merged and demultiplexed by adding cell barcode to each read. Demultiplexed pair-end reads were aligned to mm10 using Bowtie2 (Langmead and Salzberg, 2012) with the parameters: bowtie2 -p 16 -t -X 2000-no-mixed-no-discordant. After alignment, reads were sorted by read name using samtools. The pair-end reads with low mapping quality fragments < MAPQ 30 and improperly paired fragments (SAM flag = 1804) were removed. Reads were separated based on the cell barcode and reads belonging to the same cell barcode were deduplicated. Of 1,020,363,364 sequenced read pairs, 791,158,286 (77.5%) mapped to the reference genome, with an assigned cell barcode. PCR duplicate reads (35%) and mitochondrial reads (0.2%) were removed. To check the quality of library, frequency of the insert sizes representing nucleosome patterns was plotted using ATACseqQC (Ou et al., 2018) from aggregated samples (Supplementary Fig. 2a).

snATAC-seq data quality control

To select cell barcodes, a histogram of the log-transformed number of reads per cell barcode was plotted (Supplementary Fig. 2d). The bimodal distribution indicates that cell barcodes with a low read sequencing depth are improper barcodes with background reads and cell barcodes within a high read depth distribution of reads are genuine cells. For initial filtering, we filtered out cells

which have less than 1,000 reads (Supplementary Fig. 2c). To minimize the potential bias caused by the most abundant cell populations using aggregated accessibility peak sites from all cells, we adapted the previous strategy to generate a merged peak set from diverse cell populations after initial clustering (Cusanovich *et al.*, 2018). For initial clustering, we first generated a cell-by-10kb-window sparse matrix using snapATAC (Fang *et al.*, 2021). To create this matrix, the genome was broken into uniformly sized 10kb windows and the number of reads at a given bin for each cell was counted and binarized. Any windows overlapping with the ENCODE mm10 blacklist (Amemiya et al., 2019) were filtered. Then, we used Signac, an R toolkit extension of Seurat for the analysis of single-cell chromatin data, for further analysis (Hao *et al.*, 2021; Stuart *et al.*, 2021).

Next, we normalized the cell-by-windows matrix by a TF-IDF transformation. Then, we performed shared neighbor network (SNN) graph-based clustering with the top 25 principal components except for 1st principal component. The 1st component was excluded for dimensionality reduction because it has a high correlation with sequencing depth. We visualized cell clusters by uniform manifold approximation and projection (UMAP). After identifying initial clusters, all cells in individual clusters were aggregated. For each cluster, peak calling was performed using the MACS2 (Zhang et al., 2008) ‘callpeak’ command with the parameters: -nomodel-shift -100-extsize 200-keep-dup-all -q0.05. The summits were extended ±250bp and the peak sites overlapping with the ENCODE mm10 blacklist (Amemiya *et al.*, 2019) were filtered. The peak sites identified from each cluster were merged and used to create a cell-by-peak matrix. Cells with less than 0.15 reads in peak ratio were removed. Then, we repeated clustering based on the cell-by-peak matrix. To create a gene activity

matrix, we counted the reads on gene coordinates for mouse genome from EnsembleDB extended to include the 2kb upstream (Howe et al., 2021).

Identification of doublets

Initially, we did not exclude doublets to see an impact of the doublets in our analysis. The major cluster identification was not significantly affected (Supplementary Fig. 2e). However, when we subclustered a single cluster, we consistently observed that a small fraction of cells formed a distinct cluster (Supplementary Fig. 2g,r). As an example, we observed a small cluster (cluster 2) among adipocytes (Supplementary Fig. 2g). GO analysis showed that the genes relatively more enriched in cluster 2 are associated with lymphocyte proliferation (Supplementary Fig. 2i). While accessibility of *Adipoq* was similar between cluster 1 and cluster 2, accessibility of *Ptprc* was relatively higher in cluster 2; the cluster 2 having intermediate accessibilities of marker genes for adipocytes and lymphocytes (Supplementary Fig. 2j,k). However, adipocytes and lymphocytes are less likely to share similar features. For example, PPARA motif enriched in adipocytes and ETS1 motif enriched in lymphocytes showed a negative correlation (Supplementary Fig. 2l). Therefore, we further analyzed if the cluster 2 exhibiting a hybrid feature of adipocytes and lymphocytes, the two largest clusters in our dataset, is a putative collision cluster.

The putative collision cluster could appear due to cell barcode collisions since the combinatorial indexing strategy procedure may generate barcode collision as previously reported (Cusanovich *et al.*, 2018). Thus, it is likely to misinterpret a putative collision cluster as a novel cluster if doublets are included for further analysis. To determine whether the putative collision cluster is a novel cluster or a collision cluster, we first calculated the number of reads per cell.

However, unlike the assumption that barcode collision cells have higher library complexity as they have reads from two different cells, the putative collision cluster showed the average library complexity as other subclusters in our dataset (Supplementary Fig. 2m,n). We generated '*in-silico* collisions' by combining reads from random pairs of cells from our dataset. We found that these *in-silico* collisions clustered together with putative collision clusters and take similar coordinates on UMAP. To measure a likelihood of a cell being a doublet/collision, we adapted Scrublet (Wolock et al., 2019), a scRNA-seq tool for identifying doublets by calculating fraction of a cell's neighbors that are *in-silico* doublets. The cells clustered into a putative collision cluster consistently showed high doublet scores, indicating these cells have high likelihood of being collision cells (Supplementary Fig. 2o,p). We also confirmed that the cells found in the putative collision cluster, doublets identified by Scrublet, and *in-silico* collisions have high correlations compared to singlets (Supplementary Fig. 2q). Overall, we filtered out 2,956 cells (8.3%) with a doublet score higher than 0.2 cutoff. It is consistent with the collision rate (~9%) estimated from our previous mixed species experiment (Spektor et al., 2019). After removing doublets, the putative collision clusters were no longer detected. Therefore, we performed further analysis without doublets.

Identification of cell clusters and cell type annotation

32,552 cells were used for further analysis after filtering out the low-quality cells (reads per cell < 1,000, reads in peak ratio < 0.15, and doublet score > 0.2). We repeated nonlinear dimension reduction and cell clustering based on top 50% variable peaks and 2nd to 15th components using Seurat's SNN graph clustering (Stuart *et al.*, 2019). To resolve identities of the cell clusters, we first

identified sets of genes or peaks enriched in individual cell clusters in comparison with all other cell clusters by differential accessibility analysis using 'FindAllMarker' or 'FindMarker' function in Signac (Stuart *et al.*, 2021). For the gene-based analysis, gene activity quantified by summing the fragments intersecting gene body and 2kb upstream region was used. GO and KEGG pathway analyses were performed on a set of enriched genes (adjusted p-value or FDR < 0.05 and absolute value of log2 fold change > 1.2) with ClusterProfiler (Yu et al., 2012). In addition, genomic regions enrichment of annotations tool (GREAT) (McLean *et al.*, 2010) analysis were performed on differentially accessible peaks.

After annotating cell types based on snATAC-seq data, we confirmed the cell type annotation with publicly available scRNA-seq data of SVF and snRNA-seq data of mature adipocytes from iWAT (Rajbhandari *et al.*, 2019). To transfer cell labels from the reference scRNA-seq and snRNA-seq data, scRNA-seq and snRNA-seq datasets were integrated with our snATAC-seq using SCTransform after normalizing two datasets (Stuart *et al.*, 2019). For general annotation, we merged subpopulations of the same cell types in scRNA-seq data to one major cell type (e.g., adipocyte 1 through adipocyte 16 into one adipocyte cluster). Almost 85% of cells received higher than 0.5 prediction confidence scores except for the clusters such as vascular smooth muscle cells which were not found in scRNA-seq data.

Cell abundance with Milo

In addition to evaluating cell proportion changes among discrete clusters, we performed Milo (Dann *et al.*, 2022) to test differential abundance between experimental conditions (RT at day 0 and after cold exposure or CL treatment).

Milo identifies neighborhoods based on a k-nearest neighbor (KNN) graph and assigns cells to the neighborhoods. Then, the number of cells in neighborhoods were counted and a matrix of the number of neighborhoods by the number of experimental samples was created. This revealed differential abundance between treatment conditions in a cell state rather than a pre-defined cell cluster.

Transcription factor motif analysis with chromVAR

Firstly, to analyze differentially active motifs, motif analysis was performed on a set of peaks enriched in one group of cells compared to the other groups of cells using a function implemented in Signac (Stuart *et al.*, 2021). Next, transcription factor (TF) motif activity was computed by chromVAR and a cell-by TF z-score matrix was created (Schep *et al.*, 2017). To identify the transcriptional programs underlying cell states during beiging among 726 TFs in JASPAR2020 database (Fornes *et al.*, 2020), we measured Pearson correlation between motifs using motif activity score computed by chromVAR. 64 TF motifs with motif variance higher than 1.8 were used for unsupervised hierarchical clustering based on the correlation coefficients to identify modules.

Co-accessibility with Cicero

To predict the potential *cis*-regulatory interactions, the R package Cicero was used to construct *cis*-regulatory networks by assessing co-accessibility of pairs of DNA elements and linking a promoter and its potential enhancer in distal sites (Pliner *et al.*, 2018). Cicero calculated correlation (co-accessibility) between putative regulatory elements from aggregated accessibility across groups of cells. Then, links between regulatory elements and target genes were identified as putative enhancer-promoter pairs.

Inference of cell-cell interaction with CellChat

To predict the potential cell-cell interaction from our snATAC-seq data, we utilized gene accessibility of ligands and receptors from a literature-supported signaling molecule interaction database ('CellChatDB') (Jin *et al.*, 2021). Then we predicted significant communications by identifying differentially accessible ligands and receptors for each cell cluster and associating each interaction with a probability value. Then the significant cell-cell communications were identified by a statistical test that randomly permutating cell cluster and then recalculate the interaction probability.

Pseudotime trajectory analysis

We used ArchR (Granja *et al.*, 2021) to calculate the pseudotime value for each cell and to create pseudotime trajectory in a two-dimensional space. The adipocyte cells that passed previous quality control in Signac were used without additional filtering in ArchR. The trajectory backbone was defined to provide a rough ordering of cells from the cluster including the most day 0 cells to the other cluster with the most day 7 cells. Next, ArchR calculated mean coordinates of each cluster and computed the distance to the mean coordinates for each cell. ArchR provided a pseudotime value for each cell based on the Euclidean distance to their mean coordinates and plotted a trajectory. Finally, ArchR analyzed changes in features across pseudotime in motifs and genes.

Lipidomics

40-50 mg of chopped adipose tissue was subjected to lipid extraction using a modified one step lipid extraction method to obtain fatty acid methyl esters

(FAME) (Garces and Mancha, 1993). Adipose tissue was heated with an aqueous digesting and methylating reagent (1.2 mL methanol, 0.15 mL 2,2-dimethoxypropane and 0.05 mL H_2SO_4) and an organic extraction reagent (1 mL heptane, 0.6 mL touluene) for 2 hours at 80°C. After cooling the tube at room temperature, 2 mL heptane and 2 mL saturated NaCl were added to the sample and centrifuged for 10 min at 3500 rpm. After keeping the sample at 4°C overnight, two phases were formed, and top layer was transferred to a new tube. The sample was dried down under nitrogen and 60 µL of heptane was added. FAME were quantified by Shimadzu GCMS-TQ8050 triple quadrupole mass spectrometer with a CI-MS (Shimadzu) with a BPX 70 column (25m x 0.22mm x 0.25m; SGE Inc.). An equal weight FAME mixture (462A; Nu-Chek Prep, Inc.) was used to calculate response factors. The FAME were analyzed by gas chromatography covalent adduct chemical ionization tandem mass spectrometry by molecular weight and by diagnostic ion analysis. Elongation ratio was estimated by calculating (18:0+18:1n-7+18:1n-9)/(16:0+16:1n-7). Desaturation ratio was estimated by calculating (18:1n-7+18:1n-9+16:1n-7)/(16:0+18:0).

Statistics and reproducibility

All statistical tests in our analysis were performed using R version (v3.5.0) and associated packages. In our analysis, cell proportions in Fig. 1d and lipid proportions in Fig. 7h-j were compared by ANOVA multiple comparisons test with Bonferroni's post-hoc test. In the case of comparing between two treatment conditions in Fig. 7f,g, Welch's two sample t-test was performed. Comparisons were two-sided unless otherwise noted. Alpha was set at 0.05.

Data availability

snATAC-seq data reported in this study is deposited in NCBI Gene Expression Omnibus under accession number GSE185377. Publicly available snRNA-seq data of adipocytes and scRNA-seq data of adipose SVF from mice treated with saline, cold or CL up to 4 days were obtained from GEO with the accession number GSE133486 (Rajbhandari *et al.*, 2019). The GEO accession number for PGC-1α ChIP-seq data from mouse brown adipose tissue is GSE110056 (Chang *et al.*, 2018). The publicly available ESRRα ChIP-seq data from mouse liver was obtained from GEO with the accession number GSE43638 (Chaveroux *et al.*, 2013). The MEF2α ChIP-exo data from mouse skeletal myoblasts was obtained from GEO with the accession number GSE61207 (Wales *et al.*, 2014). H3K27ac and H3K4me1 ChIP-seq data from beige adipocytes after cold exposure and white adipocytes at 30°C were obtained from GEO with the accession number GSE108077 (Roh *et al.*, 2018). All other data are available from the authors upon reasonable request.

Acknowledgements

This work was supported by National Institutes of Health (NIH) grants K01 DK109027. We thank the Cornell University Biotechnology Resource Center (BRC) for their assistance for FACS sorting and sequencing. We thank Paul Cohen at the Rockefeller University and Bethany Cummings at the University of California Davis for their discussions, and Debadrita Bhattacharya at the Cornell University for her help on the TF module analysis.

Figures

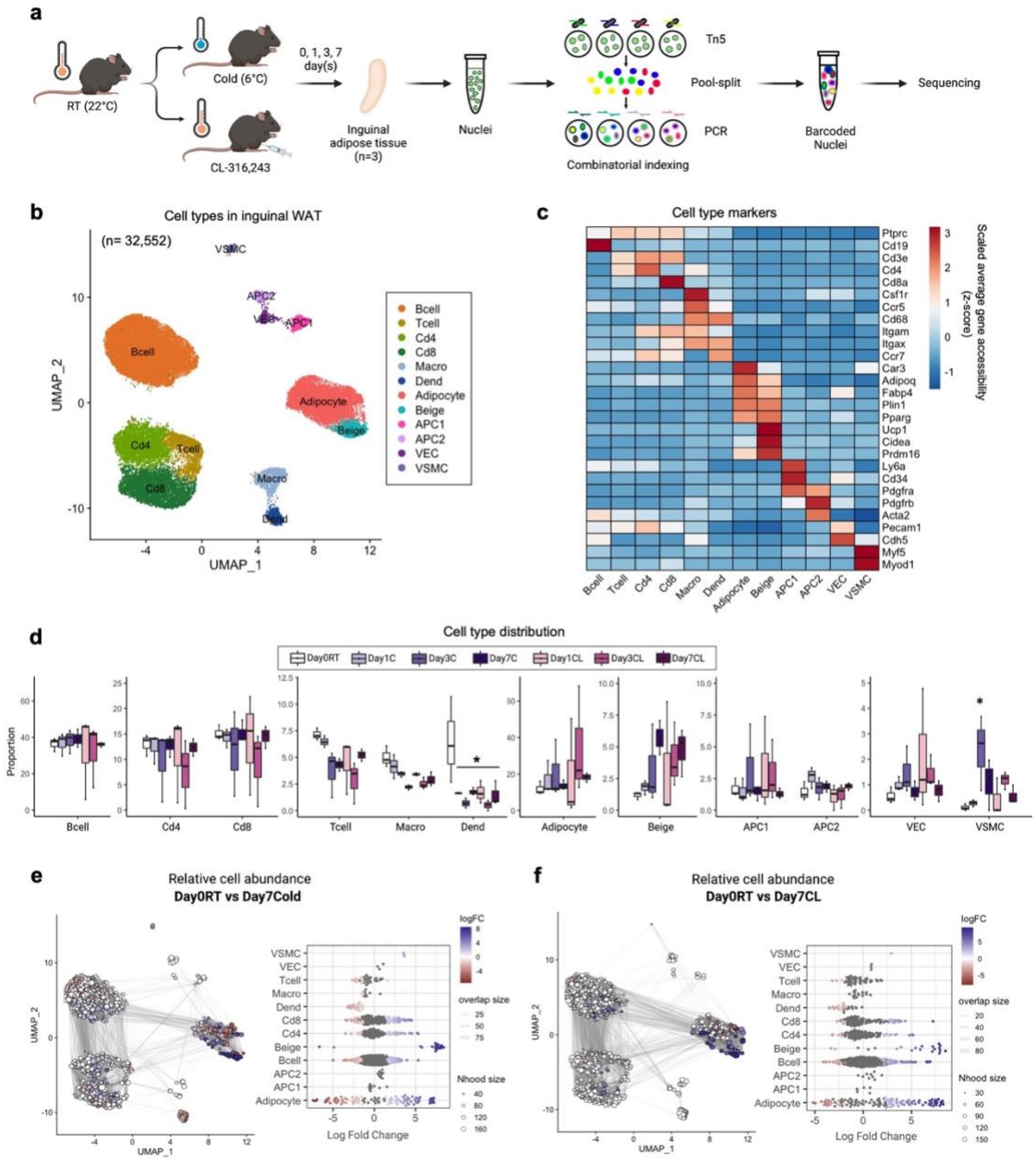

Figure 1

Cell type identification in inguinal white adipose tissue.

a, Schematic outline of the workflow. Two-month-old male C57BL/6 mice were exposed to cold (6°C) or CL-316,243 (CL; 1mg/kg/mouse/day) for 1, 3, or 7 days (n=3 per group). Inguinal adipose tissues collected at day 0, 1, 3, and 7 after

exposure was subjected to snATAC-seq. **b**, UMAP plot of 32,552 cells that passed quality control. Colors represent 12 different clusters determined by unbiased clustering. **c**, Heatmap of normalized accessibility of cell-type marker genes. **d**, Relative proportions of each cell type per group (n=3 per group). *Adjusted p-value<0.05, ANOVA multiple comparisons test with Bonferroni's post-hoc test was performed. **e**,**f**, Milo analysis of cell neighborhood abundance changes in Day 0 RT vs. Day 7 cold (**e**), or Day 7 CL (**f**) on UMAP plots. Size of points indicates the number of cells in a neighborhood; lines represent the number of cells shared between adjacent neighborhoods. Points are neighborhoods (Nhood), colored by the log fold differences at the two time points (FDR 10%). Beeswarm plots show the distribution of the log-fold in defined clusters.

Macro; Macrophage, Dend; Dendritic cell, APC1; Adipocyte progenitor cell 1, APC2; Adipocyte progenitor cell 2, VEC; Vascular endothelial cell, VSMC; Vascular smooth muscle cell.

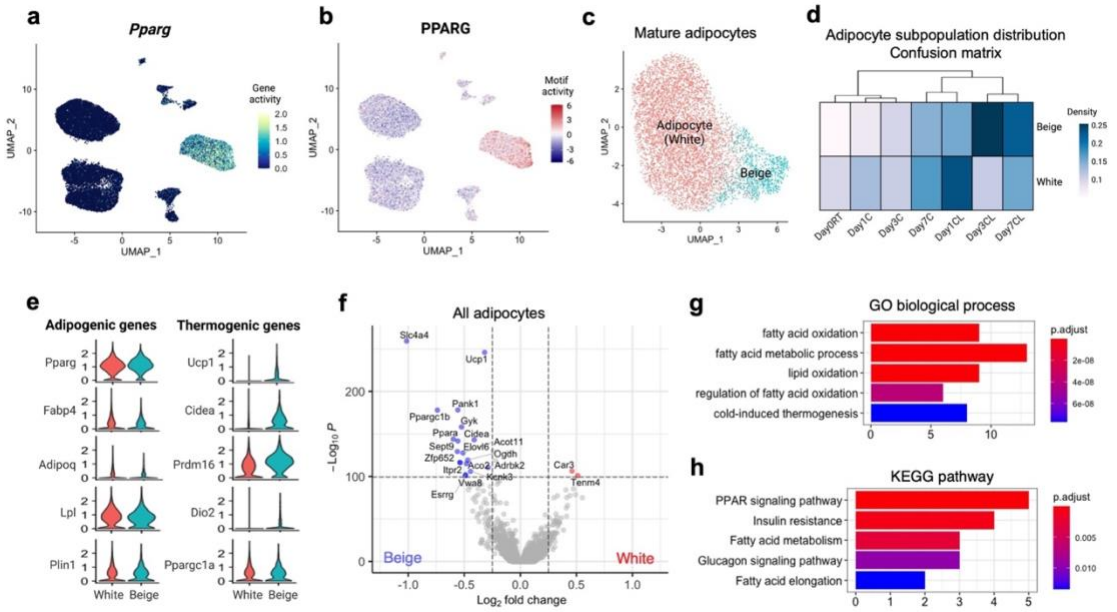

Figure 2

Identification of beige adipocytes within mature adipocytes.

a, UMAP plot of normalized *Pparg* gene accessibility. **b**, UMAP plot of normalized PPARG motif enrichment. **c**, UMAP plot of white and beige adipocytes among mature adipocytes (n=7,004). **d**, Heatmap of the relative cell abundance in white and beige adipocyte clusters for each group. **e**, Normalized accessibilities of adipogenic or common adipocyte genes and thermogenic or beige-selective genes. **f**, Differentially accessible genes between white and beige adipocytes. Positive and negative log2-fold changes respectively indicate increased accessibility in white and beige adipocytes. Genes with adjusted p-value < 10^{-100} & absolute value of log2 fold-change > 0.25 are colored and labeled. **g**,**h**, GO (**g**) and KEGG pathway (**h**) analysis of genes enriched in beige adipocytes compared to white adipocytes. X-axis indicates number of genes. Color indicates adjusted p-value.

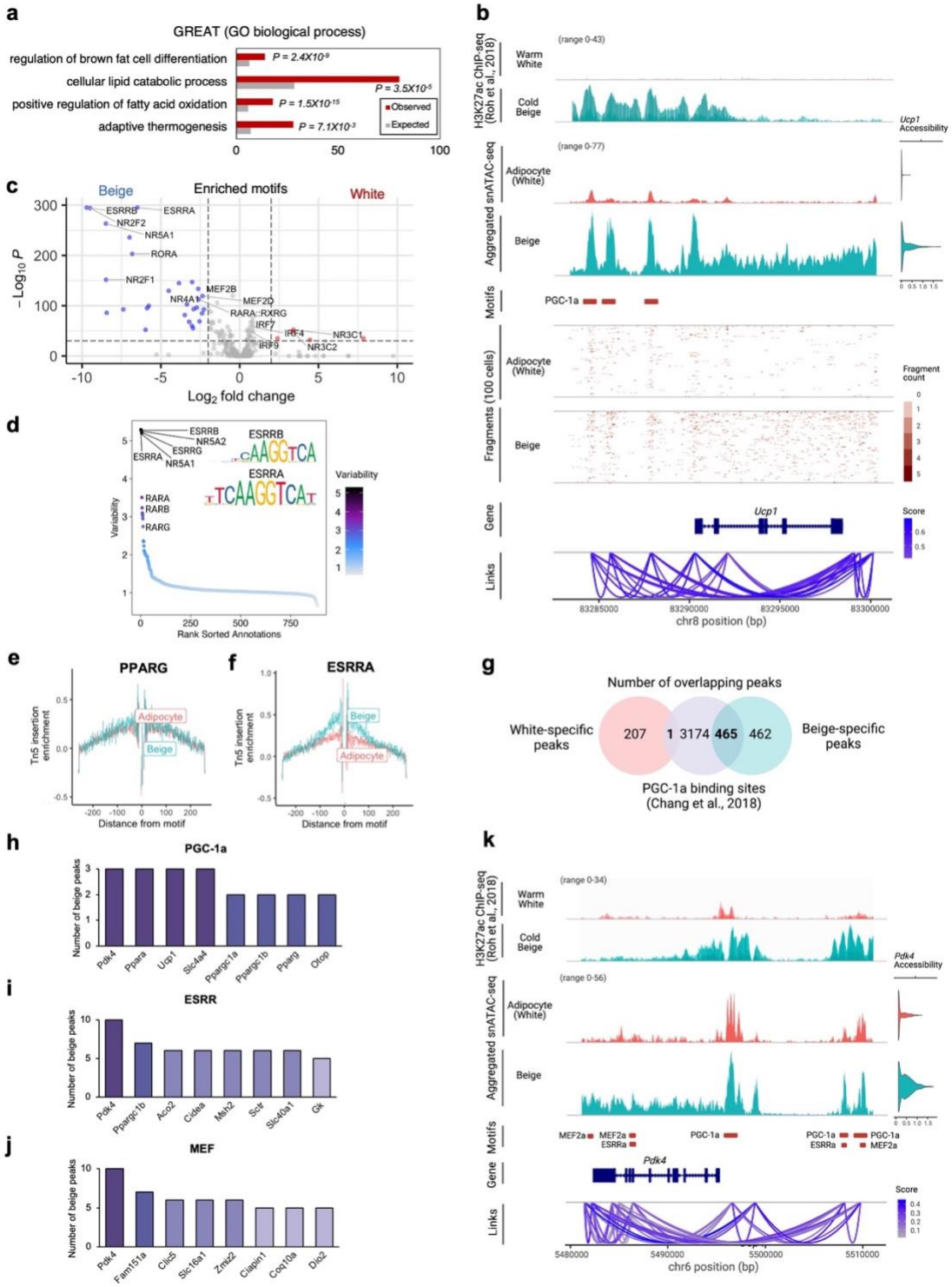

Figure 3

Beige-specific transcription factor activity and chromatin interaction networks.

a, Biological function of beige-specific peaks by GREAT analysis. **b**, Genome tracks showing the aggregated snATAC-seq profiles near the *Ucp1* locus in adipocytes. H3K27ac ChIP-seq signal tracks (n=2 for each) (Roh *et al.*, 2018) show the aggregated H3K27ac signals in white and beige adipocytes. snATAC-seq signal tracks show the aggregated snATAC-seq signals in white and beige adipocytes. Red boxes indicate beige-specific regions overlapping with PGC-1α binding sites (Chang *et al.*, 2018). Fragment coverage show the single-cell profile (each row) of randomly selected 100 single cells from white and beige adipocytes respectively. Links show *cis*-coaccessibility network with multiple connections between peaks around *Ucp1*. **c**, Motif enrichment for white and beige adipocytes. Positive and negative log2-fold changes respectively indicate enrichment in white and beige adipocytes. Motifs with adjusted *p*-value < 10^{-30} & absolute value of log2 fold-change > 2.0 are colored and labeled. **d**, Most variable TF motifs are ranked. Motif sequence logos for the top variable motifs are shown. **e**,**f**, TF footprints for PPARG (**e**) and ESRRA (**f**) from (white) adipocytes and beige adipocytes. Tn5 DNA sequence bias was normalized by subtracting the Tn5 bias from the footprinting signal. X-axis is distance to motif center (bp). **g**, Venn diagram showing the number of overlaps between white-specific or beige-specific peaks and PGC-1α binding sites (Chang *et al.*, 2018). **h-j**, The number of overlapping beige-specific peaks with PGC-1α binding sites (Chang *et al.*, 2018) (**h**), ESRRs (**i**), and MEFs (**j**) motifs from *cisbp* database (Weirauch *et al.*, 2014). The genes closest to the overlapping peaks are sorted by the number of peaks. **k**, Genome tracks showing the aggregate snATAC-seq profiles near the *Pdk4* locus in adipocytes. H3K27ac ChIP-seq signal tracks (n=2 merged) (Roh *et al.*, 2018) show the aggregated H3K27ac signals from white and beige adipocytes. snATAC-seq signal tracks show the aggregated

snATAC-seq signals in white and beige adipocytes. Red boxes indicate beige-specific regions overlapping with PGC-1α (Chang *et al.*, 2018), ESRRα (Chaveroux *et al.*, 2013), and MEF2α (Wales *et al.*, 2014) ChIP-seq binding sites. Links show *cis*-coaccessibility network with multiple connections between peaks around *Pdk4*.

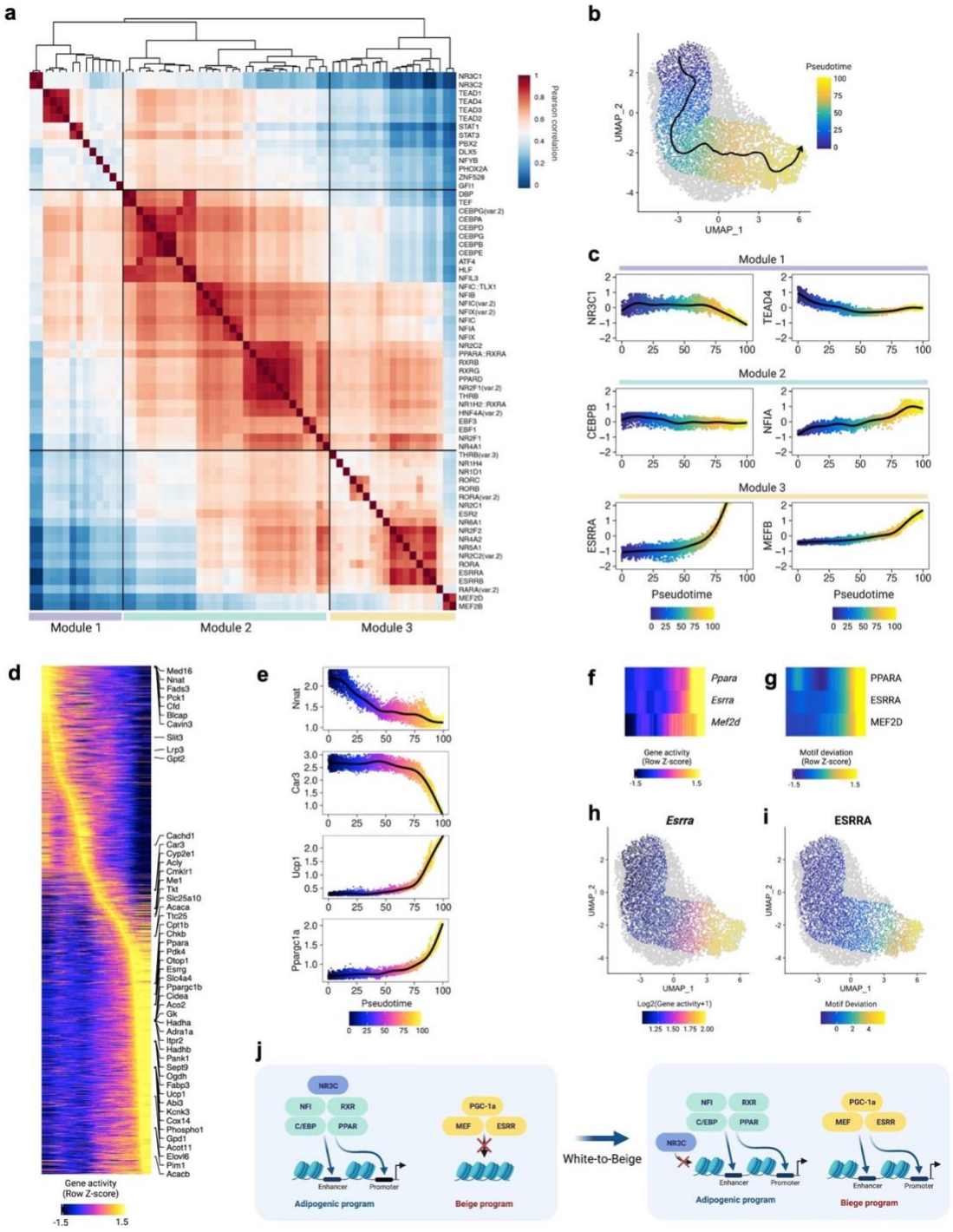

Figure 4

Uncovering transcription factor modules and beige adipocyte developmental trajectory.

a, Hierarchical clustering of top variable TF motifs (chromVAR variance >= 1.8) based on their activity scores across individual adipocytes. **b**, Adipocyte trajectory. The smoothed arrow and color represent pseudotime trajectory in the UMAP embedding. **c**, Motif enrichment dynamics along adipocyte pseudotime trajectory. **d**, Heatmap of gene accessibility along adipocyte pseudotime trajectory. Top variable genes are labeled on the right side of the heatmap. **e**, Gene accessibility dynamics along adipocyte pseudotime trajectory. **f,g**, Side-by-side heatmaps of gene accessibility scores (**f**) and motif deviation scores (**g**) for TFs, for which the inferred gene accessibility is positively correlated with the chromVAR TF deviation across adipocyte pseudotime trajectory. **h,i**, Gene accessibility of *Esrra* (**h**) and motif deviation of ESRRA (**i**) on the UMAP embedding. **j**, Model for the chromatin state dynamics at TF binding motifs through beige adipocyte development. NR3C in TF module 1 might bind to white adipocyte-selective promoters or enhancers to maintain chromatin accessibility of white adipocytes. NFI, RXR, PPAR, and C/EBP in TF module 2 might promote adipocyte development in both white and beige adipocytes. In beige adipocyte, MEF and ESRR in TF module 3 with PGC-1α might promote transcription of beige-selective genes in a coordinated manner.

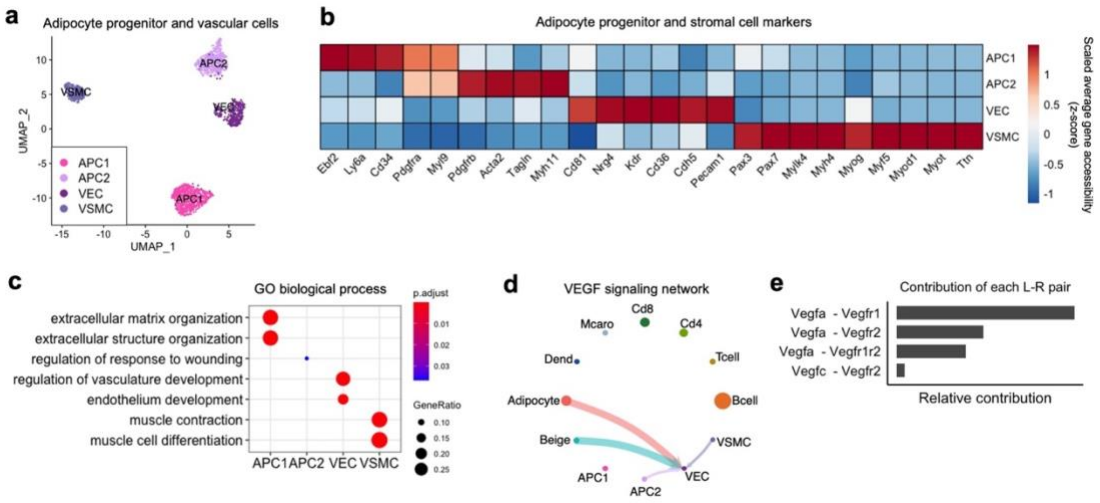

Figure 5

Cell-cell interaction for vasculature development.

a, UMAP plot of adipocyte progenitor and vascular endothelial and smooth muscle cells (n=1,861). **b**, Heatmap of normalized gene accessibility for cell-type markers. **c**, GO analysis using the top 100 differentially accessible genes for each cell type. **d**, Circle plot displaying VEGF signaling network inferred by gene accessibility of ligand-receptor pairs. Circle sizes are proportional to the size of each group. The circle and line colors represent the senders. The arrows indicate the receivers that receive signal from the corresponding senders. Thicker line indicates a stronger signal interaction. **e**, Major contributors of ligand-receptor pairs of VEGF signaling network among the senders and the receiver.

APC1; Adipocyte progenitor cell 1, APC2; Adipocyte progenitor cell 2, VEC; Vascular endothelial cell, VSMC; Vascular smooth muscle cell.

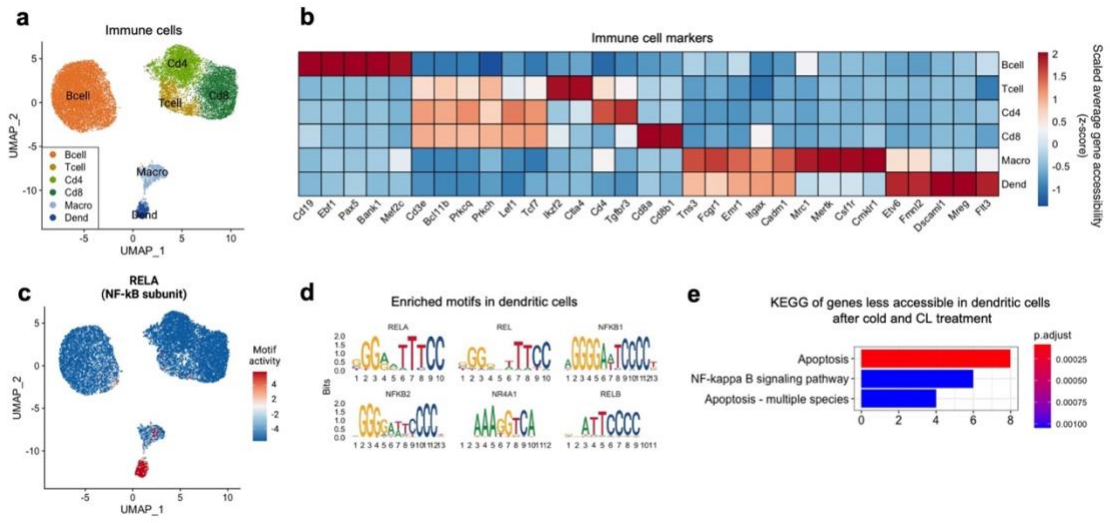

Figure 6

Alterations in pro-inflammatory immune cell compartment.

a, UMAP of immune cell populations (n=23,687). **b**, Heatmap of scaled gene accessibility for cell-type markers. **c**, UMAP of RELA motif enrichment. **d**, Motif sequences enriched in dendritic cell population. **e**, GO analysis of genes less accessible after cold and CL treatment in dendritic cells. X-axis indicates number of genes. Color indicates adjusted p-value.

Macro; Macrophage, Dend; Dendritic cell.

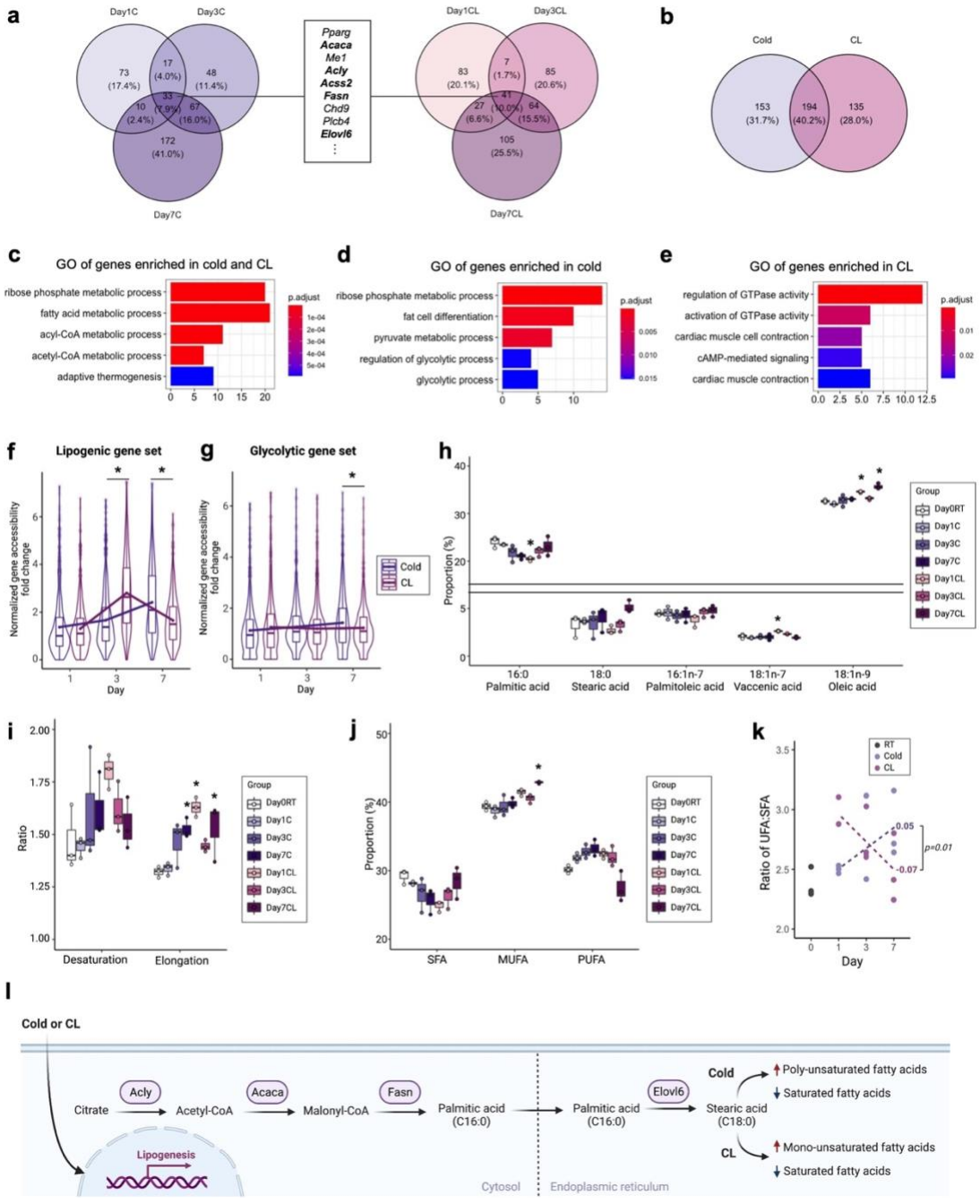

Figure 7

Shifts in lipogenic and glycolytic genes and lipid composition in response to different thermogenic stimuli.

a, Venn diagram summary showing more accessible genes at day 1, 3, and 7 after cold exposure or CL treatment compared to Day 0 RT. The genes that are commonly more accessible after cold exposure and CL treatment from day 1 to day 7 are shown in the box. Bold font indicates the genes involved in *de novo* lipogenesis (*DNL*). **b**, Venn diagram summary showing commonly or differentially more accessible genes after 3 or 7 days of cold exposure and CL treatment compared to Day 0 RT. **c**, GO analysis of genes that were commonly more accessible in both cold and CL. **d,e**, GO analysis of genes that are more accessible only in cold (**d**) or CL (**e**). X-axis indicates number of genes. Color indicates adjusted p-value. **f,g**, Violin and box plots showing the distribution of average gene accessibility of lipogenic genes (*Acaca, Acacb, Acly, Acss2, Fasn, Scd1, Elovl6*) (**f**) and glycolytic genes (*Hk1, Gpi1, Pfkl, Pfkp, Gapdh, Pgk1, Pgm1, Eno1, Pkm, Ldha*) (**g**) of fold changes after cold exposure and CL treatment compared to Day0 RT. The lower and upper hinges indicate the 25th and 75th percentiles. The horizontal line in the middle of box plot denotes the median. The mean for each day for cold and CL is connected by a line. *p-value<0.05, Welch's two sample t-test was performed. **h**, Relative concentration of quantified lipid species after cold exposure and CL treatment (n=3 per group; More lipid species in Supplementary Fig. 8c). **i**, Ratio of desaturation and elongation from lipidomics data (n=3 per group). **j**, Relative proportion of saturated fatty acids (SFA), monounsaturated fatty acids (MUFA), and polyunsaturated fatty acids (PUFA) by lipidomics analysis (n=3 per group). **k**, Ratio of unsaturated fatty acid (UFA) to saturated fatty acid (SFA) (n=3 per group). The slope for each cold and CL from day 1 to day 7 is calculated by a linear regression function. The p-value for the comparison of the slopes between cold and CL is indicated. **l**, Model for the contribution of cold

temperature and CL treatment to fatty acid metabolic process through functional accessibility changes at lipidomic genes and changes in lipid profile. *Adjusted p-value<0.05, ANOVA multiple comparisons test with Bonferroni's post-hoc test was performed for **h-j**.

Supplementary figures

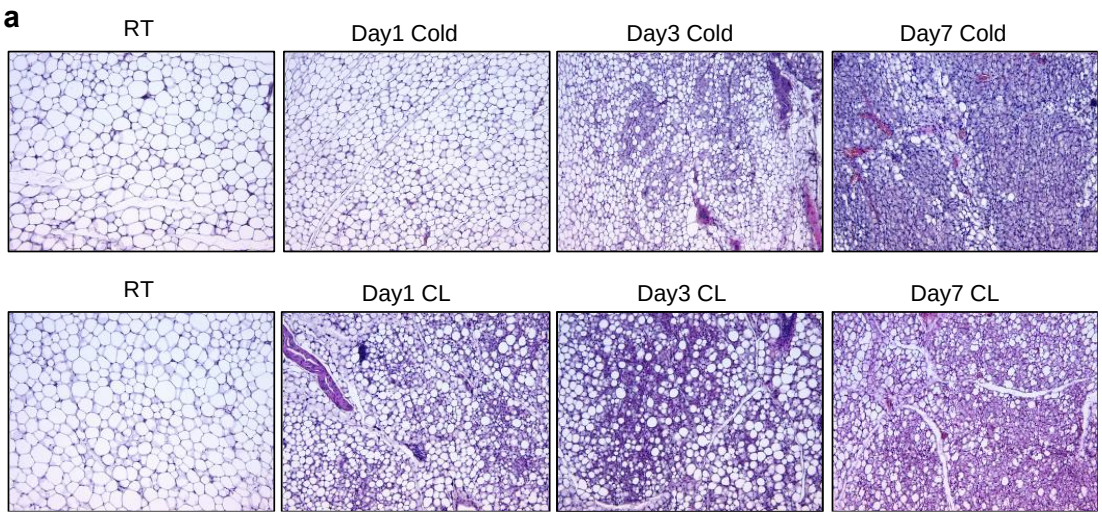

Supplementary Figure 1

Cold and CL lead to beige remodeling in inguinal adipose tissue.

a, Representative 10X H&E-stained images of sections from iWAT depots from two-month-old male C57BL/6 mice exposed to cold (6°C) or CL-316,243 (CL; 1mg/kg/mouse/day) for 1, 3, or 7 days. Scale bar = 200 µm.

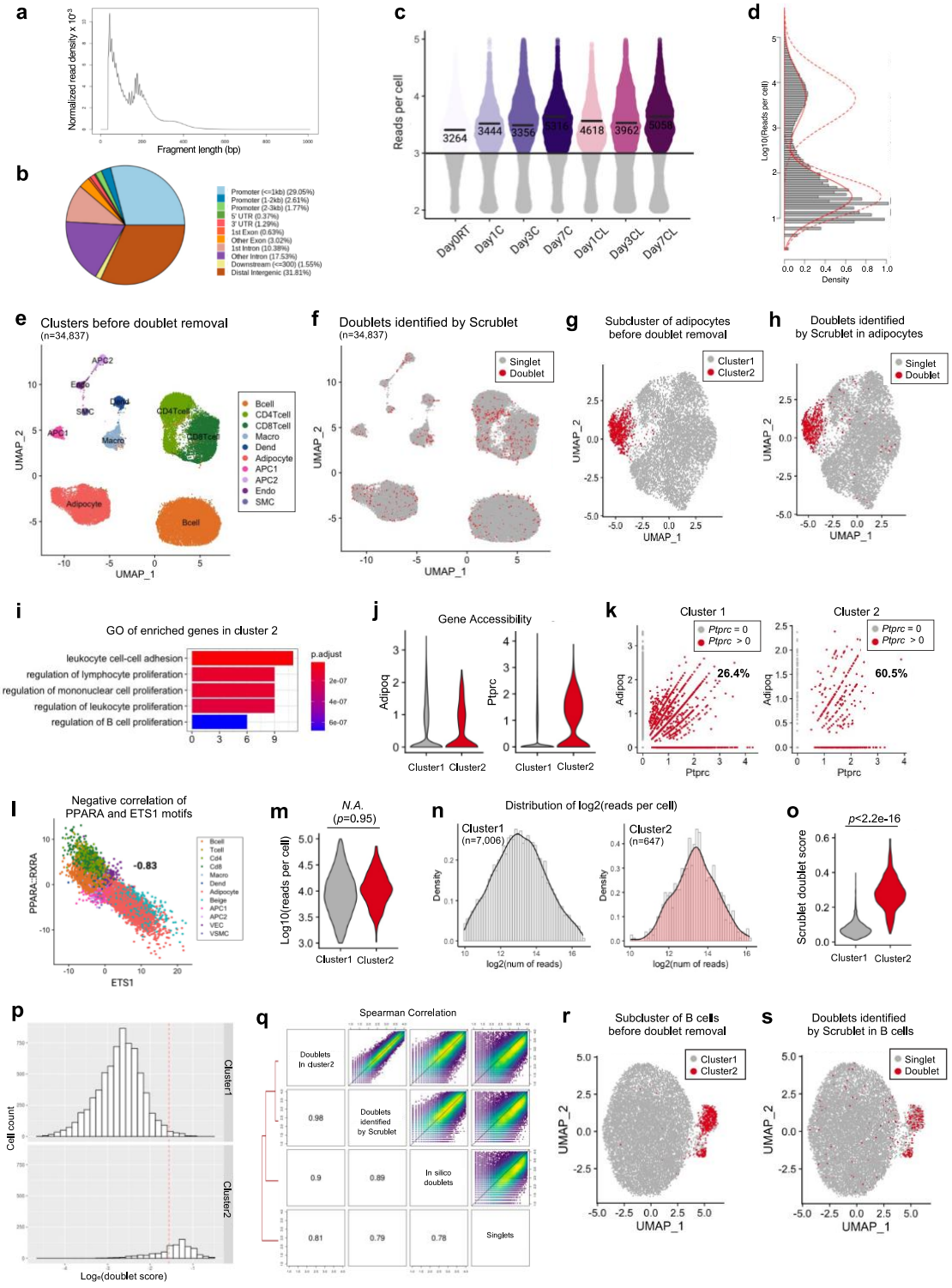

Supplementary Figure 2

Quality control metrics and doublet identification of snATAC-seq dataset.

a, Fragment size distribution plot shows peaks around 100 and 200bp, indicating enrichment of nucleosome-free and mono-nucleosome-bound fragments. **b**, Distribution of peaks on genome features shows that more than 30% of the peaks are in promoter regions, and more than half of the peaks fall into enhancer regions (distal intergenic and intronic regions). **c**, Distribution of reads per barcode for each cell from each group (n=3 for each group). The median fragment count for each group is indicated with a thick bar. The mean of log10 reads per cell of barcodes or cells passing that 1,000 reads per cell cutoff is labeled. **d**, Histogram shows the distribution of reads and a bimodal distribution, indicating that a population with low reads per cell is not real cells. Red line obtained by mixture modeling separates two populations and shows inference about where the cutoff ("split") is. **e**, UMAP plot of 34,837 cells before removing doublets. Cells are colored by cell types. **f**, UMAP plot of 34,837 cells colored by grey (singlet) or red (doublet) using Scrublet (Wolock *et al.*, 2019). **g**, UMAP plot of adipocytes (7,653 cells) before removing doublets. **h**, UMAP plot of adipocytes colored by grey (singlet) or red (doublet) using Scrublet. **i**, GO analysis of enriched genes in cluster 2. **j**, Normalized gene accessibility for adipocyte marker gene (*Adipoq*) and immune cell marker gene (*Ptprc*). **k**, Scatter plot of gene accessibility for *Adipoq* and *Ptprc*. Each dot is a cell. Red dots indicate the cells with >0 *Ptprc* accessibility. **l**, Scatter plot shows a negative correlation (-0.83 Pearson correlation) between adipocyte motif (PPARA::RXRA) and immune cell motif (ETS1). Dots are individual cells colored by cell types. **m**, Violin plot shows no statistically significant differences in reads per cell between cluster 1 and cluster 2. Welch's two sample t-test was performed. **n**, Histogram of reads per cell distribution in cluster 1 and cluster 2. **o**, Violin plot shows doublet scores of cluster 1 and cluster 2. Welch's two

sample t-test was performed. **p**, Histogram of doublet score in cluster 1 and cluster 2. Red line is the threshold. **q**, Heatmap showing Pearson correlation of doublets in putative doublet cluster, doublets identified by Scrublet, in silico doublets (doublets simulated by random sampling from snATAC-seq dataset), and singlets (not in doublet cluster or identified as doublets by Scrublet). **r**, UMAP plot of B cells (12,555 cells) before removing doublets. **s**, UMAP plot of B cells colored by grey (singlet) or red (doublet) using Scrublet.

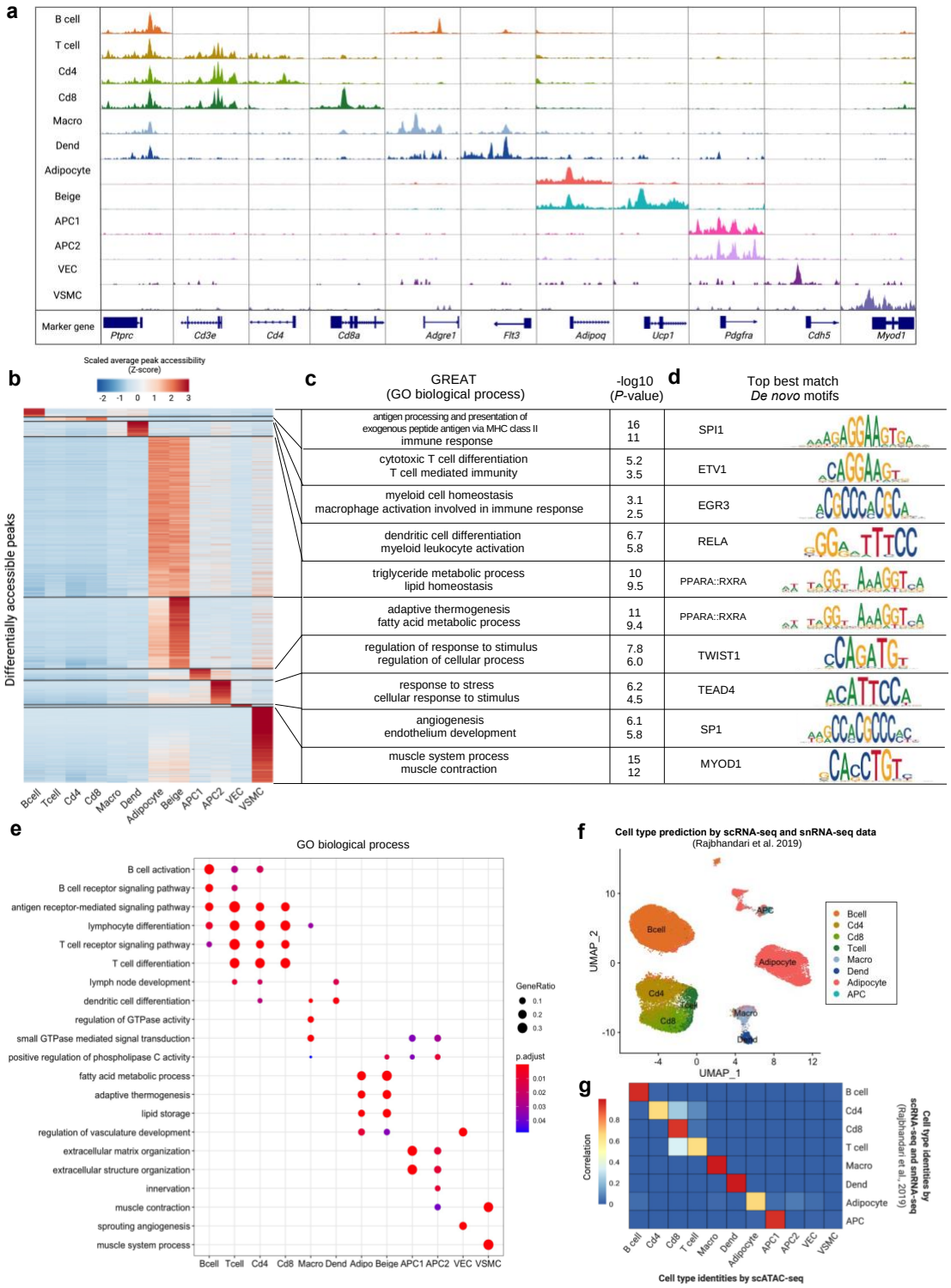

Supplementary Figure 3

Cell type identification of mouse inguinal adipose tissue.

a, Aggregated snATAC-seq accessibility profiles of the promoters for cell-type marker genes. **b**, Differentially accessible peaks (> 1.15 log2 fold-change) in each cell type. **c**, Biological function of differentially accessible regions enriched in each cell type using GREAT analysis (McLean *et al.*, 2010) and -log10 p-value of each term. **d**, Transcription factor motif enriched in highly accessible peaks in each cell type. **e**, GO analysis using the top 50 differentially accessible genes in each cell type. **f**, UMAP plot of cells annotated by predicted cell types from scRNA-seq and snRNA-seq data (Rajbhandari *et al.*, 2019). Endothelial cells and smooth muscle cells were not included in scRNA-seq data. **g**, Heatmap summarizing the accuracy of cell type identification measured by Pearson correlation between clusters identified in snATAC-seq and scRNA-seq (Rajbhandari *et al.*, 2019).

Macro; Macrophage, Dend; Dendritic cell, APC1; Adipocyte progenitor cell 1, APC2; Adipocyte progenitor cell 2, VEC; Vascular endothelial cell, VSMC; Vascular smooth muscle cell

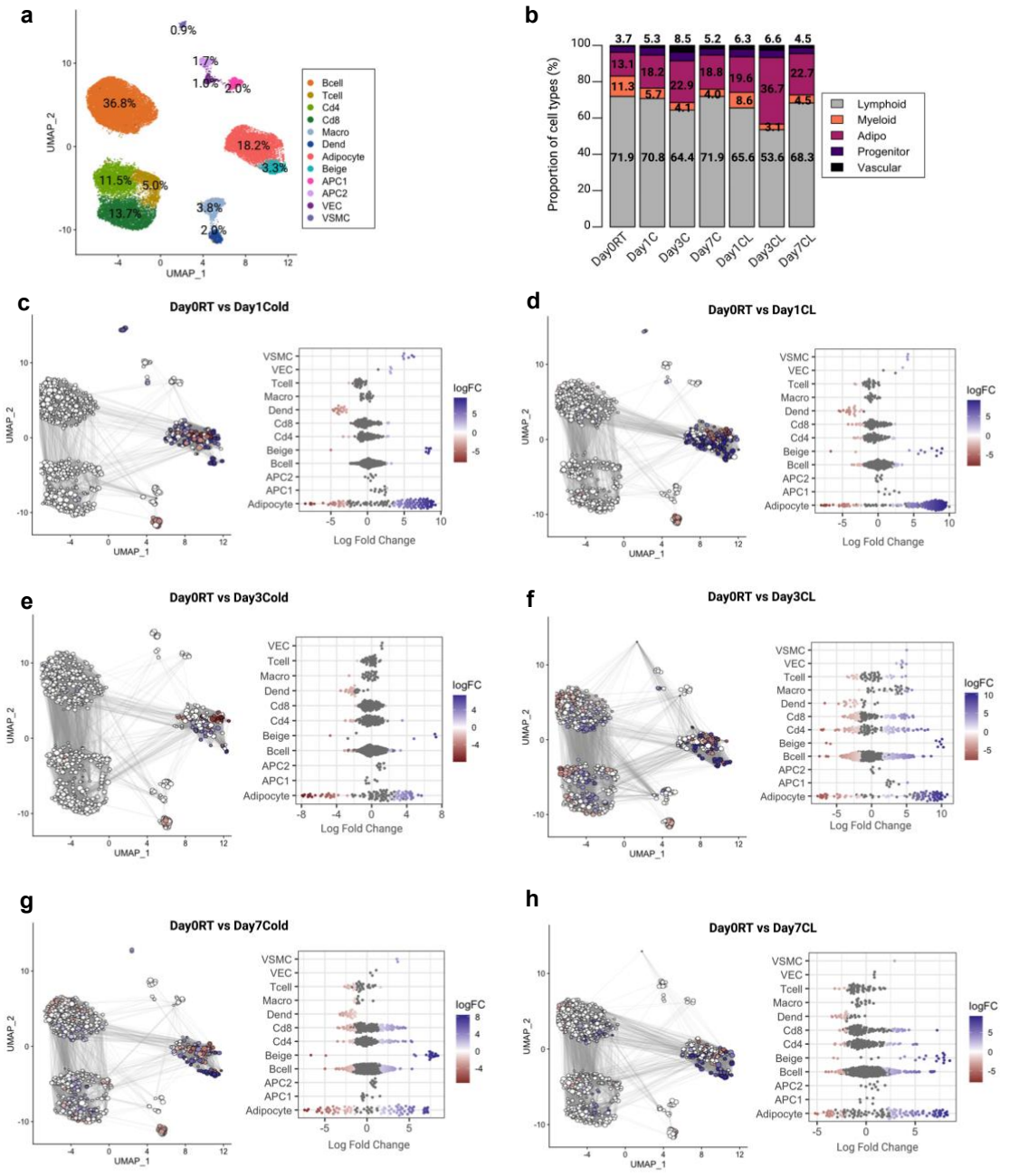

Supplementary Figure 4

Cell type distribution and differential cell abundance after cold exposure and CL treatment.

a, UMAP plot of 32,552 cells from all groups. The percentage of cell types is labeled. **b**, Proportion of major cell types in each group. **c-h**, Milo analysis (Dann

et al., 2022) of cell neighborhood abundance changes in Day 0 control vs. Day 1, 3, or 7 of cold (**c,e,g**) or CL (**d,f,h**). In UMAP, size of points indicates the number of cells in a neighborhood; lines represent the number of cells shared between adjacent neighborhoods. Points are neighborhoods (Nhood), colored by log fold differences at the two time points (FDR 10%). Beeswarm plots show the distribution of log-fold changes in defined clusters.

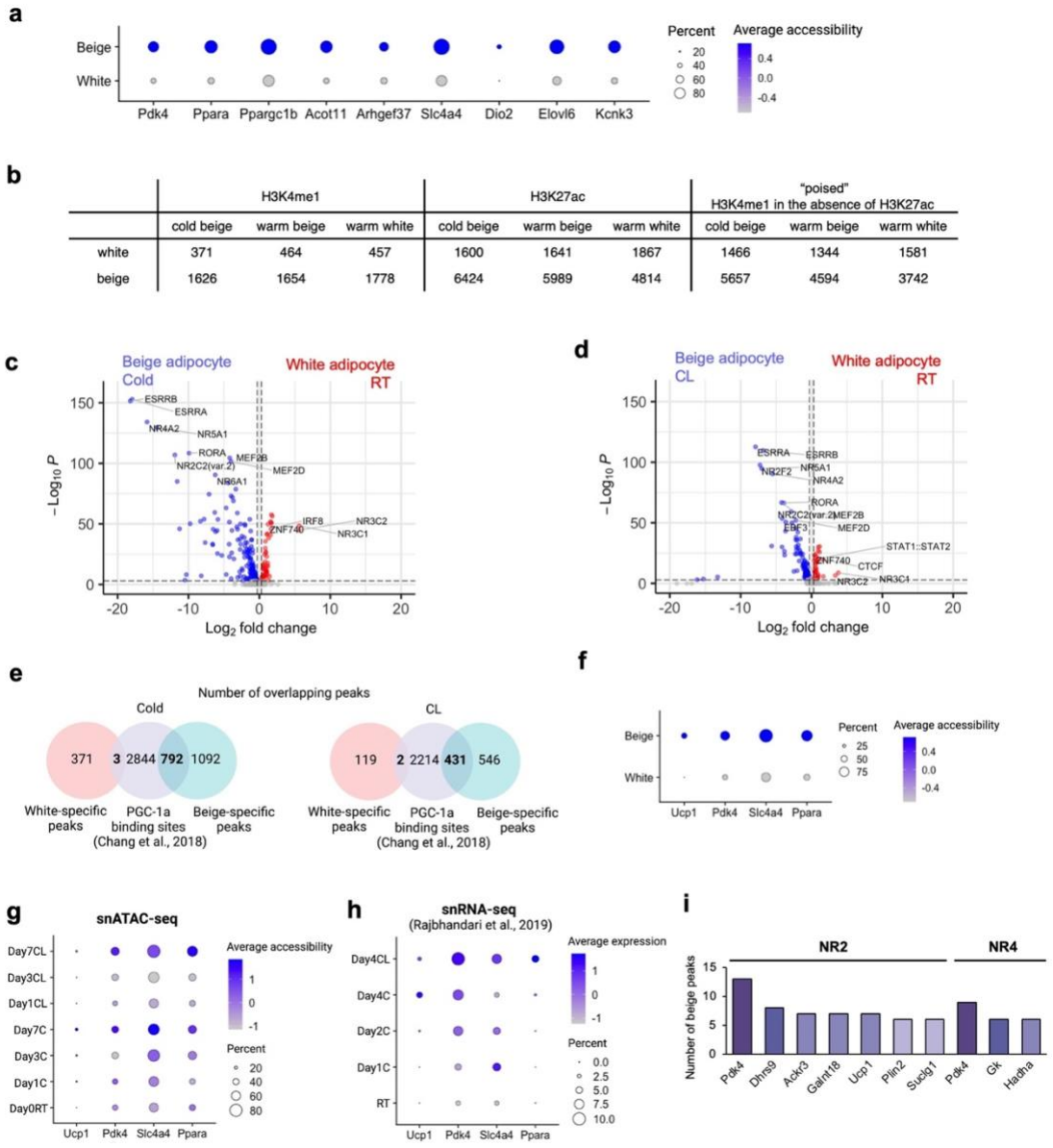

Supplementary Figure 5

Coordinating regulation of transcription factors and epigenetic modifiers in white and beige adipocytes.

a, Dot plot showing normalized accessibility of genes with more than three beige-specific peaks closest to them. Dot size depicts the percent of cells having accessibility of a given gene. **b**, The number of overlaps between white-specific or beige-specific peaks from snATAC-seq data and histone marked peaks from

H3Kme1 and H3K27ac ChIP-seq data (Roh *et al.*, 2018). White specific peaks tend to overlap with peaks enriched in warm white, while beige specific peaks tend to overlap with peaks enriched in cold beige. **c,d**, Volcano plot displaying differential motifs enrichment between white adipocytes before any intervention and beige adipocytes after cold exposure (**c**) or CL treatment (**d**). Motifs with adjusted p-value < 10^{-3} & absolute value of log2 fold-change > 0.5 are colored. **e**, Venn diagram showing the number of overlaps between white-specific or beige-specific peaks after cold exposure or CL treatment and PGC-1α ChIP-seq binding sites (Chang *et al.*, 2018). **f**, Normalized accessibilities of the genes having more than three nearby beige-specific peaks that are overlapping with PGC-1α binding sites. **g,h**, Dot plots displaying normalized snATAC-seq accessibility (**g**) and snRNA-seq expression level (Rajbhandari *et al.*, 2019) (**h**) of the genes having more than three nearby beige-specific peaks overlapping with PGC-1α binding sites. **i**, The number of overlapping beige-specific peaks with NR2 and NR4 motifs from *cisbp* database (Weirauch *et al.*, 2014). Genes are sorted by the number of overlapping peaks near them.

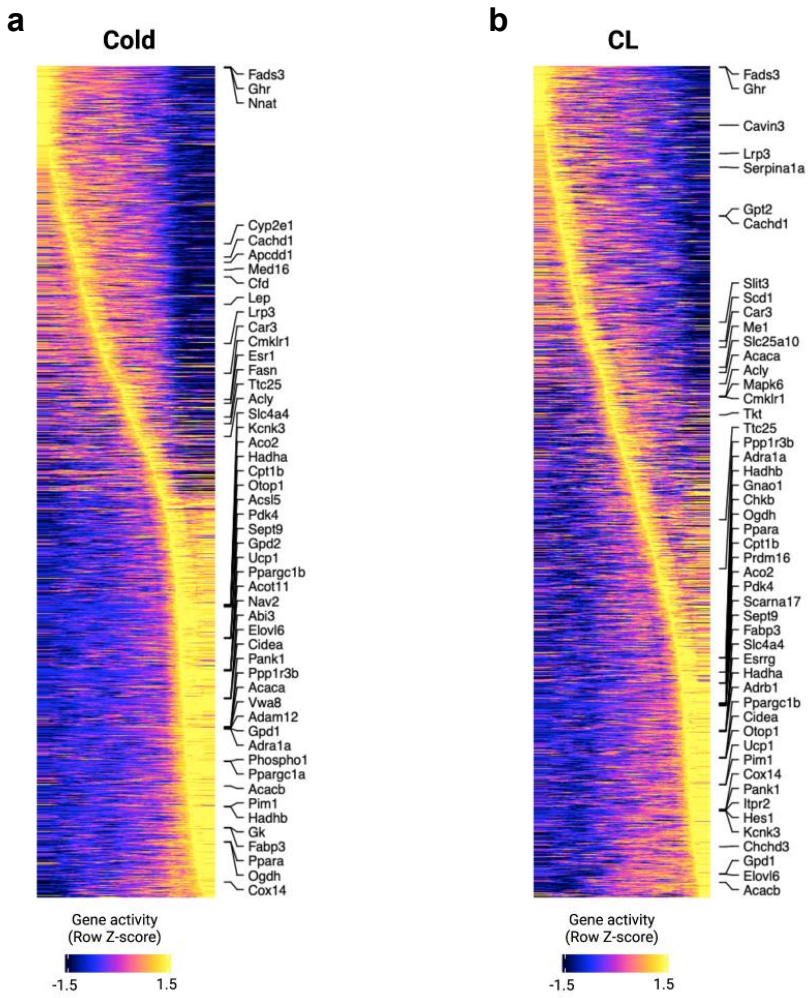

Supplementary Figure 6

Gene accessibility changes along with adipocyte pseudotime trajectory.

a,b, Heatmaps display changes in gene accessibility along adipocyte pseudotime trajectory for cold (**a**) and CL (**b**). Top variable genes are labeled on the right side of the heatmap.

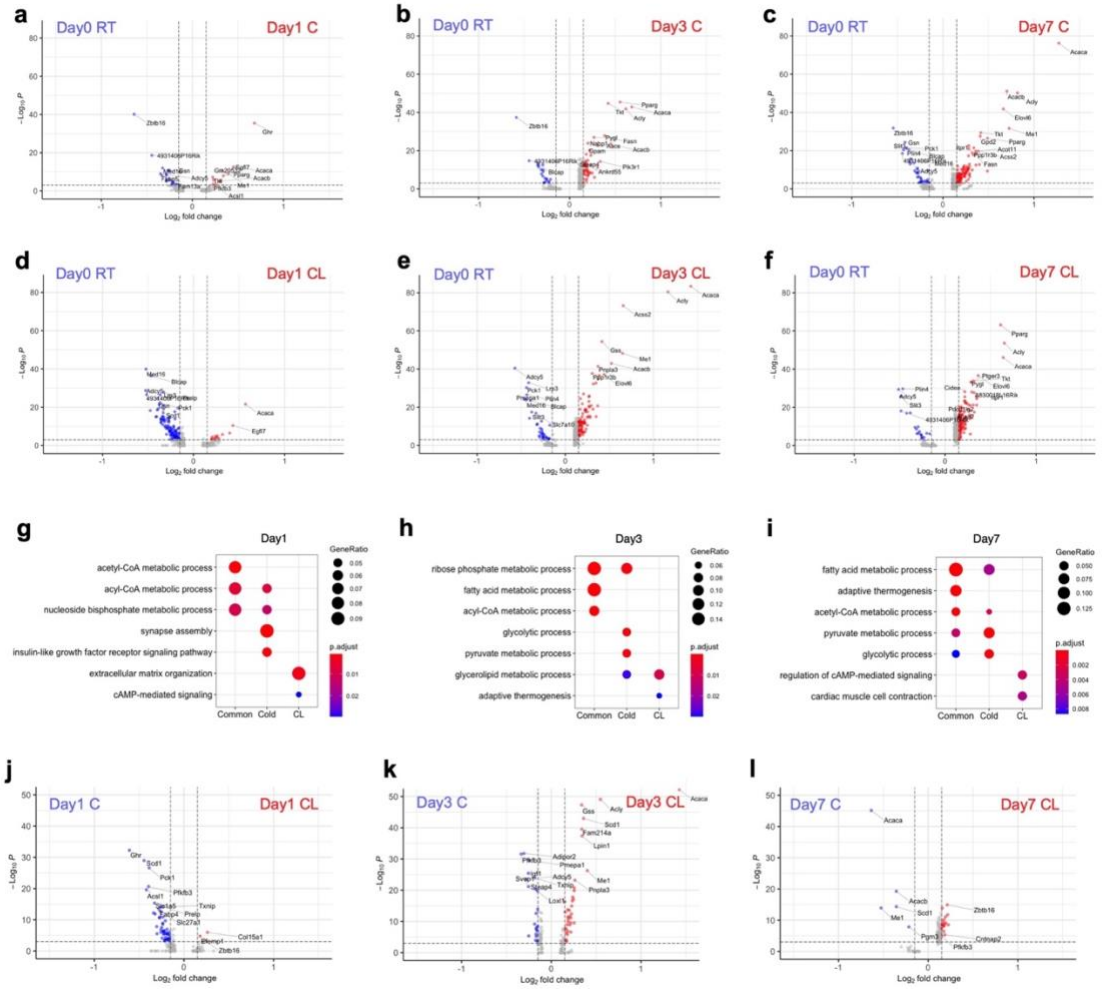

Supplementary Figure 7

Differentially accessible genes after cold exposure or CL treatment in adipocytes.

a-**f**, Volcano plots of differentially accessible genes between day 0 RT and cold (**a**,**b**,**c**) or CL (**d**,**e**,**f**) at each time point in mature adipocytes (both white and beige adipocyte). Genes with adjusted *p*-value < 0.001 & absolute value of log10 fold-change > 0.15 are colored and labeled. **g**-**i**, GO analysis of commonly more accessible genes after cold and CL treatment (common) and uniquely more accessible in cold or CL at each time point. **j**-**l**, Volcano plots of the

differentially accessible genes between cold and CL at day 1 (**j**), day 3 (**k**), and day 7 (**l**) in mature adipocytes (both white and beige). Genes with adjusted *p*-value < 0.001 & absolute value of log2 fold-change > 0.15 are colored and labeled.

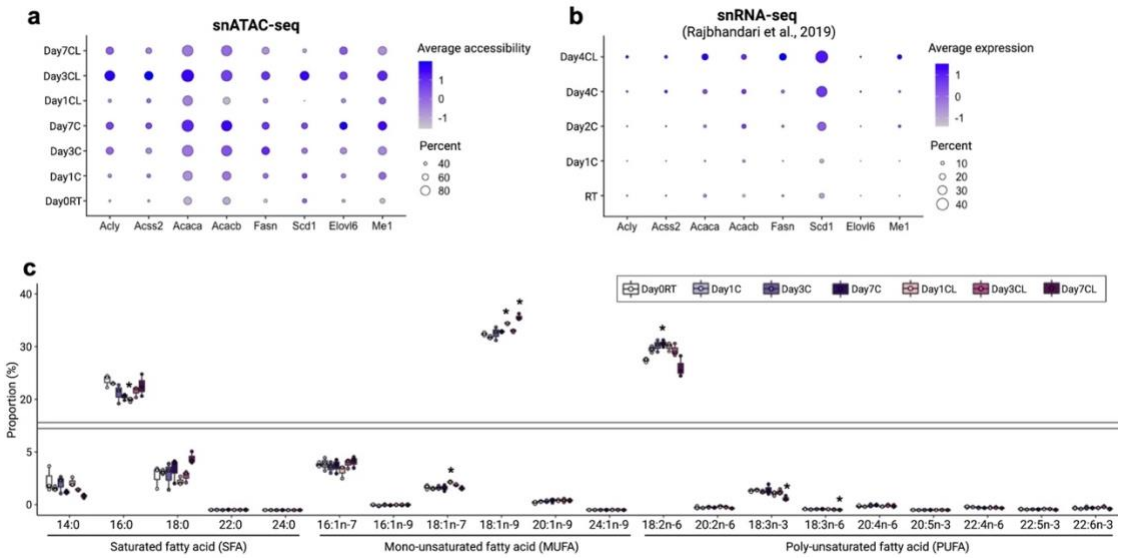

Supplementary Figure 8

Changes in accessibility and expression of genes involved in lipogenesis and proportion of lipid species after cold and CL treatment.

a,b, Dot plots displaying normalized snATAC-seq accessibility (**a**) and snRNA-seq expression level (Rajbhandari *et al.*, 2019) (**b**) of the lipogenic genes. **c**, Relative proportion of each lipid class by lipidomics analysis (n=3 per group). Color of bar indicates group. *Adjusted p-value<0.05, ANOVA multiple comparisons test with Bonferroni's post-hoc test was performed.

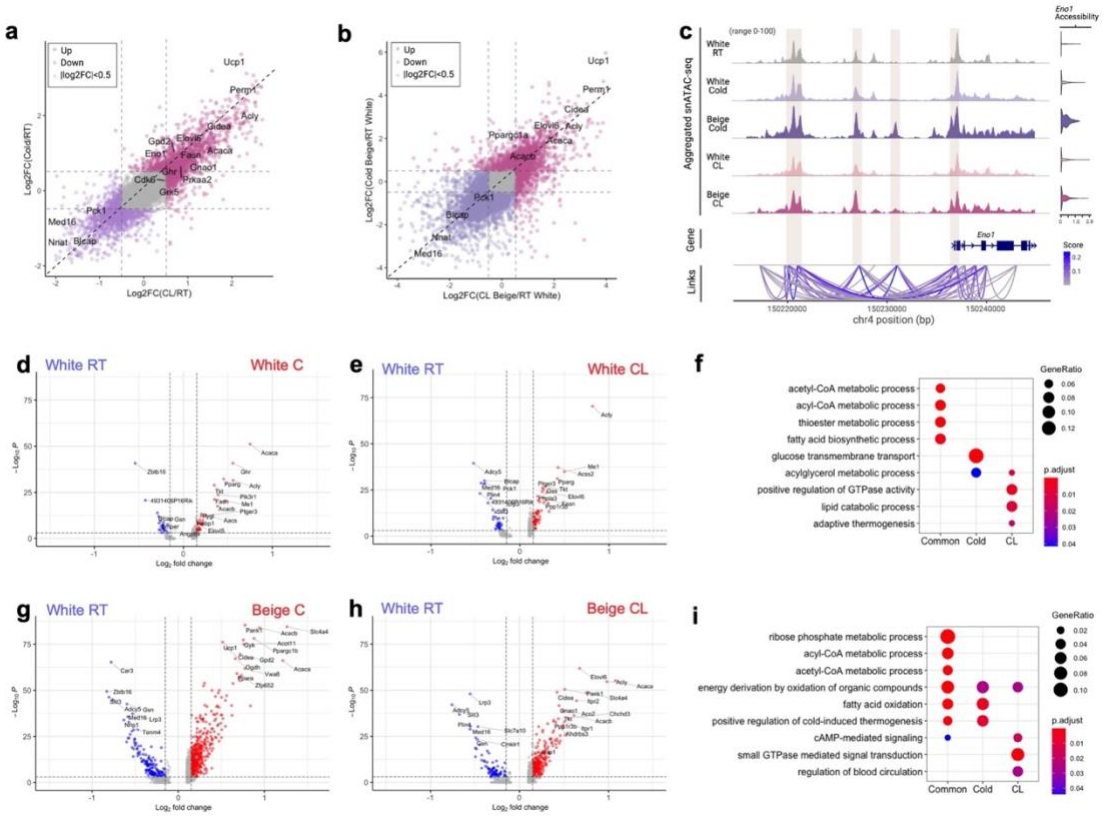

Supplementary Figure 9

Differentially accessible genes after cold exposure and CL treatment in white and beige adipocytes.

a, Scatter plot of the log2 fold-change of genes after cold exposure and CL treatment. The genes with >0.5 log2 fold changes are colored. **b**, Scatter plot of the log2 fold-change of genes in cold-induced and CL-induced beige adipocytes compared to white adipocytes at RT. The genes with > 0.5 log2 fold changes are colored. **c**, Genome tracks showing the aggregate snATAC-seq profiles of *Eno1* upstream in adipocytes. Links show *cis*-coaccessibility network with multiple connections between peaks around *Eno1*. Coaccessibility score > 0.2 regions are highlighted by brown on genome and gene track. **d,e**, Volcano plots of the differentially accessible genes between white adipocytes at day 0 RT and after cold exposure (**d**) or CL treatment (**e**) from all three time points. Genes

with adjusted p-value < 0.0001 & absolute value of log2 fold-change > 0.15 are colored. **f**, GO analysis of commonly more accessible genes after cold exposure and CL treatment (common) and uniquely more accessible after cold exposure or CL treatment in white adipocytes. **g,h**, Volcano plots of the differentially accessible genes between white adipocytes at day 0 RT and beige adipocytes after cold exposure (**g**) or CL treatment (**h**) from all three time points. Genes with adjusted p-value < 0.0001 & absolute value of log2 fold-change > 0.15 are colored. **i**, GO analysis of commonly more accessible genes after cold exposure and CL treatment (common) and uniquely more accessible after cold exposure or CL treatment in beige adipocytes.

Supplementary tables

Supplementary Table 1

Oligonucleotide sequences used in this study.

Oligos were ordered from IDT with standard desalting. Sequencing primers were ordered from IDT with PAGE purification (Vitak et al., 2017).

Oligo	Sequence (5'-3')
Tn5ME_Rev	5Phos/CTGTCTCTTATACACATCT
P5_ME_1	TCGTCGGCAGCGTCTCCACGCTATAGCCTGCGATCGAGGACGGCAGATGTGTATAAGAGACAG
P5_ME_2	TCGTCGGCAGCGTCTCCACGCATAGAGGCGCGATCGAGGACGGCAGATGTGTATAAGAGACAG
P5_ME_3	TCGTCGGCAGCGTCTCCACGCCCTATCCTGCGATCGAGGACGGCAGATGTGTATAAGAGACAG
P5_ME_4	TCGTCGGCAGCGTCTCCACGCGGCTCTGAGCGATCGAGGACGGCAGATGTGTATAAGAGACAG
P5_ME_5	TCGTCGGCAGCGTCTCCACGCAGGCGAAGGCGATCGAGGACGGCAGATGTGTATAAGAGACAG
P5_ME_6	TCGTCGGCAGCGTCTCCACGCTAATCTTAGCGATCGAGGACGGCAGATGTGTATAAGAGACAG
P5_ME_7	TCGTCGGCAGCGTCTCCACGCCAGGACGTGCGATCGAGGACGGCAGATGTGTATAAGAGACAG
P5_ME_8	TCGTCGGCAGCGTCTCCACGCGTACTGACGCGATCGAGGACGGCAGATGTGTATAAGAGACAG
P7_ME_1	GTCTCGTGGGCTCGGCTGTCCCTGTCCCGAGTAATCACCGTCTCCGCCTCAGATGTGTATAAGAGACAG
P7_ME_2	GTCTCGTGGGCTCGGCTGTCCCTGTCCTCTCCGGACACCGTCTCCGCCTCAGATGTGTATAAGAGACAG
P7_ME_3	GTCTCGTGGGCTCGGCTGTCCCTGTCCAATGAGCGCACCGTCTCCGCCTCAGATGTGTATAAGAGACAG
P7_ME_4	GTCTCGTGGGCTCGGCTGTCCCTGTCCGGAATCTCCACCGTCTCCGCCTCAGATGTGTATAAGAGACAG
P7_ME_5	GTCTCGTGGGCTCGGCTGTCCCTGTCCTTCTGAATCACCGTCTCCGCCTCAGATGTGTATAAGAGACAG
P7_ME_6	GTCTCGTGGGCTCGGCTGTCCCTGTCCACGAATTCCACCGTCTCCGCCTCAGATGTGTATAAGAGACAG
P7_ME_7	GTCTCGTGGGCTCGGCTGTCCCTGTCCAGCTTCAGCACCGTCTCCGCCTCAGATGTGTATAAGAGACAG
P7_ME_8	GTCTCGTGGGCTCGGCTGTCCCTGTCCGCGCATTACACCGTCTCCGCCTCAGATGTGTATAAGAGACAG
P7_ME_9	GTCTCGTGGGCTCGGCTGTCCCTGTCCCATAGCCGCACCGTCTCCGCCTCAGATGTGTATAAGAGACAG
P7_ME_10	GTCTCGTGGGCTCGGCTGTCCCTGTCCTTCGCGGACACCGTCTCCGCCTCAGATGTGTATAAGAGACAG
P7_ME_11	GTCTCGTGGGCTCGGCTGTCCCTGTCCGCGCGAGACACCGTCTCCGCCTCAGATGTGTATAAGAGACAG

P7_ME_12	GTCTCGTGGGCTCGGCTGTCCCTGTCCCTATCGCTCACCGTCTCCGCCTCAGAT GTGTATAAGAGACAG
I5_1	AATGATACGGCGACCACCGAGATCTACACCTCTCTATTCGTCGGCAGCGTC
I5_2	AATGATACGGCGACCACCGAGATCTACACTATCCTCTTCGTCGGCAGCGTC
I5_3	AATGATACGGCGACCACCGAGATCTACACGTAAGGAGTCGTCGGCAGCGTC
I5_4	AATGATACGGCGACCACCGAGATCTACACACTGCATATCGTCGGCAGCGTC
I5_5	AATGATACGGCGACCACCGAGATCTACACAAGGAGTATCGTCGGCAGCGTC
I5_6	AATGATACGGCGACCACCGAGATCTACACCTAAGCCTTCGTCGGCAGCGTC
I5_7	AATGATACGGCGACCACCGAGATCTACACCGTCTAATTCGTCGGCAGCGTC
I5_8	AATGATACGGCGACCACCGAGATCTACACTCTCTCCGTCGTCGGCAGCGTC
I5_9	AATGATACGGCGACCACCGAGATCTACACTCGACTAGTCGTCGGCAGCGTC
I5_10	AATGATACGGCGACCACCGAGATCTACACTTCTAGCTTCGTCGGCAGCGTC
I5_11	AATGATACGGCGACCACCGAGATCTACACCCTAGAGTTCGTCGGCAGCGTC
I5_12	AATGATACGGCGACCACCGAGATCTACACGCGTAAGATCGTCGGCAGCGTC
I5_13	AATGATACGGCGACCACCGAGATCTACACAAGGCTATTCGTCGGCAGCGTC
I5_14	AATGATACGGCGACCACCGAGATCTACACGAGCCTTATCGTCGGCAGCGTC
I5_15	AATGATACGGCGACCACCGAGATCTACACTTATGCGATCGTCGGCAGCGTC
I5_16	AATGATACGGCGACCACCGAGATCTACACATCTGAGTTCGTCGGCAGCGTC
I5_17	AATGATACGGCGACCACCGAGATCTACACGGATACTATCGTCGGCAGCGTC
I5_18	AATGATACGGCGACCACCGAGATCTACACTAAGATCCTCGTCGGCAGCGTC
I5_19	AATGATACGGCGACCACCGAGATCTACACAAGAGATGTCGTCGGCAGCGTC
I5_20	AATGATACGGCGACCACCGAGATCTACACAATGACGTTCGTCGGCAGCGTC
I5_21	AATGATACGGCGACCACCGAGATCTACACGAAGTATGTCGTCGGCAGCGTC
I5_22	AATGATACGGCGACCACCGAGATCTACACATAGCCTTTCGTCGGCAGCGTC
I5_23	AATGATACGGCGACCACCGAGATCTACACTTGGAAGTTCGTCGGCAGCGTC
I5_24	AATGATACGGCGACCACCGAGATCTACACATTCGTTGTCGTCGGCAGCGTC
I5_25	AATGATACGGCGACCACCGAGATCTACACAGGATAACTCGTCGGCAGCGTC
I5_26	AATGATACGGCGACCACCGAGATCTACACTTCATCCATCGTCGGCAGCGTC
I5_27	AATGATACGGCGACCACCGAGATCTACACAACGAACGTCGTCGGCAGCGTC
I5_28	AATGATACGGCGACCACCGAGATCTACACTGCCTTACTCGTCGGCAGCGTC
I5_29	AATGATACGGCGACCACCGAGATCTACACCGAATTCCTCGTCGGCAGCGTC
I5_30	AATGATACGGCGACCACCGAGATCTACACGGTTAGACTCGTCGGCAGCGTC
I5_31	AATGATACGGCGACCACCGAGATCTACACTCCGGTAATCGTCGGCAGCGTC
I5_32	AATGATACGGCGACCACCGAGATCTACACTTACGACCTCGTCGGCAGCGTC
I7_1	CAAGCAGAAGACGGCATACGAGATTCGCCTTAGTCTCGTGGGCTCGG
I7_2	CAAGCAGAAGACGGCATACGAGATCTAGTACGGTCTCGTGGGCTCGG
I7_3	CAAGCAGAAGACGGCATACGAGATTTCTGCCTGTCTCGTGGGCTCGG
I7_4	CAAGCAGAAGACGGCATACGAGATGCTCAGGAGTCTCGTGGGCTCGG
I7_5	CAAGCAGAAGACGGCATACGAGATAGGAGTCCGTCTCGTGGGCTCGG
I7_6	CAAGCAGAAGACGGCATACGAGATCATGCCTAGTCTCGTGGGCTCGG
I7_7	CAAGCAGAAGACGGCATACGAGATGTAGAGAGGTCTCGTGGGCTCGG
I7_8	CAAGCAGAAGACGGCATACGAGATCAGCCTCGGTCTCGTGGGCTCGG
I7_9	CAAGCAGAAGACGGCATACGAGATTGCCTCTTGTCTCGTGGGCTCGG
I7_10	CAAGCAGAAGACGGCATACGAGATTCCTCTACGTCTCGTGGGCTCGG
I7_11	CAAGCAGAAGACGGCATACGAGATTCATGAGCGTCTCGTGGGCTCGG
I7_12	CAAGCAGAAGACGGCATACGAGATCCTGAGATGTCTCGTGGGCTCGG
I7_13	CAAGCAGAAGACGGCATACGAGATTAGCGAGTGTCTCGTGGGCTCGG
I7_14	CAAGCAGAAGACGGCATACGAGATGTAGCTCCGTCTCGTGGGCTCGG
I7_15	CAAGCAGAAGACGGCATACGAGATTACTACGCGTCTCGTGGGCTCGG
I7_16	CAAGCAGAAGACGGCATACGAGATGCAGCGTAGTCTCGTGGGCTCGG
I7_17	CAAGCAGAAGACGGCATACGAGATCTGCGCATGTCTCGTGGGCTCGG

I7_18	CAAGCAGAAGACGGCATACGAGATGAGCGCTAGTCTCGTGGGCTCGG
I7_19	CAAGCAGAAGACGGCATACGAGATCGCTCAGTGTCTCGTGGGCTCGG
I7_20	CAAGCAGAAGACGGCATACGAGATGTCTTAGGGTCTCGTGGGCTCGG
I7_21	CAAGCAGAAGACGGCATACGAGATACTGATCGGTCTCGTGGGCTCGG
I7_22	CAAGCAGAAGACGGCATACGAGATTAGCTGCAGTCTCGTGGGCTCGG
I7_23	CAAGCAGAAGACGGCATACGAGATGACGTCGAGTCTCGTGGGCTCGG
I7_24	CAAGCAGAAGACGGCATACGAGATTACCAGAGGTCTCGTGGGCTCGG
I7_25	CAAGCAGAAGACGGCATACGAGATGGATGGAAGTCTCGTGGGCTCGG
I7_26	CAAGCAGAAGACGGCATACGAGATATTGAGGCGTCTCGTGGGCTCGG
I7_27	CAAGCAGAAGACGGCATACGAGATCGGATAGAGTCTCGTGGGCTCGG
I7_28	CAAGCAGAAGACGGCATACGAGATTGGTAGACGTCTCGTGGGCTCGG
I7_29	CAAGCAGAAGACGGCATACGAGATACCTGGTTGTCTCGTGGGCTCGG
I7_30	CAAGCAGAAGACGGCATACGAGATCAGTTCTGGTCTCGTGGGCTCGG
I7_31	CAAGCAGAAGACGGCATACGAGATTCGAACGTGTCTCGTGGGCTCGG
I7_32	CAAGCAGAAGACGGCATACGAGATCGTTGCTTGTCTCGTGGGCTCGG
I7_33	CAAGCAGAAGACGGCATACGAGATTACCGTTCGTCTCGTGGGCTCGG
I7_34	CAAGCAGAAGACGGCATACGAGATTAGGTTGCGTCTCGTGGGCTCGG
I7_35	CAAGCAGAAGACGGCATACGAGATGAGGCTAAGTCTCGTGGGCTCGG
I7_36	CAAGCAGAAGACGGCATACGAGATCGACCATAGTCTCGTGGGCTCGG
I7_37	CAAGCAGAAGACGGCATACGAGATAGGCAGTAGTCTCGTGGGCTCGG
I7_38	CAAGCAGAAGACGGCATACGAGATATCAAGCGGTCTCGTGGGCTCGG
I7_39	CAAGCAGAAGACGGCATACGAGATCATTGAAGGTCTCGTGGGCTCGG
I7_40	CAAGCAGAAGACGGCATACGAGATCGACTTATGTCTCGTGGGCTCGG
I7_41	CAAGCAGAAGACGGCATACGAGATTCTATACGGTCTCGTGGGCTCGG
I7_42	CAAGCAGAAGACGGCATACGAGATAGCATTAGGTCTCGTGGGCTCGG
I7_43	CAAGCAGAAGACGGCATACGAGATAATTGGCAGTCTCGTGGGCTCGG
I7_44	CAAGCAGAAGACGGCATACGAGATAGATTCGTGTCTCGTGGGCTCGG
I7_45	CAAGCAGAAGACGGCATACGAGATTTCATGACGTCTCGTGGGCTCGG
I7_46	CAAGCAGAAGACGGCATACGAGATTGAACTTGGTCTCGTGGGCTCGG
I7_47	CAAGCAGAAGACGGCATACGAGATATGGCATAGTCTCGTGGGCTCGG
I7_48	CAAGCAGAAGACGGCATACGAGATCGTAATTCGTCTCGTGGGCTCGG
Read 1 Sequencing Primer	GCGATCGAGGACGGCAGATGTGTATAAGAGACAG
Read 2 Sequencing Primer	CACCGTCTCCGCCTCAGATGTGTATAAGAGACAG
Index 1 Sequencing Primer	CTGTCTCTTATACACATCTGAGGCGGAGACGGTG
Index 2 Sequencing Primer	CTGTCTCTTATACACATCTGCCGTCCTCGATCGC

Chapter 3: Dynamic regulation of chromatin accessibility during melanocyte stem cell activation

Seoyeon Lee[1], Luye An[2], Andrew C. White[3], Paul D. Soloway[1,3]

[1]Division of Nutritional Sciences, College of Agriculture and Life Sciences, Cornell University, Ithaca, New York 14853, USA.
[2]Department of Biochemistry, Molecular, and Cell Biology, Cornell University, Ithaca, New York 14853, USA.
[3]Department of Biomedical Sciences, College of Veterinary Medicine, Cornell University, Ithaca, New York 14853, USA.

Author contributions:

S.L., P.D.S., and A.C.W. conceived this project. S.L. carried out snATAC-seq library preparation and data analyses. L.A. performed mouse and immunostaining experiments. S.L. wrote the manuscript. P.D.S. and A.C.W. supervised this study.

Abstract

Melanocytes that generate skin pigment come from melanocyte stem cells (McSCs) during each hair follicle cycle activation. McSCs are also able to migrate upwards to the epidermis and generate skin pigment through activation by ultraviolet-B (UVB). However, our current knowledge of the mechanisms regulating McSC stemness, differentiation and activation remains limited. Here, we perform single-nucleus assay for transposase-accessible chromatin with high-throughput sequencing (snATAC-seq) on sorted melanocytes at different stages of the hair follicle cycle and after UVB irradiation of mice. We show three

melanocyte lineages: quiescent McSC (qMcSC), activated McSC (aMcSC), and differentiated melanocyte (dMC) and differentially accessible genes and enriched *cis*-regulatory elements and motifs for each melanocyte lineage. Our findings reveal the potential gene regulators that make the melanocyte cell states different and provide new insights into how intrinsic and extrinsic cues regulate chromatin states of different melanocyte cell states.

Introduction

Melanocytes are neural crest-derived cells that produce melanin, a skin pigment giving colors to the skin and hair (Slominski and Paus, 1993). The activation and differentiation of melanocytes are tightly regulated with the hair follicle cycle (Slominski and Paus, 1993). Hair follicles go through three major phases associated with hair growth: anagen, catagen, and telogen. Anagen is the active hair growing phase. During the anagen phase, the hair follicle forms a new hair shaft and grows downward into the dermis. In this phase, cells proliferate rapidly to make hair continue to grow. After the period of growth, cells in the lower hair follicle stop dividing and undergo apoptosis during the transitional phase, called catagen (Tobin et al., 1998). After the regression phase, cells enter the resting phase, called telogen. Subsequently, anagen is initiated with the start of a new hair growth cycle (Fuchs et al., 2001).

Throughout the hair cycles, melanocytes are continuously repopulated by the differentiation of melanocyte stem cells (McSCs) in adult skin (Fuchs *et al.*, 2001). McSCs found in the bulge, a stem cell niche, are usually in a quiescent state during telogen (Nishimura et al., 2002). During telogen-anagen transition, McSCs translocate towards the base of the growing hair follicle, called hair bulb. McSCs then give rise to proliferative progeny which then differentiate into

mature melanocytes (Nishimura *et al.*, 2002). The fully mature or differentiated melanocytes (dMCs) produce melanin and transfer mature melanosomes to keratinocytes (Hearing, 2005). During this process, a small number of the McSCs remain in the bulge area (Tanimura et al., 2011). The McSCs in the hair bulge are capable of self-renewal and of supplying melanocyte progeny (Nishimura *et al.*, 2002). Loss of McSCs leads to failure of hair and skin pigmentation (Nishimura et al., 2005; Steingrimsson et al., 2005). Vitiligo is a common hypopigmentation disease in which epidermal melanocytes in skin are lost (Cui et al., 1991). In contrast, improper proliferation of McSCs can lead to melanoma, the deadliest skin cancer derived from melanocytes (Siegel et al., 2019). Therefore, maintenance of McSCs is critical for sustaining proper melanocyte regeneration.

Without anagen transition, McSCs can be activated by environmental cues such as ultraviolet-B (UVB), a component of sunlight with a wavelength between 280nm-315nm (Chou et al., 2013; Moon et al., 2017). Under UVB-irradiation, activated McSCs (aMcSCs) migrate upwards into the epidermis and regenerate epidermal melanocytes producing melanin (Nishimura, 2011). Moon *et al.* showed that UVB-irradiation induces McSC migration without initiating anagen transition in quiescent McSCs (qMcSCs) in telogen (Moon *et al.*, 2017). These properties of McSCs have gained attention as a potential therapeutic target for clinical therapies of vitiligo (Lee and Fisher, 2014; Mull et al., 2015). Despite the importance of McSCs providing cell source for vitiligo, the mechanisms of how McSCs are activated upon stimulation by UVB-irradiated to the top layer of skin and translocate to the epidermis remain still largely unclear.

To study McSC lineage, melanocyte-specific genes such as tyrosinase (*Tyr*), tyrosinase-related protein 1 and 2 (*Tyrp1*, *Tyrp2*/*Dct*) have been used for

labeling melanocyte lineages with GFP or *LacZ* (Plonka et al., 2009). Nishimura *et al*. used *Dct-LacZ* transgenic mice carrying *lacZ* reporter under the control of the *Dct* promoter, previously identified as a marker for the melanoblast lineage (Nishimura *et al.*, 2002). Over decades, many genes and signaling pathways involved in melanocyte differentiation and melanosome formation including WNT and BMP signaling have been identified (Botchkareva et al., 2003; Infarinato et al., 2020; Levy et al., 2006). Studies have shown that microphthalmia-associated transcription factor (MITF) is a critical transcription factor for regulating melanocyte development and promoting melanocyte differentiation (Levy *et al.*, 2006). Yet, there are no exclusive markers for McSCs (Lang et al., 2013). With lineage tracing systems, distinguishing McSCs and their progeny has been largely depending on their anatomic locations. While majority of McSC progeny translocate to the hair bulb during the anagen phase, a small percentage of McSCs remain in the bulge area and normally quiescent during the telogen phase (Nishimura *et al.*, 2002). Once spatial information of individual cells is lost during tissue dissociation, it is challenging to distinguish McSCs and their progeny. Moreover, McSCs only exist at a very small proportion (1-10%) in the skin tissue (Chung et al., 2011). Recent single-cell RNA-sequencing (scRNA-seq) data showed in mouse skin, melanocytes comprise 0.6% of cells in telogen and 4% in anagen (Joost et al., 2020). The lack of exclusive markers and rarity make the study of McSCs challenging.

Chromatin accessibility assays have successfully identified different cell types or states and profiled their unique chromatin states (Cusanovich *et al.*, 2018). Here, we hypothesized that different chromatin states exist for McSCs and their progenitors. We used single-nucleus the assay for transposase-accessible chromatin with sequencing (snATAC-seq) to characterize molecular

signatures underlying behaviors of McSCs and their progenitors under different stages of hair follicle cycle-induced proliferation and after UVB-irradiation. Melanocytes comprise a very small proportion in the skin, necessitating their purification. However, it is challenging to isolate pure melanocyte populations even with exclusion of many different cell type markers (Infarinato *et al.*, 2020). Therefore, we used *Dct*-rtTA; Tre-H2B-GFP transgenic mice, in which the tetracycline activated artificial transcription factor rtTA expressed from the *Dct* promoter, is used to drive nuclear expression of H2B-GFP, marking melanocyte lineages (Zaidi et al., 2011). Then we performed snATAC-seq on GFP+ melanocytes isolated from skin at different stages of the hair follicle cycle and after UVB irradiation of mice. Our data provide a comprehensive map of chromatin accessibility in qMcSC, aMcSC, and dMC. We characterized them by identifying enriched genes, transcription factor binding motifs, and putative *cis*-regulatory elements in each population. Specifically, features uniquely enriched in aMcSC can be potential regulators for McSC activation and migration induced by UVB. Our data show how chromatin accessibility are regulated by intrinsic cues of the hair follicle cycle and by extrinsic environmental stimuli such as UVB and can be used in the future studies to study the function of potential regulators in controlling McSC stemness, activation and differentiation.

Results

Isolating and identifying melanocyte lineages

We isolated melanocyte lineages from mice in telogen phase, anagen phase after depilation, and after three exposures to UVB during telogen (Fig. 1a). To isolate melanocyte lineages, we used *Dct*-rtTA; Tre-H2B-GFP mice in which all melanocyte lineages have nuclear labeling with GFP. We first isolated skin, prepared a single-cell suspension using collagenase, and extracted nuclei from dorsal skin. Then GFP+ nuclei were sorted by fluorescence-activated nuclei sorting (FANS), followed by snATAC-seq library preparation and sequencing (Fig. 1b). To see if the distribution of melanocyte lineages is consistent with our expectation (Fig. 1c), we confirmed the localization of GFP+ cells in the hair bulge in telogen and in the hair bulb in anagen, and some actively migrating to the epidermis after UVB exposure (Fig. 1d).

After applying quality control cutoffs (Fig. S1a,b), we acquired chromatin accessibility profiles from 14,674 cells (telogen 2,585 cells, anagen 5,474 cells, UVB 6,615 cells). By unsupervised clustering of the snATAC data after dimensional reduction, 8 clusters were identified (Fig. 2a). To assign cell types to the clusters, we used gene ontology (GO) enrichment for the top 100 differentially accessible genes from each cluster, which provides insights into biological processes (Fig. S2a). We then confirmed the cell type assignment using known marker genes (Fig. S2b). We noted that despite FANS, which enabled melanocyte enrichment, nuclei from additional skin cell types were present in the enriched population. Among 8 clusters, three clusters exhibited robust accessibility of *Dct* gene, the lineage marker for melanocyte, and increased accessibility of peaks in the *Dct* promoter, not observed in other

clusters (Fig. 2b,c). Therefore, we attribute these three clusters (melanocyte1-3) as melanocyte lineages.

The cell type annotation was consistent with the cell type identities predicted by publicly available mouse skin scRNA-seq (Joost *et al.*, 2020) (Fig. S2c). Yet, only one of the three clusters we identified as melanocytes (melanocyte 1-3) was predicted as melanocytes based on mouse skin scRNA-seq data. We reasoned that this could be because of their use of whole skin and their analysis of fewer total melanocytes from mouse skin scRNA-seq data.

Single-cell chromatin profiling of three melanocyte lineages

Next, we focused on the three melanocyte lineages and re-clustered 5,695 cells (Fig. 2d). Then we assigned predicted cell states to the three clusters based on the expected cell proportion from the hair follicle cycle and after UVB exposure, differential gene accessibility, and motif enrichment. About 96% of cells in dMC were from mice in anagen phase, whereas only 7% of all cells from mice in anagen phase were qMcSC (Fig. 2e). More than 85% of cells from mice exposed to UVB were aMcSC (Fig. 2e). There were also aMcSC from mice in telogen phase, which indicate heterogeneity among McSC populations. In addition to analyzing cell proportion in predefined cell clusters, we used Milo (Dann *et al.*, 2022) to test differential cell abundance between phases and experimental conditions by comparing cell neighborhoods. Compared to the cells from mice in telogen phase, the cells from mice in anagen phase had more dMCs, while aMcSC were more abundant after UVB exposure (Fig. 2f,g). Moreover, we compared the melanocyte cell type categorizations based on our ATAC-seq data to the previous scRNA-seq data from sorted McSC (telogen around P60), aMcSC (anagen at P21), and McSC progeny (anagen at P10)

(Infarinato *et al.*, 2020). We found that the majority of the cells predicted as qMcSC were found in qMcSC cluster (Fig. S2d). Then we compared accessibility of “stemness” and “differentiation” genes identified from the scRNA-seq data (Infarinato *et al.*, 2020). qMcSC showed high accessibility of genes including *Sbno2,* whereas dMC exhibited higher accessibility on genes involved in melanocyte differentiation and melanin synthesis such as *Mitf*, *Kit*, *Tyrp1*, *Tyr*, *Mlana*, *Mc1r*, and *Oca2* (Fig. 2h).

Distinct gene accessibility profiles of melanocyte lineages

Having identified the melanocyte lineages in our data, we compared the accessibility of genes between one cell population to other cell populations to further understand the molecular heterogeneity among three melanocyte lineages. Comparison of the relative gene accessibility revealed that *Lamb1*, *Col27a1*, *Mbp*, *Kcna1*, *Kcna5*, *Kcnj10*, and *Kcnh8* were relatively more enriched in qMcSC, whereas *Trpm1*, *Oca2*, *Pde10a*, *Slc24a4*, *Slc7a8*, and *Ago2* were more accessible in dMC (Fig. 3a,b). Consistently, the genes more accessible in dMC were indeed more expressed in melanocytes compared to other cell types in mouse skin and McSC progeny among McSC lineages based on publicly available scRNA-seq data (Infarinato *et al.*, 2020; Joost *et al.*, 2020) (Fig. S2e,f). To confirm our analysis, we performed immunofluorescence of Laminib1 (LAMB1) and Argonaute2 (AGO2) and quantified GFP+ melanocytes with overlapping LAMB1 or AGO2 expression (Fig. S3a-d). We observed a higher proportion of melanocytes overlapped with LAMB1 in the hair bulge in telogen phase, while a higher proportion of melanocytes overlapped with Argonuate2 in the hair bulb in anagen phase. In addition to finding differences in qMcSC and

dMC, we found aMcSCs had higher accessibility at *Ldb2*, *Dnm3*, *Cubn*, *Leprel1*, and *Sema3a* (Fig. 3c).

Next, we performed GO analysis of the top 50 differentially accessible genes from each cluster (Fig. 3d). The genes with higher accessibility in qMcSC were associated with axonogenesis and gliogenesis, consistent with their neural crest origin, and their identity as an earlier melanocyte progenitor. The genes more accessible in dMC were involved in pigmentation and melanin biosynthetic process, suggesting these are more mature and differentiated compared to the other two clusters. The genes relatively more accessible in aMcSC were involved in regionalization and stem cell differentiation, consistent with their transitioning from progenitors to melanocytes that can produce melanin.

Sema3a, a gene encoding a secreted protein Semaphorin3A (SEMA3A), was one of the genes more accessible in aMcSC from mice exposed to UVB. *Sema3a* is known to regulate axon/dendrite growth and neuronal migration as well as promote hepatocellular carcinoma and glioblastoma proliferation and migration by autocrine and paracrine actions (Bagci et al., 2009; Chen et al., 2008; Hu et al., 2016; Shelly et al., 2011). As SEMA3A can modulate intercellular communication between the same or different cell types in both autocrine and paracrine fashions, we performed cell-cell interaction analysis using CellChat (Jin *et al.*, 2021). For this analysis, we used all other cell types found in our snATAC-seq data except for dMC as there are only few cells from mice exposed to UVB. The analysis revealed that SEMA3 is one of the significant cell-to-cell interactions sent from aMcSC (Fig. S4a,b). Given the role of *Sema3* in other systems and the cell-cell communication analysis, it is possible that SEMA3 signaling might play a role in McSC activation and migration in the skin after UVB activation.

Changes in accessibility at transcription factor binding motifs

We next analyzed the changes in transcription factor motif enrichments at sites of differentially accessibility among three melanocyte lineages (Fig. 3e). We found nuclear factor I (NFI), Specificity protein (SP), and Krüppel-like factor (KLF) family motifs were enriched in qMcSC. A recent study suggested that NFI factors as candidate regulators of stemness by governing chromatin accessibility of master transcription factors regulating stemness genes in hair follicle stem cells (Adam et al., 2020). They also showed that stemness chromatin landscape is lost in the isolated bulge stem cells from NFIB/NFIX knockout mice (Adam *et al.*, 2020). KLF family was shown to regulate pluripotent state of mouse embryonic stem cells (Jiang et al., 2008). Especially, KLF2, KLF4, and KLF5 were shown to regulate expression of key pluripotency factors such as OCT4, SOX2 and Nanog (Jiang *et al.*, 2008). We also examined relative accessibility of genes encoding the transcription factors identified from the motif analysis (Fig. 3f). It showed that many genes encoding the motifs enriched in qMcSC were relatively more accessible in both qMcSC and aMcSC. Collectively, these transcription factors might play key roles in maintaining stemness of McSC. In contrast, binding motifs for MITF, TCF7, and LEF1 family were enriched in dMC. This is in accordance with the results from a recent ATAC-seq data from FACS-purified qMcSC in telogen in the hair bulge and McSC progeny in anagen hair bulb (Infarinato *et al.*, 2020). Consistently, the gene accessibilities of *Mitf*, *Tcf7*, and *Lef1* were relatively higher in dMC (Fig. 3f). MITF is a key transcription factor for melanocyte differentiation and regulates expression of pigmentation genes (Kawakami and Fisher, 2017). LEF/TCFs mediate the activity of nuclear β-catenin and canonical Wnt signaling, activating

MITF and promoting melanocyte proliferation and McSC differentiation (Behrens et al., 1996; Guo et al., 2016).

To understand the potential regulatory mechanisms underlying McSC activation, we identified transcription factor motifs enriched in aMcSC. We found transcription factor AP2 (TFAP2) binding sites were relatively enriched in aMcSC after UVB exposure (Fig. 3e). Mutations in *Tfap2a* gene lead to premature hair graying in human and showed defects in melanocyte differentiation in mice and zebrafish (Praetorius et al., 2013; Seberg et al., 2017). Moreover, *Tfap2b* was shown to be essential for McSC-dependent melanocyte regeneration in zebrafish (Brombin et al., 2022). In chick neural crest cells, TFAP2B was enriched in migratory cranial neural crest cells (Bhattacharya et al., 2020). It was shown that TFAP2 binding sites are enriched during differentiation of mouse embryonic stem cells and TFAP2 can bind to nucleosomes and regulate chromatin condensation (Fernandez Garcia et al., 2019; Sherwood et al., 2014). Specifically, among the TFAP2 family, *Tfap2a* gene was relatively more accessible in aMcSC (Fig. 3f).

To identify potential functions of TFAP2A in aMcSC, we identified overlapping peaks that are more enriched in aMcSC compared to qMcSC or dMC with TFAP2A binding motifs obtained from TFAP2A ChIP-seq data from mouse Melan-A cells (Seberg *et al.*, 2017). Almost 50% of aMcSC-specific peaks compared to qMcSC have binding motifs for TFAP2A, and the nearest genes to these peaks are associated with melanocyte differentiation and neural crest cell migration (Fig. 4a). More than 50% of aMcSC-specific peaks compared to dMC overlapped with TFAP2A binding sites, and the nearest genes to these peaks are involved in vasculature development and epithelial migration (Fig. 4b). Lastly, we found that the significantly enriched peaks in

aMcSC within *Sema3a* and *Sema3c* genes were binding motifs for TFAP2A (Fig. 4c,d). It was reported that TFAP2A binding sites were more likely to be found within introns (Seberg *et al.*, 2017). Furthermore, TFAP2 paralogs function as pioneer factors for MITF (Kenny et al., 2022). Overall, TFAP2A might play important roles in McSC activation as transcription factors and pioneer factors.

Discussion

Here we provide a comprehensive chromatin accessibility landscape of melanocytes at different stages of the hair follicle cycle and after UVB irradiation of mice at single-nucleus resolution. Our analyses show changes in cell abundances, gene accessibility, and motif enrichment of three melanocyte lineages by intrinsic cues of the hair follicle cycle and by extrinsic environmental stimuli. Our data suggest a potential gene regulatory network underlying McSC maintenance, activation and differentiation.

We identified that *Lamb1* and *Ago2* were more accessible in qMcSC and dMC respectively (Fig. 3a,b). Consistent with our findings, LAMB1 was more expressed in hair bulge where most of qMcSCs are located, whereas AGO2 was more expressed in hair bulb where dMCs are found (Fig. S3a-d). Yet, the roles of *Lamb1* and *Ago2* in melanocyte function remain to be further studied. Laminins are extracellular matrix (ECM) glycoproteins (Lee et al., 2021). *Lamb1* was shown to be involved in cell proliferation and invasion in several cancers (Lee *et al.*, 2021). These outcomes in cancers may be consequences of imbalances of expression of laminins, leading to dysregulated cell proliferation and localization. *Lamb1* may help preserve the quiescent state and tissue localization of qMcSCs under normal conditions. Argonaute proteins are known for their roles in RNA-mediated gene silencing (Hutvagner and Simard, 2008).

Our finding about *Ago2* raises the possibility that changes in microRNA (miRNA) regulation may be important for emergence or functions of dMCs. This may motivate the characterization of cluster-specific miRNA expression and identification of their target genes.

In our study, *Sema3a* was identified to be more accessible in aMcSC compared to other melanocyte lineages. Yet, what extent *Sema3a* regulates activation and migration of aMcSC after UVB irradiation needs to be further studied. The effects of SEMA3A on McSC activation and migration can be assessed by using a wound healing assay with adding exogenous SEMA3A or using siRNA knockdown of endogenous SEMA3A, as it was previously tested in cultured fibroblasts (Jeon et al., 2020). Additionally, for *in vivo* study, mice can be treated with a SEMA3A inhibitor SM-345431 (vinaxanthone) (Omoto et al., 2012) to block SEMA3 signaling and McSC activation can be compared to control mice.

SEMA3 signaling between aMcSc and fibroblast2 was inferred by our cell-cell interaction analysis. It revealed that aMcSC is likely to send SEMA3 signals to fibroblast2. Fibroblast2 is a subpopulation of fibroblasts that is more abundant in mice exposed to UVB (Fig. S4c). It was reported that UVB can cross the epidermis and reach the upper dermis which is mainly composed of fibroblasts (Rosette and Karin, 1996). Compared to fibroblast1, genes that are more accessible in fibroblast2 are associated with ECM remodeling (Fig. S4d). The ECM is a pivotal factor for regulating cell migration through the matrix by the neural crest cell-ECM interaction (Perris, 1997). Moreover, it was reported that SEMA3A can regulate TGFβ-induced myofibroblast differentiation and ECM production (Jeon *et al.*, 2020). Overexpression of TGFβ was shown to increase migration and invasion of colorectal cancer (Chuo et al., 2019). We also found

that genes involved in TGFβ signaling, especially *Tgfbr3* were relatively more enriched in fibroblast2 (Fig. S4e). Collectively, it is tempting to speculate that the local cell signaling between fibroblast2 and melanocyte might be a potential mechanism how UVB phototherapy stimulates McSCs in the hair bulge to undergo activation and migrate upwards.

Our current study using a genomic assay is limited by the requirement for cell dissociation from tissues and thus losing spatial context. Although the melanocyte cell states are predictable since quiescence, activation, and differentiation of melanocytes can be controlled by activation of anagen phase by depilation or activation of McSCs by UVB irradiation, we do not match spatial location with their chromatin states characterized in our study. Although we validated our findings by staining two markers LAMB1 and AGO2, it is highly desirable if we can map multiple molecular markers within the same spatial contexts. In the future studies, spatial genomic methods can be used to characterize the rare melanocyte populations in the skin by profiling the gene activity in a tissue sample, while preserving spatial location of the cells. Specifically, MERFISH (Chen et al., 2015) or seqFISH (Lubeck et al., 2014) can be used to profile the mRNA expression level at single-cell resolution.

In summary, snATAC-seq identified potential gene markers for melanocyte cell lineages and transcriptional regulators for McSC stemness, activation, and differentiation. Our results suggested a potential mechanism for activation of McSC through SEMA3 signaling pathway. Future studies may illuminate whether such mechanism might be a key regulator for McSC activation and migration induced by UVB irradiation. Our study identified regulatory sequences that are specifically enriched in a specific cell type and generated biological hypotheses for manipulating cell types *in vivo* to address unsolved questions.

Materials and Methods

Animals

All animal experiments were performed in accordance with protocols approved by the Institutional Animal Care and Use Committee (IACUC) at Cornell University (IAUCU #2014-0096). 7-week-old *Dct*-rtTA; Tre-H2B-GFP mice were used in this study (Tumbar et al., 2004). For telogen samples, drinking water containing doxycycline (20 mg dissolved in 100 ml sterilized water) was continuously provided for 5 days. For chemical depilation, mice were shortly anesthetized using isoflurane and the level of oxygen and isoflurane was controlled by Matrx VIP3000 vaporizer. Before chemical application, hairs on the dorsal skin were first shaved using a small animal clipper, then hair remover lotion (Nair cream) was applied onto the dorsal skin region. After hair removal, the skin was gently wiped with wet tissues to prevent any cutaneous irritation by Nair cream. After anagen development reaching anagen stage, drinking water containing doxycycline (20 mg dissolved in 100 ml sterilized water) was continuously provided for 5 days. For UVB irradiation, mice were provided with drinking water containing doxycycline (20 mg dissolved in 100 ml sterilized water) for 5 days and irradiated with UVB (2.2mJ/cm^2) on the dorsal skin three times a week.

Tissue immunostaining

Dorsal skins were collected and fixed in 10% neutral buffered formalin at 4°C overnight. Tissues were embedded in OCT compound (Tissue-Tek) and snap-frozen on dry ice. After fixing frozen tissues in 10% neutral buffered formalin for 10 min, tissues were sectioned 7μm. The sections were serially washed

(rehydrated) with PBS twice for 10 mins. Fluoroshield mounting medium with DAPI (Abcam) was used for nuclei staining. For LAMB1 and AGO2 immunostaining, the sections were blocked with 10% normal donkey serum in PBST. Primary antibodies were diluted in blocking buffer and incubated with anti-LAMB1 (Abcam) and anti-AGO2 (Abcam) at 4°C overnight. After washing with PBST, the sections were than incubated with fluorochrome conjugated secondary antibodies: Alexaflour 488- or 594- conjugated donkey anti-rabbit or anti-rat IgGs (Abcam and Thermo Fisher) at room temperature for 60min. Images were captured using a Leica DM2500 upright microscope with a DFC7000T camera.

Nuclei isolation from mouse dorsal skin

Isolation of epidermal cells from mouse dorsal skin was performed as described previously (Soteriou et al., 2016). Hairs on mouse dorsal skin were shaved using clippers. Dorsal skin was collected and fat tissue under the dermis was removed using a blunt scalpel. The skin was then incubated in 4 mL of prewarmed Collagenase I (20 mg/mL in DMEM/F-12) at 37°C for 1 hour. 3 mL of keratinocyte serum-free medium (KSFM-Ca++) was added into cell suspension. The cell suspension was filtered using 100 μM cell strainer and the chunks were incubated in 2 mL of Trypsin/EDTA 0.25% solution for another 10 min. The cell suspension was filtered using 40 μM cell strainer and then centrifuged for 10 min at 200 g at 4°C. The pellet was washed with PBS and centrifuged for 10min at 200 g at 4°C. The cell pellet was resuspended in 1 mL of PBS and centrifuged for 5 min at 300 g at 4°C.

After cell isolation, nuclei isolation was performed as described previously (Corces *et al.*, 2017). Cell pellets were resuspended in 100 uL of cold ATAC-

seq resuspension buffer (10 mM Tris-HCl pH 7.4, 10 mM NaCl, and 3mM $MgCl_2$ in water) containing 0.1% NP40, 0.1% Twwen-20, and 0.01% digitonin, and then, centrifuged for 10 min at 500 g in a pre-chilled (4°C) fixed-angle centrifuge. After removing the supernatant, nuclei were resuspended in 1 mL PBS buffer and filtered through 40 μM cell strainer. GFP+ nuclei were collected using a BD FACS Aria Fusion.

snATAC-seq with combinatorial indexing

Based on collected volume from FANS, 5X Tagmentation buffer (50mM Tris pH 7.5, 25mM $MgCl_2$, 50% DMF, 0.5% Tween 20, 0.05% Digitonin) was added to be final 1.25X. Nuclei concentration was adjusted to about 1,000 nuclei per well based on FANS estimated number of nuclei. 8 μL of nuclei were distributed into each well of a 96-well plate containing 1 μL of each ME-A or ME-B carrying barcoded transposome per well at ~1.5 μM. Tagmentation was performed at 50°C for 30 min. Following tagmentation, 10 μL of 40 μM EDTA was added and the plate was incubated at 37°C for 15 min to terminate the Tn5 reaction. After adding 10 μL of sort buffer (2 % BSA and 2 mM EDTA in PBS), all wells were pooled and centrifuged for 5 min at 500 g. Nuclei were resuspended in 1 mL of sort buffer, filtered through a 35 μm mesh (352235, Corning) and stained with 3 μM Draq7 (ab109202, Abcam). 20 Draq7+ nuclei were sorted into each well of another 96-well plates containing 16.5 μL of elution buffer (2 % BSA and 10 mM Tris pH 8.0) using a BD FASC Melody. After sorting, plates were frozen at -80°C.

After thawing, 2 μL of 0.2% SDS was added and the plate was incubated for 7 min at 55°C followed by adding 2.5 μL of 10% Triton X-100. For PCR amplification, 1.5 μL of 25 μM Primer i5 and 1.5 μL of 25 μM Primer i7 were added and the plate was gently vortexed and spun down briefly. 25 μL of PCR

mix (Q5 DNA polymerase (M0491, NEB), 2 mM dNTP, Q5 buffer and 1X GC Enhancer) were added. PCR was performed using the following protocol: 72°C 5 min, 98°C 30 sec, 17 cycles of: [98°C 10 sec, 63°C 30 sec, 72°C 30 sec], 72°C 5 min, held at 4°C. Amplified DNA libraries were pooled and purified using MinElute columns (28004, Qiagen) using a vacuum apparatus (19413, Qiagen). Size selection was performed using Ampure XP Bead (A63880, Beckman Coulter). Libraries were sequenced on a mid-lane output PE 150bp on a Nextseq500 sequencer (Illumina) with custom recipe for the following, read 1: [36 imaged cycles], Index 1: [8 imaged cycles, 27 dark cycles, 8 imaged cycles], Index 2: [8 imaged cycles, 21 dark cycles, 8 imaged cycles], Read 2: [36 imaged cycles].

snATAC-seq data pre-processing

Fastq files were demultiplexed by adding cell barcodes to each read. Then demultiplexed reads were aligned to mm10 using Bowtie2 and sorted by read name using samtools. Pair-end reads with mapping quality lower than 30 and improperly paired or duplicated fragments were filtered out. Cells with less than 1,000 reads and smaller than 5 transcription start stie (TSS) enrichment score were removed further. After identifying initial clusters with cell-by-bin (window) matrix, peak calling was performed using MACS2 callpeak (Zhang *et al.*, 2008). Gene activity was predicted by counting the reads on the gene coordinates extended to include the 2kb upstream.

Identification of cell clusters and cell type annotation

Total of 14,674 cells from 8 Anagen mice (3F, 5M), 13 Telogen mice (7F, 6M), 15 UV mice (7F, 8M) passed quality control (reads per cell > 1,000 and

TSS enrichment score > 5). Then we used cell-by-peak matrix normalized by a TF-IDF transformation for shared neighbor network (SNN) graph-based clustering with the top 30 principal components except for the first principal component (Hao *et al.*, 2021; Stuart *et al.*, 2019). Cell clusters were visualized by uniform manifold approximation and projection (UMAP). This revealed 8 major clusters.

To resolve identities of the cell clusters, we first identified sets of genes or peaks enriched in individual cell clusters in comparison with all other cell clusters by differential accessibility analysis using 'FindAllMarker' or 'FindMarker' function in Signac (Stuart *et al.*, 2021). GO term enrichment analysis was performed on a set of enriched genes (adjusted p-value or FDR < 0.05 and absolute log2 fold change > 1.2) with ClusterProfiler (Yu *et al.*, 2012). After annotating cell types based on snATAC-seq data, we confirmed the cell type annotation with publicly available scRNA-seq data of mouse skin and scRNA-seq data of FACS-purified melanocytes. To transfer cell labels from the reference scRNA-seq and snRNA-seq data, scRNA-seq and snRNA-seq datasets were integrated with our snATAC-seq using SCTransform after normalizing two datasets (Hao *et al.*, 2021; Stuart *et al.*, 2019).

Cell abundance test with Milo

We performed differential cell abundance test between two hair follicle phases and after UVB exposure using Milo (Dann *et al.*, 2022). Milo identifies cell neighborhoods based on the k-nearest neighbor graph and assigns cells to the neighborhoods. The number of cells in neighborhoods were counted and log-fold changes between two experimental conditions were calculated.

Transcription factor motif analysis with chromVAR

Motif activity scores were computed by chromVAR (Schep *et al.*, 2017). To identify potential regulatory sequences for each cell type, differentially enriched motifs among cell types were identified by computing average differences in *z*-score.

Co-accessibility with Cicero

We predicted *cis*-regulatory networks by cicero, a R package assessing co-accessibility pairs of DNA elements (Pliner *et al.*, 2018). It calculates co-accessibility between open regulatory elements across groups of cells and links a promoter to its potential distal enhancer.

Inference of cell-cell interaction with CellChat

To infer potential cell-cell interactions from our snATAC-seq data, gene accessibility of ligands and receptors from a literature-supported signaling interaction database ('CellChatDB') was used (Jin *et al.*, 2021). Significant communications were predicted by identifying differentially accessible ligands and receptors for cell clusters and associating interaction pairs with probability values.

Publicly available scRNA-seq and ChIP-seq data availability

Publicly available scRNA-seq data were obtained from NCBI Gene Expression Omnibus (GEO). The published scRNA-seq data of mouse skin was obtained from GEO accession number GSE129218 (Joost *et al.*, 2020). The published scRNA-seq data of sorted melanocytes was obtained from GEO accession number GSE147299 (Infarinato *et al.*, 2020). The published TFAP2A

ChIP-seq data of mouse immortalized melanocytes was obtained from GEO accession number GSE72953 (Seberg *et al.*, 2017).

Figures

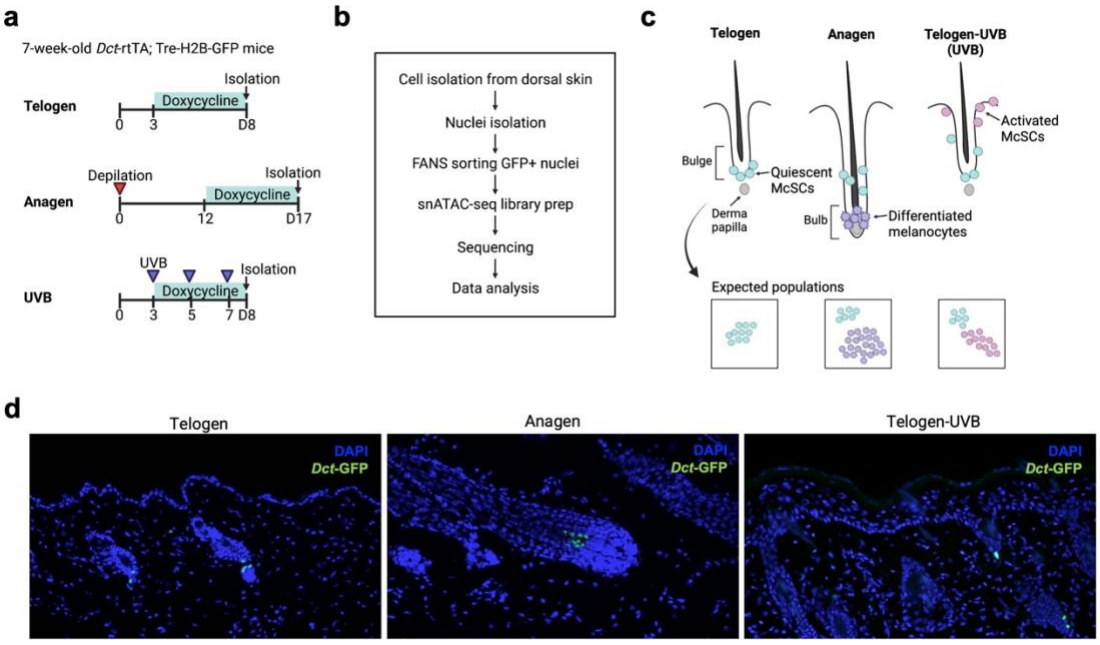

Figure 1

Melanocyte lineages throughout hair follicle cycle and UVB irradiation.

a,**b**, Experimental approach to isolate melanocytes from skin at different stages of the hair follicle cycles (telogen and anagen) and after UVB irradiation of mice and to generate snATAC-seq library. **c**, Schematic of melanocyte cell states in telogen and anagen phase of the hair follicle cycles and after UVB exposure. **d**, GFP lineage tracing and immunostaining of DAPI in telogen and anagen phase and after UVB exposure. Location of melanocyte lineages are shown by expression of *Dct*-GFP at the hair bulge and hair bulb.

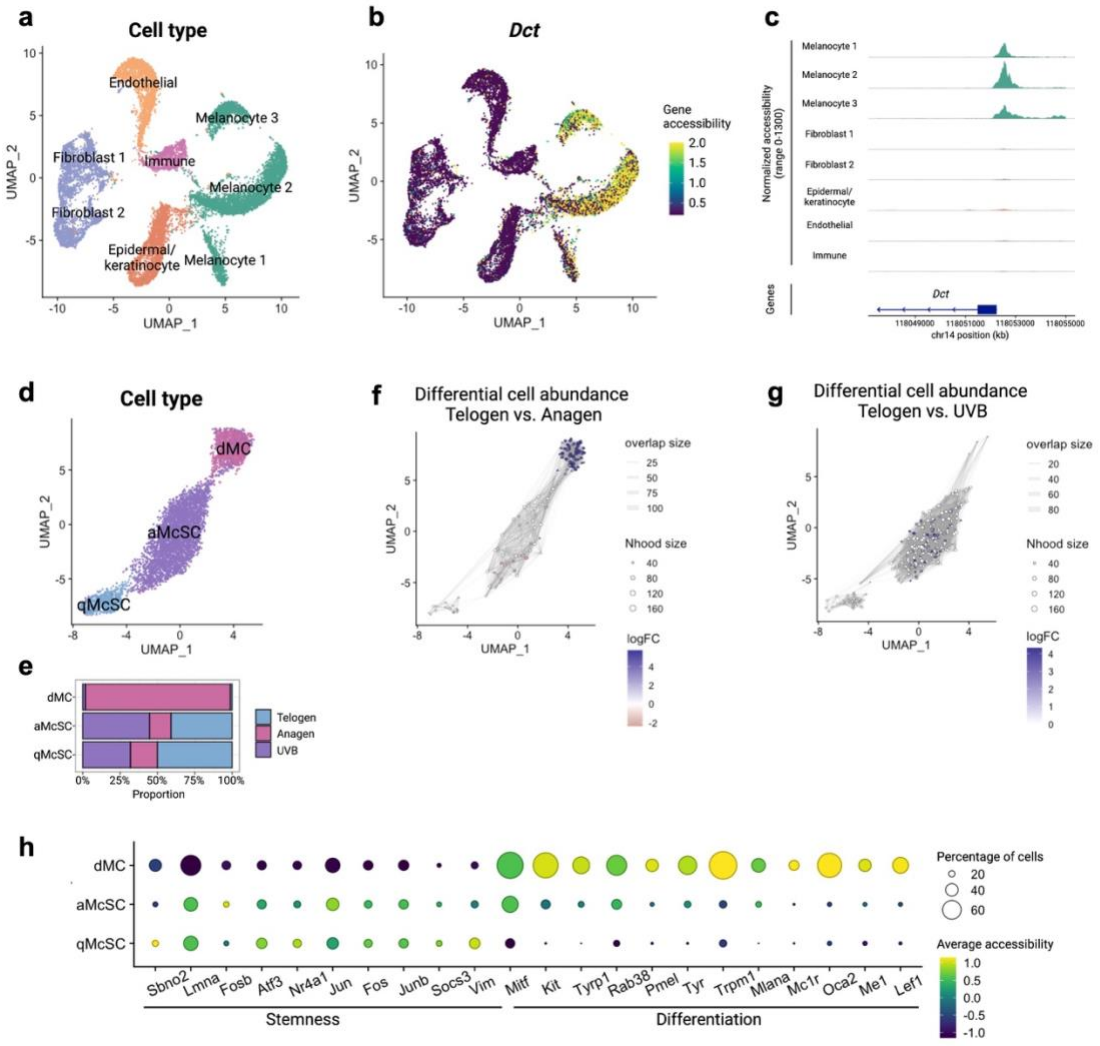

Figure 2

Single-nucleus chromatin accessibility of melanocyte lineage cells.

a, UMAP plot of 14,674 cells (telogen 2,585 cells, anagen 5,474 cells, UVB 6,615 cells) that passed quality control. 8 different clusters were identified by unbiased clustering and colors represent 5 major cell types. **b**, UMAP plot of *Dct* gene accessibility. **c**, Genome tracks showing aggregated snATAC-seq profiles near the *Dct* locus in 8 different clusters. **d**, UMAP plot of 5,695 cells from the three melanocyte clusters. Colors represent three melanocyte lineage cell clusters. **e**, Relative cell proportion of cells from mice in telogen and anagen

phase or after UVB exposure. **f**,**g**, Milo analysis (Dann *et al.*, 2022) of cell neighborhood abundance changes in anagen phase (**f**) or after UVB exposure (**g**) compared to telogen phase. Size of points (Nhood size) represents the number of cells in a neighborhood; Thickness of lines (overlap size) indicates the number of cells shared between neighborhoods. Colors indicate the log-fold differences (logFC). The more purple colors indicate, the more cells were for a neighborhood in anagen phase (**f**) or after UVB exposure (**g**). **h**, Normalized gene accessibility of stemness and differentiation genes.

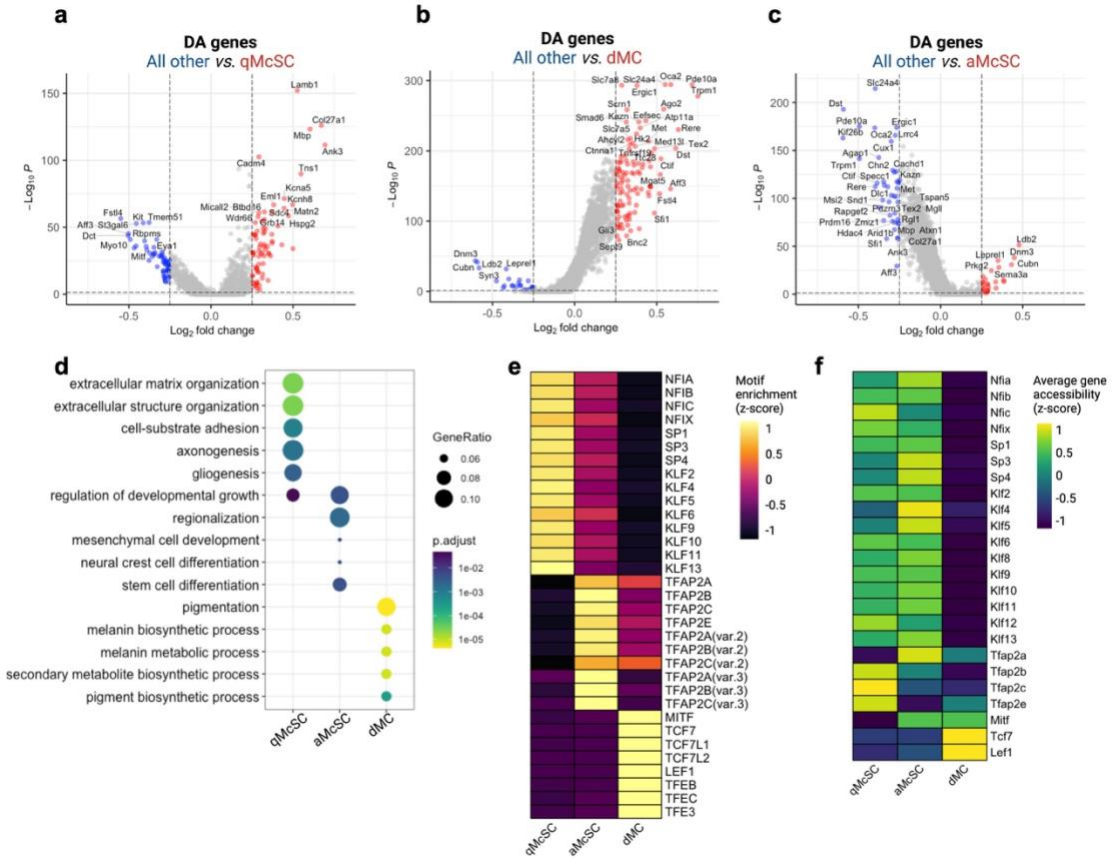

Figure 3

Differential gene accessibility and transcription factor motif of three melanocyte lineages.

a-c, Gene accessibility differences for each melanocyte lineage cell cluster compared to other melanocyte lineage cells. Positive log2-fold change indicates increased accessibility in qMcSC (**a**), dMC (**b**), and aMcSC (**c**). **d**, Gene ontology (GO) enrichment for biological process for the top 50 most significantly more accessible genes. **e**, Transcription factor motif enrichment in differentially accessible peaks. **f**, Normalized accessibility of genes encoding the transcription factors that have enriched binding sites from the motif analysis.

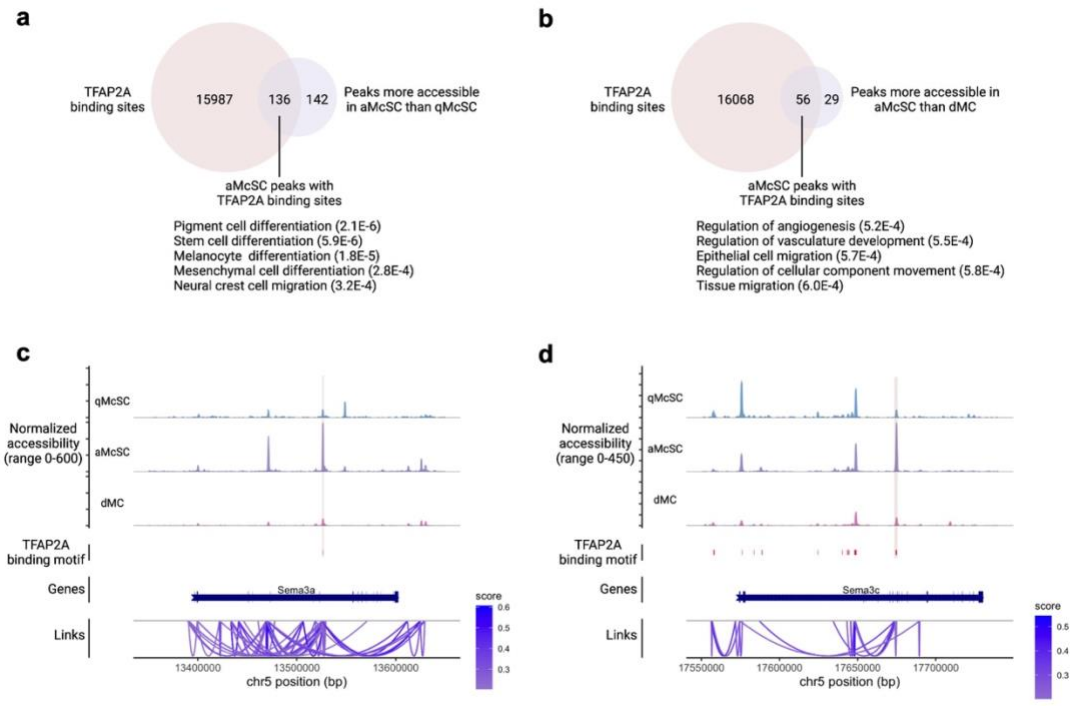

Figure 4

Enrichment of TFAP2A motifs in activated McSCs-specific peaks.

a,**b**, Number of TFAP2A binding sites from publicly available ChIP-seq data of mouse immortalized melanocytes (Seberg *et al.*, 2017) overlapping with peaks enriched in aMcSC compared to qMcSC (**a**) and dMC (**b**). Gene ontology (GO) enrichment for biological process using the nearest genes (<100kb) to the peaks enriched in aMcSC having TFAP2A motifs. **c**,**d**, Genome tracks showing aggregated snATAC-seq profiles near the *Sema3a* locus (**c**) and *Sema3c* locus (**d**). Red boxes represent TFAP2A binding motifs from publicly available ChIP-seq data (Seberg *et al.*, 2017). Links show *cis*-coaccessibility of peaks.

Supplementary figures

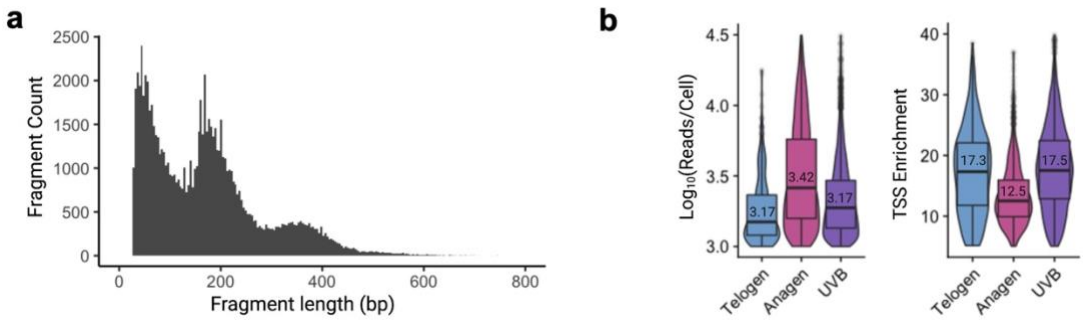

Supplementary Figure 1

Quality control metrices of snATAC-seq data.

a, Fragment size distribution plot of snATAC-seq data. **b**, Fragment count distributions and transcription start site (TSS) enrichment per cell from mice in telogen and anagen phase and after UVB exposure. Cells with 1,000 or more fragments and 5 or more TSS enrichment were used in this study. The median fragment count and TSS enrichment for each experimental condition are indicated.

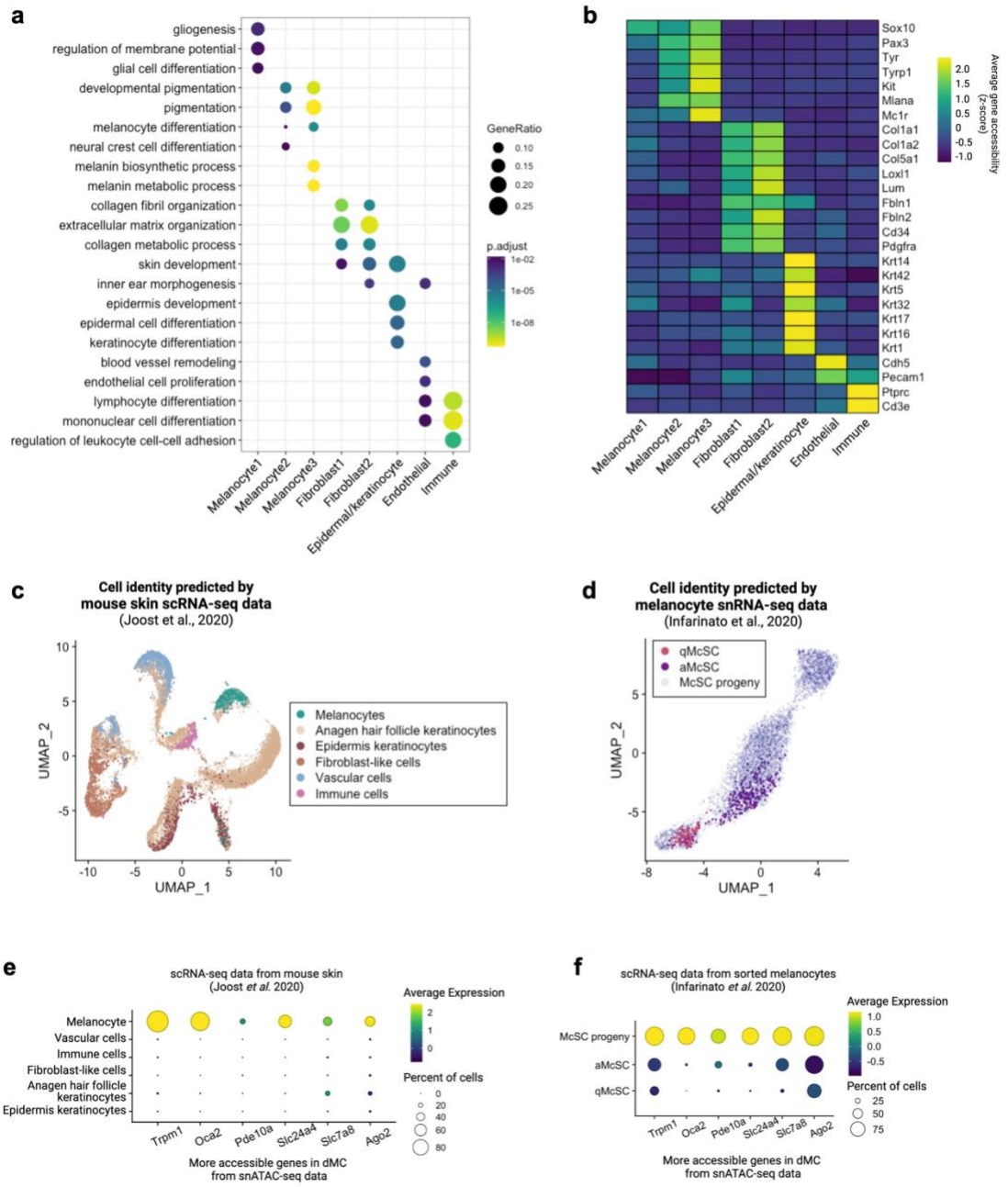

Supplementary Figure 2

Cell type identification.

a, Gene ontology enrichment for biological process for the top 50 most significantly more accessible genes in each cluster. **b**, Heatmap of normalized accessibility of cell-type marker genes. **c**, UMAP plot of cells colored by

predicted cell types from publicly available mouse skin scRNA-seq data (Joost *et al.*, 2020). **d**, UMAP plot of melanocyte lineage cells colored by predicted cell types from publicly available scRNA-seq data from sorted melanocyte lineage cells (Infarinato *et al.*, 2020). **e**,**f**, Average expression of genes more accessible in dMC in snATAC-seq data from publicly available scRNA-seq data from mouse skin (Joost *et al.*, 2020) (**e**) and sorted melanocyte lineage cells (Infarinato *et al.*, 2020) (**f**).

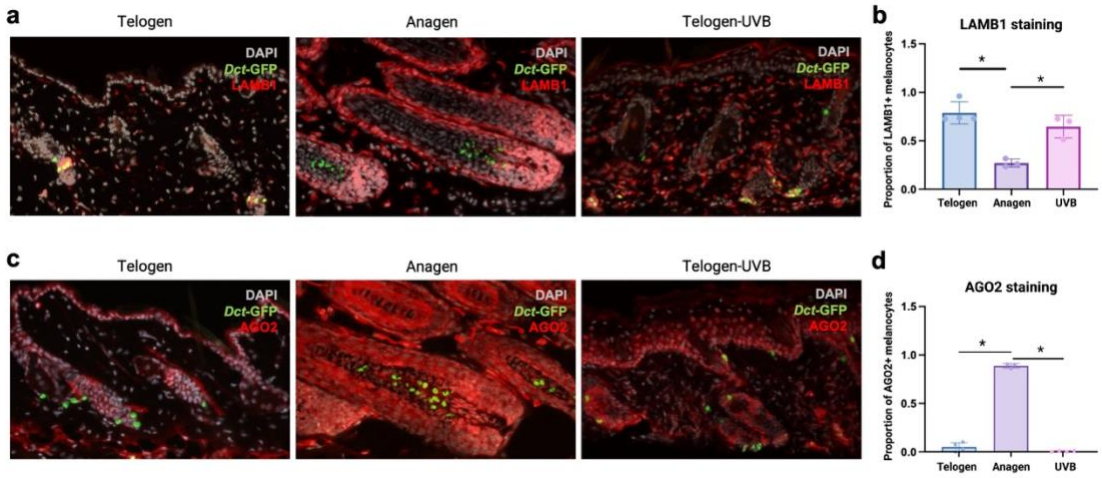

Supplementary Figure 3

Immunostaining of LAMB1 and Argonaute2.

a, Immunostaining of LAMB1 in telogen and anagen phase and after UVB exposure. Melanocyte lineages are shown by expression of *Dct*-GFP at the hair bulge and hair bulb. DAPI (grey), *Dct*-GFP (green) and LAMB1(red). **b**, Proportion of GFP+ melanocytes overlapped with LAMB1. *p-value < 0.05 by t-test. **c,** Immunostaining of AGO2 in telogen and anagen phase and after UVB exposure. DAPI (grey), *Dct*-GFP (green) and Argonuate2 (red). **d**, Proportion of GFP+ melanocytes overlapped with Argonaute2. *p-value < 0.05 by t-test.

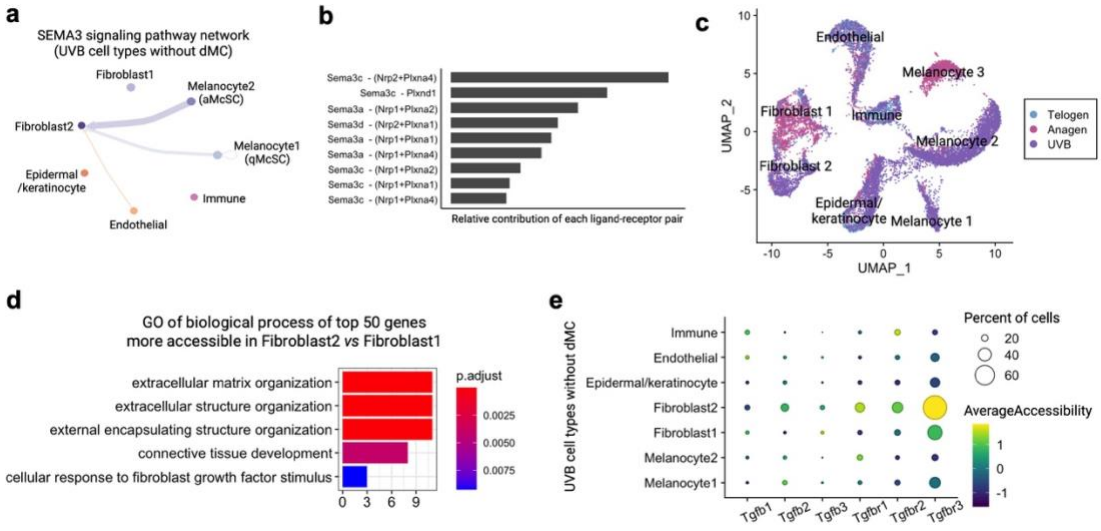

Supplementary Figure 4

Cell-cell interaction analysis of the SEMA3 signaling between activated McSCs and fibroblast2 after UVB irradiation.

a, Circle plot displaying SEMA3 signaling pathway network inferred by gene accessibility of ligand-receptor pairs among the cell types from mice exposed to UVB without dMC using CellChat (Jin *et al.*, 2021). The colors of circles and lines represent the senders. The arrows indicate the receivers that receive signal from the corresponding senders. The thicker line indicates a stronger signal interaction. **b**, Major contributors of ligand-receptor pairs of SEMA3 signaling network. **c**, UMAP plot of cells colored by hair follicle stages and experimental condition. **d**, Gene ontology (GO) analysis of biological process using the top 50 more accessible genes in fibroblast1 compared to fibroblast2. **e**, Average gene accessibility of *Tgfb* and *Tgfb* receptor isoforms among the cell types from mice exposed to UVB without dMC.

Chapter 4: Extended Discussion

In my thesis, I conducted single-cell analysis of accessible chromatin and characterized adipose tissue and melanocytes under different physiological conditions. Yet, there are many more details to be discovered about the molecular or tissue-level changes arising during adipose beiging and melanocyte activation that could be elaborated by applying additional methodologies. And there are opportunities for further functional validation of our findings that would require manipulations of genes, transcription factors, or enhancers and pathways identified in our study. Therefore, this chapter will focus on discussing these issues. Lastly, a key environmental factor that we are exposed throughout the lifetime is our diet. I will discuss nutrition's effects through epigenetic modifications from a nutritional standpoint.

1. Joint profiling for single-cell multiomics

In my thesis, I showed changes in chromatin accessibility that occur during adipose beiging and melanocyte stem cell activation with unprecedented resolution using snATAC-seq. Although we query the changes in gene activity based on chromatin accessibility and publicly available snRNA-seq dataset, the weakness of this study is that we do not measure changes in gene expression from the same tissues or cells. Although ATAC-seq is closely associated with gene activity, it was also reported that changes in accessibility do not always correlate to increased transcription (Jia et al., 2018), which shows the importance of profiling both within the same cells. Integrating scATAC-seq and scRNA-seq enables us

to identify gene regulatory elements and transcription factors that control gene regulatory networks and understand how genes are expressed. The simultaneous profiling of RNA and chromatin accessibility at single-cell level has the potential to reveal regulatory relationships. As I mentioned in the first chapter, single-cell methods for joint profiling of scATAC-seq and scRNA-seq, such as sci-CAR (Cao *et al.*, 2018), SNARE-seq (Chen *et al.*, 2019b), Paired-seq (Zhu *et al.*, 2019), and SHARE-seq (Ma *et al.*, 2020) successfully correlated changes in accessibility and gene expression. Currently, our lab has optimized our protocol to generate snRNA-seq library from the same tissue or cells after tagmentation. With this, we have begun to jointly profile chromatin accessibility and transcriptomics and applied to different tissue types, disease models, and organisms.

More techniques for joint profiling of multiple classes of molecules or other epigenetic layers together with chromatin accessibility in single cells have been developed. scNMT-seq (Clark et al., 2018) and scNOMeRe-seq (Wang et al., 2021) are approaches that simultaneously profile chromatin accessibility, DNA methylation and transcription. TEA-seq allows joint analysis of chromatin accessibility, transcriptomics, and epitopes (Swanson et al., 2021), while NEAT-seq enables profiling of chromatin accessibility, gene expression, and intra-nuclear proteins (Chen et al., 2022). Profiling each molecular or epigenetic layer provides unique insights into cellular and molecular processes. Single-cell methods that measure more than one type of data enable us to identify the associations between molecular layers, dynamics of epigenome interactions, and regulatory relationships along dynamic trajectories of heterogeneous cell types across developmental or

cell fate transitions. Future studies would benefit from these single-cell multiomics techniques.

2. Imputation of unknown epigenome information

In the second and third chapter of my thesis, I presented several omics data using publicly available scRNA-seq and ChIP-seq datasets. As high-throughput sequencing technologies have become more accessible and more widely used, more data from high-throughput sequencing studies have been deposited in repositories such as the Gene Expression Omnibus (GEO) and European Nucleotide Archive (ENA). These publicly available datasets can be used as references or reanalyzed to provide different biological information content for other studies. However, publicly available experimental datasets are still limited. For example, often only a subset of histone epigenetic marks is experimentally measured. In the second chapter of my thesis, I was able to obtain publicly available H3K27ac and H3K4me1 ChIP-seq data for adipocytes, but not other histone marks such as H3K27me3.

Recently, machine learning approaches have been used to address this problem by leveraging available information from existing datasets. Ocelot (optimized complementation of epigenomes by neural network and tree-based modeling) predicts histone modifications using available ChIP-seq datasets from other cell types of the same histone marks or other histone marks in the same cell types (Li and Guan, 2022). Another recent method imputes histone marks based on nascent transcription (Wang et al., 2022). This method showed high correlation between imputation and experimental

data (Wang *et al.*, 2022). They can be especially useful when experimental data are hard to obtain in the future.

3. Single-cell spatial technologies

In the third chapter of my thesis, I performed snATAC-seq to comprehensively profile the chromatin accessibility of different cell states from melanocyte populations. Despite the advantages of this approach, spatial information is lost as this approach requires dissociation of tissues into cells. Although we took advantage of known cell populations at different hair follicle cycles, anatomic localization of melanocyte stem cells (McSCs) and melanocytes in the hair follicle is one of the most important features that segregate them into different populations and predict their cell states as quiescent, proliferating, and differentiating. Therefore, it would be desirable if we can preserve spatial information and track melanocytes as they migrate, while investigating their chromatin accessibility at single-cell level.

In the second chapter of my thesis, I identified 12 cell types in adipose tissue and revealed cell-cell interaction during adipose beiging. Recent studies have shown that the distribution and localization of cell types in a tissue as well as the spatial pattern are also important for cell-cell communication based on cell contact (Li and Yang, 2022). The neighboring cells are more likely to have some types of interactions than random and non-neighboring cells that are far away from each other within a tissue. Therefore, to reconstruct cell interaction networks in a more comprehensive manner, it is highly desirable to map the spatial localization of the cell types in a tissue. In addition, it was reported that within the same adipose tissue, there is regional variation in beige fat biogenesis revealed by three-

dimensional adipose tissue imaging (Chi et al., 2018). Mapping the spatial localization of different cells will help us discern specific functional domains within a tissue.

Standard histology methods such as Hematoxylin and Eosin (H&E) staining and immunohistochemical antigen labeling have been used to array changes in tissue composition and morphology in adipose tissue sections (Cinti et al., 2001). RNA fluorescence *in situ* hybridization (FISH) (Raj et al., 2006) and RNAscope (Wang et al., 2012) can also be applied to visualize RNA expression of cell type-specific marker genes *in situ*, which help localize cell types in tissue sections. Alternatively, transgenic reporter mouse assays can be used to label specific cell types within a tissue based on cell type-specific genes and enhancers, though developing such reporter mice could be challenging. Nevertheless, the above-mentioned methods are limited by imaging a few molecular or cell types. It is highly desirable if we can correlate changes in genomic, epigenomic, transcriptomic, proteomic and/or metabolic level with spatial context in a tissue.

The limitation can be partially addressed by the recent advances in spatially resolved methods. Capture-based spatial techniques such as Slide-seq (Rodriques et al., 2019) use spatially barcoded oligonucleotides to capture mRNAs from tissue. The spatial information of the mRNAs is encoded by the barcodes, which can be read with mRNA sequence by high-throughput sequencing. In terms of spatial ATAC-seq methods, Spatial-ATAC-seq utilizes microfluidic channels to introduce a set of DNA barcodes to the tissue slide for *in situ* ligation (Deng et al., 2021). In parallel, ATAC-seq method with combinatorial indexing strategy was integrated with multiregional sampling, called sciMAP-ATAC (Thornton et al., 2021). This

preserves spatial information based on the spatial orientation of multiple regions from the tissue collected by microbiopsy sampling and profiles chromatin accessibility of single cells. Nevertheless, the data points obtained by these methods are in near single-cell resolution, not necessarily representing single cells. On the other hand, imaging-based spatially resolved transcriptomic methods, such as multiplexed error-robust fluorescence *in situ* hybridization (MERFISH) (Chen *et al.*, 2015) and sequential fluorescence *in situ* hybridization (seqFISH) (Lubeck *et al.*, 2014), utilize FISH and image mRNA molecules in single cells using combinatorial FISH labeling. Moreover, the spatial transcriptomic technologies have enabled mapping of gene expression and recently have been extended to DNA imaging to capture 3D organization and spatial epigenetic information. DNA-MERFISH enables mapping chromatin structure at the genome scale (Su et al., 2020). And the same group further expanded the spatial tools to identify chromatin loci with epigenetic modifications *in situ* (Lu et al., 2022). A variety of single-cell spatial analysis methods are rapidly evolving and will bridge the gap between single-cell sequencing and spatial analysis in the future.

4. Functional analysis of high-throughput data

Studies in my thesis can be extended in several ways to assess the functional importance of changes in chromatin accessibility we observed. In the second chapter of my thesis, we observed increased accessibility of genes involved in *de novo* lipogenesis (*DNL*) and in fatty acid (FA) elongation, and increased elongation ratio in FA composition correlated with changes in chromatin accessibility. Yet, whether *DNL* in adipose tissue is

essential for beige adipocyte formation and thermogenesis is unclear. To test if impairments in lipogenic genes affect responses to thermogenic stimuli, we can use mice with adipocyte-specific deletion of *Acaca*, a gene encoding ACC in charge of the rate-limiting step in FA synthesis, or *Fasn*, a gene encoding FA synthase. Furthermore, we can also use mice with adipocyte-specific deletion of *Elovl6* to test if longer chain FA production in adipocytes is required for beige adipocyte function. Similarly, in the third chapter of my thesis, I showed that *Sema3a* was more accessible in activated McSCs (aMcSCs). As I mentioned in the discussion of the third chapter, we can use pharmacologic inhibition of endogenous *Sema3a* to block SEMA3A signaling and evaluate the role of SEMA3A signaling in McSC activation and migration.

The above-mentioned studies are mainly focused on protein-coding genes. Gene expression is mediated by coordinated control of *cis*-regulatory elements, such as promoters and enhancers. Differences in the chromatin landscape between cell states and cell types reveal putative regulatory regions that might change gene regulatory architecture substantially. However, there is still a major gap in our knowledge about the function of the noncoding DNA regulatory regions. Moreover, the *cis*-regulatory elements can be bound and regulated by transcription factors. How disrupting transcription factor binding dynamics drive changes in epigenetic state remains to be further studied. In the second and third chapter of my thesis, I identified putative enhancers for adipose beiging and McSC activation on a genome wide scale using snATAC-seq. To assess the importance of the *cis*-regulatory regions, traditional genetic approaches can be used to uncover *cis*-regulatory regions that lead to changes in gene

expression patterns with transgenic mouse reporter assays (Nord et al., 2013). The development of CRISPR-Cas9 (clustered, regularly interspaced, short palindromic repeats (CRISPR) and the CRISPR-associated protein 9 (Cas9)) has allowed us to achieve genome-wide targeted editing, even noncoding regions of the genome (Sanjana et al., 2016). And a catalytically inactive Cas9 (dCas9) has been used for the transcriptional activation (Konermann et al., 2015) or repression (Gilbert et al., 2013; Larson et al., 2013). Based on CRISPR/dCas9 enhancer-targeting epigenetic editing systems, functional enhancers can be investigated in an unbiased way. However, a major challenge for knockout of noncoding regions is that a small deletion or targeting one noncoding region may not necessarily lead to functional changes. Therefore, more effective methods are needed for validating tens of thousands of putative enhancers simultaneously. To this point, functional genomic screens can be employed to explore the consequences of perturbation of hundreds or thousands of candidate enhancers and to reveal gene-enhancer relationships on a large-scale. Pooled CRISPR screening utilizing multiple distinct single guide RNAs (gRNA) is a powerful tool for mapping perturbations and phenotypes. One such method, called Perturb-seq (Dixit et al., 2016), integrates scRNA-seq and CRISPR system for genome editing and transcriptional profiling at genome wide scale to understand gene function and regulation of transcription factors. A key advantage of this method is that multiple noncoding elements can be targeted, and complex phenotypes can be measured. In our snATAC-seq data, putative enhancers, and their potential target genes were predicted computationally by cicero (Pliner *et al.*, 2018). To elucidate their function and map the transcriptional effects associated

with manipulations on genes, cell states, and signaling pathways, Perturb-seq can be applied to our study to unravel the function of the essential promoters and putative enhancers discovered by our snATAC-seq. gRNA libraries can therefore be designed to targets putative enhancers and Perturb-seq can screen and map those enhancers and their target genes. With this method, candidate enhancers can be investigated in a systematic and unbiased way, without disrupting one by one. Currently, these strategies are typically applied to cell culture systems. In order to apply to our systems, we can use 3T3 preadipocyte cell lines or preadipocyte cells from mouse inguinal adipose stromal vascular fraction (Aune et al., 2013), and Melan-A cell line, an immortal melanocyte cell line derived from embryonic mouse skin (Bennett et al., 1987).

Readout used in the above-mentioned Perturb-seq method was gene expression. However, to identify the effects associated with perturbation of genomic elements on chromatin states and gene regulatory networks, it is desirable to profile chromatin accessibility and identify single guide RNA (sgRNA) sequences from individual single cells at once. Rubin *et al*. developed Perturb-ATAC, a method utilizing multiplexed CRISPR interference (CRISPRi) or knockout with chromatin accessibility profiling, which allows simultaneous measurements of perturbations and ATAC-seq profiles in single cells (Rubin et al., 2019). Also, the same group who developed ATAC-seq developed Spear-ATAC which can perturb transcription factor expression and evaluate the effects of perturbations on gene regulatory networks (Pierce et al., 2021). This method modified droplet-based scATAC-seq protocol for perturbing and evaluating changes in single-cell epigenetic states. Lastly, pooled CRISPR screens with

scATAC-seq with combinatorial indexing strategy, called CRISPR-sciATAC was also developed (Liscovitch-Brauer et al., 2021). These methods allow determination of the roles of a set of *cis*-regulatory elements and *trans*-regulatory factors such as transcription factors and chromatin modifiers. Therefore, these methods can be used to demonstrate the function of the noncoding genomic regions that were differentially more or less accessible in our snATAC-seq dataset. In the future, these methods can be applied to create *cis*- and *trans*-regulatory element interaction maps and expand our understanding of how gene regulatory networks are regulated.

5. Nutritional epigenetics

In my thesis, I studied changes in chromatin accessibility in response to environmental cues, such as temperature and light. Besides these environmental cues, nutrition plays a significant role in regulating chromatin and gene activity. Nutritional epigenetics is the study of environmental and nutritional impacts on the epigenome (Landecker, 2011). Our diet broadly impacts development, aging, and diseases through epigenetic mechanisms (Landecker, 2011). Numerous studies have shown that nutrients can affect structure of chromatin and regulate gene activity (Russo et al., 2017). Nutrients and dietary components influence on chromatin by interacting with histone modifying and chromatin remodeling enzymes or modulating the availability of substrates for enzyme reactions (Choi and Friso, 2010). For example, dietary compounds such as polyphenols from garlic and green tea and butyrate, a product of fiber fermentation by gut microbes, inhibit histone deacetylases (HDACs) (Kasubuchi et al., 2015; Mierziak et al., 2021). Another epigenetic process related to the chromatin states is DNA

methylation. Several studies have shown that a low-calorie diet leads to significant differences in DNA methylation patterns (Milagro et al., 2011). In this regard, nutritional epigenetics can be an alternative and safer tool to reverse or change epigenetic modifications to activate physiologic and pathologic processes, such as adipose beiging in my thesis. In addition to cold-induced thermogenesis, diet-induced thermogenesis is another nonshivering thermogenesis (Westerterp, 2004). Recently, several dietary compounds have been shown to activate white-to-beige adipose tissue with beneficial health effects. Some examples of the ingredients that induce thermogenesis are capsaicin from hot pepper (Baskaran et al., 2016), resveratrol found in grapes and red wine (Wang et al., 2015), green tea (Chen et al., 2017), and omega-3 polyunsaturated fatty acids (PUFAs) (Kim et al., 2015). They were shown to promote UCP1 and PGC-1a expression and increase recruiting of beige adipocytes. Further studies are needed to determine if these compounds share the same mechanisms and can be used as a safe clinical strategy in human. In addition to affecting physiological processes through epigenetic mechanisms, nutrients influence on interactions between epigenetics, transcriptomics, metabolomics, and lipidomics. As an example, fatty acids can not only regulate gene activity by modifying epigenetic mechanisms, but also impact on metabolic outcomes and signaling pathways. Fatty acids are critical components of the body that serve as energy sources and membrane constitution. And long chain PUFAs can play anti-inflammatory roles (Shek et al., 2012). Therefore, multiomics profiling studies will shed light on the response to food and how nutrients influence metabolism and critical pathways. Overall, nutritional interventions may represent a useful non-pharmacological and non-invasive means to

maintain and improve health and sustainable alternative for disease management.

REFERENCES: Chapter 1

Adey, A., Morrison, H.G., Asan, Xun, X., Kitzman, J.O., Turner, E.H., Stackhouse, B., MacKenzie, A.P., Caruccio, N.C., Zhang, X., and Shendure, J. (2010). Rapid, low-input, low-bias construction of shotgun fragment libraries by high-density in vitro transposition. Genome Biol *11*, R119. 10.1186/gb-2010-11-12-r119.

Arnaudo, A.M., and Garcia, B.A. (2013). Proteomic characterization of novel histone post-translational modifications. Epigenetics Chromatin *6*, 24. 10.1186/1756-8935-6-24.

Barski, A., Cuddapah, S., Cui, K., Roh, T.Y., Schones, D.E., Wang, Z., Wei, G., Chepelev, I., and Zhao, K. (2007). High-resolution profiling of histone methylations in the human genome. Cell *129*, 823-837. 10.1016/j.cell.2007.05.009.

Bernstein, B.E., Kamal, M., Lindblad-Toh, K., Bekiranov, S., Bailey, D.K., Huebert, D.J., McMahon, S., Karlsson, E.K., Kulbokas, E.J., 3rd, Gingeras, T.R., et al. (2005). Genomic maps and comparative analysis of histone modifications in human and mouse. Cell *120*, 169-181. 10.1016/j.cell.2005.01.001.

Boyadjiev, S.A., and Jabs, E.W. (2000). Online Mendelian Inheritance in Man (OMIM) as a knowledgebase for human developmental disorders. Clin Genet *57*, 253-266. 10.1034/j.1399-0004.2000.570403.x.

Boyle, A.P., Davis, S., Shulha, H.P., Meltzer, P., Margulies, E.H., Weng, Z., Furey, T.S., and Crawford, G.E. (2008). High-resolution mapping and characterization of open chromatin across the genome. Cell *132*, 311-322. 10.1016/j.cell.2007.12.014.

Bradner, J.E., Hnisz, D., and Young, R.A. (2017). Transcriptional Addiction in Cancer. Cell *168*, 629-643. 10.1016/j.cell.2016.12.013.

Bruno, M., Flaus, A., Stockdale, C., Rencurel, C., Ferreira, H., and Owen-Hughes, T. (2003). Histone H2A/H2B Dimer Exchange by ATP-Dependent Chromatin Remodeling Activities. Molecular Cell *12*, 1599-1606. 10.1016/s1097-2765(03)00499-4.

Buenrostro, J.D., Giresi, P.G., Zaba, L.C., Chang, H.Y., and Greenleaf, W.J. (2013). Transposition of native chromatin for fast and sensitive epigenomic profiling of open chromatin, DNA-binding proteins and nucleosome position. Nat Methods *10*, 1213-1218. 10.1038/nmeth.2688.

Buenrostro, J.D., Wu, B., Litzenburger, U.M., Ruff, D., Gonzales, M.L., Snyder, M.P., Chang, H.Y., and Greenleaf, W.J. (2015). Single-cell chromatin accessibility reveals principles of regulatory variation. Nature *523*, 486-490. 10.1038/nature14590.

Cao, J., Cusanovich, D.A., Ramani, V., Aghamirzaie, D., Pliner, H.A., Hill, A.J., Daza, R.M., McFaline-Figueroa, J.L., Packer, J.S., Christiansen, L., et al. (2018). Joint profiling of chromatin accessibility and gene expression in thousands of single cells. Science *361*, 1380-1385. 10.1126/science.aau0730.

Chen, H., Lareau, C., Andreani, T., Vinyard, M.E., Garcia, S.P., Clement, K., Andrade-Navarro, M.A., Buenrostro, J.D., and Pinello, L. (2019a). Assessment of computational methods for the analysis of single-cell ATAC-seq data. Genome Biol *20*, 241. 10.1186/s13059-019-1854-5.

Chen, S., Lake, B.B., and Zhang, K. (2019b). High-throughput sequencing of the transcriptome and chromatin accessibility in the same cell. Nat Biotechnol *37*, 1452-1457. 10.1038/s41587-019-0290-0.

Chen, X., Miragaia, R.J., Natarajan, K.N., and Teichmann, S.A. (2018). A rapid and robust method for single cell chromatin accessibility profiling. Nat Commun *9*, 5345. 10.1038/s41467-018-07771-0.

Cheng, H., Pui, H.-p., Lentini, A., Kolbeinsdóttir, S., Andrews, N., Pei, Y., Reinius, B., Deng, Q., and Enge, M. (2021). Smart3-ATAC: a highly sensitive method for joint accessibility and full-length transcriptome analysis in single cells. bioRxiv. https://doi.org/10.1101/2021.12.02.470912.

Chu, T., Rice, E.J., Booth, G.T., Salamanca, H.H., Wang, Z., Core, L.J., Longo, S.L., Corona, R.J., Chin, L.S., Lis, J.T., et al. (2018). Chromatin run-on and sequencing maps the transcriptional regulatory landscape of glioblastoma multiforme. Nat Genet *50*, 1553-1564. 10.1038/s41588-018-0244-3.

Corces, M.R., Trevino, A.E., Hamilton, E.G., Greenside, P.G., Sinnott-Armstrong, N.A., Vesuna, S., Satpathy, A.T., Rubin, A.J., Montine, K.S., Wu, B., et al. (2017). An improved ATAC-seq protocol reduces background and enables interrogation of frozen tissues. Nat Methods *14*, 959-962. 10.1038/nmeth.4396.

Cusanovich, D.A., Daza, R., Adey, A., Pliner, H.A., Christiansen, L., Gunderson, K.L., Steemers, F.J., Trapnell, C., and Shendure, J. (2015). Multiplex single cell profiling of chromatin accessibility by combinatorial cellular indexing. Science *348*, 910-914. 10.1126/science.aab1601.

Domcke, S., Hill, A.J., Daza, R.M., Cao, J., O'Day, D.R., Pliner, H.A., Aldinger, K.A., Pokholok, D., Zhang, F., Milbank, J.H., et al. (2020). A human cell atlas of fetal chromatin accessibility. Science *370*. 10.1126/science.aba7612.

Fang, R., Preissl, S., Li, Y., Hou, X., Lucero, J., Wang, X., Motamedi, A., Shiau, A.K., Zhou, X., Xie, F., et al. (2021). Comprehensive analysis of single cell ATAC-seq data with SnapATAC. Nat Commun *12*, 1337. 10.1038/s41467-021-21583-9.

Gillette, T.G., and Hill, J.A. (2015). Readers, writers, and erasers: chromatin as the whiteboard of heart disease. Circ Res *116*, 1245-1253. 10.1161/CIRCRESAHA.116.303630.

Giresi, P.G., Kim, J., McDaniell, R.M., Iyer, V.R., and Lieb, J.D. (2007). FAIRE (Formaldehyde-Assisted Isolation of Regulatory Elements) isolates active regulatory elements from human chromatin. Genome Res *17*, 877-885. 10.1101/gr.5533506.

Goryshin, I.Y., and Reznikoff, W.S. (1998). Tn5 in vitro transposition. J Biol Chem *273*, 7367-7374. 10.1074/jbc.273.13.7367.

Granja, J.M., Corces, M.R., Pierce, S.E., Bagdatli, S.T., Choudhry, H., Chang, H.Y., and Greenleaf, W.J. (2021). ArchR is a scalable software package for

integrative single-cell chromatin accessibility analysis. Nat Genet *53*, 403-411. 10.1038/s41588-021-00790-6.

Hamiche, A., Sandaltzopoulos, R., Gdula, D.A., and Wu, C. (1999). ATP-Dependent Histone Octamer Sliding Mediated by the Chromatin Remodeling Complex NURF. Cell *97*, 833-842. 10.1016/s0092-8674(00)80796-5.

Heintzman, N.D., Stuart, R.K., Hon, G., Fu, Y., Ching, C.W., Hawkins, R.D., Barrera, L.O., Van Calcar, S., Qu, C., Ching, K.A., et al. (2007). Distinct and predictive chromatin signatures of transcriptional promoters and enhancers in the human genome. Nat Genet *39*, 311-318. 10.1038/ng1966.

Henikoff, S. (2008). Nucleosome destabilization in the epigenetic regulation of gene expression. Nat Rev Genet *9*, 15-26. 10.1038/nrg2206.

Iwafuchi-Doi, M., and Zaret, K.S. (2016). Cell fate control by pioneer transcription factors. Development *143*, 1833-1837. 10.1242/dev.133900.

Johnson, D.S., Mortazavi, A., Myers, R.M., and Wold, B. (2007). Genome-wide mapping of in vivo protein-DNA interactions. Science *316*, 1497-1502. 10.1126/science.1141319.

Kaya-Okur, H.S., Wu, S.J., Codomo, C.A., Pledger, E.S., Bryson, T.D., Henikoff, J.G., Ahmad, K., and Henikoff, S. (2019). CUT&Tag for efficient epigenomic profiling of small samples and single cells. Nat Commun *10*, 1930. 10.1038/s41467-019-09982-5.

Kornberg, R.D. (1974). Chromatin structure: a repeating unit of histones and DNA. Science *184*, 868-871. 10.1126/science.184.4139.868.

Kouzarides, T. (2007). Chromatin modifications and their function. Cell *128*, 693-705. 10.1016/j.cell.2007.02.005.

Kwak, H., Fuda, N.J., Core, L.J., and Lis, J.T. (2013). Precise maps of RNA polymerase reveal how promoters direct initiation and pausing. Science *339*, 950-953. 10.1126/science.1229386.

Längst, G., Bonte, E.J., Corona, D.F.V., and Becker, P.B. (1999). Nucleosome Movement by CHRAC and ISWI without Disruption or trans-Displacement of the Histone Octamer. Cell *97*, 843-852. 10.1016/s0092-8674(00)80797-7.

Lareau, C.A., Duarte, F.M., Chew, J.G., Kartha, V.K., Burkett, Z.D., Kohlway, A.S., Pokholok, D., Aryee, M.J., Steemers, F.J., Lebofsky, R., and Buenrostro, J.D. (2019). Droplet-based combinatorial indexing for massive-scale single-cell chromatin accessibility. Nat Biotechnol *37*, 916-924. 10.1038/s41587-019-0147-6.

Larson, E.D., Marsh, A.J., and Harrison, M.M. (2021). Pioneering the developmental frontier. Mol Cell *81*, 1640-1650. 10.1016/j.molcel.2021.02.020.

Lee, C.K., Shibata, Y., Rao, B., Strahl, B.D., and Lieb, J.D. (2004). Evidence for nucleosome depletion at active regulatory regions genome-wide. Nat Genet *36*, 900-905. 10.1038/ng1400.

Lee, T.I., and Young, R.A. (2013). Transcriptional regulation and its misregulation in disease. Cell *152*, 1237-1251. 10.1016/j.cell.2013.02.014.

Lister, R., Pelizzola, M., Dowen, R.H., Hawkins, R.D., Hon, G., Tonti-Filippini, J., Nery, J.R., Lee, L., Ye, Z., Ngo, Q.M., et al. (2009). Human DNA

methylomes at base resolution show widespread epigenomic differences. Nature *462*, 315-322. 10.1038/nature08514.

Lorch, Y., Zhang, M., and Kornberg, R.D. (1999). Histone Octamer Transfer by a Chromatin-Remodeling Complex. Cell *96*, 389-392. 10.1016/s0092-8674(00)80551-6.

Luger, K., Mader, A.W., Richmond, R.K., Sargent, D.F., and Richmond, T.J. (1997). Crystal structure of the nucleosome core particle at 2.8 A resolution. Nature *389*, 251-260. 10.1038/38444.

Ma, S., Zhang, B., LaFave, L.M., Earl, A.S., Chiang, Z., Hu, Y., Ding, J., Brack, A., Kartha, V.K., Tay, T., et al. (2020). Chromatin Potential Identified by Shared Single-Cell Profiling of RNA and Chromatin. Cell *183*, 1103-1116 e1120. 10.1016/j.cell.2020.09.056.

Mayran, A., and Drouin, J. (2018). Pioneer transcription factors shape the epigenetic landscape. J Biol Chem *293*, 13795-13804. 10.1074/jbc.R117.001232.

Mimitou, E.P., Lareau, C.A., Chen, K.Y., Zorzetto-Fernandes, A.L., Hao, Y., Takeshima, Y., Luo, W., Huang, T.S., Yeung, B.Z., Papalexi, E., et al. (2021). Scalable, multimodal profiling of chromatin accessibility, gene expression and protein levels in single cells. Nat Biotechnol *39*, 1246-1258. 10.1038/s41587-021-00927-2.

Musselman, C.A., Lalonde, M.E., Cote, J., and Kutateladze, T.G. (2012). Perceiving the epigenetic landscape through histone readers. Nat Struct Mol Biol *19*, 1218-1227. 10.1038/nsmb.2436.

Pliner, H.A., Packer, J.S., McFaline-Figueroa, J.L., Cusanovich, D.A., Daza, R.M., Aghamirzaie, D., Srivatsan, S., Qiu, X., Jackson, D., Minkina, A., et al. (2018). Cicero Predicts cis-Regulatory DNA Interactions from Single-Cell Chromatin Accessibility Data. Mol Cell *71*, 858-871 e858. 10.1016/j.molcel.2018.06.044.

Rhee, H.S., and Pugh, B.F. (2011). Comprehensive genome-wide protein-DNA interactions detected at single-nucleotide resolution. Cell *147*, 1408-1419. 10.1016/j.cell.2011.11.013.

Rosenberg, A.B., Roco, C.M., Muscat, R.A., Kuchina, A., Sample, P., Yao, Z., Graybuck, L.T., Peeler, D.J., Mukherjee, S., Chen, W., et al. (2018). Single-cell profiling of the developing mouse brain and spinal cord with split-pool barcoding. Science *360*, 176-182. 10.1126/science.aam8999.

Schep, A.N., Wu, B., Buenrostro, J.D., and Greenleaf, W.J. (2017). chromVAR: inferring transcription-factor-associated accessibility from single-cell epigenomic data. Nat Methods *14*, 975-978. 10.1038/nmeth.4401.

Schlesinger, F., Smith, A.D., Gingeras, T.R., Hannon, G.J., and Hodges, E. (2013). De novo DNA demethylation and noncoding transcription define active intergenic regulatory elements. Genome Res *23*, 1601-1614. 10.1101/gr.157271.113.

Schones, D.E., Cui, K., Cuddapah, S., Roh, T.Y., Barski, A., Wang, Z., Wei, G., and Zhao, K. (2008). Dynamic regulation of nucleosome positioning in the human genome. Cell *132*, 887-898. 10.1016/j.cell.2008.02.022.

Sims, R.J., 3rd, and Reinberg, D. (2004). From chromatin to cancer: a new histone lysine methyltransferase enters the mix. Nat Cell Biol *6*, 685-687. 10.1038/ncb0804-685.

Skene, P.J., and Henikoff, S. (2017). An efficient targeted nuclease strategy for high-resolution mapping of DNA binding sites. Elife *6*. 10.7554/eLife.21856.

Staub, E., Grone, J., Mennerich, D., Ropcke, S., Klamann, I., Hinzmann, B., Castanos-Velez, E., Mann, B., Pilarsky, C., Brummendorf, T., et al. (2006). A genome-wide map of aberrantly expressed chromosomal islands in colorectal cancer. Mol Cancer *5*, 37. 10.1186/1476-4598-5-37.

Stuart, T., Butler, A., Hoffman, P., Hafemeister, C., Papalexi, E., Mauck, W.M., 3rd, Hao, Y., Stoeckius, M., Smibert, P., and Satija, R. (2019). Comprehensive Integration of Single-Cell Data. Cell *177*, 1888-1902 e1821. 10.1016/j.cell.2019.05.031.

Stuart, T., Srivastava, A., Madad, S., Lareau, C.A., and Satija, R. (2021). Single-cell chromatin state analysis with Signac. Nat Methods *18*, 1333-1341. 10.1038/s41592-021-01282-5.

Swanson, E., Lord, C., Reading, J., Heubeck, A.T., Genge, P.C., Thomson, Z., Weiss, M.D., Li, X.J., Savage, A.K., Green, R.R., et al. (2021). Simultaneous trimodal single-cell measurement of transcripts, epitopes, and chromatin accessibility using TEA-seq. Elife *10*. 10.7554/eLife.63632.

Trapnell, C., Cacchiarelli, D., Grimsby, J., Pokharel, P., Li, S., Morse, M., Lennon, N.J., Livak, K.J., Mikkelsen, T.S., and Rinn, J.L. (2014). The dynamics and regulators of cell fate decisions are revealed by pseudotemporal ordering of single cells. Nat Biotechnol *32*, 381-386. 10.1038/nbt.2859.

Wu, C., Wong, Y.C., and Elgin, S.C. (1979). The chromatin structure of specific genes: II. Disruption of chromatin structure during gene activity. Cell *16*, 807-814. 10.1016/0092-8674(79)90096-5.

Yue, F., Cheng, Y., Breschi, A., Vierstra, J., Wu, W., Ryba, T., Sandstrom, R., Ma, Z., Davis, C., Pope, B.D., et al. (2014). A comparative encyclopedia of DNA elements in the mouse genome. Nature *515*, 355-364. 10.1038/nature13992.

Zaret, K.S., and Mango, S.E. (2016). Pioneer transcription factors, chromatin dynamics, and cell fate control. Curr Opin Genet Dev *37*, 76-81. 10.1016/j.gde.2015.12.003.

Zhang, Y., LeRoy, G., Seelig, H.-P., Lane, W.S., and Reinberg, D. (1998). The Dermatomyositis-Specific Autoantigen Mi2 Is a Component of a Complex Containing Histone Deacetylase and Nucleosome Remodeling Activities. Cell *95*, 279-289. 10.1016/s0092-8674(00)81758-4.

Zhong, Z., Feng, S., Duttke, S.H., Potok, M.E., Zhang, Y., Gallego-Bartolome, J., Liu, W., and Jacobsen, S.E. (2021). DNA methylation-linked chromatin accessibility affects genomic architecture in Arabidopsis. Proc Natl Acad Sci U S A *118*. 10.1073/pnas.2023347118.

Zhu, C., Yu, M., Huang, H., Juric, I., Abnousi, A., Hu, R., Lucero, J., Behrens, M.M., Hu, M., and Ren, B. (2019). An ultra high-throughput method for

single-cell joint analysis of open chromatin and transcriptome. Nat Struct Mol Biol *26*, 1063-1070. 10.1038/s41594-019-0323-x.

REFERENCES: Chapter 2

Adey, A., Morrison, H.G., Asan, Xun, X., Kitzman, J.O., Turner, E.H., Stackhouse, B., MacKenzie, A.P., Caruccio, N.C., Zhang, X., and Shendure, J. (2010). Rapid, low-input, low-bias construction of shotgun fragment libraries by high-density in vitro transposition. Genome Biol *11*, R119. 10.1186/gb-2010-11-12-r119.

Altschuler, S.J., and Wu, L.F. (2010). Cellular heterogeneity: do differences make a difference? Cell *141*, 559-563. 10.1016/j.cell.2010.04.033.

Amemiya, H.M., Kundaje, A., and Boyle, A.P. (2019). The ENCODE Blacklist: Identification of Problematic Regions of the Genome. Sci Rep *9*, 9354. 10.1038/s41598-019-45839-z.

Arany, Z., Foo, S.Y., Ma, Y., Ruas, J.L., Bommi-Reddy, A., Girnun, G., Cooper, M., Laznik, D., Chinsomboon, J., Rangwala, S.M., et al. (2008). HIF-independent regulation of VEGF and angiogenesis by the transcriptional coactivator PGC-1alpha. Nature *451*, 1008-1012. 10.1038/nature06613.

Arch, J.R. (2011). Challenges in beta(3)-Adrenoceptor Agonist Drug Development. Ther Adv Endocrinol Metab *2*, 59-64. 10.1177/2042018811398517.

Arnaudo, A.M., and Garcia, B.A. (2013). Proteomic characterization of novel histone post-translational modifications. Epigenetics Chromatin *6*, 24. 10.1186/1756-8935-6-24.

Baker, R.G., Hayden, M.S., and Ghosh, S. (2011). NF-kappaB, inflammation, and metabolic disease. Cell Metab *13*, 11-22. 10.1016/j.cmet.2010.12.008.

Barbatelli, G., Murano, I., Madsen, L., Hao, Q., Jimenez, M., Kristiansen, K., Giacobino, J.P., De Matteis, R., and Cinti, S. (2010). The emergence of cold-induced brown adipocytes in mouse white fat depots is determined predominantly by white to brown adipocyte transdifferentiation. Am J Physiol Endocrinol Metab *298*, E1244-1253. 10.1152/ajpendo.00600.2009.

Barquissau, V., Beuzelin, D., Pisani, D.F., Beranger, G.E., Mairal, A., Montagner, A., Roussel, B., Tavernier, G., Marques, M.A., Moro, C., et al. (2016). White-to-brite conversion in human adipocytes promotes metabolic reprogramming towards fatty acid anabolic and catabolic pathways. Mol Metab *5*, 352-365. 10.1016/j.molmet.2016.03.002.

Barski, A., Cuddapah, S., Cui, K., Roh, T.Y., Schones, D.E., Wang, Z., Wei, G., Chepelev, I., and Zhao, K. (2007). High-resolution profiling of histone methylations in the human genome. Cell *129*, 823-837. 10.1016/j.cell.2007.05.009.

Bernstein, B.E., Kamal, M., Lindblad-Toh, K., Bekiranov, S., Bailey, D.K., Huebert, D.J., McMahon, S., Karlsson, E.K., Kulbokas, E.J., 3rd, Gingeras, T.R., et al. (2005). Genomic maps and comparative analysis of histone modifications in human and mouse. Cell *120*, 169-181. 10.1016/j.cell.2005.01.001.

Berry, D.C., Jiang, Y., and Graff, J.M. (2016). Mouse strains to study cold-inducible beige progenitors and beige adipocyte formation and function. Nat

Commun *7*, 10184. 10.1038/ncomms10184.
Biagi, C.A.O., Jr., Cury, S.S., Alves, C.P., Rabhi, N., Silva, W.A., Jr., Farmer, S.R., Carvalho, R.F., and Batista, M.L., Jr. (2021). Multidimensional Single-Nuclei RNA-Seq Reconstruction of Adipose Tissue Reveals Adipocyte Plasticity Underlying Thermogenic Response. Cells *10*. 10.3390/cells10113073.
Boyadjiev, S.A., and Jabs, E.W. (2000). Online Mendelian Inheritance in Man (OMIM) as a knowledgebase for human developmental disorders. Clin Genet *57*, 253-266. 10.1034/j.1399-0004.2000.570403.x.
Boyle, A.P., Davis, S., Shulha, H.P., Meltzer, P., Margulies, E.H., Weng, Z., Furey, T.S., and Crawford, G.E. (2008). High-resolution mapping and characterization of open chromatin across the genome. Cell *132*, 311-322. 10.1016/j.cell.2007.12.014.
Bradner, J.E., Hnisz, D., and Young, R.A. (2017). Transcriptional Addiction in Cancer. Cell *168*, 629-643. 10.1016/j.cell.2016.12.013.
Brown, E.L., Hazen, B.C., Eury, E., Wattez, J.S., Gantner, M.L., Albert, V., Chau, S., Sanchez-Alavez, M., Conti, B., and Kralli, A. (2018). Estrogen-Related Receptors Mediate the Adaptive Response of Brown Adipose Tissue to Adrenergic Stimulation. iScience *2*, 221-237. 10.1016/j.isci.2018.03.005.
Bruno, M., Flaus, A., Stockdale, C., Rencurel, C., Ferreira, H., and Owen-Hughes, T. (2003). Histone H2A/H2B Dimer Exchange by ATP-Dependent Chromatin Remodeling Activities. Molecular Cell *12*, 1599-1606. 10.1016/s1097-2765(03)00499-4.
Buenrostro, J.D., Giresi, P.G., Zaba, L.C., Chang, H.Y., and Greenleaf, W.J. (2013). Transposition of native chromatin for fast and sensitive epigenomic profiling of open chromatin, DNA-binding proteins and nucleosome position. Nat Methods *10*, 1213-1218. 10.1038/nmeth.2688.
Buenrostro, J.D., Wu, B., Litzenburger, U.M., Ruff, D., Gonzales, M.L., Snyder, M.P., Chang, H.Y., and Greenleaf, W.J. (2015). Single-cell chromatin accessibility reveals principles of regulatory variation. Nature *523*, 486-490. 10.1038/nature14590.
Burl, R.B., Ramseyer, V.D., Rondini, E.A., Pique-Regi, R., Lee, Y.H., and Granneman, J.G. (2018). Deconstructing Adipogenesis Induced by beta3-Adrenergic Receptor Activation with Single-Cell Expression Profiling. Cell Metab *28*, 300-309 e304. 10.1016/j.cmet.2018.05.025.
Cadoudal, T., Distel, E., Durant, S., Fouque, F., Blouin, J.M., Collinet, M., Bortoli, S., Forest, C., and Benelli, C. (2008). Pyruvate dehydrogenase kinase 4: regulation by thiazolidinediones and implication in glyceroneogenesis in adipose tissue. Diabetes *57*, 2272-2279. 10.2337/db08-0477.
Cao, J., Cusanovich, D.A., Ramani, V., Aghamirzaie, D., Pliner, H.A., Hill, A.J., Daza, R.M., McFaline-Figueroa, J.L., Packer, J.S., Christiansen, L., et al. (2018). Joint profiling of chromatin accessibility and gene expression in thousands of single cells. Science *361*, 1380-1385.

10.1126/science.aau0730.
Cao, J., Spielmann, M., Qiu, X., Huang, X., Ibrahim, D.M., Hill, A.J., Zhang, F., Mundlos, S., Christiansen, L., Steemers, F.J., et al. (2019). The single-cell transcriptional landscape of mammalian organogenesis. Nature *566*, 496-502. 10.1038/s41586-019-0969-x.
Chandra, V., Huang, P., Hamuro, Y., Raghuram, S., Wang, Y., Burris, T.P., and Rastinejad, F. (2008). Structure of the intact PPAR-gamma-RXR- nuclear receptor complex on DNA. Nature *456*, 350-356. 10.1038/nature07413.
Chang, J.S., Ghosh, S., Newman, S., and Salbaum, J.M. (2018). A map of the PGC-1alpha- and NT-PGC-1alpha-regulated transcriptional network in brown adipose tissue. Sci Rep *8*, 7876. 10.1038/s41598-018-26244-4.
Chaveroux, C., Eichner, L.J., Dufour, C.R., Shatnawi, A., Khoutorsky, A., Bourque, G., Sonenberg, N., and Giguere, V. (2013). Molecular and genetic crosstalks between mTOR and ERRalpha are key determinants of rapamycin-induced nonalcoholic fatty liver. Cell Metab *17*, 586-598. 10.1016/j.cmet.2013.03.003.
Chen, H., Lareau, C., Andreani, T., Vinyard, M.E., Garcia, S.P., Clement, K., Andrade-Navarro, M.A., Buenrostro, J.D., and Pinello, L. (2019a). Assessment of computational methods for the analysis of single-cell ATAC-seq data. Genome Biol *20*, 241. 10.1186/s13059-019-1854-5.
Chen, S., Lake, B.B., and Zhang, K. (2019b). High-throughput sequencing of the transcriptome and chromatin accessibility in the same cell. Nat Biotechnol *37*, 1452-1457. 10.1038/s41587-019-0290-0.
Chen, X., Miragaia, R.J., Natarajan, K.N., and Teichmann, S.A. (2018). A rapid and robust method for single cell chromatin accessibility profiling. Nat Commun *9*, 5345. 10.1038/s41467-018-07771-0.
Chen, Y., Ikeda, K., Yoneshiro, T., Scaramozza, A., Tajima, K., Wang, Q., Kim, K., Shinoda, K., Sponton, C.H., Brown, Z., et al. (2019c). Thermal stress induces glycolytic beige fat formation via a myogenic state. Nature *565*, 180-185. 10.1038/s41586-018-0801-z.
Cheng, H., Pui, H.-p., Lentini, A., Kolbeinsdóttir, S., Andrews, N., Pei, Y., Reinius, B., Deng, Q., and Enge, M. (2021). Smart3-ATAC: a highly sensitive method for joint accessibility and full-length transcriptome analysis in single cells. bioRxiv. https://doi.org/10.1101/2021.12.02.470912.
Chiang, S.H., Bazuine, M., Lumeng, C.N., Geletka, L.M., Mowers, J., White, N.M., Ma, J.T., Zhou, J., Qi, N., Westcott, D., et al. (2009). The protein kinase IKKepsilon regulates energy balance in obese mice. Cell *138*, 961-975. 10.1016/j.cell.2009.06.046.
Choe, S.S., Huh, J.Y., Hwang, I.J., Kim, J.I., and Kim, J.B. (2016). Adipose Tissue Remodeling: Its Role in Energy Metabolism and Metabolic Disorders. Front Endocrinol (Lausanne) *7*, 30. 10.3389/fendo.2016.00030.
Chu, T., Rice, E.J., Booth, G.T., Salamanca, H.H., Wang, Z., Core, L.J., Longo, S.L., Corona, R.J., Chin, L.S., Lis, J.T., et al. (2018). Chromatin run-on and sequencing maps the transcriptional regulatory landscape of glioblastoma multiforme. Nat Genet *50*, 1553-1564. 10.1038/s41588-018-0244-3.

Corces, M.R., Trevino, A.E., Hamilton, E.G., Greenside, P.G., Sinnott-Armstrong, N.A., Vesuna, S., Satpathy, A.T., Rubin, A.J., Montine, K.S., Wu, B., et al. (2017). An improved ATAC-seq protocol reduces background and enables interrogation of frozen tissues. Nat Methods *14*, 959-962. 10.1038/nmeth.4396.

Cox, A.R., Chernis, N., Bader, D.A., Saha, P.K., Masschelin, P.M., Felix, J.B., Sharp, R., Lian, Z., Putluri, V., Rajapakshe, K., et al. (2020). STAT1 Dissociates Adipose Tissue Inflammation From Insulin Sensitivity in Obesity. Diabetes *69*, 2630-2641. 10.2337/db20-0384.

Cusanovich, D.A., Daza, R., Adey, A., Pliner, H.A., Christiansen, L., Gunderson, K.L., Steemers, F.J., Trapnell, C., and Shendure, J. (2015). Multiplex single cell profiling of chromatin accessibility by combinatorial cellular indexing. Science *348*, 910-914. 10.1126/science.aab1601.

Cusanovich, D.A., Hill, A.J., Aghamirzaie, D., Daza, R.M., Pliner, H.A., Berletch, J.B., Filippova, G.N., Huang, X., Christiansen, L., DeWitt, W.S., et al. (2018). A Single-Cell Atlas of In Vivo Mammalian Chromatin Accessibility. Cell *174*, 1309-1324 e1318. 10.1016/j.cell.2018.06.052.

Cypess, A.M., and Kahn, C.R. (2010a). Brown fat as a therapy for obesity and diabetes. Curr Opin Endocrinol Diabetes Obes *17*, 143-149. 10.1097/MED.0b013e328337a81f.

Cypess, A.M., and Kahn, C.R. (2010b). The role and importance of brown adipose tissue in energy homeostasis. Curr Opin Pediatr *22*, 478-484. 10.1097/MOP.0b013e32833a8d6e.

Czubryt, M.P., McAnally, J., Fishman, G.I., and Olson, E.N. (2003). Regulation of peroxisome proliferator-activated receptor gamma coactivator 1 alpha (PGC-1 alpha) and mitochondrial function by MEF2 and HDAC5. Proc Natl Acad Sci U S A *100*, 1711-1716. 10.1073/pnas.0337639100.

Dann, E., Henderson, N.C., Teichmann, S.A., Morgan, M.D., and Marioni, J.C. (2022). Differential abundance testing on single-cell data using k-nearest neighbor graphs. Nat Biotechnol *40*, 245-253. 10.1038/s41587-021-01033-z.

Domcke, S., Hill, A.J., Daza, R.M., Cao, J., O'Day, D.R., Pliner, H.A., Aldinger, K.A., Pokholok, D., Zhang, F., Milbank, J.H., et al. (2020). A human cell atlas of fetal chromatin accessibility. Science *370*. 10.1126/science.aba7612.

Fang, R., Preissl, S., Li, Y., Hou, X., Lucero, J., Wang, X., Motamedi, A., Shiau, A.K., Zhou, X., Xie, F., et al. (2021). Comprehensive analysis of single cell ATAC-seq data with SnapATAC. Nat Commun *12*, 1337. 10.1038/s41467-021-21583-9.

Ferrara, N., Gerber, H.P., and LeCouter, J. (2003). The biology of VEGF and its receptors. Nat Med *9*, 669-676. 10.1038/nm0603-669.

Finck, B.N., and Kelly, D.P. (2006). PGC-1 coactivators: inducible regulators of energy metabolism in health and disease. J Clin Invest *116*, 615-622. 10.1172/JCI27794.

Fornes, O., Castro-Mondragon, J.A., Khan, A., van der Lee, R., Zhang, X., Richmond, P.A., Modi, B.P., Correard, S., Gheorghe, M., Baranasic, D., et

al. (2020). JASPAR 2020: update of the open-access database of transcription factor binding profiles. Nucleic Acids Res *48*, D87-D92. 10.1093/nar/gkz1001.

Garces, R., and Mancha, M. (1993). One-step lipid extraction and fatty acid methyl esters preparation from fresh plant tissues. Anal Biochem *211*, 139-143. 10.1006/abio.1993.1244.

Gillette, T.G., and Hill, J.A. (2015). Readers, writers, and erasers: chromatin as the whiteboard of heart disease. Circ Res *116*, 1245-1253. 10.1161/CIRCRESAHA.116.303630.

Giresi, P.G., Kim, J., McDaniell, R.M., Iyer, V.R., and Lieb, J.D. (2007). FAIRE (Formaldehyde-Assisted Isolation of Regulatory Elements) isolates active regulatory elements from human chromatin. Genome Res *17*, 877-885. 10.1101/gr.5533506.

Goryshin, I.Y., and Reznikoff, W.S. (1998). Tn5 in vitro transposition. J Biol Chem *273*, 7367-7374. 10.1074/jbc.273.13.7367.

Goto, T., Lee, J.Y., Teraminami, A., Kim, Y.I., Hirai, S., Uemura, T., Inoue, H., Takahashi, N., and Kawada, T. (2011). Activation of peroxisome proliferator-activated receptor-alpha stimulates both differentiation and fatty acid oxidation in adipocytes. J Lipid Res *52*, 873-884. 10.1194/jlr.M011320.

Granja, J.M., Corces, M.R., Pierce, S.E., Bagdatli, S.T., Choudhry, H., Chang, H.Y., and Greenleaf, W.J. (2021). ArchR is a scalable software package for integrative single-cell chromatin accessibility analysis. Nat Genet *53*, 403-411. 10.1038/s41588-021-00790-6.

Guilherme, A., Yenilmez, B., Bedard, A.H., Henriques, F., Liu, D., Lee, A., Goldstein, L., Kelly, M., Nicoloro, S.M., Chen, M., et al. (2020). Control of Adipocyte Thermogenesis and Lipogenesis through beta3-Adrenergic and Thyroid Hormone Signal Integration. Cell Rep *31*, 107598. 10.1016/j.celrep.2020.107598.

Hamiche, A., Sandaltzopoulos, R., Gdula, D.A., and Wu, C. (1999). ATP-Dependent Histone Octamer Sliding Mediated by the Chromatin Remodeling Complex NURF. Cell *97*, 833-842. 10.1016/s0092-8674(00)80796-5.

Han, J., Lee, J.E., Jin, J., Lim, J.S., Oh, N., Kim, K., Chang, S.I., Shibuya, M., Kim, H., and Koh, G.Y. (2011). The spatiotemporal development of adipose tissue. Development *138*, 5027-5037. 10.1242/dev.067686.

Han, X., Zhang, Z., He, L., Zhu, H., Li, Y., Pu, W., Han, M., Zhao, H., Liu, K., Li, Y., et al. (2021). A suite of new Dre recombinase drivers markedly expands the ability to perform intersectional genetic targeting. Cell Stem Cell *28*, 1160-1176 e1167. 10.1016/j.stem.2021.01.007.

Hao, Y., Hao, S., Andersen-Nissen, E., Mauck, W.M., 3rd, Zheng, S., Butler, A., Lee, M.J., Wilk, A.J., Darby, C., Zager, M., et al. (2021). Integrated analysis of multimodal single-cell data. Cell *184*, 3573-3587 e3529. 10.1016/j.cell.2021.04.048.

Harms, M., and Seale, P. (2013). Brown and beige fat: development, function and therapeutic potential. Nat Med *19*, 1252-1263. 10.1038/nm.3361.

Heintzman, N.D., Stuart, R.K., Hon, G., Fu, Y., Ching, C.W., Hawkins, R.D.,

Barrera, L.O., Van Calcar, S., Qu, C., Ching, K.A., et al. (2007). Distinct and predictive chromatin signatures of transcriptional promoters and enhancers in the human genome. Nat Genet *39*, 311-318. 10.1038/ng1966.

Henikoff, S. (2008). Nucleosome destabilization in the epigenetic regulation of gene expression. Nat Rev Genet *9*, 15-26. 10.1038/nrg2206.

Hiraike, Y., Waki, H., Yu, J., Nakamura, M., Miyake, K., Nagano, G., Nakaki, R., Suzuki, K., Kobayashi, H., Yamamoto, S., et al. (2017). NFIA co-localizes with PPARgamma and transcriptionally controls the brown fat gene program. Nat Cell Biol *19*, 1081-1092. 10.1038/ncb3590.

Howe, K.L., Achuthan, P., Allen, J., Allen, J., Alvarez-Jarreta, J., Amode, M.R., Armean, I.M., Azov, A.G., Bennett, R., Bhai, J., et al. (2021). Ensembl 2021. Nucleic Acids Res *49*, D884-D891. 10.1093/nar/gkaa942.

Huss, J.M., Torra, I.P., Staels, B., Giguere, V., and Kelly, D.P. (2004). Estrogen-related receptor alpha directs peroxisome proliferator-activated receptor alpha signaling in the transcriptional control of energy metabolism in cardiac and skeletal muscle. Mol Cell Biol *24*, 9079-9091. 10.1128/MCB.24.20.9079-9091.2004.

Iwafuchi-Doi, M., and Zaret, K.S. (2016). Cell fate control by pioneer transcription factors. Development *143*, 1833-1837. 10.1242/dev.133900.

Jiang, Y., Berry, D.C., and Graff, J.M. (2017a). Distinct cellular and molecular mechanisms for beta3 adrenergic receptor-induced beige adipocyte formation. Elife *6*. 10.7554/eLife.30329.

Jiang, Y., Berry, D.C., Jo, A., Tang, W., Arpke, R.W., Kyba, M., and Graff, J.M. (2017b). A PPARgamma transcriptional cascade directs adipose progenitor cell-niche interaction and niche expansion. Nat Commun *8*, 15926. 10.1038/ncomms15926.

Jiang, Y., Berry, D.C., Tang, W., and Graff, J.M. (2014). Independent stem cell lineages regulate adipose organogenesis and adipose homeostasis. Cell Rep *9*, 1007-1022. 10.1016/j.celrep.2014.09.049.

Jin, S., Guerrero-Juarez, C.F., Zhang, L., Chang, I., Ramos, R., Kuan, C.H., Myung, P., Plikus, M.V., and Nie, Q. (2021). Inference and analysis of cell-cell communication using CellChat. Nat Commun *12*, 1088. 10.1038/s41467-021-21246-9.

Johnson, D.S., Mortazavi, A., Myers, R.M., and Wold, B. (2007). Genome-wide mapping of in vivo protein-DNA interactions. Science *316*, 1497-1502. 10.1126/science.1141319.

Kaya-Okur, H.S., Wu, S.J., Codomo, C.A., Pledger, E.S., Bryson, T.D., Henikoff, J.G., Ahmad, K., and Henikoff, S. (2019). CUT&Tag for efficient epigenomic profiling of small samples and single cells. Nat Commun *10*, 1930. 10.1038/s41467-019-09982-5.

Kornberg, R.D. (1974). Chromatin structure: a repeating unit of histones and DNA. Science *184*, 868-871. 10.1126/science.184.4139.868.

Kostal, V., Sula, J., and Simek, P. (1998). Physiology of drought tolerance and cold hardiness of the Mediterranean tiger moth Cymbalophora pudica during summer diapause. Journal of Insect Physiology *44*, 165-173.

10.1016/s0022-1910(97)00047-4.
Kouzarides, T. (2007). Chromatin modifications and their function. Cell *128*, 693-705. 10.1016/j.cell.2007.02.005.
Kumar, N., Liu, D., Wang, H., Robidoux, J., and Collins, S. (2008). Orphan nuclear receptor NOR-1 enhances 3',5'-cyclic adenosine 5'-monophosphate-dependent uncoupling protein-1 gene transcription. Mol Endocrinol *22*, 1057-1064. 10.1210/me.2007-0464.
Kwak, H., Fuda, N.J., Core, L.J., and Lis, J.T. (2013). Precise maps of RNA polymerase reveal how promoters direct initiation and pausing. Science *339*, 950-953. 10.1126/science.1229386.
Langmead, B., and Salzberg, S.L. (2012). Fast gapped-read alignment with Bowtie 2. Nat Methods *9*, 357-359. 10.1038/nmeth.1923.
Längst, G., Bonte, E.J., Corona, D.F.V., and Becker, P.B. (1999). Nucleosome Movement by CHRAC and ISWI without Disruption or trans-Displacement of the Histone Octamer. Cell *97*, 843-852. 10.1016/s0092-8674(00)80797-7.
Lareau, C.A., Duarte, F.M., Chew, J.G., Kartha, V.K., Burkett, Z.D., Kohlway, A.S., Pokholok, D., Aryee, M.J., Steemers, F.J., Lebofsky, R., and Buenrostro, J.D. (2019). Droplet-based combinatorial indexing for massive-scale single-cell chromatin accessibility. Nat Biotechnol *37*, 916-924. 10.1038/s41587-019-0147-6.
Larson, E.D., Marsh, A.J., and Harrison, M.M. (2021). Pioneering the developmental frontier. Mol Cell *81*, 1640-1650. 10.1016/j.molcel.2021.02.020.
Lawrence, T. (2009). The nuclear factor NF-kappaB pathway in inflammation. Cold Spring Harb Perspect Biol *1*, a001651. 10.1101/cshperspect.a001651.
Lee, C.K., Shibata, Y., Rao, B., Strahl, B.D., and Lieb, J.D. (2004). Evidence for nucleosome depletion at active regulatory regions genome-wide. Nat Genet *36*, 900-905. 10.1038/ng1400.
Lee, T.I., and Young, R.A. (2013). Transcriptional regulation and its misregulation in disease. Cell *152*, 1237-1251. 10.1016/j.cell.2013.02.014.
Leyton, J., Drury, P.J., and Crawford, M.A. (1987). Differential oxidation of saturated and unsaturated fatty acids in vivo in the rat. Br J Nutr *57*, 383-393. 10.1079/bjn19870046.
Li, Y., Ping, X., Zhang, Y., Li, G., Zhang, T., Chen, G., Ma, X., Wang, D., and Xu, L. (2021). Comparative Transcriptome Profiling of Cold Exposure and beta3-AR Agonist CL316,243-Induced Browning of White Fat. Front Physiol *12*, 667698. 10.3389/fphys.2021.667698.
Lim, J.H., Gerhart-Hines, Z., Dominy, J.E., Lee, Y., Kim, S., Tabata, M., Xiang, Y.K., and Puigserver, P. (2013). Oleic acid stimulates complete oxidation of fatty acids through protein kinase A-dependent activation of SIRT1-PGC1alpha complex. J Biol Chem *288*, 7117-7126. 10.1074/jbc.M112.415729.
Lister, R., Pelizzola, M., Dowen, R.H., Hawkins, R.D., Hon, G., Tonti-Filippini, J., Nery, J.R., Lee, L., Ye, Z., Ngo, Q.M., et al. (2009). Human DNA methylomes at base resolution show widespread epigenomic differences.

Nature *462*, 315-322. 10.1038/nature08514.
Lodhi, I.J., Wei, X., and Semenkovich, C.F. (2011). Lipoexpediency: de novo lipogenesis as a metabolic signal transmitter. Trends Endocrinol Metab *22*, 1-8. 10.1016/j.tem.2010.09.002.
Lorch, Y., Zhang, M., and Kornberg, R.D. (1999). Histone Octamer Transfer by a Chromatin-Remodeling Complex. Cell *96*, 389-392. 10.1016/s0092-8674(00)80551-6.
Luger, K., Mader, A.W., Richmond, R.K., Sargent, D.F., and Richmond, T.J. (1997). Crystal structure of the nucleosome core particle at 2.8 A resolution. Nature *389*, 251-260. 10.1038/38444.
Ma, S., Zhang, B., LaFave, L.M., Earl, A.S., Chiang, Z., Hu, Y., Ding, J., Brack, A., Kartha, V.K., Tay, T., et al. (2020). Chromatin Potential Identified by Shared Single-Cell Profiling of RNA and Chromatin. Cell *183*, 1103-1116 e1120. 10.1016/j.cell.2020.09.056.
Mayran, A., and Drouin, J. (2018). Pioneer transcription factors shape the epigenetic landscape. J Biol Chem *293*, 13795-13804. 10.1074/jbc.R117.001232.
McLean, C.Y., Bristor, D., Hiller, M., Clarke, S.L., Schaar, B.T., Lowe, C.B., Wenger, A.M., and Bejerano, G. (2010). GREAT improves functional interpretation of cis-regulatory regions. Nat Biotechnol *28*, 495-501. 10.1038/nbt.1630.
Michel, L.Y.M., Farah, C., and Balligand, J.L. (2020). The Beta3 Adrenergic Receptor in Healthy and Pathological Cardiovascular Tissues. Cells *9*. 10.3390/cells9122584.
Mimitou, E.P., Lareau, C.A., Chen, K.Y., Zorzetto-Fernandes, A.L., Hao, Y., Takeshima, Y., Luo, W., Huang, T.S., Yeung, B.Z., Papalexi, E., et al. (2021). Scalable, multimodal profiling of chromatin accessibility, gene expression and protein levels in single cells. Nat Biotechnol *39*, 1246-1258. 10.1038/s41587-021-00927-2.
Mottillo, E.P., Balasubramanian, P., Lee, Y.H., Weng, C., Kershaw, E.E., and Granneman, J.G. (2014). Coupling of lipolysis and de novo lipogenesis in brown, beige, and white adipose tissues during chronic beta3-adrenergic receptor activation. J Lipid Res *55*, 2276-2286. 10.1194/jlr.M050005.
Musselman, C.A., Lalonde, M.E., Cote, J., and Kutateladze, T.G. (2012). Perceiving the epigenetic landscape through histone readers. Nat Struct Mol Biol *19*, 1218-1227. 10.1038/nsmb.2436.
Nie, B., Nie, T., Hui, X., Gu, P., Mao, L., Li, K., Yuan, R., Zheng, J., Wang, H., Li, K., et al. (2017). Brown Adipogenic Reprogramming Induced by a Small Molecule. Cell Rep *18*, 624-635. 10.1016/j.celrep.2016.12.062.
Ohno, H., Shinoda, K., Spiegelman, B.M., and Kajimura, S. (2012). PPARgamma agonists induce a white-to-brown fat conversion through stabilization of PRDM16 protein. Cell Metab *15*, 395-404. 10.1016/j.cmet.2012.01.019.
Ou, J., Liu, H., Yu, J., Kelliher, M.A., Castilla, L.H., Lawson, N.D., and Zhu, L.J. (2018). ATACseqQC: a Bioconductor package for post-alignment quality

assessment of ATAC-seq data. BMC Genomics *19*, 169. 10.1186/s12864-018-4559-3.

Picelli, S., Bjorklund, A.K., Reinius, B., Sagasser, S., Winberg, G., and Sandberg, R. (2014). Tn5 transposase and tagmentation procedures for massively scaled sequencing projects. Genome Res *24*, 2033-2040. 10.1101/gr.177881.114.

Pliner, H.A., Packer, J.S., McFaline-Figueroa, J.L., Cusanovich, D.A., Daza, R.M., Aghamirzaie, D., Srivatsan, S., Qiu, X., Jackson, D., Minkina, A., et al. (2018). Cicero Predicts cis-Regulatory DNA Interactions from Single-Cell Chromatin Accessibility Data. Mol Cell *71*, 858-871 e858. 10.1016/j.molcel.2018.06.044.

Preissl, S., Fang, R., Huang, H., Zhao, Y., Raviram, R., Gorkin, D.U., Zhang, Y., Sos, B.C., Afzal, V., Dickel, D.E., et al. (2018). Single-nucleus analysis of accessible chromatin in developing mouse forebrain reveals cell-type-specific transcriptional regulation. Nat Neurosci *21*, 432-439. 10.1038/s41593-018-0079-3.

Rabhi, N., Belkina, A.C., Desevin, K., Cortez, B.N., and Farmer, S.R. (2020). Shifts of Immune Cell Populations Differ in Response to Different Effectors of Beige Remodeling of Adipose Tissue. iScience *23*, 101765. 10.1016/j.isci.2020.101765.

Rajbhandari, P., Arneson, D., Hart, S.K., Ahn, I.S., Diamante, G., Santos, L.C., Zaghari, N., Feng, A.C., Thomas, B.J., Vergnes, L., et al. (2019). Single cell analysis reveals immune cell-adipocyte crosstalk regulating the transcription of thermogenic adipocytes. Elife *8*. 10.7554/eLife.49501.

Rhee, H.S., and Pugh, B.F. (2011). Comprehensive genome-wide protein-DNA interactions detected at single-nucleotide resolution. Cell *147*, 1408-1419. 10.1016/j.cell.2011.11.013.

Roh, H.C., Tsai, L.T.Y., Shao, M., Tenen, D., Shen, Y., Kumari, M., Lyubetskaya, A., Jacobs, C., Dawes, B., Gupta, R.K., and Rosen, E.D. (2018). Warming Induces Significant Reprogramming of Beige, but Not Brown, Adipocyte Cellular Identity. Cell Metab *27*, 1121-1137 e1125. 10.1016/j.cmet.2018.03.005.

Rosen, E.D., Hsu, C.H., Wang, X., Sakai, S., Freeman, M.W., Gonzalez, F.J., and Spiegelman, B.M. (2002). C/EBPalpha induces adipogenesis through PPARgamma: a unified pathway. Genes Dev *16*, 22-26. 10.1101/gad.948702.

Rosen, E.D., and Spiegelman, B.M. (2014). What we talk about when we talk about fat. Cell *156*, 20-44. 10.1016/j.cell.2013.12.012.

Rosenberg, A.B., Roco, C.M., Muscat, R.A., Kuchina, A., Sample, P., Yao, Z., Graybuck, L.T., Peeler, D.J., Mukherjee, S., Chen, W., et al. (2018). Single-cell profiling of the developing mouse brain and spinal cord with split-pool barcoding. Science *360*, 176-182. 10.1126/science.aam8999.

Rosenwald, M., Perdikari, A., Rulicke, T., and Wolfrum, C. (2013). Bi-directional interconversion of brite and white adipocytes. Nat Cell Biol *15*, 659-667. 10.1038/ncb2740.

Schep, A.N., Wu, B., Buenrostro, J.D., and Greenleaf, W.J. (2017). chromVAR: inferring transcription-factor-associated accessibility from single-cell epigenomic data. Nat Methods *14*, 975-978. 10.1038/nmeth.4401.

Schlesinger, F., Smith, A.D., Gingeras, T.R., Hannon, G.J., and Hodges, E. (2013). De novo DNA demethylation and noncoding transcription define active intergenic regulatory elements. Genome Res *23*, 1601-1614. 10.1101/gr.157271.113.

Schones, D.E., Cui, K., Cuddapah, S., Roh, T.Y., Barski, A., Wang, Z., Wei, G., and Zhao, K. (2008). Dynamic regulation of nucleosome positioning in the human genome. Cell *132*, 887-898. 10.1016/j.cell.2008.02.022.

Schreiber, S.N., Emter, R., Hock, M.B., Knutti, D., Cardenas, J., Podvinec, M., Oakeley, E.J., and Kralli, A. (2004). The estrogen-related receptor alpha (ERRalpha) functions in PPARgamma coactivator 1alpha (PGC-1alpha)-induced mitochondrial biogenesis. Proc Natl Acad Sci U S A *101*, 6472-6477. 10.1073/pnas.0308686101.

Sims, R.J., 3rd, and Reinberg, D. (2004). From chromatin to cancer: a new histone lysine methyltransferase enters the mix. Nat Cell Biol *6*, 685-687. 10.1038/ncb0804-685.

Skene, P.J., and Henikoff, S. (2017). An efficient targeted nuclease strategy for high-resolution mapping of DNA binding sites. Elife *6*. 10.7554/eLife.21856.

Soumano, K. (2000). Glucocorticoids inhibit the transcriptional response of the uncoupling protein-1 gene to adrenergic stimulation in a brown adipose cell line. Molecular and Cellular Endocrinology *165*, 7-15. 10.1016/s0303-7207(00)00276-8.

Spektor, R., Yang, J.W., Lee, S., and Soloway, P.D. (2019). Single cell ATAC-seq identifies broad changes in neuronal abundance and chromatin accessibility in Down Syndrome. bioRxiv. 10.1101/561191.

Staub, E., Grone, J., Mennerich, D., Ropcke, S., Klamann, I., Hinzmann, B., Castanos-Velez, E., Mann, B., Pilarsky, C., Brummendorf, T., et al. (2006). A genome-wide map of aberrantly expressed chromosomal islands in colorectal cancer. Mol Cancer *5*, 37. 10.1186/1476-4598-5-37.

Strack, A.M., Bradbury, M.J., and Dallman, M.F. (1995). Corticosterone decreases nonshivering thermogenesis and increases lipid storage in brown adipose tissue. Am J Physiol *268*, R183-191. 10.1152/ajpregu.1995.268.1.R183.

Stuart, T., Butler, A., Hoffman, P., Hafemeister, C., Papalexi, E., Mauck, W.M., 3rd, Hao, Y., Stoeckius, M., Smibert, P., and Satija, R. (2019). Comprehensive Integration of Single-Cell Data. Cell *177*, 1888-1902 e1821. 10.1016/j.cell.2019.05.031.

Stuart, T., Srivastava, A., Madad, S., Lareau, C.A., and Satija, R. (2021). Single-cell chromatin state analysis with Signac. Nat Methods *18*, 1333-1341. 10.1038/s41592-021-01282-5.

Sun, W., Dong, H., Balaz, M., Slyper, M., Drokhlyansky, E., Colleluori, G., Giordano, A., Kovanicova, Z., Stefanicka, P., Balazova, L., et al. (2020). snRNA-seq reveals a subpopulation of adipocytes that regulates

thermogenesis. Nature *587*, 98-102. 10.1038/s41586-020-2856-x.
Swanson, E., Lord, C., Reading, J., Heubeck, A.T., Genge, P.C., Thomson, Z., Weiss, M.D., Li, X.J., Savage, A.K., Green, R.R., et al. (2021). Simultaneous trimodal single-cell measurement of transcripts, epitopes, and chromatin accessibility using TEA-seq. Elife *10*. 10.7554/eLife.63632.
Thiele, A., Luettges, K., Ritter, D., Beyhoff, N., Smeir, E., Grune, J., Steinhoff, J.S., Schupp, M., Klopfleisch, R., Rothe, M., et al. (2021). Pharmacological inhibition of adipose tissue Adipose Triglyceride Lipase (ATGL) by Atglistatin prevents catecholamine-induced myocardial damage. Cardiovasc Res. 10.1093/cvr/cvab182.
Thuzar, M., Law, W.P., Ratnasingam, J., Jang, C., Dimeski, G., and Ho, K.K.Y. (2018). Glucocorticoids suppress brown adipose tissue function in humans: A double-blind placebo-controlled study. Diabetes Obes Metab *20*, 840-848. 10.1111/dom.13157.
Tiku, P.E., Gracey, A.Y., Macartney, A.I., Beynon, R.J., and Cossins, A.R. (1996). Cold-induced expression of delta 9-desaturase in carp by transcriptional and posttranslational mechanisms. Science *271*, 815-818. 10.1126/science.271.5250.815.
Trapnell, C., Cacchiarelli, D., Grimsby, J., Pokharel, P., Li, S., Morse, M., Lennon, N.J., Livak, K.J., Mikkelsen, T.S., and Rinn, J.L. (2014). The dynamics and regulators of cell fate decisions are revealed by pseudotemporal ordering of single cells. Nat Biotechnol *32*, 381-386. 10.1038/nbt.2859.
Vega, R.B., Huss, J.M., and Kelly, D.P. (2000). The coactivator PGC-1 cooperates with peroxisome proliferator-activated receptor alpha in transcriptional control of nuclear genes encoding mitochondrial fatty acid oxidation enzymes. Mol Cell Biol *20*, 1868-1876. 10.1128/MCB.20.5.1868-1876.2000.
Viengchareun, S., Penfornis, P., Zennaro, M.C., and Lombes, M. (2001). Mineralocorticoid and glucocorticoid receptors inhibit UCP expression and function in brown adipocytes. Am J Physiol Endocrinol Metab *280*, E640-649. 10.1152/ajpendo.2001.280.4.E640.
Vijay, J., Gauthier, M.F., Biswell, R.L., Louiselle, D.A., Johnston, J.J., Cheung, W.A., Belden, B., Pramatarova, A., Biertho, L., Gibson, M., et al. (2020). Single-cell analysis of human adipose tissue identifies depot and disease specific cell types. Nat Metab *2*, 97-109. 10.1038/s42255-019-0152-6.
Vitak, S.A., Torkenczy, K.A., Rosenkrantz, J.L., Fields, A.J., Christiansen, L., Wong, M.H., Carbone, L., Steemers, F.J., and Adey, A. (2017). Sequencing thousands of single-cell genomes with combinatorial indexing. Nat Methods *14*, 302-308. 10.1038/nmeth.4154.
Wales, S., Hashemi, S., Blais, A., and McDermott, J.C. (2014). Global MEF2 target gene analysis in cardiac and skeletal muscle reveals novel regulation of DUSP6 by p38MAPK-MEF2 signaling. Nucleic Acids Res *42*, 11349-11362. 10.1093/nar/gku813.
Weirauch, M.T., Yang, A., Albu, M., Cote, A.G., Montenegro-Montero, A.,

Drewe, P., Najafabadi, H.S., Lambert, S.A., Mann, I., Cook, K., et al. (2014). Determination and inference of eukaryotic transcription factor sequence specificity. Cell *158*, 1431-1443. 10.1016/j.cell.2014.08.009.

Wolock, S.L., Lopez, R., and Klein, A.M. (2019). Scrublet: Computational Identification of Cell Doublets in Single-Cell Transcriptomic Data. Cell Syst *8*, 281-291 e289. 10.1016/j.cels.2018.11.005.

Wu, C., Wong, Y.C., and Elgin, S.C. (1979). The chromatin structure of specific genes: II. Disruption of chromatin structure during gene activity. Cell *16*, 807-814. 10.1016/0092-8674(79)90096-5.

Wu, J., Bostrom, P., Sparks, L.M., Ye, L., Choi, J.H., Giang, A.H., Khandekar, M., Virtanen, K.A., Nuutila, P., Schaart, G., et al. (2012). Beige adipocytes are a distinct type of thermogenic fat cell in mouse and human. Cell *150*, 366-376. 10.1016/j.cell.2012.05.016.

Yu, G., Wang, L.G., Han, Y., and He, Q.Y. (2012). clusterProfiler: an R package for comparing biological themes among gene clusters. OMICS *16*, 284-287. 10.1089/omi.2011.0118.

Yue, F., Cheng, Y., Breschi, A., Vierstra, J., Wu, W., Ryba, T., Sandstrom, R., Ma, Z., Davis, C., Pope, B.D., et al. (2014). A comparative encyclopedia of DNA elements in the mouse genome. Nature *515*, 355-364. 10.1038/nature13992.

Zaret, K.S., and Mango, S.E. (2016). Pioneer transcription factors, chromatin dynamics, and cell fate control. Curr Opin Genet Dev *37*, 76-81. 10.1016/j.gde.2015.12.003.

Zhang, W., Xu, J., Li, J., Guo, T., Jiang, D., Feng, X., Ma, X., He, L., Wu, W., Yin, M., et al. (2018). The TEA domain family transcription factor TEAD4 represses murine adipogenesis by recruiting the cofactors VGLL4 and CtBP2 into a transcriptional complex. J Biol Chem *293*, 17119-17134. 10.1074/jbc.RA118.003608.

Zhang, Y., LeRoy, G., Seelig, H.-P., Lane, W.S., and Reinberg, D. (1998). The Dermatomyositis-Specific Autoantigen Mi2 Is a Component of a Complex Containing Histone Deacetylase and Nucleosome Remodeling Activities. Cell *95*, 279-289. 10.1016/s0092-8674(00)81758-4.

Zhang, Y., Liu, T., Meyer, C.A., Eeckhoute, J., Johnson, D.S., Bernstein, B.E., Nusbaum, C., Myers, R.M., Brown, M., Li, W., and Liu, X.S. (2008). Model-based analysis of ChIP-Seq (MACS). Genome Biol *9*, R137. 10.1186/gb-2008-9-9-r137.

Zhong, Z., Feng, S., Duttke, S.H., Potok, M.E., Zhang, Y., Gallego-Bartolome, J., Liu, W., and Jacobsen, S.E. (2021). DNA methylation-linked chromatin accessibility affects genomic architecture in Arabidopsis. Proc Natl Acad Sci U S A *118*. 10.1073/pnas.2023347118.

Zhu, C., Yu, M., Huang, H., Juric, I., Abnousi, A., Hu, R., Lucero, J., Behrens, M.M., Hu, M., and Ren, B. (2019). An ultra high-throughput method for single-cell joint analysis of open chromatin and transcriptome. Nat Struct Mol Biol *26*, 1063-1070. 10.1038/s41594-019-0323-x.

REFERENCES: Chapter 3

Adam, R.C., Yang, H., Ge, Y., Infarinato, N.R., Gur-Cohen, S., Miao, Y., Wang, P., Zhao, Y., Lu, C.P., Kim, J.E., et al. (2020). NFI transcription factors provide chromatin access to maintain stem cell identity while preventing unintended lineage fate choices. Nat Cell Biol *22*, 640-650. 10.1038/s41556-020-0513-0.

Adey, A., Morrison, H.G., Asan, Xun, X., Kitzman, J.O., Turner, E.H., Stackhouse, B., MacKenzie, A.P., Caruccio, N.C., Zhang, X., and Shendure, J. (2010). Rapid, low-input, low-bias construction of shotgun fragment libraries by high-density in vitro transposition. Genome Biol *11*, R119. 10.1186/gb-2010-11-12-r119.

Altschuler, S.J., and Wu, L.F. (2010). Cellular heterogeneity: do differences make a difference? Cell *141*, 559-563. 10.1016/j.cell.2010.04.033.

Amemiya, H.M., Kundaje, A., and Boyle, A.P. (2019). The ENCODE Blacklist: Identification of Problematic Regions of the Genome. Sci Rep *9*, 9354. 10.1038/s41598-019-45839-z.

Arany, Z., Foo, S.Y., Ma, Y., Ruas, J.L., Bommi-Reddy, A., Girnun, G., Cooper, M., Laznik, D., Chinsomboon, J., Rangwala, S.M., et al. (2008). HIF-independent regulation of VEGF and angiogenesis by the transcriptional coactivator PGC-1alpha. Nature *451*, 1008-1012. 10.1038/nature06613.

Arch, J.R. (2011). Challenges in beta(3)-Adrenoceptor Agonist Drug Development. Ther Adv Endocrinol Metab *2*, 59-64. 10.1177/2042018811398517.

Arnaudo, A.M., and Garcia, B.A. (2013). Proteomic characterization of novel histone post-translational modifications. Epigenetics Chromatin *6*, 24. 10.1186/1756-8935-6-24.

Aune, U.L., Ruiz, L., and Kajimura, S. (2013). Isolation and differentiation of stromal vascular cells to beige/brite cells. J Vis Exp. 10.3791/50191.

Bagci, T., Wu, J.K., Pfannl, R., Ilag, L.L., and Jay, D.G. (2009). Autocrine semaphorin 3A signaling promotes glioblastoma dispersal. Oncogene *28*, 3537-3550. 10.1038/onc.2009.204.

Baker, R.G., Hayden, M.S., and Ghosh, S. (2011). NF-kappaB, inflammation, and metabolic disease. Cell Metab *13*, 11-22. 10.1016/j.cmet.2010.12.008.

Barbatelli, G., Murano, I., Madsen, L., Hao, Q., Jimenez, M., Kristiansen, K., Giacobino, J.P., De Matteis, R., and Cinti, S. (2010). The emergence of cold-induced brown adipocytes in mouse white fat depots is determined predominantly by white to brown adipocyte transdifferentiation. Am J Physiol Endocrinol Metab *298*, E1244-1253. 10.1152/ajpendo.00600.2009.

Barquissau, V., Beuzelin, D., Pisani, D.F., Beranger, G.E., Mairal, A., Montagner, A., Roussel, B., Tavernier, G., Marques, M.A., Moro, C., et al. (2016). White-to-brite conversion in human adipocytes promotes metabolic reprogramming towards fatty acid anabolic and catabolic pathways. Mol Metab *5*, 352-365. 10.1016/j.molmet.2016.03.002.

Barski, A., Cuddapah, S., Cui, K., Roh, T.Y., Schones, D.E., Wang, Z., Wei, G.,

Chepelev, I., and Zhao, K. (2007). High-resolution profiling of histone methylations in the human genome. Cell *129*, 823-837. 10.1016/j.cell.2007.05.009.

Behrens, J., von Kries, J.P., Kuhl, M., Bruhn, L., Wedlich, D., Grosschedl, R., and Birchmeier, W. (1996). Functional interaction of beta-catenin with the transcription factor LEF-1. Nature *382*, 638-642. 10.1038/382638a0.

Bennett, D.C., Cooper, P.J., and Hart, I.R. (1987). A line of non-tumorigenic mouse melanocytes, syngeneic with the B16 melanoma and requiring a tumour promoter for growth. Int J Cancer *39*, 414-418. 10.1002/ijc.2910390324.

Bernstein, B.E., Kamal, M., Lindblad-Toh, K., Bekiranov, S., Bailey, D.K., Huebert, D.J., McMahon, S., Karlsson, E.K., Kulbokas, E.J., 3rd, Gingeras, T.R., et al. (2005). Genomic maps and comparative analysis of histone modifications in human and mouse. Cell *120*, 169-181. 10.1016/j.cell.2005.01.001.

Berry, D.C., Jiang, Y., and Graff, J.M. (2016). Mouse strains to study cold-inducible beige progenitors and beige adipocyte formation and function. Nat Commun *7*, 10184. 10.1038/ncomms10184.

Bhattacharya, D., Azambuja, A.P., and Simoes-Costa, M. (2020). Metabolic Reprogramming Promotes Neural Crest Migration via Yap/Tead Signaling. Dev Cell *53*, 199-211 e196. 10.1016/j.devcel.2020.03.005.

Biagi, C.A.O., Jr., Cury, S.S., Alves, C.P., Rabhi, N., Silva, W.A., Jr., Farmer, S.R., Carvalho, R.F., and Batista, M.L., Jr. (2021). Multidimensional Single-Nuclei RNA-Seq Reconstruction of Adipose Tissue Reveals Adipocyte Plasticity Underlying Thermogenic Response. Cells *10*. 10.3390/cells10113073.

Botchkareva, N.V., Botchkarev, V.A., and Gilchrest, B.A. (2003). Fate of melanocytes during development of the hair follicle pigmentary unit. J Investig Dermatol Symp Proc *8*, 76-79. 10.1046/j.1523-1747.2003.12176.x.

Boyadjiev, S.A., and Jabs, E.W. (2000). Online Mendelian Inheritance in Man (OMIM) as a knowledgebase for human developmental disorders. Clin Genet *57*, 253-266. 10.1034/j.1399-0004.2000.570403.x.

Boyle, A.P., Davis, S., Shulha, H.P., Meltzer, P., Margulies, E.H., Weng, Z., Furey, T.S., and Crawford, G.E. (2008). High-resolution mapping and characterization of open chromatin across the genome. Cell *132*, 311-322. 10.1016/j.cell.2007.12.014.

Bradner, J.E., Hnisz, D., and Young, R.A. (2017). Transcriptional Addiction in Cancer. Cell *168*, 629-643. 10.1016/j.cell.2016.12.013.

Brombin, A., Simpson, D.J., Travnickova, J., Brunsdon, H., Zeng, Z., Lu, Y., Young, A.I.J., Chandra, T., and Patton, E.E. (2022). Tfap2b specifies an embryonic melanocyte stem cell that retains adult multifate potential. Cell Rep *38*, 110234. 10.1016/j.celrep.2021.110234.

Brown, E.L., Hazen, B.C., Eury, E., Wattez, J.S., Gantner, M.L., Albert, V., Chau, S., Sanchez-Alavez, M., Conti, B., and Kralli, A. (2018). Estrogen-Related Receptors Mediate the Adaptive Response of Brown Adipose

Tissue to Adrenergic Stimulation. iScience *2*, 221-237. 10.1016/j.isci.2018.03.005.

Bruno, M., Flaus, A., Stockdale, C., Rencurel, C., Ferreira, H., and Owen-Hughes, T. (2003). Histone H2A/H2B Dimer Exchange by ATP-Dependent Chromatin Remodeling Activities. Molecular Cell *12*, 1599-1606. 10.1016/s1097-2765(03)00499-4.

Buenrostro, J.D., Giresi, P.G., Zaba, L.C., Chang, H.Y., and Greenleaf, W.J. (2013). Transposition of native chromatin for fast and sensitive epigenomic profiling of open chromatin, DNA-binding proteins and nucleosome position. Nat Methods *10*, 1213-1218. 10.1038/nmeth.2688.

Buenrostro, J.D., Wu, B., Litzenburger, U.M., Ruff, D., Gonzales, M.L., Snyder, M.P., Chang, H.Y., and Greenleaf, W.J. (2015). Single-cell chromatin accessibility reveals principles of regulatory variation. Nature *523*, 486-490. 10.1038/nature14590.

Burl, R.B., Ramseyer, V.D., Rondini, E.A., Pique-Regi, R., Lee, Y.H., and Granneman, J.G. (2018). Deconstructing Adipogenesis Induced by beta3-Adrenergic Receptor Activation with Single-Cell Expression Profiling. Cell Metab *28*, 300-309 e304. 10.1016/j.cmet.2018.05.025.

Cadoudal, T., Distel, E., Durant, S., Fouque, F., Blouin, J.M., Collinet, M., Bortoli, S., Forest, C., and Benelli, C. (2008). Pyruvate dehydrogenase kinase 4: regulation by thiazolidinediones and implication in glyceroneogenesis in adipose tissue. Diabetes *57*, 2272-2279. 10.2337/db08-0477.

Cao, J., Cusanovich, D.A., Ramani, V., Aghamirzaie, D., Pliner, H.A., Hill, A.J., Daza, R.M., McFaline-Figueroa, J.L., Packer, J.S., Christiansen, L., et al. (2018). Joint profiling of chromatin accessibility and gene expression in thousands of single cells. Science *361*, 1380-1385. 10.1126/science.aau0730.

Cao, J., Spielmann, M., Qiu, X., Huang, X., Ibrahim, D.M., Hill, A.J., Zhang, F., Mundlos, S., Christiansen, L., Steemers, F.J., et al. (2019). The single-cell transcriptional landscape of mammalian organogenesis. Nature *566*, 496-502. 10.1038/s41586-019-0969-x.

Chandra, V., Huang, P., Hamuro, Y., Raghuram, S., Wang, Y., Burris, T.P., and Rastinejad, F. (2008). Structure of the intact PPAR-gamma-RXR- nuclear receptor complex on DNA. Nature *456*, 350-356. 10.1038/nature07413.

Chang, J.S., Ghosh, S., Newman, S., and Salbaum, J.M. (2018). A map of the PGC-1alpha- and NT-PGC-1alpha-regulated transcriptional network in brown adipose tissue. Sci Rep *8*, 7876. 10.1038/s41598-018-26244-4.

Chaveroux, C., Eichner, L.J., Dufour, C.R., Shatnawi, A., Khoutorsky, A., Bourque, G., Sonenberg, N., and Giguere, V. (2013). Molecular and genetic crosstalks between mTOR and ERRalpha are key determinants of rapamycin-induced nonalcoholic fatty liver. Cell Metab *17*, 586-598. 10.1016/j.cmet.2013.03.003.

Chen, A.F., Parks, B., Kathiria, A.S., Ober-Reynolds, B., Goronzy, J.J., and Greenleaf, W.J. (2022). NEAT-seq: simultaneous profiling of intra-nuclear

proteins, chromatin accessibility and gene expression in single cells. Nat Methods *19*, 547-553. 10.1038/s41592-022-01461-y.

Chen, G., Sima, J., Jin, M., Wang, K.Y., Xue, X.J., Zheng, W., Ding, Y.Q., and Yuan, X.B. (2008). Semaphorin-3A guides radial migration of cortical neurons during development. Nat Neurosci *11*, 36-44. 10.1038/nn2018.

Chen, H., Lareau, C., Andreani, T., Vinyard, M.E., Garcia, S.P., Clement, K., Andrade-Navarro, M.A., Buenrostro, J.D., and Pinello, L. (2019a). Assessment of computational methods for the analysis of single-cell ATAC-seq data. Genome Biol *20*, 241. 10.1186/s13059-019-1854-5.

Chen, K.H., Boettiger, A.N., Moffitt, J.R., Wang, S., and Zhuang, X. (2015). RNA imaging. Spatially resolved, highly multiplexed RNA profiling in single cells. Science *348*, aaa6090. 10.1126/science.aaa6090.

Chen, S., Lake, B.B., and Zhang, K. (2019b). High-throughput sequencing of the transcriptome and chromatin accessibility in the same cell. Nat Biotechnol *37*, 1452-1457. 10.1038/s41587-019-0290-0.

Chen, X., Miragaia, R.J., Natarajan, K.N., and Teichmann, S.A. (2018). A rapid and robust method for single cell chromatin accessibility profiling. Nat Commun *9*, 5345. 10.1038/s41467-018-07771-0.

Chen, Y., Ikeda, K., Yoneshiro, T., Scaramozza, A., Tajima, K., Wang, Q., Kim, K., Shinoda, K., Sponton, C.H., Brown, Z., et al. (2019c). Thermal stress induces glycolytic beige fat formation via a myogenic state. Nature *565*, 180-185. 10.1038/s41586-018-0801-z.

Cheng, H., Pui, H.-p., Lentini, A., Kolbeinsdóttir, S., Andrews, N., Pei, Y., Reinius, B., Deng, Q., and Enge, M. (2021). Smart3-ATAC: a highly sensitive method for joint accessibility and full-length transcriptome analysis in single cells. bioRxiv. https://doi.org/10.1101/2021.12.02.470912.

Chi, J., Wu, Z., Choi, C.H.J., Nguyen, L., Tegegne, S., Ackerman, S.E., Crane, A., Marchildon, F., Tessier-Lavigne, M., and Cohen, P. (2018). Three-Dimensional Adipose Tissue Imaging Reveals Regional Variation in Beige Fat Biogenesis and PRDM16-Dependent Sympathetic Neurite Density. Cell Metab *27*, 226-236 e223. 10.1016/j.cmet.2017.12.011.

Chiang, S.H., Bazuine, M., Lumeng, C.N., Geletka, L.M., Mowers, J., White, N.M., Ma, J.T., Zhou, J., Qi, N., Westcott, D., et al. (2009). The protein kinase IKKepsilon regulates energy balance in obese mice. Cell *138*, 961-975. 10.1016/j.cell.2009.06.046.

Choe, S.S., Huh, J.Y., Hwang, I.J., Kim, J.I., and Kim, J.B. (2016). Adipose Tissue Remodeling: Its Role in Energy Metabolism and Metabolic Disorders. Front Endocrinol (Lausanne) *7*, 30. 10.3389/fendo.2016.00030.

Chou, W.C., Takeo, M., Rabbani, P., Hu, H., Lee, W., Chung, Y.R., Carucci, J., Overbeek, P., and Ito, M. (2013). Direct migration of follicular melanocyte stem cells to the epidermis after wounding or UVB irradiation is dependent on Mc1r signaling. Nat Med *19*, 924-929. 10.1038/nm.3194.

Chu, T., Rice, E.J., Booth, G.T., Salamanca, H.H., Wang, Z., Core, L.J., Longo, S.L., Corona, R.J., Chin, L.S., Lis, J.T., et al. (2018). Chromatin run-on and sequencing maps the transcriptional regulatory landscape of glioblastoma

multiforme. Nat Genet *50*, 1553-1564. 10.1038/s41588-018-0244-3.
Chung, H., Suh, E.K., Han, I.O., and Oh, E.S. (2011). Keratinocyte-derived laminin-332 promotes adhesion and migration in melanocytes and melanoma. J Biol Chem *286*, 13438-13447. 10.1074/jbc.M110.166751.
Chuo, D., Liu, F., Chen, Y., and Yin, M. (2019). LncRNA MIR503HG is downregulated in Han Chinese with colorectal cancer and inhibits cell migration and invasion mediated by TGF-beta2. Gene *713*, 143960. 10.1016/j.gene.2019.143960.
Cinti, S., Zingaretti, M.C., Cancello, R., Ceresi, E., and Ferrara, P. (2001). Morphologic techniques for the study of brown adipose tissue and white adipose tissue. Methods Mol Biol *155*, 21-51. 10.1385/1-59259-231-7:021.
Clark, S.J., Argelaguet, R., Kapourani, C.A., Stubbs, T.M., Lee, H.J., Alda-Catalinas, C., Krueger, F., Sanguinetti, G., Kelsey, G., Marioni, J.C., et al. (2018). scNMT-seq enables joint profiling of chromatin accessibility DNA methylation and transcription in single cells. Nat Commun *9*, 781. 10.1038/s41467-018-03149-4.
Corces, M.R., Trevino, A.E., Hamilton, E.G., Greenside, P.G., Sinnott-Armstrong, N.A., Vesuna, S., Satpathy, A.T., Rubin, A.J., Montine, K.S., Wu, B., et al. (2017). An improved ATAC-seq protocol reduces background and enables interrogation of frozen tissues. Nat Methods *14*, 959-962. 10.1038/nmeth.4396.
Cox, A.R., Chernis, N., Bader, D.A., Saha, P.K., Masschelin, P.M., Felix, J.B., Sharp, R., Lian, Z., Putluri, V., Rajapakshe, K., et al. (2020). STAT1 Dissociates Adipose Tissue Inflammation From Insulin Sensitivity in Obesity. Diabetes *69*, 2630-2641. 10.2337/db20-0384.
Cui, J., Shen, L.Y., and Wang, G.C. (1991). Role of hair follicles in the repigmentation of vitiligo. J Invest Dermatol *97*, 410-416. 10.1111/1523-1747.ep12480997.
Cusanovich, D.A., Daza, R., Adey, A., Pliner, H.A., Christiansen, L., Gunderson, K.L., Steemers, F.J., Trapnell, C., and Shendure, J. (2015). Multiplex single cell profiling of chromatin accessibility by combinatorial cellular indexing. Science *348*, 910-914. 10.1126/science.aab1601.
Cusanovich, D.A., Hill, A.J., Aghamirzaie, D., Daza, R.M., Pliner, H.A., Berletch, J.B., Filippova, G.N., Huang, X., Christiansen, L., DeWitt, W.S., et al. (2018). A Single-Cell Atlas of In Vivo Mammalian Chromatin Accessibility. Cell *174*, 1309-1324 e1318. 10.1016/j.cell.2018.06.052.
Cypess, A.M., and Kahn, C.R. (2010a). Brown fat as a therapy for obesity and diabetes. Curr Opin Endocrinol Diabetes Obes *17*, 143-149. 10.1097/MED.0b013e328337a81f.
Cypess, A.M., and Kahn, C.R. (2010b). The role and importance of brown adipose tissue in energy homeostasis. Curr Opin Pediatr *22*, 478-484. 10.1097/MOP.0b013e32833a8d6e.
Czubryt, M.P., McAnally, J., Fishman, G.I., and Olson, E.N. (2003). Regulation of peroxisome proliferator-activated receptor gamma coactivator 1 alpha (PGC-1 alpha) and mitochondrial function by MEF2 and HDAC5. Proc Natl

Acad Sci U S A *100*, 1711-1716. 10.1073/pnas.0337639100.
Dann, E., Henderson, N.C., Teichmann, S.A., Morgan, M.D., and Marioni, J.C. (2022). Differential abundance testing on single-cell data using k-nearest neighbor graphs. Nat Biotechnol *40*, 245-253. 10.1038/s41587-021-01033-z.
Deng, Y., Bartosovic, M., Ma, S., Zhang, D., Liu, Y., Qin, X., Su, G., Xu, M.L., Halene, S., Craft, J.E., et al. (2021). Spatial-ATAC-seq: spatially resolved chromatin accessibility profiling of tissues at genome scale and cellular level. bioRxiv. 10.1101/2021.06.06.447244.
Dixit, A., Parnas, O., Li, B., Chen, J., Fulco, C.P., Jerby-Arnon, L., Marjanovic, N.D., Dionne, D., Burks, T., Raychowdhury, R., et al. (2016). Perturb-Seq: Dissecting Molecular Circuits with Scalable Single-Cell RNA Profiling of Pooled Genetic Screens. Cell *167*, 1853-1866 e1817. 10.1016/j.cell.2016.11.038.
Domcke, S., Hill, A.J., Daza, R.M., Cao, J., O'Day, D.R., Pliner, H.A., Aldinger, K.A., Pokholok, D., Zhang, F., Milbank, J.H., et al. (2020). A human cell atlas of fetal chromatin accessibility. Science *370*. 10.1126/science.aba7612.
Fang, R., Preissl, S., Li, Y., Hou, X., Lucero, J., Wang, X., Motamedi, A., Shiau, A.K., Zhou, X., Xie, F., et al. (2021). Comprehensive analysis of single cell ATAC-seq data with SnapATAC. Nat Commun *12*, 1337. 10.1038/s41467-021-21583-9.
Fernandez Garcia, M., Moore, C.D., Schulz, K.N., Alberto, O., Donague, G., Harrison, M.M., Zhu, H., and Zaret, K.S. (2019). Structural Features of Transcription Factors Associating with Nucleosome Binding. Mol Cell *75*, 921-932 e926. 10.1016/j.molcel.2019.06.009.
Ferrara, N., Gerber, H.P., and LeCouter, J. (2003). The biology of VEGF and its receptors. Nat Med *9*, 669-676. 10.1038/nm0603-669.
Finck, B.N., and Kelly, D.P. (2006). PGC-1 coactivators: inducible regulators of energy metabolism in health and disease. J Clin Invest *116*, 615-622. 10.1172/JCI27794.
Fornes, O., Castro-Mondragon, J.A., Khan, A., van der Lee, R., Zhang, X., Richmond, P.A., Modi, B.P., Correard, S., Gheorghe, M., Baranasic, D., et al. (2020). JASPAR 2020: update of the open-access database of transcription factor binding profiles. Nucleic Acids Res *48*, D87-D92. 10.1093/nar/gkz1001.
Fuchs, E., Merrill, B.J., Jamora, C., and DasGupta, R. (2001). At the Roots of a Never-Ending Cycle. Developmental Cell *1*, 13-25. 10.1016/s1534-5807(01)00022-3.
Garces, R., and Mancha, M. (1993). One-step lipid extraction and fatty acid methyl esters preparation from fresh plant tissues. Anal Biochem *211*, 139-143. 10.1006/abio.1993.1244.
Gilbert, L.A., Larson, M.H., Morsut, L., Liu, Z., Brar, G.A., Torres, S.E., Stern-Ginossar, N., Brandman, O., Whitehead, E.H., Doudna, J.A., et al. (2013). CRISPR-mediated modular RNA-guided regulation of transcription in eukaryotes. Cell *154*, 442-451. 10.1016/j.cell.2013.06.044.

Gillette, T.G., and Hill, J.A. (2015). Readers, writers, and erasers: chromatin as the whiteboard of heart disease. Circ Res *116*, 1245-1253. 10.1161/CIRCRESAHA.116.303630.

Giresi, P.G., Kim, J., McDaniell, R.M., Iyer, V.R., and Lieb, J.D. (2007). FAIRE (Formaldehyde-Assisted Isolation of Regulatory Elements) isolates active regulatory elements from human chromatin. Genome Res *17*, 877-885. 10.1101/gr.5533506.

Goryshin, I.Y., and Reznikoff, W.S. (1998). Tn5 in vitro transposition. J Biol Chem *273*, 7367-7374. 10.1074/jbc.273.13.7367.

Goto, T., Lee, J.Y., Teraminami, A., Kim, Y.I., Hirai, S., Uemura, T., Inoue, H., Takahashi, N., and Kawada, T. (2011). Activation of peroxisome proliferator-activated receptor-alpha stimulates both differentiation and fatty acid oxidation in adipocytes. J Lipid Res *52*, 873-884. 10.1194/jlr.M011320.

Granja, J.M., Corces, M.R., Pierce, S.E., Bagdatli, S.T., Choudhry, H., Chang, H.Y., and Greenleaf, W.J. (2021). ArchR is a scalable software package for integrative single-cell chromatin accessibility analysis. Nat Genet *53*, 403-411. 10.1038/s41588-021-00790-6.

Guilherme, A., Yenilmez, B., Bedard, A.H., Henriques, F., Liu, D., Lee, A., Goldstein, L., Kelly, M., Nicoloro, S.M., Chen, M., et al. (2020). Control of Adipocyte Thermogenesis and Lipogenesis through beta3-Adrenergic and Thyroid Hormone Signal Integration. Cell Rep *31*, 107598. 10.1016/j.celrep.2020.107598.

Guo, H., Xing, Y., Liu, Y., Luo, Y., Deng, F., Yang, T., Yang, K., and Li, Y. (2016). Wnt/beta-catenin signaling pathway activates melanocyte stem cells in vitro and in vivo. J Dermatol Sci *83*, 45-51. 10.1016/j.jdermsci.2016.04.005.

Hamiche, A., Sandaltzopoulos, R., Gdula, D.A., and Wu, C. (1999). ATP-Dependent Histone Octamer Sliding Mediated by the Chromatin Remodeling Complex NURF. Cell *97*, 833-842. 10.1016/s0092-8674(00)80796-5.

Han, J., Lee, J.E., Jin, J., Lim, J.S., Oh, N., Kim, K., Chang, S.I., Shibuya, M., Kim, H., and Koh, G.Y. (2011). The spatiotemporal development of adipose tissue. Development *138*, 5027-5037. 10.1242/dev.067686.

Han, X., Zhang, Z., He, L., Zhu, H., Li, Y., Pu, W., Han, M., Zhao, H., Liu, K., Li, Y., et al. (2021). A suite of new Dre recombinase drivers markedly expands the ability to perform intersectional genetic targeting. Cell Stem Cell *28*, 1160-1176 e1167. 10.1016/j.stem.2021.01.007.

Hao, Y., Hao, S., Andersen-Nissen, E., Mauck, W.M., 3rd, Zheng, S., Butler, A., Lee, M.J., Wilk, A.J., Darby, C., Zager, M., et al. (2021). Integrated analysis of multimodal single-cell data. Cell *184*, 3573-3587 e3529. 10.1016/j.cell.2021.04.048.

Harms, M., and Seale, P. (2013). Brown and beige fat: development, function and therapeutic potential. Nat Med *19*, 1252-1263. 10.1038/nm.3361.

Hearing, V.J. (2005). Biogenesis of pigment granules: a sensitive way to regulate melanocyte function. J Dermatol Sci *37*, 3-14. 10.1016/j.jdermsci.2004.08.014.

Heintzman, N.D., Stuart, R.K., Hon, G., Fu, Y., Ching, C.W., Hawkins, R.D.,

Barrera, L.O., Van Calcar, S., Qu, C., Ching, K.A., et al. (2007). Distinct and predictive chromatin signatures of transcriptional promoters and enhancers in the human genome. Nat Genet *39*, 311-318. 10.1038/ng1966.

Henikoff, S. (2008). Nucleosome destabilization in the epigenetic regulation of gene expression. Nat Rev Genet *9*, 15-26. 10.1038/nrg2206.

Hiraike, Y., Waki, H., Yu, J., Nakamura, M., Miyake, K., Nagano, G., Nakaki, R., Suzuki, K., Kobayashi, H., Yamamoto, S., et al. (2017). NFIA co-localizes with PPARgamma and transcriptionally controls the brown fat gene program. Nat Cell Biol *19*, 1081-1092. 10.1038/ncb3590.

Howe, K.L., Achuthan, P., Allen, J., Allen, J., Alvarez-Jarreta, J., Amode, M.R., Armean, I.M., Azov, A.G., Bennett, R., Bhai, J., et al. (2021). Ensembl 2021. Nucleic Acids Res *49*, D884-D891. 10.1093/nar/gkaa942.

Hu, Z.Q., Zhou, S.L., Zhou, Z.J., Luo, C.B., Chen, E.B., Zhan, H., Wang, P.C., Dai, Z., Zhou, J., Fan, J., and Huang, X.W. (2016). Overexpression of semaphorin 3A promotes tumor progression and predicts poor prognosis in hepatocellular carcinoma after curative resection. Oncotarget *7*, 51733-51746. 10.18632/oncotarget.10104.

Huss, J.M., Torra, I.P., Staels, B., Giguere, V., and Kelly, D.P. (2004). Estrogen-related receptor alpha directs peroxisome proliferator-activated receptor alpha signaling in the transcriptional control of energy metabolism in cardiac and skeletal muscle. Mol Cell Biol *24*, 9079-9091. 10.1128/MCB.24.20.9079-9091.2004.

Hutvagner, G., and Simard, M.J. (2008). Argonaute proteins: key players in RNA silencing. Nat Rev Mol Cell Biol *9*, 22-32. 10.1038/nrm2321.

Infarinato, N.R., Stewart, K.S., Yang, Y., Gomez, N.C., Pasolli, H.A., Hidalgo, L., Polak, L., Carroll, T.S., and Fuchs, E. (2020). BMP signaling: at the gate between activated melanocyte stem cells and differentiation. Genes Dev *34*, 1713-1734. 10.1101/gad.340281.120.

Iwafuchi-Doi, M., and Zaret, K.S. (2016). Cell fate control by pioneer transcription factors. Development *143*, 1833-1837. 10.1242/dev.133900.

Jeon, K.I., Nehrke, K., and Huxlin, K.R. (2020). Semaphorin 3A potentiates the profibrotic effects of transforming growth factor-beta1 in the cornea. Biochem Biophys Res Commun *521*, 333-339. 10.1016/j.bbrc.2019.10.107.

Jia, G., Preussner, J., Chen, X., Guenther, S., Yuan, X., Yekelchyk, M., Kuenne, C., Looso, M., Zhou, Y., Teichmann, S., and Braun, T. (2018). Single cell RNA-seq and ATAC-seq analysis of cardiac progenitor cell transition states and lineage settlement. Nat Commun *9*, 4877. 10.1038/s41467-018-07307-6.

Jiang, J., Chan, Y.S., Loh, Y.H., Cai, J., Tong, G.Q., Lim, C.A., Robson, P., Zhong, S., and Ng, H.H. (2008). A core Klf circuitry regulates self-renewal of embryonic stem cells. Nat Cell Biol *10*, 353-360. 10.1038/ncb1698.

Jiang, Y., Berry, D.C., and Graff, J.M. (2017a). Distinct cellular and molecular mechanisms for beta3 adrenergic receptor-induced beige adipocyte formation. Elife *6*. 10.7554/eLife.30329.

Jiang, Y., Berry, D.C., Jo, A., Tang, W., Arpke, R.W., Kyba, M., and Graff, J.M.

(2017b). A PPARgamma transcriptional cascade directs adipose progenitor cell-niche interaction and niche expansion. Nat Commun *8*, 15926. 10.1038/ncomms15926.

Jiang, Y., Berry, D.C., Tang, W., and Graff, J.M. (2014). Independent stem cell lineages regulate adipose organogenesis and adipose homeostasis. Cell Rep *9*, 1007-1022. 10.1016/j.celrep.2014.09.049.

Jin, S., Guerrero-Juarez, C.F., Zhang, L., Chang, I., Ramos, R., Kuan, C.H., Myung, P., Plikus, M.V., and Nie, Q. (2021). Inference and analysis of cell-cell communication using CellChat. Nat Commun *12*, 1088. 10.1038/s41467-021-21246-9.

Johnson, D.S., Mortazavi, A., Myers, R.M., and Wold, B. (2007). Genome-wide mapping of in vivo protein-DNA interactions. Science *316*, 1497-1502. 10.1126/science.1141319.

Joost, S., Annusver, K., Jacob, T., Sun, X., Dalessandri, T., Sivan, U., Sequeira, I., Sandberg, R., and Kasper, M. (2020). The Molecular Anatomy of Mouse Skin during Hair Growth and Rest. Cell Stem Cell *26*, 441-457 e447. 10.1016/j.stem.2020.01.012.

Kawakami, A., and Fisher, D.E. (2017). The master role of microphthalmia-associated transcription factor in melanocyte and melanoma biology. Lab Invest *97*, 649-656. 10.1038/labinvest.2017.9.

Kaya-Okur, H.S., Wu, S.J., Codomo, C.A., Pledger, E.S., Bryson, T.D., Henikoff, J.G., Ahmad, K., and Henikoff, S. (2019). CUT&Tag for efficient epigenomic profiling of small samples and single cells. Nat Commun *10*, 1930. 10.1038/s41467-019-09982-5.

Kenny, C., Dilshat, R., Seberg, H., Otterloo, E.V., Bonde, G., Helverson, A., Franke, C.M., Steingrímsson, E., and Cornell, R.A. (2022). TFAP2 paralogs facilitate chromatin access for MITF at pigmentation genes but inhibit expression of cell-cell adhesion genes independently of MITF. bioRxiv *2021.11.23.469757*. https://doi.org/10.1101/2021.11.23.469757.

Konermann, S., Brigham, M.D., Trevino, A.E., Joung, J., Abudayyeh, O.O., Barcena, C., Hsu, P.D., Habib, N., Gootenberg, J.S., Nishimasu, H., et al. (2015). Genome-scale transcriptional activation by an engineered CRISPR-Cas9 complex. Nature *517*, 583-588. 10.1038/nature14136.

Kornberg, R.D. (1974). Chromatin structure: a repeating unit of histones and DNA. Science *184*, 868-871. 10.1126/science.184.4139.868.

Kostal, V., Sula, J., and Simek, P. (1998). Physiology of drought tolerance and cold hardiness of the Mediterranean tiger moth Cymbalophora pudica during summer diapause. Journal of Insect Physiology *44*, 165-173. 10.1016/s0022-1910(97)00047-4.

Kouzarides, T. (2007). Chromatin modifications and their function. Cell *128*, 693-705. 10.1016/j.cell.2007.02.005.

Kumar, N., Liu, D., Wang, H., Robidoux, J., and Collins, S. (2008). Orphan nuclear receptor NOR-1 enhances 3',5'-cyclic adenosine 5'-monophosphate-dependent uncoupling protein-1 gene transcription. Mol Endocrinol *22*, 1057-1064. 10.1210/me.2007-0464.

Kwak, H., Fuda, N.J., Core, L.J., and Lis, J.T. (2013). Precise maps of RNA polymerase reveal how promoters direct initiation and pausing. Science *339*, 950-953. 10.1126/science.1229386.

Lang, D., Mascarenhas, J.B., and Shea, C.R. (2013). Melanocytes, melanocyte stem cells, and melanoma stem cells. Clin Dermatol *31*, 166-178. 10.1016/j.clindermatol.2012.08.014.

Langmead, B., and Salzberg, S.L. (2012). Fast gapped-read alignment with Bowtie 2. Nat Methods *9*, 357-359. 10.1038/nmeth.1923.

Längst, G., Bonte, E.J., Corona, D.F.V., and Becker, P.B. (1999). Nucleosome Movement by CHRAC and ISWI without Disruption or trans-Displacement of the Histone Octamer. Cell *97*, 843-852. 10.1016/s0092-8674(00)80797-7.

Lareau, C.A., Duarte, F.M., Chew, J.G., Kartha, V.K., Burkett, Z.D., Kohlway, A.S., Pokholok, D., Aryee, M.J., Steemers, F.J., Lebofsky, R., and Buenrostro, J.D. (2019). Droplet-based combinatorial indexing for massive-scale single-cell chromatin accessibility. Nat Biotechnol *37*, 916-924. 10.1038/s41587-019-0147-6.

Larson, E.D., Marsh, A.J., and Harrison, M.M. (2021). Pioneering the developmental frontier. Mol Cell *81*, 1640-1650. 10.1016/j.molcel.2021.02.020.

Larson, M.H., Gilbert, L.A., Wang, X., Lim, W.A., Weissman, J.S., and Qi, L.S. (2013). CRISPR interference (CRISPRi) for sequence-specific control of gene expression. Nat Protoc *8*, 2180-2196. 10.1038/nprot.2013.132.

Lawrence, T. (2009). The nuclear factor NF-kappaB pathway in inflammation. Cold Spring Harb Perspect Biol *1*, a001651. 10.1101/cshperspect.a001651.

Lee, C.K., Shibata, Y., Rao, B., Strahl, B.D., and Lieb, J.D. (2004). Evidence for nucleosome depletion at active regulatory regions genome-wide. Nat Genet *36*, 900-905. 10.1038/ng1400.

Lee, H., Kim, W.J., Kang, H.G., Jang, J.H., Choi, I.J., Chun, K.H., and Kim, S.J. (2021). Upregulation of LAMB1 via ERK/c-Jun Axis Promotes Gastric Cancer Growth and Motility. Int J Mol Sci *22*. 10.3390/ijms22020626.

Lee, J.H., and Fisher, D.E. (2014). Melanocyte stem cells as potential therapeutics in skin disorders. Expert Opin Biol Ther *14*, 1569-1579. 10.1517/14712598.2014.935331.

Lee, T.I., and Young, R.A. (2013). Transcriptional regulation and its misregulation in disease. Cell *152*, 1237-1251. 10.1016/j.cell.2013.02.014.

Levy, C., Khaled, M., and Fisher, D.E. (2006). MITF: master regulator of melanocyte development and melanoma oncogene. Trends Mol Med *12*, 406-414. 10.1016/j.molmed.2006.07.008.

Leyton, J., Drury, P.J., and Crawford, M.A. (1987). Differential oxidation of saturated and unsaturated fatty acids in vivo in the rat. Br J Nutr *57*, 383-393. 10.1079/bjn19870046.

Li, H., and Guan, Y. (2022). Asymmetric Predictive Relationships Across Histone Modifications. Nat Mach Intell *4*, 288-299. 10.1038/s42256-022-00455-x.

Li, R., and Yang, X. (2022). De novo reconstruction of cell interaction

landscapes from single-cell spatial transcriptome data with DeepLinc. Genome Biol *23*, 124. 10.1186/s13059-022-02692-0.

Li, Y., Ping, X., Zhang, Y., Li, G., Zhang, T., Chen, G., Ma, X., Wang, D., and Xu, L. (2021). Comparative Transcriptome Profiling of Cold Exposure and beta3-AR Agonist CL316,243-Induced Browning of White Fat. Front Physiol *12*, 667698. 10.3389/fphys.2021.667698.

Lim, J.H., Gerhart-Hines, Z., Dominy, J.E., Lee, Y., Kim, S., Tabata, M., Xiang, Y.K., and Puigserver, P. (2013). Oleic acid stimulates complete oxidation of fatty acids through protein kinase A-dependent activation of SIRT1-PGC1alpha complex. J Biol Chem *288*, 7117-7126. 10.1074/jbc.M112.415729.

Liscovitch-Brauer, N., Montalbano, A., Deng, J., Mendez-Mancilla, A., Wessels, H.H., Moss, N.G., Kung, C.Y., Sookdeo, A., Guo, X., Geller, E., et al. (2021). Profiling the genetic determinants of chromatin accessibility with scalable single-cell CRISPR screens. Nat Biotechnol *39*, 1270-1277. 10.1038/s41587-021-00902-x.

Lister, R., Pelizzola, M., Dowen, R.H., Hawkins, R.D., Hon, G., Tonti-Filippini, J., Nery, J.R., Lee, L., Ye, Z., Ngo, Q.M., et al. (2009). Human DNA methylomes at base resolution show widespread epigenomic differences. Nature *462*, 315-322. 10.1038/nature08514.

Lodhi, I.J., Wei, X., and Semenkovich, C.F. (2011). Lipoexpediency: de novo lipogenesis as a metabolic signal transmitter. Trends Endocrinol Metab *22*, 1-8. 10.1016/j.tem.2010.09.002.

Lorch, Y., Zhang, M., and Kornberg, R.D. (1999). Histone Octamer Transfer by a Chromatin-Remodeling Complex. Cell *96*, 389-392. 10.1016/s0092-8674(00)80551-6.

Lu, T., Ang, C.E., and Zhuang, X. (2022). Spatially resolved epigenomic profiling of single cells in complex tissues. bioRxiv. 10.1101/2022.02.17.480825.

Lubeck, E., Coskun, A.F., Zhiyentayev, T., Ahmad, M., and Cai, L. (2014). Single-cell in situ RNA profiling by sequential hybridization. Nat Methods *11*, 360-361. 10.1038/nmeth.2892.

Luger, K., Mader, A.W., Richmond, R.K., Sargent, D.F., and Richmond, T.J. (1997). Crystal structure of the nucleosome core particle at 2.8 A resolution. Nature *389*, 251-260. 10.1038/38444.

Ma, S., Zhang, B., LaFave, L.M., Earl, A.S., Chiang, Z., Hu, Y., Ding, J., Brack, A., Kartha, V.K., Tay, T., et al. (2020). Chromatin Potential Identified by Shared Single-Cell Profiling of RNA and Chromatin. Cell *183*, 1103-1116 e1120. 10.1016/j.cell.2020.09.056.

Mayran, A., and Drouin, J. (2018). Pioneer transcription factors shape the epigenetic landscape. J Biol Chem *293*, 13795-13804. 10.1074/jbc.R117.001232.

McLean, C.Y., Bristor, D., Hiller, M., Clarke, S.L., Schaar, B.T., Lowe, C.B., Wenger, A.M., and Bejerano, G. (2010). GREAT improves functional interpretation of cis-regulatory regions. Nat Biotechnol *28*, 495-501. 10.1038/nbt.1630.

Michel, L.Y.M., Farah, C., and Balligand, J.L. (2020). The Beta3 Adrenergic Receptor in Healthy and Pathological Cardiovascular Tissues. Cells *9*. 10.3390/cells9122584.

Moon, H., Donahue, L.R., Choi, E., Scumpia, P.O., Lowry, W.E., Grenier, J.K., Zhu, J., and White, A.C. (2017). Melanocyte Stem Cell Activation and Translocation Initiate Cutaneous Melanoma in Response to UV Exposure. Cell Stem Cell *21*, 665-678 e666. 10.1016/j.stem.2017.09.001.

Mottillo, E.P., Balasubramanian, P., Lee, Y.H., Weng, C., Kershaw, E.E., and Granneman, J.G. (2014). Coupling of lipolysis and de novo lipogenesis in brown, beige, and white adipose tissues during chronic beta3-adrenergic receptor activation. J Lipid Res *55*, 2276-2286. 10.1194/jlr.M050005.

Mull, A.N., Zolekar, A., and Wang, Y.C. (2015). Understanding Melanocyte Stem Cells for Disease Modeling and Regenerative Medicine Applications. Int J Mol Sci *16*, 30458-30469. 10.3390/ijms161226207.

Musselman, C.A., Lalonde, M.E., Cote, J., and Kutateladze, T.G. (2012). Perceiving the epigenetic landscape through histone readers. Nat Struct Mol Biol *19*, 1218-1227. 10.1038/nsmb.2436.

Nie, B., Nie, T., Hui, X., Gu, P., Mao, L., Li, K., Yuan, R., Zheng, J., Wang, H., Li, K., et al. (2017). Brown Adipogenic Reprogramming Induced by a Small Molecule. Cell Rep *18*, 624-635. 10.1016/j.celrep.2016.12.062.

Nishimura, E.K. (2011). Melanocyte stem cells: a melanocyte reservoir in hair follicles for hair and skin pigmentation. Pigment Cell Melanoma Res *24*, 401-410. 10.1111/j.1755-148X.2011.00855.x.

Nishimura, E.K., Granter, S.R., and Fisher, D.E. (2005). Mechanisms of hair graying: incomplete melanocyte stem cell maintenance in the niche. Science *307*, 720-724. 10.1126/science.1099593.

Nishimura, E.K., Jordan, S.A., Oshima, H., Yoshida, H., Osawa, M., Moriyama, M., Jackson, I.J., Barrandon, Y., Miyachi, Y., and Nishikawa, S. (2002). Dominant role of the niche in melanocyte stem-cell fate determination. Nature *416*, 854-860. 10.1038/416854a.

Nord, A.S., Blow, M.J., Attanasio, C., Akiyama, J.A., Holt, A., Hosseini, R., Phouanenavong, S., Plajzer-Frick, I., Shoukry, M., Afzal, V., et al. (2013). Rapid and pervasive changes in genome-wide enhancer usage during mammalian development. Cell *155*, 1521-1531. 10.1016/j.cell.2013.11.033.

Ohno, H., Shinoda, K., Spiegelman, B.M., and Kajimura, S. (2012). PPARgamma agonists induce a white-to-brown fat conversion through stabilization of PRDM16 protein. Cell Metab *15*, 395-404. 10.1016/j.cmet.2012.01.019.

Omoto, M., Yoshida, S., Miyashita, H., Kawakita, T., Yoshida, K., Kishino, A., Kimura, T., Shibata, S., Tsubota, K., Okano, H., and Shimmura, S. (2012). The semaphorin 3A inhibitor SM-345431 accelerates peripheral nerve regeneration and sensitivity in a murine corneal transplantation model. PLoS One *7*, e47716. 10.1371/journal.pone.0047716.

Ou, J., Liu, H., Yu, J., Kelliher, M.A., Castilla, L.H., Lawson, N.D., and Zhu, L.J. (2018). ATACseqQC: a Bioconductor package for post-alignment quality

assessment of ATAC-seq data. BMC Genomics *19*, 169. 10.1186/s12864-018-4559-3.

Perris, R. (1997). The extracellular matrix in neural crest-cell migration. Trends in Neurosciences *20*, 23-31. 10.1016/s0166-2236(96)10063-1.

Picelli, S., Bjorklund, A.K., Reinius, B., Sagasser, S., Winberg, G., and Sandberg, R. (2014). Tn5 transposase and tagmentation procedures for massively scaled sequencing projects. Genome Res *24*, 2033-2040. 10.1101/gr.177881.114.

Pierce, S.E., Granja, J.M., and Greenleaf, W.J. (2021). High-throughput single-cell chromatin accessibility CRISPR screens enable unbiased identification of regulatory networks in cancer. Nat Commun *12*, 2969. 10.1038/s41467-021-23213-w.

Pliner, H.A., Packer, J.S., McFaline-Figueroa, J.L., Cusanovich, D.A., Daza, R.M., Aghamirzaie, D., Srivatsan, S., Qiu, X., Jackson, D., Minkina, A., et al. (2018). Cicero Predicts cis-Regulatory DNA Interactions from Single-Cell Chromatin Accessibility Data. Mol Cell *71*, 858-871 e858. 10.1016/j.molcel.2018.06.044.

Plonka, P.M., Passeron, T., Brenner, M., Tobin, D.J., Shibahara, S., Thomas, A., Slominski, A., Kadekaro, A.L., Hershkovitz, D., Peters, E., et al. (2009). What are melanocytes really doing all day long...? Exp Dermatol *18*, 799-819. 10.1111/j.1600-0625.2009.00912.x.

Praetorius, C., Grill, C., Stacey, S.N., Metcalf, A.M., Gorkin, D.U., Robinson, K.C., Van Otterloo, E., Kim, R.S., Bergsteinsdottir, K., Ogmundsdottir, M.H., et al. (2013). A polymorphism in IRF4 affects human pigmentation through a tyrosinase-dependent MITF/TFAP2A pathway. Cell *155*, 1022-1033. 10.1016/j.cell.2013.10.022.

Preissl, S., Fang, R., Huang, H., Zhao, Y., Raviram, R., Gorkin, D.U., Zhang, Y., Sos, B.C., Afzal, V., Dickel, D.E., et al. (2018). Single-nucleus analysis of accessible chromatin in developing mouse forebrain reveals cell-type-specific transcriptional regulation. Nat Neurosci *21*, 432-439. 10.1038/s41593-018-0079-3.

Rabhi, N., Belkina, A.C., Desevin, K., Cortez, B.N., and Farmer, S.R. (2020). Shifts of Immune Cell Populations Differ in Response to Different Effectors of Beige Remodeling of Adipose Tissue. iScience *23*, 101765. 10.1016/j.isci.2020.101765.

Raj, A., Peskin, C.S., Tranchina, D., Vargas, D.Y., and Tyagi, S. (2006). Stochastic mRNA synthesis in mammalian cells. PLoS Biol *4*, e309. 10.1371/journal.pbio.0040309.

Rajbhandari, P., Arneson, D., Hart, S.K., Ahn, I.S., Diamante, G., Santos, L.C., Zaghari, N., Feng, A.C., Thomas, B.J., Vergnes, L., et al. (2019). Single cell analysis reveals immune cell-adipocyte crosstalk regulating the transcription of thermogenic adipocytes. Elife *8*. 10.7554/eLife.49501.

Rhee, H.S., and Pugh, B.F. (2011). Comprehensive genome-wide protein-DNA interactions detected at single-nucleotide resolution. Cell *147*, 1408-1419. 10.1016/j.cell.2011.11.013.

Roh, H.C., Tsai, L.T.Y., Shao, M., Tenen, D., Shen, Y., Kumari, M., Lyubetskaya, A., Jacobs, C., Dawes, B., Gupta, R.K., and Rosen, E.D. (2018). Warming Induces Significant Reprogramming of Beige, but Not Brown, Adipocyte Cellular Identity. Cell Metab *27*, 1121-1137 e1125. 10.1016/j.cmet.2018.03.005.

Rosen, E.D., Hsu, C.H., Wang, X., Sakai, S., Freeman, M.W., Gonzalez, F.J., and Spiegelman, B.M. (2002). C/EBPalpha induces adipogenesis through PPARgamma: a unified pathway. Genes Dev *16*, 22-26. 10.1101/gad.948702.

Rosen, E.D., and Spiegelman, B.M. (2014). What we talk about when we talk about fat. Cell *156*, 20-44. 10.1016/j.cell.2013.12.012.

Rosenberg, A.B., Roco, C.M., Muscat, R.A., Kuchina, A., Sample, P., Yao, Z., Graybuck, L.T., Peeler, D.J., Mukherjee, S., Chen, W., et al. (2018). Single-cell profiling of the developing mouse brain and spinal cord with split-pool barcoding. Science *360*, 176-182. 10.1126/science.aam8999.

Rosenwald, M., Perdikari, A., Rulicke, T., and Wolfrum, C. (2013). Bi-directional interconversion of brite and white adipocytes. Nat Cell Biol *15*, 659-667. 10.1038/ncb2740.

Rosette, C., and Karin, M. (1996). Ultraviolet light and osmotic stress: activation of the JNK cascade through multiple growth factor and cytokine receptors. Science *274*, 1194-1197. 10.1126/science.274.5290.1194.

Rubin, A.J., Parker, K.R., Satpathy, A.T., Qi, Y., Wu, B., Ong, A.J., Mumbach, M.R., Ji, A.L., Kim, D.S., Cho, S.W., et al. (2019). Coupled Single-Cell CRISPR Screening and Epigenomic Profiling Reveals Causal Gene Regulatory Networks. Cell *176*, 361-376 e317. 10.1016/j.cell.2018.11.022.

Sanjana, N.E., Wright, J., Zheng, K., Shalem, O., Fontanillas, P., Joung, J., Cheng, C., Regev, A., and Zhang, F. (2016). High-resolution interrogation of functional elements in the noncoding genome. Science *353*, 1545-1549. 10.1126/science.aaf7613.

Schep, A.N., Wu, B., Buenrostro, J.D., and Greenleaf, W.J. (2017). chromVAR: inferring transcription-factor-associated accessibility from single-cell epigenomic data. Nat Methods *14*, 975-978. 10.1038/nmeth.4401.

Schlesinger, F., Smith, A.D., Gingeras, T.R., Hannon, G.J., and Hodges, E. (2013). De novo DNA demethylation and noncoding transcription define active intergenic regulatory elements. Genome Res *23*, 1601-1614. 10.1101/gr.157271.113.

Schones, D.E., Cui, K., Cuddapah, S., Roh, T.Y., Barski, A., Wang, Z., Wei, G., and Zhao, K. (2008). Dynamic regulation of nucleosome positioning in the human genome. Cell *132*, 887-898. 10.1016/j.cell.2008.02.022.

Schreiber, S.N., Emter, R., Hock, M.B., Knutti, D., Cardenas, J., Podvinec, M., Oakeley, E.J., and Kralli, A. (2004). The estrogen-related receptor alpha (ERRalpha) functions in PPARgamma coactivator 1alpha (PGC-1alpha)-induced mitochondrial biogenesis. Proc Natl Acad Sci U S A *101*, 6472-6477. 10.1073/pnas.0308686101.

Seberg, H.E., Van Otterloo, E., Loftus, S.K., Liu, H., Bonde, G., Sompallae, R.,

Gildea, D.E., Santana, J.F., Manak, J.R., Pavan, W.J., et al. (2017). TFAP2 paralogs regulate melanocyte differentiation in parallel with MITF. PLoS Genet *13*, e1006636. 10.1371/journal.pgen.1006636.

Shelly, M., Cancedda, L., Lim, B.K., Popescu, A.T., Cheng, P.L., Gao, H., and Poo, M.M. (2011). Semaphorin3A regulates neuronal polarization by suppressing axon formation and promoting dendrite growth. Neuron *71*, 433-446. 10.1016/j.neuron.2011.06.041.

Sherwood, R.I., Hashimoto, T., O'Donnell, C.W., Lewis, S., Barkal, A.A., van Hoff, J.P., Karun, V., Jaakkola, T., and Gifford, D.K. (2014). Discovery of directional and nondirectional pioneer transcription factors by modeling DNase profile magnitude and shape. Nat Biotechnol *32*, 171-178. 10.1038/nbt.2798.

Siegel, R.L., Miller, K.D., and Jemal, A. (2019). Cancer statistics, 2019. CA Cancer J Clin *69*, 7-34. 10.3322/caac.21551.

Sims, R.J., 3rd, and Reinberg, D. (2004). From chromatin to cancer: a new histone lysine methyltransferase enters the mix. Nat Cell Biol *6*, 685-687. 10.1038/ncb0804-685.

Skene, P.J., and Henikoff, S. (2017). An efficient targeted nuclease strategy for high-resolution mapping of DNA binding sites. Elife *6*. 10.7554/eLife.21856.

Slominski, A., and Paus, R. (1993). Melanogenesis is coupled to murine anagen: Toward new concepts for the role of melanocytes and the regulation of melanogenesis in hair growth. Journal of Investigative Dermatology *101*, S90-S97. 10.1016/0022-202x(93)90507-e.

Soteriou, D., Kostic, L., Sedov, E., Yosefzon, Y., Steller, H., and Fuchs, Y. (2016). Isolating Hair Follicle Stem Cells and Epidermal Keratinocytes from Dorsal Mouse Skin. J Vis Exp. 10.3791/53931.

Soumano, K. (2000). Glucocorticoids inhibit the transcriptional response of the uncoupling protein-1 gene to adrenergic stimulation in a brown adipose cell line. Molecular and Cellular Endocrinology *165*, 7-15. 10.1016/s0303-7207(00)00276-8.

Spektor, R., Yang, J.W., Lee, S., and Soloway, P.D. (2019). Single cell ATAC-seq identifies broad changes in neuronal abundance and chromatin accessibility in Down Syndrome. bioRxiv. 10.1101/561191.

Staub, E., Grone, J., Mennerich, D., Ropcke, S., Klamann, I., Hinzmann, B., Castanos-Velez, E., Mann, B., Pilarsky, C., Brummendorf, T., et al. (2006). A genome-wide map of aberrantly expressed chromosomal islands in colorectal cancer. Mol Cancer *5*, 37. 10.1186/1476-4598-5-37.

Steingrimsson, E., Copeland, N.G., and Jenkins, N.A. (2005). Melanocyte stem cell maintenance and hair graying. Cell *121*, 9-12. 10.1016/j.cell.2005.03.021.

Strack, A.M., Bradbury, M.J., and Dallman, M.F. (1995). Corticosterone decreases nonshivering thermogenesis and increases lipid storage in brown adipose tissue. Am J Physiol *268*, R183-191. 10.1152/ajpregu.1995.268.1.R183.

Stuart, T., Butler, A., Hoffman, P., Hafemeister, C., Papalexi, E., Mauck, W.M.,

3rd, Hao, Y., Stoeckius, M., Smibert, P., and Satija, R. (2019). Comprehensive Integration of Single-Cell Data. Cell *177*, 1888-1902 e1821. 10.1016/j.cell.2019.05.031.

Stuart, T., Srivastava, A., Madad, S., Lareau, C.A., and Satija, R. (2021). Single-cell chromatin state analysis with Signac. Nat Methods *18*, 1333-1341. 10.1038/s41592-021-01282-5.

Su, J.H., Zheng, P., Kinrot, S.S., Bintu, B., and Zhuang, X. (2020). Genome-Scale Imaging of the 3D Organization and Transcriptional Activity of Chromatin. Cell *182*, 1641-1659 e1626. 10.1016/j.cell.2020.07.032.

Sun, W., Dong, H., Balaz, M., Slyper, M., Drokhlyansky, E., Colleluori, G., Giordano, A., Kovanicova, Z., Stefanicka, P., Balazova, L., et al. (2020). snRNA-seq reveals a subpopulation of adipocytes that regulates thermogenesis. Nature *587*, 98-102. 10.1038/s41586-020-2856-x.

Swanson, E., Lord, C., Reading, J., Heubeck, A.T., Genge, P.C., Thomson, Z., Weiss, M.D., Li, X.J., Savage, A.K., Green, R.R., et al. (2021). Simultaneous trimodal single-cell measurement of transcripts, epitopes, and chromatin accessibility using TEA-seq. Elife *10*. 10.7554/eLife.63632.

Tanimura, S., Tadokoro, Y., Inomata, K., Binh, N.T., Nishie, W., Yamazaki, S., Nakauchi, H., Tanaka, Y., McMillan, J.R., Sawamura, D., et al. (2011). Hair follicle stem cells provide a functional niche for melanocyte stem cells. Cell Stem Cell *8*, 177-187. 10.1016/j.stem.2010.11.029.

Thiele, A., Luettges, K., Ritter, D., Beyhoff, N., Smeir, E., Grune, J., Steinhoff, J.S., Schupp, M., Klopfleisch, R., Rothe, M., et al. (2021). Pharmacological inhibition of adipose tissue Adipose Triglyceride Lipase (ATGL) by Atglistatin prevents catecholamine-induced myocardial damage. Cardiovasc Res. 10.1093/cvr/cvab182.

Thornton, C.A., Mulqueen, R.M., Torkenczy, K.A., Nishida, A., Lowenstein, E.G., Fields, A.J., Steemers, F.J., Zhang, W., McConnell, H.L., Woltjer, R.L., et al. (2021). Spatially mapped single-cell chromatin accessibility. Nat Commun *12*, 1274. 10.1038/s41467-021-21515-7.

Thuzar, M., Law, W.P., Ratnasingam, J., Jang, C., Dimeski, G., and Ho, K.K.Y. (2018). Glucocorticoids suppress brown adipose tissue function in humans: A double-blind placebo-controlled study. Diabetes Obes Metab *20*, 840-848. 10.1111/dom.13157.

Tiku, P.E., Gracey, A.Y., Macartney, A.I., Beynon, R.J., and Cossins, A.R. (1996). Cold-induced expression of delta 9-desaturase in carp by transcriptional and posttranslational mechanisms. Science *271*, 815-818. 10.1126/science.271.5250.815.

Tobin, D.J., Hagen, E., Botchkarev, V.A., and Paus, R. (1998). Do hair bulb melanocytes undergo apoptosis during hair follicle regression (catagen)? J Invest Dermatol *111*, 941-947. 10.1046/j.1523-1747.1998.00417.x.

Trapnell, C., Cacchiarelli, D., Grimsby, J., Pokharel, P., Li, S., Morse, M., Lennon, N.J., Livak, K.J., Mikkelsen, T.S., and Rinn, J.L. (2014). The dynamics and regulators of cell fate decisions are revealed by pseudotemporal ordering of single cells. Nat Biotechnol *32*, 381-386.

10.1038/nbt.2859.
Tumbar, T., Guasch, G., Greco, V., Blanpain, C., Lowry, W.E., Rendl, M., and Fuchs, E. (2004). Defining the epithelial stem cell niche in skin. Science *303*, 359-363. 10.1126/science.1092436.
Vega, R.B., Huss, J.M., and Kelly, D.P. (2000). The coactivator PGC-1 cooperates with peroxisome proliferator-activated receptor alpha in transcriptional control of nuclear genes encoding mitochondrial fatty acid oxidation enzymes. Mol Cell Biol *20*, 1868-1876. 10.1128/MCB.20.5.1868-1876.2000.
Viengchareun, S., Penfornis, P., Zennaro, M.C., and Lombes, M. (2001). Mineralocorticoid and glucocorticoid receptors inhibit UCP expression and function in brown adipocytes. Am J Physiol Endocrinol Metab *280*, E640-649. 10.1152/ajpendo.2001.280.4.E640.
Vijay, J., Gauthier, M.F., Biswell, R.L., Louiselle, D.A., Johnston, J.J., Cheung, W.A., Belden, B., Pramatarova, A., Biertho, L., Gibson, M., et al. (2020). Single-cell analysis of human adipose tissue identifies depot and disease specific cell types. Nat Metab *2*, 97-109. 10.1038/s42255-019-0152-6.
Vitak, S.A., Torkenczy, K.A., Rosenkrantz, J.L., Fields, A.J., Christiansen, L., Wong, M.H., Carbone, L., Steemers, F.J., and Adey, A. (2017). Sequencing thousands of single-cell genomes with combinatorial indexing. Nat Methods *14*, 302-308. 10.1038/nmeth.4154.
Wales, S., Hashemi, S., Blais, A., and McDermott, J.C. (2014). Global MEF2 target gene analysis in cardiac and skeletal muscle reveals novel regulation of DUSP6 by p38MAPK-MEF2 signaling. Nucleic Acids Res *42*, 11349-11362. 10.1093/nar/gku813.
Wang, F., Flanagan, J., Su, N., Wang, L.C., Bui, S., Nielson, A., Wu, X., Vo, H.T., Ma, X.J., and Luo, Y. (2012). RNAscope: a novel in situ RNA analysis platform for formalin-fixed, paraffin-embedded tissues. J Mol Diagn *14*, 22-29. 10.1016/j.jmoldx.2011.08.002.
Wang, Y., Yuan, P., Yan, Z., Yang, M., Huo, Y., Nie, Y., Zhu, X., Qiao, J., and Yan, L. (2021). Single-cell multiomics sequencing reveals the functional regulatory landscape of early embryos. Nat Commun *12*, 1247. 10.1038/s41467-021-21409-8.
Wang, Z., Chivu, A.G., Choate, L.A., Rice, E.J., Miller, D.C., Chu, T., Chou, S.P., Kingsley, N.B., Petersen, J.L., Finno, C.J., et al. (2022). Prediction of histone post-translational modification patterns based on nascent transcription data. Nat Genet *54*, 295-305. 10.1038/s41588-022-01026-x.
Weirauch, M.T., Yang, A., Albu, M., Cote, A.G., Montenegro-Montero, A., Drewe, P., Najafabadi, H.S., Lambert, S.A., Mann, I., Cook, K., et al. (2014). Determination and inference of eukaryotic transcription factor sequence specificity. Cell *158*, 1431-1443. 10.1016/j.cell.2014.08.009.
Wolock, S.L., Lopez, R., and Klein, A.M. (2019). Scrublet: Computational Identification of Cell Doublets in Single-Cell Transcriptomic Data. Cell Syst *8*, 281-291 e289. 10.1016/j.cels.2018.11.005.
Wu, C., Wong, Y.C., and Elgin, S.C. (1979). The chromatin structure of specific

genes: II. Disruption of chromatin structure during gene activity. Cell *16*, 807-814. 10.1016/0092-8674(79)90096-5.

Wu, J., Bostrom, P., Sparks, L.M., Ye, L., Choi, J.H., Giang, A.H., Khandekar, M., Virtanen, K.A., Nuutila, P., Schaart, G., et al. (2012). Beige adipocytes are a distinct type of thermogenic fat cell in mouse and human. Cell *150*, 366-376. 10.1016/j.cell.2012.05.016.

Yu, G., Wang, L.G., Han, Y., and He, Q.Y. (2012). clusterProfiler: an R package for comparing biological themes among gene clusters. OMICS *16*, 284-287. 10.1089/omi.2011.0118.

Yue, F., Cheng, Y., Breschi, A., Vierstra, J., Wu, W., Ryba, T., Sandstrom, R., Ma, Z., Davis, C., Pope, B.D., et al. (2014). A comparative encyclopedia of DNA elements in the mouse genome. Nature *515*, 355-364. 10.1038/nature13992.

Zaidi, M.R., Hornyak, T.J., and Merlino, G. (2011). A genetically engineered mouse model with inducible GFP expression in melanocytes. Pigment Cell and Melanoma Research *24*, 393-394. 10.1111/j.1755-148X.2011.00832.x.

Zaret, K.S., and Mango, S.E. (2016). Pioneer transcription factors, chromatin dynamics, and cell fate control. Curr Opin Genet Dev *37*, 76-81. 10.1016/j.gde.2015.12.003.

Zhang, W., Xu, J., Li, J., Guo, T., Jiang, D., Feng, X., Ma, X., He, L., Wu, W., Yin, M., et al. (2018). The TEA domain family transcription factor TEAD4 represses murine adipogenesis by recruiting the cofactors VGLL4 and CtBP2 into a transcriptional complex. J Biol Chem *293*, 17119-17134. 10.1074/jbc.RA118.003608.

Zhang, Y., LeRoy, G., Seelig, H.-P., Lane, W.S., and Reinberg, D. (1998). The Dermatomyositis-Specific Autoantigen Mi2 Is a Component of a Complex Containing Histone Deacetylase and Nucleosome Remodeling Activities. Cell *95*, 279-289. 10.1016/s0092-8674(00)81758-4.

Zhang, Y., Liu, T., Meyer, C.A., Eeckhoute, J., Johnson, D.S., Bernstein, B.E., Nusbaum, C., Myers, R.M., Brown, M., Li, W., and Liu, X.S. (2008). Model-based analysis of ChIP-Seq (MACS). Genome Biol *9*, R137. 10.1186/gb-2008-9-9-r137.

Zhong, Z., Feng, S., Duttke, S.H., Potok, M.E., Zhang, Y., Gallego-Bartolome, J., Liu, W., and Jacobsen, S.E. (2021). DNA methylation-linked chromatin accessibility affects genomic architecture in Arabidopsis. Proc Natl Acad Sci U S A *118*. 10.1073/pnas.2023347118.

Zhu, C., Yu, M., Huang, H., Juric, I., Abnousi, A., Hu, R., Lucero, J., Behrens, M.M., Hu, M., and Ren, B. (2019). An ultra high-throughput method for single-cell joint analysis of open chromatin and transcriptome. Nat Struct Mol Biol *26*, 1063-1070. 10.1038/s41594-019-0323-x.

REFERENCES: Chapter 4

Adam, R.C., Yang, H., Ge, Y., Infarinato, N.R., Gur-Cohen, S., Miao, Y., Wang, P., Zhao, Y., Lu, C.P., Kim, J.E., et al. (2020). NFI transcription factors provide chromatin access to maintain stem cell identity while preventing unintended lineage fate choices. Nat Cell Biol *22*, 640-650. 10.1038/s41556-020-0513-0.

Adey, A., Morrison, H.G., Asan, Xun, X., Kitzman, J.O., Turner, E.H., Stackhouse, B., MacKenzie, A.P., Caruccio, N.C., Zhang, X., and Shendure, J. (2010). Rapid, low-input, low-bias construction of shotgun fragment libraries by high-density in vitro transposition. Genome Biol *11*, R119. 10.1186/gb-2010-11-12-r119.

Altschuler, S.J., and Wu, L.F. (2010). Cellular heterogeneity: do differences make a difference? Cell *141*, 559-563. 10.1016/j.cell.2010.04.033.

Amemiya, H.M., Kundaje, A., and Boyle, A.P. (2019). The ENCODE Blacklist: Identification of Problematic Regions of the Genome. Sci Rep *9*, 9354. 10.1038/s41598-019-45839-z.

Arany, Z., Foo, S.Y., Ma, Y., Ruas, J.L., Bommi-Reddy, A., Girnun, G., Cooper, M., Laznik, D., Chinsomboon, J., Rangwala, S.M., et al. (2008). HIF-independent regulation of VEGF and angiogenesis by the transcriptional coactivator PGC-1alpha. Nature *451*, 1008-1012. 10.1038/nature06613.

Arch, J.R. (2011). Challenges in beta(3)-Adrenoceptor Agonist Drug Development. Ther Adv Endocrinol Metab *2*, 59-64. 10.1177/2042018811398517.

Arnaudo, A.M., and Garcia, B.A. (2013). Proteomic characterization of novel histone post-translational modifications. Epigenetics Chromatin *6*, 24. 10.1186/1756-8935-6-24.

Aune, U.L., Ruiz, L., and Kajimura, S. (2013). Isolation and differentiation of stromal vascular cells to beige/brite cells. J Vis Exp. 10.3791/50191.

Bagci, T., Wu, J.K., Pfannl, R., Ilag, L.L., and Jay, D.G. (2009). Autocrine semaphorin 3A signaling promotes glioblastoma dispersal. Oncogene *28*, 3537-3550. 10.1038/onc.2009.204.

Baker, R.G., Hayden, M.S., and Ghosh, S. (2011). NF-kappaB, inflammation, and metabolic disease. Cell Metab *13*, 11-22. 10.1016/j.cmet.2010.12.008.

Barbatelli, G., Murano, I., Madsen, L., Hao, Q., Jimenez, M., Kristiansen, K., Giacobino, J.P., De Matteis, R., and Cinti, S. (2010). The emergence of cold-induced brown adipocytes in mouse white fat depots is determined predominantly by white to brown adipocyte transdifferentiation. Am J Physiol Endocrinol Metab *298*, E1244-1253. 10.1152/ajpendo.00600.2009.

Barquissau, V., Beuzelin, D., Pisani, D.F., Beranger, G.E., Mairal, A., Montagner, A., Roussel, B., Tavernier, G., Marques, M.A., Moro, C., et al. (2016). White-to-brite conversion in human adipocytes promotes metabolic reprogramming towards fatty acid anabolic and catabolic pathways. Mol Metab *5*, 352-365. 10.1016/j.molmet.2016.03.002.

Barski, A., Cuddapah, S., Cui, K., Roh, T.Y., Schones, D.E., Wang, Z., Wei, G.,

Chepelev, I., and Zhao, K. (2007). High-resolution profiling of histone methylations in the human genome. Cell *129*, 823-837. 10.1016/j.cell.2007.05.009.

Baskaran, P., Krishnan, V., Ren, J., and Thyagarajan, B. (2016). Capsaicin induces browning of white adipose tissue and counters obesity by activating TRPV1 channel-dependent mechanisms. Br J Pharmacol *173*, 2369-2389. 10.1111/bph.13514.

Behrens, J., von Kries, J.P., Kuhl, M., Bruhn, L., Wedlich, D., Grosschedl, R., and Birchmeier, W. (1996). Functional interaction of beta-catenin with the transcription factor LEF-1. Nature *382*, 638-642. 10.1038/382638a0.

Bennett, D.C., Cooper, P.J., and Hart, I.R. (1987). A line of non-tumorigenic mouse melanocytes, syngeneic with the B16 melanoma and requiring a tumour promoter for growth. Int J Cancer *39*, 414-418. 10.1002/ijc.2910390324.

Bernstein, B.E., Kamal, M., Lindblad-Toh, K., Bekiranov, S., Bailey, D.K., Huebert, D.J., McMahon, S., Karlsson, E.K., Kulbokas, E.J., 3rd, Gingeras, T.R., et al. (2005). Genomic maps and comparative analysis of histone modifications in human and mouse. Cell *120*, 169-181. 10.1016/j.cell.2005.01.001.

Berry, D.C., Jiang, Y., and Graff, J.M. (2016). Mouse strains to study cold-inducible beige progenitors and beige adipocyte formation and function. Nat Commun *7*, 10184. 10.1038/ncomms10184.

Bhattacharya, D., Azambuja, A.P., and Simoes-Costa, M. (2020). Metabolic Reprogramming Promotes Neural Crest Migration via Yap/Tead Signaling. Dev Cell *53*, 199-211 e196. 10.1016/j.devcel.2020.03.005.

Biagi, C.A.O., Jr., Cury, S.S., Alves, C.P., Rabhi, N., Silva, W.A., Jr., Farmer, S.R., Carvalho, R.F., and Batista, M.L., Jr. (2021). Multidimensional Single-Nuclei RNA-Seq Reconstruction of Adipose Tissue Reveals Adipocyte Plasticity Underlying Thermogenic Response. Cells *10*. 10.3390/cells10113073.

Botchkareva, N.V., Botchkarev, V.A., and Gilchrest, B.A. (2003). Fate of melanocytes during development of the hair follicle pigmentary unit. J Investig Dermatol Symp Proc *8*, 76-79. 10.1046/j.1523-1747.2003.12176.x.

Boyadjiev, S.A., and Jabs, E.W. (2000). Online Mendelian Inheritance in Man (OMIM) as a knowledgebase for human developmental disorders. Clin Genet *57*, 253-266. 10.1034/j.1399-0004.2000.570403.x.

Boyle, A.P., Davis, S., Shulha, H.P., Meltzer, P., Margulies, E.H., Weng, Z., Furey, T.S., and Crawford, G.E. (2008). High-resolution mapping and characterization of open chromatin across the genome. Cell *132*, 311-322. 10.1016/j.cell.2007.12.014.

Bradner, J.E., Hnisz, D., and Young, R.A. (2017). Transcriptional Addiction in Cancer. Cell *168*, 629-643. 10.1016/j.cell.2016.12.013.

Brombin, A., Simpson, D.J., Travnickova, J., Brunsdon, H., Zeng, Z., Lu, Y., Young, A.I.J., Chandra, T., and Patton, E.E. (2022). Tfap2b specifies an embryonic melanocyte stem cell that retains adult multifate potential. Cell

Rep *38*, 110234. 10.1016/j.celrep.2021.110234.
Brown, E.L., Hazen, B.C., Eury, E., Wattez, J.S., Gantner, M.L., Albert, V., Chau, S., Sanchez-Alavez, M., Conti, B., and Kralli, A. (2018). Estrogen-Related Receptors Mediate the Adaptive Response of Brown Adipose Tissue to Adrenergic Stimulation. iScience *2*, 221-237. 10.1016/j.isci.2018.03.005.
Bruno, M., Flaus, A., Stockdale, C., Rencurel, C., Ferreira, H., and Owen-Hughes, T. (2003). Histone H2A/H2B Dimer Exchange by ATP-Dependent Chromatin Remodeling Activities. Molecular Cell *12*, 1599-1606. 10.1016/s1097-2765(03)00499-4.
Buenrostro, J.D., Giresi, P.G., Zaba, L.C., Chang, H.Y., and Greenleaf, W.J. (2013). Transposition of native chromatin for fast and sensitive epigenomic profiling of open chromatin, DNA-binding proteins and nucleosome position. Nat Methods *10*, 1213-1218. 10.1038/nmeth.2688.
Buenrostro, J.D., Wu, B., Litzenburger, U.M., Ruff, D., Gonzales, M.L., Snyder, M.P., Chang, H.Y., and Greenleaf, W.J. (2015). Single-cell chromatin accessibility reveals principles of regulatory variation. Nature *523*, 486-490. 10.1038/nature14590.
Burl, R.B., Ramseyer, V.D., Rondini, E.A., Pique-Regi, R., Lee, Y.H., and Granneman, J.G. (2018). Deconstructing Adipogenesis Induced by beta3-Adrenergic Receptor Activation with Single-Cell Expression Profiling. Cell Metab *28*, 300-309 e304. 10.1016/j.cmet.2018.05.025.
Cadoudal, T., Distel, E., Durant, S., Fouque, F., Blouin, J.M., Collinet, M., Bortoli, S., Forest, C., and Benelli, C. (2008). Pyruvate dehydrogenase kinase 4: regulation by thiazolidinediones and implication in glyceroneogenesis in adipose tissue. Diabetes *57*, 2272-2279. 10.2337/db08-0477.
Cao, J., Cusanovich, D.A., Ramani, V., Aghamirzaie, D., Pliner, H.A., Hill, A.J., Daza, R.M., McFaline-Figueroa, J.L., Packer, J.S., Christiansen, L., et al. (2018). Joint profiling of chromatin accessibility and gene expression in thousands of single cells. Science *361*, 1380-1385. 10.1126/science.aau0730.
Cao, J., Spielmann, M., Qiu, X., Huang, X., Ibrahim, D.M., Hill, A.J., Zhang, F., Mundlos, S., Christiansen, L., Steemers, F.J., et al. (2019). The single-cell transcriptional landscape of mammalian organogenesis. Nature *566*, 496-502. 10.1038/s41586-019-0969-x.
Chandra, V., Huang, P., Hamuro, Y., Raghuram, S., Wang, Y., Burris, T.P., and Rastinejad, F. (2008). Structure of the intact PPAR-gamma-RXR- nuclear receptor complex on DNA. Nature *456*, 350-356. 10.1038/nature07413.
Chang, J.S., Ghosh, S., Newman, S., and Salbaum, J.M. (2018). A map of the PGC-1alpha- and NT-PGC-1alpha-regulated transcriptional network in brown adipose tissue. Sci Rep *8*, 7876. 10.1038/s41598-018-26244-4.
Chaveroux, C., Eichner, L.J., Dufour, C.R., Shatnawi, A., Khoutorsky, A., Bourque, G., Sonenberg, N., and Giguere, V. (2013). Molecular and genetic crosstalks between mTOR and ERRalpha are key determinants of

rapamycin-induced nonalcoholic fatty liver. Cell Metab *17*, 586-598. 10.1016/j.cmet.2013.03.003.

Chen, A.F., Parks, B., Kathiria, A.S., Ober-Reynolds, B., Goronzy, J.J., and Greenleaf, W.J. (2022). NEAT-seq: simultaneous profiling of intra-nuclear proteins, chromatin accessibility and gene expression in single cells. Nat Methods *19*, 547-553. 10.1038/s41592-022-01461-y.

Chen, G., Sima, J., Jin, M., Wang, K.Y., Xue, X.J., Zheng, W., Ding, Y.Q., and Yuan, X.B. (2008). Semaphorin-3A guides radial migration of cortical neurons during development. Nat Neurosci *11*, 36-44. 10.1038/nn2018.

Chen, H., Lareau, C., Andreani, T., Vinyard, M.E., Garcia, S.P., Clement, K., Andrade-Navarro, M.A., Buenrostro, J.D., and Pinello, L. (2019a). Assessment of computational methods for the analysis of single-cell ATAC-seq data. Genome Biol *20*, 241. 10.1186/s13059-019-1854-5.

Chen, K.H., Boettiger, A.N., Moffitt, J.R., Wang, S., and Zhuang, X. (2015). RNA imaging. Spatially resolved, highly multiplexed RNA profiling in single cells. Science *348*, aaa6090. 10.1126/science.aaa6090.

Chen, L.H., Chien, Y.W., Liang, C.T., Chan, C.H., Fan, M.H., and Huang, H.Y. (2017). Green tea extract induces genes related to browning of white adipose tissue and limits weight-gain in high energy diet-fed rat. Food Nutr Res *61*, 1347480. 10.1080/16546628.2017.1347480.

Chen, S., Lake, B.B., and Zhang, K. (2019b). High-throughput sequencing of the transcriptome and chromatin accessibility in the same cell. Nat Biotechnol *37*, 1452-1457. 10.1038/s41587-019-0290-0.

Chen, X., Miragaia, R.J., Natarajan, K.N., and Teichmann, S.A. (2018). A rapid and robust method for single cell chromatin accessibility profiling. Nat Commun *9*, 5345. 10.1038/s41467-018-07771-0.

Chen, Y., Ikeda, K., Yoneshiro, T., Scaramozza, A., Tajima, K., Wang, Q., Kim, K., Shinoda, K., Sponton, C.H., Brown, Z., et al. (2019c). Thermal stress induces glycolytic beige fat formation via a myogenic state. Nature *565*, 180-185. 10.1038/s41586-018-0801-z.

Cheng, H., Pui, H.-p., Lentini, A., Kolbeinsdóttir, S., Andrews, N., Pei, Y., Reinius, B., Deng, Q., and Enge, M. (2021). Smart3-ATAC: a highly sensitive method for joint accessibility and full-length transcriptome analysis in single cells. bioRxiv. https://doi.org/10.1101/2021.12.02.470912.

Chi, J., Wu, Z., Choi, C.H.J., Nguyen, L., Tegegne, S., Ackerman, S.E., Crane, A., Marchildon, F., Tessier-Lavigne, M., and Cohen, P. (2018). Three-Dimensional Adipose Tissue Imaging Reveals Regional Variation in Beige Fat Biogenesis and PRDM16-Dependent Sympathetic Neurite Density. Cell Metab *27*, 226-236 e223. 10.1016/j.cmet.2017.12.011.

Chiang, S.H., Bazuine, M., Lumeng, C.N., Geletka, L.M., Mowers, J., White, N.M., Ma, J.T., Zhou, J., Qi, N., Westcott, D., et al. (2009). The protein kinase IKKepsilon regulates energy balance in obese mice. Cell *138*, 961-975. 10.1016/j.cell.2009.06.046.

Choe, S.S., Huh, J.Y., Hwang, I.J., Kim, J.I., and Kim, J.B. (2016). Adipose Tissue Remodeling: Its Role in Energy Metabolism and Metabolic Disorders.

Front Endocrinol (Lausanne) *7*, 30. 10.3389/fendo.2016.00030.
Choi, S.W., and Friso, S. (2010). Epigenetics: A New Bridge between Nutrition and Health. Adv Nutr *1*, 8-16. 10.3945/an.110.1004.
Chou, W.C., Takeo, M., Rabbani, P., Hu, H., Lee, W., Chung, Y.R., Carucci, J., Overbeek, P., and Ito, M. (2013). Direct migration of follicular melanocyte stem cells to the epidermis after wounding or UVB irradiation is dependent on Mc1r signaling. Nat Med *19*, 924-929. 10.1038/nm.3194.
Chu, T., Rice, E.J., Booth, G.T., Salamanca, H.H., Wang, Z., Core, L.J., Longo, S.L., Corona, R.J., Chin, L.S., Lis, J.T., et al. (2018). Chromatin run-on and sequencing maps the transcriptional regulatory landscape of glioblastoma multiforme. Nat Genet *50*, 1553-1564. 10.1038/s41588-018-0244-3.
Chung, H., Suh, E.K., Han, I.O., and Oh, E.S. (2011). Keratinocyte-derived laminin-332 promotes adhesion and migration in melanocytes and melanoma. J Biol Chem *286*, 13438-13447. 10.1074/jbc.M110.166751.
Chuo, D., Liu, F., Chen, Y., and Yin, M. (2019). LncRNA MIR503HG is downregulated in Han Chinese with colorectal cancer and inhibits cell migration and invasion mediated by TGF-beta2. Gene *713*, 143960. 10.1016/j.gene.2019.143960.
Cinti, S., Zingaretti, M.C., Cancello, R., Ceresi, E., and Ferrara, P. (2001). Morphologic techniques for the study of brown adipose tissue and white adipose tissue. Methods Mol Biol *155*, 21-51. 10.1385/1-59259-231-7:021.
Clark, S.J., Argelaguet, R., Kapourani, C.A., Stubbs, T.M., Lee, H.J., Alda-Catalinas, C., Krueger, F., Sanguinetti, G., Kelsey, G., Marioni, J.C., et al. (2018). scNMT-seq enables joint profiling of chromatin accessibility DNA methylation and transcription in single cells. Nat Commun *9*, 781. 10.1038/s41467-018-03149-4.
Corces, M.R., Trevino, A.E., Hamilton, E.G., Greenside, P.G., Sinnott-Armstrong, N.A., Vesuna, S., Satpathy, A.T., Rubin, A.J., Montine, K.S., Wu, B., et al. (2017). An improved ATAC-seq protocol reduces background and enables interrogation of frozen tissues. Nat Methods *14*, 959-962. 10.1038/nmeth.4396.
Cox, A.R., Chernis, N., Bader, D.A., Saha, P.K., Masschelin, P.M., Felix, J.B., Sharp, R., Lian, Z., Putluri, V., Rajapakshe, K., et al. (2020). STAT1 Dissociates Adipose Tissue Inflammation From Insulin Sensitivity in Obesity. Diabetes *69*, 2630-2641. 10.2337/db20-0384.
Cui, J., Shen, L.Y., and Wang, G.C. (1991). Role of hair follicles in the repigmentation of vitiligo. J Invest Dermatol *97*, 410-416. 10.1111/1523-1747.ep12480997.
Cusanovich, D.A., Daza, R., Adey, A., Pliner, H.A., Christiansen, L., Gunderson, K.L., Steemers, F.J., Trapnell, C., and Shendure, J. (2015). Multiplex single cell profiling of chromatin accessibility by combinatorial cellular indexing. Science *348*, 910-914. 10.1126/science.aab1601.
Cusanovich, D.A., Hill, A.J., Aghamirzaie, D., Daza, R.M., Pliner, H.A., Berletch, J.B., Filippova, G.N., Huang, X., Christiansen, L., DeWitt, W.S., et al. (2018). A Single-Cell Atlas of In Vivo Mammalian Chromatin Accessibility. Cell *174*,

1309-1324 e1318. 10.1016/j.cell.2018.06.052.
Cypess, A.M., and Kahn, C.R. (2010a). Brown fat as a therapy for obesity and diabetes. Curr Opin Endocrinol Diabetes Obes *17*, 143-149. 10.1097/MED.0b013e328337a81f.
Cypess, A.M., and Kahn, C.R. (2010b). The role and importance of brown adipose tissue in energy homeostasis. Curr Opin Pediatr *22*, 478-484. 10.1097/MOP.0b013e32833a8d6e.
Czubryt, M.P., McAnally, J., Fishman, G.I., and Olson, E.N. (2003). Regulation of peroxisome proliferator-activated receptor gamma coactivator 1 alpha (PGC-1 alpha) and mitochondrial function by MEF2 and HDAC5. Proc Natl Acad Sci U S A *100*, 1711-1716. 10.1073/pnas.0337639100.
Dann, E., Henderson, N.C., Teichmann, S.A., Morgan, M.D., and Marioni, J.C. (2022). Differential abundance testing on single-cell data using k-nearest neighbor graphs. Nat Biotechnol *40*, 245-253. 10.1038/s41587-021-01033-z.
Deng, Y., Bartosovic, M., Ma, S., Zhang, D., Liu, Y., Qin, X., Su, G., Xu, M.L., Halene, S., Craft, J.E., et al. (2021). Spatial-ATAC-seq: spatially resolved chromatin accessibility profiling of tissues at genome scale and cellular level. bioRxiv. 10.1101/2021.06.06.447244.
Dixit, A., Parnas, O., Li, B., Chen, J., Fulco, C.P., Jerby-Arnon, L., Marjanovic, N.D., Dionne, D., Burks, T., Raychowdhury, R., et al. (2016). Perturb-Seq: Dissecting Molecular Circuits with Scalable Single-Cell RNA Profiling of Pooled Genetic Screens. Cell *167*, 1853-1866 e1817. 10.1016/j.cell.2016.11.038.
Domcke, S., Hill, A.J., Daza, R.M., Cao, J., O'Day, D.R., Pliner, H.A., Aldinger, K.A., Pokholok, D., Zhang, F., Milbank, J.H., et al. (2020). A human cell atlas of fetal chromatin accessibility. Science *370*. 10.1126/science.aba7612.
Fang, R., Preissl, S., Li, Y., Hou, X., Lucero, J., Wang, X., Motamedi, A., Shiau, A.K., Zhou, X., Xie, F., et al. (2021). Comprehensive analysis of single cell ATAC-seq data with SnapATAC. Nat Commun *12*, 1337. 10.1038/s41467-021-21583-9.
Fernandez Garcia, M., Moore, C.D., Schulz, K.N., Alberto, O., Donague, G., Harrison, M.M., Zhu, H., and Zaret, K.S. (2019). Structural Features of Transcription Factors Associating with Nucleosome Binding. Mol Cell *75*, 921-932 e926. 10.1016/j.molcel.2019.06.009.
Ferrara, N., Gerber, H.P., and LeCouter, J. (2003). The biology of VEGF and its receptors. Nat Med *9*, 669-676. 10.1038/nm0603-669.
Finck, B.N., and Kelly, D.P. (2006). PGC-1 coactivators: inducible regulators of energy metabolism in health and disease. J Clin Invest *116*, 615-622. 10.1172/JCI27794.
Fornes, O., Castro-Mondragon, J.A., Khan, A., van der Lee, R., Zhang, X., Richmond, P.A., Modi, B.P., Correard, S., Gheorghe, M., Baranasic, D., et al. (2020). JASPAR 2020: update of the open-access database of transcription factor binding profiles. Nucleic Acids Res *48*, D87-D92. 10.1093/nar/gkz1001.

Fuchs, E., Merrill, B.J., Jamora, C., and DasGupta, R. (2001). At the Roots of a Never-Ending Cycle. Developmental Cell *1*, 13-25. 10.1016/s1534-5807(01)00022-3.

Garces, R., and Mancha, M. (1993). One-step lipid extraction and fatty acid methyl esters preparation from fresh plant tissues. Anal Biochem *211*, 139-143. 10.1006/abio.1993.1244.

Gilbert, L.A., Larson, M.H., Morsut, L., Liu, Z., Brar, G.A., Torres, S.E., Stern-Ginossar, N., Brandman, O., Whitehead, E.H., Doudna, J.A., et al. (2013). CRISPR-mediated modular RNA-guided regulation of transcription in eukaryotes. Cell *154*, 442-451. 10.1016/j.cell.2013.06.044.

Gillette, T.G., and Hill, J.A. (2015). Readers, writers, and erasers: chromatin as the whiteboard of heart disease. Circ Res *116*, 1245-1253. 10.1161/CIRCRESAHA.116.303630.

Giresi, P.G., Kim, J., McDaniell, R.M., Iyer, V.R., and Lieb, J.D. (2007). FAIRE (Formaldehyde-Assisted Isolation of Regulatory Elements) isolates active regulatory elements from human chromatin. Genome Res *17*, 877-885. 10.1101/gr.5533506.

Goryshin, I.Y., and Reznikoff, W.S. (1998). Tn5 in vitro transposition. J Biol Chem *273*, 7367-7374. 10.1074/jbc.273.13.7367.

Goto, T., Lee, J.Y., Teraminami, A., Kim, Y.I., Hirai, S., Uemura, T., Inoue, H., Takahashi, N., and Kawada, T. (2011). Activation of peroxisome proliferator-activated receptor-alpha stimulates both differentiation and fatty acid oxidation in adipocytes. J Lipid Res *52*, 873-884. 10.1194/jlr.M011320.

Granja, J.M., Corces, M.R., Pierce, S.E., Bagdatli, S.T., Choudhry, H., Chang, H.Y., and Greenleaf, W.J. (2021). ArchR is a scalable software package for integrative single-cell chromatin accessibility analysis. Nat Genet *53*, 403-411. 10.1038/s41588-021-00790-6.

Guilherme, A., Yenilmez, B., Bedard, A.H., Henriques, F., Liu, D., Lee, A., Goldstein, L., Kelly, M., Nicoloro, S.M., Chen, M., et al. (2020). Control of Adipocyte Thermogenesis and Lipogenesis through beta3-Adrenergic and Thyroid Hormone Signal Integration. Cell Rep *31*, 107598. 10.1016/j.celrep.2020.107598.

Guo, H., Xing, Y., Liu, Y., Luo, Y., Deng, F., Yang, T., Yang, K., and Li, Y. (2016). Wnt/beta-catenin signaling pathway activates melanocyte stem cells in vitro and in vivo. J Dermatol Sci *83*, 45-51. 10.1016/j.jdermsci.2016.04.005.

Hamiche, A., Sandaltzopoulos, R., Gdula, D.A., and Wu, C. (1999). ATP-Dependent Histone Octamer Sliding Mediated by the Chromatin Remodeling Complex NURF. Cell *97*, 833-842. 10.1016/s0092-8674(00)80796-5.

Han, J., Lee, J.E., Jin, J., Lim, J.S., Oh, N., Kim, K., Chang, S.I., Shibuya, M., Kim, H., and Koh, G.Y. (2011). The spatiotemporal development of adipose tissue. Development *138*, 5027-5037. 10.1242/dev.067686.

Han, X., Zhang, Z., He, L., Zhu, H., Li, Y., Pu, W., Han, M., Zhao, H., Liu, K., Li, Y., et al. (2021). A suite of new Dre recombinase drivers markedly expands the ability to perform intersectional genetic targeting. Cell Stem Cell *28*, 1160-1176 e1167. 10.1016/j.stem.2021.01.007.

Hao, Y., Hao, S., Andersen-Nissen, E., Mauck, W.M., 3rd, Zheng, S., Butler, A., Lee, M.J., Wilk, A.J., Darby, C., Zager, M., et al. (2021). Integrated analysis of multimodal single-cell data. Cell *184*, 3573-3587 e3529. 10.1016/j.cell.2021.04.048.

Harms, M., and Seale, P. (2013). Brown and beige fat: development, function and therapeutic potential. Nat Med *19*, 1252-1263. 10.1038/nm.3361.

Hearing, V.J. (2005). Biogenesis of pigment granules: a sensitive way to regulate melanocyte function. J Dermatol Sci *37*, 3-14. 10.1016/j.jdermsci.2004.08.014.

Heintzman, N.D., Stuart, R.K., Hon, G., Fu, Y., Ching, C.W., Hawkins, R.D., Barrera, L.O., Van Calcar, S., Qu, C., Ching, K.A., et al. (2007). Distinct and predictive chromatin signatures of transcriptional promoters and enhancers in the human genome. Nat Genet *39*, 311-318. 10.1038/ng1966.

Henikoff, S. (2008). Nucleosome destabilization in the epigenetic regulation of gene expression. Nat Rev Genet *9*, 15-26. 10.1038/nrg2206.

Hiraike, Y., Waki, H., Yu, J., Nakamura, M., Miyake, K., Nagano, G., Nakaki, R., Suzuki, K., Kobayashi, H., Yamamoto, S., et al. (2017). NFIA co-localizes with PPARgamma and transcriptionally controls the brown fat gene program. Nat Cell Biol *19*, 1081-1092. 10.1038/ncb3590.

Howe, K.L., Achuthan, P., Allen, J., Allen, J., Alvarez-Jarreta, J., Amode, M.R., Armean, I.M., Azov, A.G., Bennett, R., Bhai, J., et al. (2021). Ensembl 2021. Nucleic Acids Res *49*, D884-D891. 10.1093/nar/gkaa942.

Hu, Z.Q., Zhou, S.L., Zhou, Z.J., Luo, C.B., Chen, E.B., Zhan, H., Wang, P.C., Dai, Z., Zhou, J., Fan, J., and Huang, X.W. (2016). Overexpression of semaphorin 3A promotes tumor progression and predicts poor prognosis in hepatocellular carcinoma after curative resection. Oncotarget *7*, 51733-51746. 10.18632/oncotarget.10104.

Huss, J.M., Torra, I.P., Staels, B., Giguere, V., and Kelly, D.P. (2004). Estrogen-related receptor alpha directs peroxisome proliferator-activated receptor alpha signaling in the transcriptional control of energy metabolism in cardiac and skeletal muscle. Mol Cell Biol *24*, 9079-9091. 10.1128/MCB.24.20.9079-9091.2004.

Hutvagner, G., and Simard, M.J. (2008). Argonaute proteins: key players in RNA silencing. Nat Rev Mol Cell Biol *9*, 22-32. 10.1038/nrm2321.

Infarinato, N.R., Stewart, K.S., Yang, Y., Gomez, N.C., Pasolli, H.A., Hidalgo, L., Polak, L., Carroll, T.S., and Fuchs, E. (2020). BMP signaling: at the gate between activated melanocyte stem cells and differentiation. Genes Dev *34*, 1713-1734. 10.1101/gad.340281.120.

Iwafuchi-Doi, M., and Zaret, K.S. (2016). Cell fate control by pioneer transcription factors. Development *143*, 1833-1837. 10.1242/dev.133900.

Jeon, K.I., Nehrke, K., and Huxlin, K.R. (2020). Semaphorin 3A potentiates the profibrotic effects of transforming growth factor-beta1 in the cornea. Biochem Biophys Res Commun *521*, 333-339. 10.1016/j.bbrc.2019.10.107.

Jia, G., Preussner, J., Chen, X., Guenther, S., Yuan, X., Yekelchyk, M., Kuenne, C., Looso, M., Zhou, Y., Teichmann, S., and Braun, T. (2018). Single cell

RNA-seq and ATAC-seq analysis of cardiac progenitor cell transition states and lineage settlement. Nat Commun *9*, 4877. 10.1038/s41467-018-07307-6.

Jiang, J., Chan, Y.S., Loh, Y.H., Cai, J., Tong, G.Q., Lim, C.A., Robson, P., Zhong, S., and Ng, H.H. (2008). A core Klf circuitry regulates self-renewal of embryonic stem cells. Nat Cell Biol *10*, 353-360. 10.1038/ncb1698.

Jiang, Y., Berry, D.C., and Graff, J.M. (2017a). Distinct cellular and molecular mechanisms for beta3 adrenergic receptor-induced beige adipocyte formation. Elife *6*. 10.7554/eLife.30329.

Jiang, Y., Berry, D.C., Jo, A., Tang, W., Arpke, R.W., Kyba, M., and Graff, J.M. (2017b). A PPARgamma transcriptional cascade directs adipose progenitor cell-niche interaction and niche expansion. Nat Commun *8*, 15926. 10.1038/ncomms15926.

Jiang, Y., Berry, D.C., Tang, W., and Graff, J.M. (2014). Independent stem cell lineages regulate adipose organogenesis and adipose homeostasis. Cell Rep *9*, 1007-1022. 10.1016/j.celrep.2014.09.049.

Jin, S., Guerrero-Juarez, C.F., Zhang, L., Chang, I., Ramos, R., Kuan, C.H., Myung, P., Plikus, M.V., and Nie, Q. (2021). Inference and analysis of cell-cell communication using CellChat. Nat Commun *12*, 1088. 10.1038/s41467-021-21246-9.

Johnson, D.S., Mortazavi, A., Myers, R.M., and Wold, B. (2007). Genome-wide mapping of in vivo protein-DNA interactions. Science *316*, 1497-1502. 10.1126/science.1141319.

Joost, S., Annusver, K., Jacob, T., Sun, X., Dalessandri, T., Sivan, U., Sequeira, I., Sandberg, R., and Kasper, M. (2020). The Molecular Anatomy of Mouse Skin during Hair Growth and Rest. Cell Stem Cell *26*, 441-457 e447. 10.1016/j.stem.2020.01.012.

Kasubuchi, M., Hasegawa, S., Hiramatsu, T., Ichimura, A., and Kimura, I. (2015). Dietary gut microbial metabolites, short-chain fatty acids, and host metabolic regulation. Nutrients *7*, 2839-2849. 10.3390/nu7042839.

Kawakami, A., and Fisher, D.E. (2017). The master role of microphthalmia-associated transcription factor in melanocyte and melanoma biology. Lab Invest *97*, 649-656. 10.1038/labinvest.2017.9.

Kaya-Okur, H.S., Wu, S.J., Codomo, C.A., Pledger, E.S., Bryson, T.D., Henikoff, J.G., Ahmad, K., and Henikoff, S. (2019). CUT&Tag for efficient epigenomic profiling of small samples and single cells. Nat Commun *10*, 1930. 10.1038/s41467-019-09982-5.

Kenny, C., Dilshat, R., Seberg, H., Otterloo, E.V., Bonde, G., Helverson, A., Franke, C.M., Steingrímsson, E., and Cornell, R.A. (2022). TFAP2 paralogs facilitate chromatin access for MITF at pigmentation genes but inhibit expression of cell-cell adhesion genes independently of MITF. bioRxiv *2021.11.23.469757*. https://doi.org/10.1101/2021.11.23.469757.

Kim, M., Goto, T., Yu, R., Uchida, K., Tominaga, M., Kano, Y., Takahashi, N., and Kawada, T. (2015). Fish oil intake induces UCP1 upregulation in brown and white adipose tissue via the sympathetic nervous system. Sci Rep *5*,

18013. 10.1038/srep18013.
Konermann, S., Brigham, M.D., Trevino, A.E., Joung, J., Abudayyeh, O.O., Barcena, C., Hsu, P.D., Habib, N., Gootenberg, J.S., Nishimasu, H., et al. (2015). Genome-scale transcriptional activation by an engineered CRISPR-Cas9 complex. Nature *517*, 583-588. 10.1038/nature14136.
Kornberg, R.D. (1974). Chromatin structure: a repeating unit of histones and DNA. Science *184*, 868-871. 10.1126/science.184.4139.868.
Kostal, V., Sula, J., and Simek, P. (1998). Physiology of drought tolerance and cold hardiness of the Mediterranean tiger moth Cymbalophora pudica during summer diapause. Journal of Insect Physiology *44*, 165-173. 10.1016/s0022-1910(97)00047-4.
Kouzarides, T. (2007). Chromatin modifications and their function. Cell *128*, 693-705. 10.1016/j.cell.2007.02.005.
Kumar, N., Liu, D., Wang, H., Robidoux, J., and Collins, S. (2008). Orphan nuclear receptor NOR-1 enhances 3',5'-cyclic adenosine 5'-monophosphate-dependent uncoupling protein-1 gene transcription. Mol Endocrinol *22*, 1057-1064. 10.1210/me.2007-0464.
Kwak, H., Fuda, N.J., Core, L.J., and Lis, J.T. (2013). Precise maps of RNA polymerase reveal how promoters direct initiation and pausing. Science *339*, 950-953. 10.1126/science.1229386.
Landecker, H. (2011). Food as exposure: Nutritional epigenetics and the new metabolism. Biosocieties *6*, 167-194. 10.1057/biosoc.2011.1.
Lang, D., Mascarenhas, J.B., and Shea, C.R. (2013). Melanocytes, melanocyte stem cells, and melanoma stem cells. Clin Dermatol *31*, 166-178. 10.1016/j.clindermatol.2012.08.014.
Langmead, B., and Salzberg, S.L. (2012). Fast gapped-read alignment with Bowtie 2. Nat Methods *9*, 357-359. 10.1038/nmeth.1923.
Längst, G., Bonte, E.J., Corona, D.F.V., and Becker, P.B. (1999). Nucleosome Movement by CHRAC and ISWI without Disruption or trans-Displacement of the Histone Octamer. Cell *97*, 843-852. 10.1016/s0092-8674(00)80797-7.
Lareau, C.A., Duarte, F.M., Chew, J.G., Kartha, V.K., Burkett, Z.D., Kohlway, A.S., Pokholok, D., Aryee, M.J., Steemers, F.J., Lebofsky, R., and Buenrostro, J.D. (2019). Droplet-based combinatorial indexing for massive-scale single-cell chromatin accessibility. Nat Biotechnol *37*, 916-924. 10.1038/s41587-019-0147-6.
Larson, E.D., Marsh, A.J., and Harrison, M.M. (2021). Pioneering the developmental frontier. Mol Cell *81*, 1640-1650. 10.1016/j.molcel.2021.02.020.
Larson, M.H., Gilbert, L.A., Wang, X., Lim, W.A., Weissman, J.S., and Qi, L.S. (2013). CRISPR interference (CRISPRi) for sequence-specific control of gene expression. Nat Protoc *8*, 2180-2196. 10.1038/nprot.2013.132.
Lawrence, T. (2009). The nuclear factor NF-kappaB pathway in inflammation. Cold Spring Harb Perspect Biol *1*, a001651. 10.1101/cshperspect.a001651.
Lee, C.K., Shibata, Y., Rao, B., Strahl, B.D., and Lieb, J.D. (2004). Evidence for nucleosome depletion at active regulatory regions genome-wide. Nat Genet

36, 900-905. 10.1038/ng1400.
Lee, H., Kim, W.J., Kang, H.G., Jang, J.H., Choi, I.J., Chun, K.H., and Kim, S.J. (2021). Upregulation of LAMB1 via ERK/c-Jun Axis Promotes Gastric Cancer Growth and Motility. Int J Mol Sci *22*. 10.3390/ijms22020626.
Lee, J.H., and Fisher, D.E. (2014). Melanocyte stem cells as potential therapeutics in skin disorders. Expert Opin Biol Ther *14*, 1569-1579. 10.1517/14712598.2014.935331.
Lee, T.I., and Young, R.A. (2013). Transcriptional regulation and its misregulation in disease. Cell *152*, 1237-1251. 10.1016/j.cell.2013.02.014.
Levy, C., Khaled, M., and Fisher, D.E. (2006). MITF: master regulator of melanocyte development and melanoma oncogene. Trends Mol Med *12*, 406-414. 10.1016/j.molmed.2006.07.008.
Leyton, J., Drury, P.J., and Crawford, M.A. (1987). Differential oxidation of saturated and unsaturated fatty acids in vivo in the rat. Br J Nutr *57*, 383-393. 10.1079/bjn19870046.
Li, H., and Guan, Y. (2022). Asymmetric Predictive Relationships Across Histone Modifications. Nat Mach Intell *4*, 288-299. 10.1038/s42256-022-00455-x.
Li, R., and Yang, X. (2022). De novo reconstruction of cell interaction landscapes from single-cell spatial transcriptome data with DeepLinc. Genome Biol *23*, 124. 10.1186/s13059-022-02692-0.
Li, Y., Ping, X., Zhang, Y., Li, G., Zhang, T., Chen, G., Ma, X., Wang, D., and Xu, L. (2021). Comparative Transcriptome Profiling of Cold Exposure and beta3-AR Agonist CL316,243-Induced Browning of White Fat. Front Physiol *12*, 667698. 10.3389/fphys.2021.667698.
Lim, J.H., Gerhart-Hines, Z., Dominy, J.E., Lee, Y., Kim, S., Tabata, M., Xiang, Y.K., and Puigserver, P. (2013). Oleic acid stimulates complete oxidation of fatty acids through protein kinase A-dependent activation of SIRT1-PGC1alpha complex. J Biol Chem *288*, 7117-7126. 10.1074/jbc.M112.415729.
Liscovitch-Brauer, N., Montalbano, A., Deng, J., Mendez-Mancilla, A., Wessels, H.H., Moss, N.G., Kung, C.Y., Sookdeo, A., Guo, X., Geller, E., et al. (2021). Profiling the genetic determinants of chromatin accessibility with scalable single-cell CRISPR screens. Nat Biotechnol *39*, 1270-1277. 10.1038/s41587-021-00902-x.
Lister, R., Pelizzola, M., Dowen, R.H., Hawkins, R.D., Hon, G., Tonti-Filippini, J., Nery, J.R., Lee, L., Ye, Z., Ngo, Q.M., et al. (2009). Human DNA methylomes at base resolution show widespread epigenomic differences. Nature *462*, 315-322. 10.1038/nature08514.
Lodhi, I.J., Wei, X., and Semenkovich, C.F. (2011). Lipoexpediency: de novo lipogenesis as a metabolic signal transmitter. Trends Endocrinol Metab *22*, 1-8. 10.1016/j.tem.2010.09.002.
Lorch, Y., Zhang, M., and Kornberg, R.D. (1999). Histone Octamer Transfer by a Chromatin-Remodeling Complex. Cell *96*, 389-392. 10.1016/s0092-8674(00)80551-6.

Lu, T., Ang, C.E., and Zhuang, X. (2022). Spatially resolved epigenomic profiling of single cells in complex tissues. bioRxiv. 10.1101/2022.02.17.480825.
Lubeck, E., Coskun, A.F., Zhiyentayev, T., Ahmad, M., and Cai, L. (2014). Single-cell in situ RNA profiling by sequential hybridization. Nat Methods *11*, 360-361. 10.1038/nmeth.2892.
Luger, K., Mader, A.W., Richmond, R.K., Sargent, D.F., and Richmond, T.J. (1997). Crystal structure of the nucleosome core particle at 2.8 A resolution. Nature *389*, 251-260. 10.1038/38444.
Ma, S., Zhang, B., LaFave, L.M., Earl, A.S., Chiang, Z., Hu, Y., Ding, J., Brack, A., Kartha, V.K., Tay, T., et al. (2020). Chromatin Potential Identified by Shared Single-Cell Profiling of RNA and Chromatin. Cell *183*, 1103-1116 e1120. 10.1016/j.cell.2020.09.056.
Mayran, A., and Drouin, J. (2018). Pioneer transcription factors shape the epigenetic landscape. J Biol Chem *293*, 13795-13804. 10.1074/jbc.R117.001232.
McLean, C.Y., Bristor, D., Hiller, M., Clarke, S.L., Schaar, B.T., Lowe, C.B., Wenger, A.M., and Bejerano, G. (2010). GREAT improves functional interpretation of cis-regulatory regions. Nat Biotechnol *28*, 495-501. 10.1038/nbt.1630.
Michel, L.Y.M., Farah, C., and Balligand, J.L. (2020). The Beta3 Adrenergic Receptor in Healthy and Pathological Cardiovascular Tissues. Cells *9*. 10.3390/cells9122584.
Mierziak, J., Kostyn, K., Boba, A., Czemplik, M., Kulma, A., and Wojtasik, W. (2021). Influence of the Bioactive Diet Components on the Gene Expression Regulation. Nutrients *13*. 10.3390/nu13113673.
Milagro, F.I., Campion, J., Cordero, P., Goyenechea, E., Gomez-Uriz, A.M., Abete, I., Zulet, M.A., and Martinez, J.A. (2011). A dual epigenomic approach for the search of obesity biomarkers: DNA methylation in relation to diet-induced weight loss. FASEB J *25*, 1378-1389. 10.1096/fj.10-170365.
Moon, H., Donahue, L.R., Choi, E., Scumpia, P.O., Lowry, W.E., Grenier, J.K., Zhu, J., and White, A.C. (2017). Melanocyte Stem Cell Activation and Translocation Initiate Cutaneous Melanoma in Response to UV Exposure. Cell Stem Cell *21*, 665-678 e666. 10.1016/j.stem.2017.09.001.
Mottillo, E.P., Balasubramanian, P., Lee, Y.H., Weng, C., Kershaw, E.E., and Granneman, J.G. (2014). Coupling of lipolysis and de novo lipogenesis in brown, beige, and white adipose tissues during chronic beta3-adrenergic receptor activation. J Lipid Res *55*, 2276-2286. 10.1194/jlr.M050005.
Mull, A.N., Zolekar, A., and Wang, Y.C. (2015). Understanding Melanocyte Stem Cells for Disease Modeling and Regenerative Medicine Applications. Int J Mol Sci *16*, 30458-30469. 10.3390/ijms161226207.
Musselman, C.A., Lalonde, M.E., Cote, J., and Kutateladze, T.G. (2012). Perceiving the epigenetic landscape through histone readers. Nat Struct Mol Biol *19*, 1218-1227. 10.1038/nsmb.2436.
Nie, B., Nie, T., Hui, X., Gu, P., Mao, L., Li, K., Yuan, R., Zheng, J., Wang, H., Li, K., et al. (2017). Brown Adipogenic Reprogramming Induced by a Small

Molecule. Cell Rep *18*, 624-635. 10.1016/j.celrep.2016.12.062.
Nishimura, E.K. (2011). Melanocyte stem cells: a melanocyte reservoir in hair follicles for hair and skin pigmentation. Pigment Cell Melanoma Res *24*, 401-410. 10.1111/j.1755-148X.2011.00855.x.
Nishimura, E.K., Granter, S.R., and Fisher, D.E. (2005). Mechanisms of hair graying: incomplete melanocyte stem cell maintenance in the niche. Science *307*, 720-724. 10.1126/science.1099593.
Nishimura, E.K., Jordan, S.A., Oshima, H., Yoshida, H., Osawa, M., Moriyama, M., Jackson, I.J., Barrandon, Y., Miyachi, Y., and Nishikawa, S. (2002). Dominant role of the niche in melanocyte stem-cell fate determination. Nature *416*, 854-860. 10.1038/416854a.
Nord, A.S., Blow, M.J., Attanasio, C., Akiyama, J.A., Holt, A., Hosseini, R., Phouanenavong, S., Plajzer-Frick, I., Shoukry, M., Afzal, V., et al. (2013). Rapid and pervasive changes in genome-wide enhancer usage during mammalian development. Cell *155*, 1521-1531. 10.1016/j.cell.2013.11.033.
Ohno, H., Shinoda, K., Spiegelman, B.M., and Kajimura, S. (2012). PPARgamma agonists induce a white-to-brown fat conversion through stabilization of PRDM16 protein. Cell Metab *15*, 395-404. 10.1016/j.cmet.2012.01.019.
Omoto, M., Yoshida, S., Miyashita, H., Kawakita, T., Yoshida, K., Kishino, A., Kimura, T., Shibata, S., Tsubota, K., Okano, H., and Shimmura, S. (2012). The semaphorin 3A inhibitor SM-345431 accelerates peripheral nerve regeneration and sensitivity in a murine corneal transplantation model. PLoS One *7*, e47716. 10.1371/journal.pone.0047716.
Ou, J., Liu, H., Yu, J., Kelliher, M.A., Castilla, L.H., Lawson, N.D., and Zhu, L.J. (2018). ATACseqQC: a Bioconductor package for post-alignment quality assessment of ATAC-seq data. BMC Genomics *19*, 169. 10.1186/s12864-018-4559-3.
Perris, R. (1997). The extracellular matrix in neural crest-cell migration. Trends in Neurosciences *20*, 23-31. 10.1016/s0166-2236(96)10063-1.
Picelli, S., Bjorklund, A.K., Reinius, B., Sagasser, S., Winberg, G., and Sandberg, R. (2014). Tn5 transposase and tagmentation procedures for massively scaled sequencing projects. Genome Res *24*, 2033-2040. 10.1101/gr.177881.114.
Pierce, S.E., Granja, J.M., and Greenleaf, W.J. (2021). High-throughput single-cell chromatin accessibility CRISPR screens enable unbiased identification of regulatory networks in cancer. Nat Commun *12*, 2969. 10.1038/s41467-021-23213-w.
Pliner, H.A., Packer, J.S., McFaline-Figueroa, J.L., Cusanovich, D.A., Daza, R.M., Aghamirzaie, D., Srivatsan, S., Qiu, X., Jackson, D., Minkina, A., et al. (2018). Cicero Predicts cis-Regulatory DNA Interactions from Single-Cell Chromatin Accessibility Data. Mol Cell *71*, 858-871 e858. 10.1016/j.molcel.2018.06.044.
Plonka, P.M., Passeron, T., Brenner, M., Tobin, D.J., Shibahara, S., Thomas, A., Slominski, A., Kadekaro, A.L., Hershkovitz, D., Peters, E., et al. (2009).

What are melanocytes really doing all day long...? Exp Dermatol *18*, 799-819. 10.1111/j.1600-0625.2009.00912.x.

Praetorius, C., Grill, C., Stacey, S.N., Metcalf, A.M., Gorkin, D.U., Robinson, K.C., Van Otterloo, E., Kim, R.S., Bergsteinsdottir, K., Ogmundsdottir, M.H., et al. (2013). A polymorphism in IRF4 affects human pigmentation through a tyrosinase-dependent MITF/TFAP2A pathway. Cell *155*, 1022-1033. 10.1016/j.cell.2013.10.022.

Preissl, S., Fang, R., Huang, H., Zhao, Y., Raviram, R., Gorkin, D.U., Zhang, Y., Sos, B.C., Afzal, V., Dickel, D.E., et al. (2018). Single-nucleus analysis of accessible chromatin in developing mouse forebrain reveals cell-type-specific transcriptional regulation. Nat Neurosci *21*, 432-439. 10.1038/s41593-018-0079-3.

Rabhi, N., Belkina, A.C., Desevin, K., Cortez, B.N., and Farmer, S.R. (2020). Shifts of Immune Cell Populations Differ in Response to Different Effectors of Beige Remodeling of Adipose Tissue. iScience *23*, 101765. 10.1016/j.isci.2020.101765.

Raj, A., Peskin, C.S., Tranchina, D., Vargas, D.Y., and Tyagi, S. (2006). Stochastic mRNA synthesis in mammalian cells. PLoS Biol *4*, e309. 10.1371/journal.pbio.0040309.

Rajbhandari, P., Arneson, D., Hart, S.K., Ahn, I.S., Diamante, G., Santos, L.C., Zaghari, N., Feng, A.C., Thomas, B.J., Vergnes, L., et al. (2019). Single cell analysis reveals immune cell-adipocyte crosstalk regulating the transcription of thermogenic adipocytes. Elife *8*. 10.7554/eLife.49501.

Rhee, H.S., and Pugh, B.F. (2011). Comprehensive genome-wide protein-DNA interactions detected at single-nucleotide resolution. Cell *147*, 1408-1419. 10.1016/j.cell.2011.11.013.

Roh, H.C., Tsai, L.T.Y., Shao, M., Tenen, D., Shen, Y., Kumari, M., Lyubetskaya, A., Jacobs, C., Dawes, B., Gupta, R.K., and Rosen, E.D. (2018). Warming Induces Significant Reprogramming of Beige, but Not Brown, Adipocyte Cellular Identity. Cell Metab *27*, 1121-1137 e1125. 10.1016/j.cmet.2018.03.005.

Rosen, E.D., Hsu, C.H., Wang, X., Sakai, S., Freeman, M.W., Gonzalez, F.J., and Spiegelman, B.M. (2002). C/EBPalpha induces adipogenesis through PPARgamma: a unified pathway. Genes Dev *16*, 22-26. 10.1101/gad.948702.

Rosen, E.D., and Spiegelman, B.M. (2014). What we talk about when we talk about fat. Cell *156*, 20-44. 10.1016/j.cell.2013.12.012.

Rosenberg, A.B., Roco, C.M., Muscat, R.A., Kuchina, A., Sample, P., Yao, Z., Graybuck, L.T., Peeler, D.J., Mukherjee, S., Chen, W., et al. (2018). Single-cell profiling of the developing mouse brain and spinal cord with split-pool barcoding. Science *360*, 176-182. 10.1126/science.aam8999.

Rosenwald, M., Perdikari, A., Rulicke, T., and Wolfrum, C. (2013). Bi-directional interconversion of brite and white adipocytes. Nat Cell Biol *15*, 659-667. 10.1038/ncb2740.

Rosette, C., and Karin, M. (1996). Ultraviolet light and osmotic stress: activation

of the JNK cascade through multiple growth factor and cytokine receptors. Science *274*, 1194-1197. 10.1126/science.274.5290.1194.

Rubin, A.J., Parker, K.R., Satpathy, A.T., Qi, Y., Wu, B., Ong, A.J., Mumbach, M.R., Ji, A.L., Kim, D.S., Cho, S.W., et al. (2019). Coupled Single-Cell CRISPR Screening and Epigenomic Profiling Reveals Causal Gene Regulatory Networks. Cell *176*, 361-376 e317. 10.1016/j.cell.2018.11.022.

Russo, G.L., Vastolo, V., Ciccarelli, M., Albano, L., Macchia, P.E., and Ungaro, P. (2017). Dietary polyphenols and chromatin remodeling. Crit Rev Food Sci Nutr *57*, 2589-2599. 10.1080/10408398.2015.1062353.

Sanjana, N.E., Wright, J., Zheng, K., Shalem, O., Fontanillas, P., Joung, J., Cheng, C., Regev, A., and Zhang, F. (2016). High-resolution interrogation of functional elements in the noncoding genome. Science *353*, 1545-1549. 10.1126/science.aaf7613.

Schep, A.N., Wu, B., Buenrostro, J.D., and Greenleaf, W.J. (2017). chromVAR: inferring transcription-factor-associated accessibility from single-cell epigenomic data. Nat Methods *14*, 975-978. 10.1038/nmeth.4401.

Schlesinger, F., Smith, A.D., Gingeras, T.R., Hannon, G.J., and Hodges, E. (2013). De novo DNA demethylation and noncoding transcription define active intergenic regulatory elements. Genome Res *23*, 1601-1614. 10.1101/gr.157271.113.

Schones, D.E., Cui, K., Cuddapah, S., Roh, T.Y., Barski, A., Wang, Z., Wei, G., and Zhao, K. (2008). Dynamic regulation of nucleosome positioning in the human genome. Cell *132*, 887-898. 10.1016/j.cell.2008.02.022.

Schreiber, S.N., Emter, R., Hock, M.B., Knutti, D., Cardenas, J., Podvinec, M., Oakeley, E.J., and Kralli, A. (2004). The estrogen-related receptor alpha (ERRalpha) functions in PPARgamma coactivator 1alpha (PGC-1alpha)-induced mitochondrial biogenesis. Proc Natl Acad Sci U S A *101*, 6472-6477. 10.1073/pnas.0308686101.

Seberg, H.E., Van Otterloo, E., Loftus, S.K., Liu, H., Bonde, G., Sompallae, R., Gildea, D.E., Santana, J.F., Manak, J.R., Pavan, W.J., et al. (2017). TFAP2 paralogs regulate melanocyte differentiation in parallel with MITF. PLoS Genet *13*, e1006636. 10.1371/journal.pgen.1006636.

Shek, L.P., Chong, M.F., Lim, J.Y., Soh, S.E., and Chong, Y.S. (2012). Role of dietary long-chain polyunsaturated fatty acids in infant allergies and respiratory diseases. Clin Dev Immunol *2012*, 730568. 10.1155/2012/730568.

Shelly, M., Cancedda, L., Lim, B.K., Popescu, A.T., Cheng, P.L., Gao, H., and Poo, M.M. (2011). Semaphorin3A regulates neuronal polarization by suppressing axon formation and promoting dendrite growth. Neuron *71*, 433-446. 10.1016/j.neuron.2011.06.041.

Sherwood, R.I., Hashimoto, T., O'Donnell, C.W., Lewis, S., Barkal, A.A., van Hoff, J.P., Karun, V., Jaakkola, T., and Gifford, D.K. (2014). Discovery of directional and nondirectional pioneer transcription factors by modeling DNase profile magnitude and shape. Nat Biotechnol *32*, 171-178. 10.1038/nbt.2798.

Siegel, R.L., Miller, K.D., and Jemal, A. (2019). Cancer statistics, 2019. CA Cancer J Clin *69*, 7-34. 10.3322/caac.21551.

Sims, R.J., 3rd, and Reinberg, D. (2004). From chromatin to cancer: a new histone lysine methyltransferase enters the mix. Nat Cell Biol *6*, 685-687. 10.1038/ncb0804-685.

Skene, P.J., and Henikoff, S. (2017). An efficient targeted nuclease strategy for high-resolution mapping of DNA binding sites. Elife *6*. 10.7554/eLife.21856.

Slominski, A., and Paus, R. (1993). Melanogenesis is coupled to murine anagen: Toward new concepts for the role of melanocytes and the regulation of melanogenesis in hair growth. Journal of Investigative Dermatology *101*, S90-S97. 10.1016/0022-202x(93)90507-e.

Soteriou, D., Kostic, L., Sedov, E., Yosefzon, Y., Steller, H., and Fuchs, Y. (2016). Isolating Hair Follicle Stem Cells and Epidermal Keratinocytes from Dorsal Mouse Skin. J Vis Exp. 10.3791/53931.

Soumano, K. (2000). Glucocorticoids inhibit the transcriptional response of the uncoupling protein-1 gene to adrenergic stimulation in a brown adipose cell line. Molecular and Cellular Endocrinology *165*, 7-15. 10.1016/s0303-7207(00)00276-8.

Spektor, R., Yang, J.W., Lee, S., and Soloway, P.D. (2019). Single cell ATAC-seq identifies broad changes in neuronal abundance and chromatin accessibility in Down Syndrome. bioRxiv. 10.1101/561191.

Staub, E., Grone, J., Mennerich, D., Ropcke, S., Klamann, I., Hinzmann, B., Castanos-Velez, E., Mann, B., Pilarsky, C., Brummendorf, T., et al. (2006). A genome-wide map of aberrantly expressed chromosomal islands in colorectal cancer. Mol Cancer *5*, 37. 10.1186/1476-4598-5-37.

Steingrimsson, E., Copeland, N.G., and Jenkins, N.A. (2005). Melanocyte stem cell maintenance and hair graying. Cell *121*, 9-12. 10.1016/j.cell.2005.03.021.

Strack, A.M., Bradbury, M.J., and Dallman, M.F. (1995). Corticosterone decreases nonshivering thermogenesis and increases lipid storage in brown adipose tissue. Am J Physiol *268*, R183-191. 10.1152/ajpregu.1995.268.1.R183.

Stuart, T., Butler, A., Hoffman, P., Hafemeister, C., Papalexi, E., Mauck, W.M., 3rd, Hao, Y., Stoeckius, M., Smibert, P., and Satija, R. (2019). Comprehensive Integration of Single-Cell Data. Cell *177*, 1888-1902 e1821. 10.1016/j.cell.2019.05.031.

Stuart, T., Srivastava, A., Madad, S., Lareau, C.A., and Satija, R. (2021). Single-cell chromatin state analysis with Signac. Nat Methods *18*, 1333-1341. 10.1038/s41592-021-01282-5.

Su, J.H., Zheng, P., Kinrot, S.S., Bintu, B., and Zhuang, X. (2020). Genome-Scale Imaging of the 3D Organization and Transcriptional Activity of Chromatin. Cell *182*, 1641-1659 e1626. 10.1016/j.cell.2020.07.032.

Sun, W., Dong, H., Balaz, M., Slyper, M., Drokhlyansky, E., Colleluori, G., Giordano, A., Kovanicova, Z., Stefanicka, P., Balazova, L., et al. (2020). snRNA-seq reveals a subpopulation of adipocytes that regulates

thermogenesis. Nature *587*, 98-102. 10.1038/s41586-020-2856-x.
Swanson, E., Lord, C., Reading, J., Heubeck, A.T., Genge, P.C., Thomson, Z., Weiss, M.D., Li, X.J., Savage, A.K., Green, R.R., et al. (2021). Simultaneous trimodal single-cell measurement of transcripts, epitopes, and chromatin accessibility using TEA-seq. Elife *10*. 10.7554/eLife.63632.
Tanimura, S., Tadokoro, Y., Inomata, K., Binh, N.T., Nishie, W., Yamazaki, S., Nakauchi, H., Tanaka, Y., McMillan, J.R., Sawamura, D., et al. (2011). Hair follicle stem cells provide a functional niche for melanocyte stem cells. Cell Stem Cell *8*, 177-187. 10.1016/j.stem.2010.11.029.
Thiele, A., Luettges, K., Ritter, D., Beyhoff, N., Smeir, E., Grune, J., Steinhoff, J.S., Schupp, M., Klopfleisch, R., Rothe, M., et al. (2021). Pharmacological inhibition of adipose tissue Adipose Triglyceride Lipase (ATGL) by Atglistatin prevents catecholamine-induced myocardial damage. Cardiovasc Res. 10.1093/cvr/cvab182.
Thornton, C.A., Mulqueen, R.M., Torkenczy, K.A., Nishida, A., Lowenstein, E.G., Fields, A.J., Steemers, F.J., Zhang, W., McConnell, H.L., Woltjer, R.L., et al. (2021). Spatially mapped single-cell chromatin accessibility. Nat Commun *12*, 1274. 10.1038/s41467-021-21515-7.
Thuzar, M., Law, W.P., Ratnasingam, J., Jang, C., Dimeski, G., and Ho, K.K.Y. (2018). Glucocorticoids suppress brown adipose tissue function in humans: A double-blind placebo-controlled study. Diabetes Obes Metab *20*, 840-848. 10.1111/dom.13157.
Tiku, P.E., Gracey, A.Y., Macartney, A.I., Beynon, R.J., and Cossins, A.R. (1996). Cold-induced expression of delta 9-desaturase in carp by transcriptional and posttranslational mechanisms. Science *271*, 815-818. 10.1126/science.271.5250.815.
Tobin, D.J., Hagen, E., Botchkarev, V.A., and Paus, R. (1998). Do hair bulb melanocytes undergo apoptosis during hair follicle regression (catagen)? J Invest Dermatol *111*, 941-947. 10.1046/j.1523-1747.1998.00417.x.
Trapnell, C., Cacchiarelli, D., Grimsby, J., Pokharel, P., Li, S., Morse, M., Lennon, N.J., Livak, K.J., Mikkelsen, T.S., and Rinn, J.L. (2014). The dynamics and regulators of cell fate decisions are revealed by pseudotemporal ordering of single cells. Nat Biotechnol *32*, 381-386. 10.1038/nbt.2859.
Tumbar, T., Guasch, G., Greco, V., Blanpain, C., Lowry, W.E., Rendl, M., and Fuchs, E. (2004). Defining the epithelial stem cell niche in skin. Science *303*, 359-363. 10.1126/science.1092436.
Vega, R.B., Huss, J.M., and Kelly, D.P. (2000). The coactivator PGC-1 cooperates with peroxisome proliferator-activated receptor alpha in transcriptional control of nuclear genes encoding mitochondrial fatty acid oxidation enzymes. Mol Cell Biol *20*, 1868-1876. 10.1128/MCB.20.5.1868-1876.2000.
Viengchareun, S., Penfornis, P., Zennaro, M.C., and Lombes, M. (2001). Mineralocorticoid and glucocorticoid receptors inhibit UCP expression and function in brown adipocytes. Am J Physiol Endocrinol Metab *280*, E640-

649. 10.1152/ajpendo.2001.280.4.E640.
Vijay, J., Gauthier, M.F., Biswell, R.L., Louiselle, D.A., Johnston, J.J., Cheung, W.A., Belden, B., Pramatarova, A., Biertho, L., Gibson, M., et al. (2020). Single-cell analysis of human adipose tissue identifies depot and disease specific cell types. Nat Metab *2*, 97-109. 10.1038/s42255-019-0152-6.
Vitak, S.A., Torkenczy, K.A., Rosenkrantz, J.L., Fields, A.J., Christiansen, L., Wong, M.H., Carbone, L., Steemers, F.J., and Adey, A. (2017). Sequencing thousands of single-cell genomes with combinatorial indexing. Nat Methods *14*, 302-308. 10.1038/nmeth.4154.
Wales, S., Hashemi, S., Blais, A., and McDermott, J.C. (2014). Global MEF2 target gene analysis in cardiac and skeletal muscle reveals novel regulation of DUSP6 by p38MAPK-MEF2 signaling. Nucleic Acids Res *42*, 11349-11362. 10.1093/nar/gku813.
Wang, F., Flanagan, J., Su, N., Wang, L.C., Bui, S., Nielson, A., Wu, X., Vo, H.T., Ma, X.J., and Luo, Y. (2012). RNAscope: a novel in situ RNA analysis platform for formalin-fixed, paraffin-embedded tissues. J Mol Diagn *14*, 22-29. 10.1016/j.jmoldx.2011.08.002.
Wang, S., Liang, X., Yang, Q., Fu, X., Rogers, C.J., Zhu, M., Rodgers, B.D., Jiang, Q., Dodson, M.V., and Du, M. (2015). Resveratrol induces brown-like adipocyte formation in white fat through activation of AMP-activated protein kinase (AMPK) alpha1. Int J Obes (Lond) *39*, 967-976. 10.1038/ijo.2015.23.
Wang, Y., Yuan, P., Yan, Z., Yang, M., Huo, Y., Nie, Y., Zhu, X., Qiao, J., and Yan, L. (2021). Single-cell multiomics sequencing reveals the functional regulatory landscape of early embryos. Nat Commun *12*, 1247. 10.1038/s41467-021-21409-8.
Wang, Z., Chivu, A.G., Choate, L.A., Rice, E.J., Miller, D.C., Chu, T., Chou, S.P., Kingsley, N.B., Petersen, J.L., Finno, C.J., et al. (2022). Prediction of histone post-translational modification patterns based on nascent transcription data. Nat Genet *54*, 295-305. 10.1038/s41588-022-01026-x.
Weirauch, M.T., Yang, A., Albu, M., Cote, A.G., Montenegro-Montero, A., Drewe, P., Najafabadi, H.S., Lambert, S.A., Mann, I., Cook, K., et al. (2014). Determination and inference of eukaryotic transcription factor sequence specificity. Cell *158*, 1431-1443. 10.1016/j.cell.2014.08.009.
Westerterp, K.R. (2004). Diet induced thermogenesis. Nutr Metab (Lond) *1*, 5. 10.1186/1743-7075-1-5.
Wolock, S.L., Lopez, R., and Klein, A.M. (2019). Scrublet: Computational Identification of Cell Doublets in Single-Cell Transcriptomic Data. Cell Syst *8*, 281-291 e289. 10.1016/j.cels.2018.11.005.
Wu, C., Wong, Y.C., and Elgin, S.C. (1979). The chromatin structure of specific genes: II. Disruption of chromatin structure during gene activity. Cell *16*, 807-814. 10.1016/0092-8674(79)90096-5.
Wu, J., Bostrom, P., Sparks, L.M., Ye, L., Choi, J.H., Giang, A.H., Khandekar, M., Virtanen, K.A., Nuutila, P., Schaart, G., et al. (2012). Beige adipocytes are a distinct type of thermogenic fat cell in mouse and human. Cell *150*, 366-376. 10.1016/j.cell.2012.05.016.

Yu, G., Wang, L.G., Han, Y., and He, Q.Y. (2012). clusterProfiler: an R package for comparing biological themes among gene clusters. OMICS *16*, 284-287. 10.1089/omi.2011.0118.

Yue, F., Cheng, Y., Breschi, A., Vierstra, J., Wu, W., Ryba, T., Sandstrom, R., Ma, Z., Davis, C., Pope, B.D., et al. (2014). A comparative encyclopedia of DNA elements in the mouse genome. Nature *515*, 355-364. 10.1038/nature13992.

Zaidi, M.R., Hornyak, T.J., and Merlino, G. (2011). A genetically engineered mouse model with inducible GFP expression in melanocytes. Pigment Cell and Melanoma Research *24*, 393-394. 10.1111/j.1755-148X.2011.00832.x.

Zaret, K.S., and Mango, S.E. (2016). Pioneer transcription factors, chromatin dynamics, and cell fate control. Curr Opin Genet Dev *37*, 76-81. 10.1016/j.gde.2015.12.003.

Zhang, W., Xu, J., Li, J., Guo, T., Jiang, D., Feng, X., Ma, X., He, L., Wu, W., Yin, M., et al. (2018). The TEA domain family transcription factor TEAD4 represses murine adipogenesis by recruiting the cofactors VGLL4 and CtBP2 into a transcriptional complex. J Biol Chem *293*, 17119-17134. 10.1074/jbc.RA118.003608.

Zhang, Y., LeRoy, G., Seelig, H.-P., Lane, W.S., and Reinberg, D. (1998). The Dermatomyositis-Specific Autoantigen Mi2 Is a Component of a Complex Containing Histone Deacetylase and Nucleosome Remodeling Activities. Cell *95*, 279-289. 10.1016/s0092-8674(00)81758-4.

Zhang, Y., Liu, T., Meyer, C.A., Eeckhoute, J., Johnson, D.S., Bernstein, B.E., Nusbaum, C., Myers, R.M., Brown, M., Li, W., and Liu, X.S. (2008). Model-based analysis of ChIP-Seq (MACS). Genome Biol *9*, R137. 10.1186/gb-2008-9-9-r137.

Zhong, Z., Feng, S., Duttke, S.H., Potok, M.E., Zhang, Y., Gallego-Bartolome, J., Liu, W., and Jacobsen, S.E. (2021). DNA methylation-linked chromatin accessibility affects genomic architecture in Arabidopsis. Proc Natl Acad Sci U S A *118*. 10.1073/pnas.2023347118.

Zhu, C., Yu, M., Huang, H., Juric, I., Abnousi, A., Hu, R., Lucero, J., Behrens, M.M., Hu, M., and Ren, B. (2019). An ultra high-throughput method for single-cell joint analysis of open chromatin and transcriptome. Nat Struct Mol Biol *26*, 1063-1070. 10.1038/s41594-019-0323-x.

APPENDIX

The following publications are results of collaborative work conducted during doctoral study:

1. Roman Spektor, Jee Won Yang, **Seoyeon Lee**, Paul Soloway. Single cell ATAC-seq identifies broad changes in neuronal abundance and chromatin accessibility in Down Syndrome. *bioRxiv* 561191; doi: https://doi.org/10.1101/561191 *Manuscript under review*

   I was responsible for figure 1d. I mixed human and mouse cells, A549 cells and Hepa1-6 cells respectively, then generated snATAC-seq library. Then reads were counted for each barcode and mapped to hg19 or mm19 genome. Any cell barcodes containing both human and mouse reads were counted as a collision (doublet).

2. Chieh-Ren Hsia, Jawuanna McAllister, Ovais Hasan, Julius Judd, **Seoyeon Lee**, Richa Agrawal, Chao-Yuan Chang, Cedric Feschotte, Paul Soloway, Jan Lammerding. Confined Migration Induces Heterochromatin Formation and Alters Chromatin Accessibility. *bioRxiv* 2021.09.22.461293; doi: https://doi.org/10.1101/2021.09.22.461293 *Manuscript accepted by iScience*

   I was responsible for figure 6a and 6c and table 1 and 2. I annotated genomic location of differentially accessible peaks and identified the distribution of peaks from transcription start sties of its associated genes and their potential function predicted by its associated genes. I calculated the proportion of differentially accessible peaks nearby centromeres or telomeres.